

PROCEEDINGS OF THE
SEVENTH ANNUAL
PACIFIC CLIMATE (PACLIM) WORKSHOP

Asilomar, California – April 1990

Edited by
Julio L. Betancourt and Vera L. Tharp

Technical Report 26
of the
Interagency Ecological Studies Program
for the
Sacramento-San Joaquin Estuary

April 1991

Copies of this report may be obtained without charge from:

California Department of Water Resources
P.O. Box 942836
Sacramento, CA 94236-0001

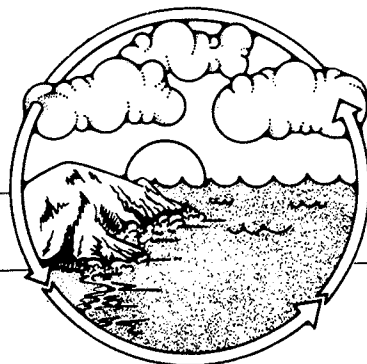
PROCEEDINGS OF THE SEVENTH ANNUAL PACIFIC CLIMATE (PACLIM) WORKSHOP

Asilomar, California – April 1990

Edited by
Julio L. Betancourt and Vera L. Tharp

Technical Report 26
of the
Interagency Ecological Studies Program
for the
Sacramento-San Joaquin Estuary

PACLIM



**Climate Variability
of the
Eastern North Pacific
and
Western North America**

The Seventh Annual Pacific Climate Workshop was sponsored by the

U.S. Geological Survey

Monterey Bay Aquarium Research Institute

National Oceanic and Atmospheric Administration,
Geophysical Data Center

Environmental Protection Agency, Global Change Program

California Department of Water Resources

Publication of this proceedings has been sponsored by the

Interagency Ecological Studies Program
for the
Sacramento-San Joaquin Estuary

A Cooperative Study by:

California Department of Water Resources
State Water Resources Control Board
U.S. Bureau of Reclamation

U.S. Army Corps of Engineers

California Department of Fish and Game
U.S. Fish and Wildlife Service
U.S. Geological Survey

These proceedings were published by the Interagency Ecological Studies Program for the
Sacramento-San Joaquin Estuary (Interagency Program)
in a cooperative effort with the

U.S. Geological Survey Research Project Office, Tucson, Arizona.

Although the Research Project Office is not a member of the Interagency Program,
information generated by the PACLIM workshop provides the
Interagency Program with a climatological perspective that cannot be obtained from its own studies.
Views and conclusions contained in this publication do not necessarily reflect the opinions of the
Interagency Program or its member agencies.

Contents

Sponsors	iii
Authors of Papers	vii
Introduction	1
<i>Julio L. Betancourt</i>	
GCM-Data Intercomparison: The Good News and The Bad	5
<i>Stanley L. Grotch</i>	
Land Surface Hydrology in a General Circulation Model: Global and Regional Fields Needed for Validation	17
<i>Robert E. Dickinson and Patrick J. Kennedy</i>	
Simulation and Diagnosis of Large-Scale Atmospheric Moisture and Surface Hydrology Over North America	25
<i>John O. Roads, Shyh-Chin Chen, David Langley, Chih-Yue Kao, Jordan Alpert, and Gary A. Glatzmaier</i>	
Toward a Rule-Based Biome Model	35
<i>Ronald P. Neilson, George A. King, and Greg Koerper</i>	
Skill of Monthly Forecasts during the Northern Hemisphere Summer	53
<i>Kingtse C. Mo</i>	
Wind Climate Trends in the Pacific Northwest and the Implications to Renewable Energy Supply	59
<i>John E. Wade and Kelly T. Redmond</i>	
Climate Variability and Crater Lake Water Levels	67
<i>Kelly T. Redmond</i>	
The Influence of Seasonal Precipitation and Temperature Variations on Runoff in California and Southwestern Oregon	75
<i>Larry G. Riddle, Daniel R. Cayan, and Edward Aguado</i>	
“Cool” vs. “Warm” Winter Precipitation and its Effect on Streamflow in California	91
<i>Daniel R. Cayan</i>	
Air Temperature Trends in California	101
<i>James D. Goodridge</i>	
One Hundred Years of Rainfall Trends in California	109
<i>James D. Goodridge</i>	

1976 Step in the Pacific Climate: Forty Environmental Changes Between 1968-1975 and 1977-1984	115
<i>Curtis C. Ebbesmeyer, Daniel R. Cayan, Douglas R. McLain, Frederic H. Nichols, David H. Peterson, and Kelly T. Redmond</i>	
Climate Forcing of Pacific Herring Recruitment and Growth in Southern British Columbia	127
<i>Daniel M. Ware</i>	
Upwelling, Offshore Transport, and the Availability of Rockfish in Central California	131
<i>David G. Ainley, William J. Sydeman, and Richard H. Parrish</i>	
The Role of Direct Observation in Predicting Climatic Change	137
<i>Roger Y. Anderson</i>	
Initial Global Perspective of Climate for the Last Thousand Years: The Ice Core Record	147
<i>Lonnie G. Thompson</i>	
Snow Accumulation Time Series and Their Climatic Interpretation	153
<i>Gerald Holdsworth</i>	
Coastal Climate Reflected in $^{13}\text{C}/^{12}\text{C}$ Ratio of Organic Carbon in Varved Sediment from Santa Barbara Basin	157
<i>Arndt Schimmelmann and Mia J. Tegner</i>	
Eastern Tropical Pacific Corals Monitor Low Latitude Climate of the Past 400 Years	165
<i>Robert B. Dunbar, Gerard M. Wellington, Mitchell W. Colgan, and Peter W. Glynn</i>	
Inter-Regional Correlation in Tree-Growth Variations in the Western United States, 1513-1964, at ENSO, Sunspot, and Longer Frequency Bands	179
<i>David M. Meko</i>	
Geochemical Evidence for Enhanced Upwelling and Organic Productivity During the Late Quaternary on the Continental Margin of Northern California	187
<i>Walter E. Dean, James V. Gardner, and Roger Y. Anderson</i>	
The Younger Dryas and Millennial-Scale Oceanographic Variability in the Sulu Sea, Tropical Western Pacific	205
<i>Braddock K. Linsley</i>	
High- and Low-Latitude Climate Interactions: Evidence for Enhanced Aridity of Asian Monsoon Dust Source Areas After 2.4 MYR from ODP Leg 117 Magnetic Susceptibility Data	217
<i>Peter deMenocal and Jan Bloemendal</i>	
Stable Isotopes in Paleosols and Origins of the Asian Monsoon	229
<i>Jay Quade and Thure E. Cerling</i>	

Authors of Papers

Seventh Annual Pacific Climate Workshop
Asilomar, California
April 10-13, 1990

Edward Aguado
Department of Geography
San Diego State University
San Diego, CA 92110

David G. Ainley
Point Reyes Bird Observatory
4990 Shoreline Highway
Stinson Beach, CA 94970

Jordan Alpert
Scripps Institution of Oceanography
University of California, San Diego
La Jolla, CA 92093-0224

Roger Y. Anderson
The University of New Mexico
Department of Geology
Albuquerque, NM 87131

Julio L. Betancourt
U.S. Geological Survey
1675 West Anklam Road
Tucson, AZ 85745

Jan Bloemendal
Graduate School of Oceanography
University of Rhode Island
Narragansett, RI 02882

Daniel R. Cayan
Climate Research Division
Scripps Institution of Oceanography
University of California, San Diego
La Jolla, CA 92093-0224

Thure E. Cerling
Department of Geology and Geophysics
University of Utah
Salt Lake City, UT 84112

Shyh-Chin Chen
Scripps Institution of Oceanography
University of California, San Diego
La Jolla, CA 92093-0224

Mitchell W. Colgan
Department of Geology
College of Charleston
Charleston, SC 29424

Walter E. Dean
U.S. Geological Survey
MS 939 Federal Center
Denver, CO 80225

Peter deMenocal
Lamont-Doherty Geological Observatory
of Columbia University
Palisades, NY 10964

Robert E. Dickinson
Interdisciplinary Climate Systems
National Center for Atmospheric Research
Post Office Box 3000
Boulder, CO 80307-3000

Robert B. Dunbar
Department of Geology and Geophysics
Rice University
Houston, TX 77251

Curtis C. Ebbesmeyer
Evans-Hamilton, Inc.
731 North Northlake Way
Seattle, WA 98103

James V. Gardner
U.S. Geological Survey
345 Middlefield Road
Menlo Park, CA 94025

Gary A. Glatzmaier
Scripps Institution of Oceanography
University of California, San Diego
La Jolla, CA 92093-0224

Peter W. Glynn
RSMAS
University of Miami
Miami, FL 33149

James D. Goodridge
Consulting Engineer
31 Rondo Court
Chico, CA 95928

Stanley L. Grotch
Atmospheric and Geophysical Sciences Division
Lawrence Livermore National Laboratory
Post Office Box 808
Livermore, CA 94550

Gerald Holdsworth
National Hydrology Research Institute
Saskatoon, Saskatchewan, Canada S7N 3H5

Chih-Yue Kao
Scripps Institution of Oceanography
University of California, San Diego
La Jolla, CA 92093-0224

Patrick J. Kennedy
Interdisciplinary Climate Systems
National Center for Atmospheric Research
Post Office Box 3000
Boulder, CO 80307-3000

George A. King
NSI Technology Services Corporation
U.S. Environmental Protection Agency
Environmental Research Laboratory
200 Southwest 35th Street
Corvallis, OR 97333

Greg Koerper
Oregon State University
U.S. Environmental Protection Agency
Environmental Research Laboratory
200 Southwest 35th Street
Corvallis, OR 97333

David Langley
Scripps Institution of Oceanography
University of California, San Diego
La Jolla, CA 92093-0224

Braddock K. Linsley
Department of Geology
University of New Mexico
Albuquerque, NM 87131

Douglas R. McLain
National Oceanic and Atmospheric Administration
Ocean Applications Group
NPS, FNOC, Building 4
Monterey, CA 93943-5005

David M. Meko
Laboratory of Tree-Ring Research
The University of Arizona
Tucson, AZ 85721

Kingtse C. Mo
National Meteorological Center
National Oceanic and Atmospheric Administration
Washington, DC 20233

Ronald P. Neilson
Oregon State University
U.S. Environmental Protection Agency
Environmental Research Laboratory
200 Southwest 35th Street
Corvallis, OR 97333

Frederic H. Nichols
U.S. Geological Survey
345 Middlefield Road
Menlo Park, CA 94025

Richard H. Parrish
National Marine Fisheries Service
Post Office Box 831
Monterey, CA 93942

Jay Quade
Department of Geology and Geophysics
University of Utah
Salt Lake City, UT 84112

Kelly T. Redmond
Western Regional Climate Center
Desert Research Institute
Post Office Box 60220
Reno, NV 89506-0220

Larry G. Riddle
Climate Research Division
Scripps Institution of Oceanography
University of California, San Diego
La Jolla, CA 92093-0224

John O. Roads
Scripps Institution of Oceanography
University of California, San Diego
La Jolla, CA 92093-0224

Arndt Schimmelmann
Scripps Institution of Oceanography
University of California, San Diego
La Jolla, CA 92093-0215

William J. Sydeman
Point Reyes Bird Observatory
4990 Shoreline Highway
Stinson Beach, CA 94970

Mia J. Tegner
Scripps Institution of Oceanography
University of California, San Diego
La Jolla, CA 92093-0215

Lonnie G. Thompson
Byrd Polar Research Center
The Ohio State University
Columbus, OH 43210-1308

John E. Wade
AeroVironment Inc.
Northwest Office
183 West Main
Monmouth, OR 97361

Daniel M. Ware
Canada Dept. of Fisheries and Oceans
Pacific Biological Station
Nanaimo, British Columbia, Canada V9R 5K6

Gerard M. Wellington
Department of Biology
University of Houston
Houston, TX 77204

Introduction

Julio L. Betancourt

In 1984, a workshop was held on “Climatic variability of the eastern North Pacific and western North America”. From it has emerged an annual series of workshops held each spring at the Asilomar Conference Center, Monterey Peninsula, California (Mooers and others 1986). These annual gatherings have come to be called PACLIM (Pacific Climate) Workshops, reflecting broad interests in the climatologies associated with the Pacific Ocean. Participants in the seven workshops that have convened since 1984 have included atmospheric scientists, hydrologists, geologists, glaciologists, oceanographers, limnologists, and both marine and terrestrial biologists. A collective goal of PACLIM is to connect these various interests with common targets. One such target is the climate system associated with El Niño-Southern Oscillation (ENSO) and its physical and biological manifestations. Another is the behavior of this system on the scale of decades, centuries and millennia, as recorded in high-resolution proxy data (*i.e.*, annual ice layers, corals, sediment varves and tree rings). Multidisciplinary collaborations fostered by previous PACLIM workshops are illustrated in Peterson (1989) and Betancourt and MacKay (1990).

PACLIM Workshops have been sponsored largely by the U.S. Geological Survey in cooperation with other federal and state agencies, as well as private institutions. PACLIM 90, which led to publication of this proceedings, was sponsored by USGS, NOAA-National Geophysical Data Center, NOAA-Climate Analysis Center, the National Park Service-Global Change Program, the American Geophysical Union, Southern California Edison, and the California Department of Water Resources.

On behalf of the sponsors, we extend our thanks to those individuals responsible for organizing and planning PACLIM 90. Ana MacKay, National Research Program, Water Resources Division, USGS, wore many hats and single-handedly made PACLIM 90 a success. Paul Weiss, comptroller at the American Geophysical Union, was incredibly efficient in managing funds from private sources. AGU’s role is critical to PACLIM, both in disseminating information about the workshop and in banking funds. Merilee Bennett, USGS, made transferring funds across federal agencies look easy.

PACLIM 90 Theme: Comparison of Observations vs. Simulations of GCMs

Less than two years into LBJ’s presidency, in the midst of the Da Nang offensive, the President’s Science Advisory Council prophesied that general circulation models would be able to predict the climatic effects of increasing atmospheric CO₂ concentrations (Revelle *et al.* 1965). For those on the sidelines, this surely meant we would be able to anticipate more or less flow in the overcommitted Colorado River or the relative success of our harvests in the Nation’s Breadbasket, the Midwest.

In the quarter-century since then, GCMs have evolved in tandem with our computer technology and alongside an explosion of knowledge about how the Earth’s climate system works. Despite our growing sophistication, if we are now sure of anything, it is that significant uncertainties exist. To wit, the greenhouse effect apparently has warmed the

Earth no more than the 0.5 ± 0.2 K observed in the instrumental record (Jones and others 1986) and far less than the 2.5 to 4.5 K predicted from doubled-CO₂ GCM experiments. Members of the 1965 President's Science Advisory Council would have been miffed to find that in 1991, the North American continent would be but a small region in a global GCM, inappropriately scaled to capture what is a complex mosaic of hydroclimatic, ecological, and economic diversity. They would also be surprised at how difficult it has been to statistically measure goodness-of-fit between GCM simulations of present climate and actual observations thereof (Livezey 1985; Katz 1988; Moss 1992). Moreover, despite the considerable efforts of a proficient and well-funded climate modeling community, GCM characterizations are not yet capable of driving policy that anticipates the future of our energy, food, and water resources.

In setting the theme for the Seventh Annual Pacific Climate (PACLIM) Workshop, "Comparison of observations vs. simulations of GCMs", it was not our intent to dwell on inadequacies of the models. Since its inception in 1984, PACLIM has favored empirical data sets, and the focus seldom has been on numerical models, that is until Hugh Elsaesser's (1989) keynote address at PACLIM 89. Participants took to heart Elsaesser's comments about the turf factor, that the CO₂ problem had become the sole province of radiation transport specialists with little input from other relevant disciplines, such as those represented at PACLIM. If the PACLIM group has an inclination, it is that there is no substitute for well-resolved time-series observations in geophysical research, and that such time series are essential for constructing and verifying conceptual and numerical models, be they geophysical or biological (Cayan *et al.* 1989)

The response to Elsaesser, then, was a conscious effort to recruit participation in PACLIM by the climate modeling community. A PACLIM workshop is a somewhat informal affair held in full view of Monterey Bay, where a glaciologist can walk the beach with a phytoplankton ecologist. If PACLIM is anything, it is an opportunity to talk across disciplines. So in part, PACLIM 90 was designed as a chance for the empiricist to get to know the modeler and vice-versa.

Stanley Grotch's keynote address, which opens the Proceedings, is related to a recently published critique of the use of GCMs to predict regional climate change (Grotch and MacCracken 1991). For seven GCMs, Grotch compared model gridpoint reconstructions with historical data for current surface air temperature and precipitation. The good news is that the models and historical data closely agree on seasonally-averaged and area-weighted global average temperatures. The bad news is illustrated by discordance in the latitudinal distribution of seasonal temperature and precipitation. For winter temperatures, simulations and observations diverge the most at high latitudes, and for winter precipitation the disagreement is 100 percent at some latitudes. Other studies have shown that even greater discrepancies, in this case between the various models, occur in longitudinal profiles of seasonal precipitation, specifically in the subtropics (Neilson *et al.* 1990). The comparison among the different models points up the advantage that several competing models have over a single "definitive" supermodel, a controversy that raged in budget meetings for fiscal year 1992 (Kerr 1990). The disparity between the various models probably stems from how well (or poorly) the models simulate present climate. Further improvement of sensitivity estimates will be bounded by the theoretical limits, both in time and space, of climate predictability (Grotch and MacCracken 1991).

No doubt, climate modeling stands to benefit from the kinds of studies that make up these proceedings: better integration of surface hydrology in the form of submodels (Dickinson and Kennedy; Roads and others; Neilson and others); validation from operational weather forecasting using GCMs (Mo); synoptic studies and in-depth analyses of the instrumental record (Wade and Redmond; Redmond; Riddle and others; Cayan; Goodridge); development of proxy records for times and places for which we have no instrumental record (Anderson; Thompson; Holdsworth; Schimmelmann and Tegner; Dunbar and others; Meko; Dean and others); and an understanding of how global climates might drive local and regional ecosystems (Ware; Ainley and others). Four papers in the volume (Ebbesmeyer and others; Linsley; de Menocal and Bloemendal; Quade and Cerling) remind us that, at various times (the late 1970s, the Younger Dryas, the onset of the Pleistocene 2.4 Myr, and 7.3 Myr, when conditions for the Asian Monsoon apparently began), the Earth's climate shifts mode, producing step-like changes in both the geologic and instrumental record. The ability of GCM models to reproduce such abrupt and directional changes offers a compelling opportunity to validate such models.

References

- Betancourt, J.L., and A.M. MacKay, eds., 1990. *Proceedings of the Sixth Annual Pacific Climate (PACCLIM) Workshop, March 5-8, 1989*. California Department of Water Resources, Interagency Ecological Studies Program Technical Report 23.
- Cayan, D.R., J.V. Gardner, J.M. Landwehr, J. Namias, and D.H. Peterson, 1989. in D.H. Peterson, ed., "Aspects of Climatic Variability in the Pacific and the western Americas". *American Geophysical Union Monograph 55*, pp. xiii-xvi.
- Elsaesser, H.W. 1990. "Atmospheric carbon dioxide and the climatic record". In J.L. Betancourt and A.M. MacKay, eds., *Proceedings of the Sixth Annual Pacific Climate (PACCLIM) Workshop, March 5-8, 1989*. California Department of Water Resources, Interagency Ecological Studies Program Technical Report 23, pp. 5-18.
- Grotch, S.L., and M.C. MacCracken, 1991. "The use of general circulation models to predict regional climatic change". *Journal of Climate* 4:286-303.
- Jones, P.D., S.C.B. Raper, R.S. Bradley, H.F. Diaz, P.M. Kelly, and T.M.L. Wigley, 1986. "Northern Hemisphere surface air temperature variations, 1851-1984". *Journal of Climate and Applied Meteorology* 25:161-179.
- Katz, R.W. 1988. "Statistical procedures for making inferences about changes in climatic variability". *Journal of Climate* 1:1057-1068.
- Kerr, R.A. 1990. "Climatologists debate how to model the world". *Science* 250:1082-1083.
- Mooers, C.N.K., D.H. Peterson, and D.R. Cayan, 1986. "The Pacific Climate Workshops": *EOS* 67:1404-1405.
- Livezey, R.E. 1985. "Statistical analysis of general circulation model climate simulations: Sensitivity and prediction experiments". *Journal of Atmospheric Sciences* 42:1139-1149.

- Moss, M.E. 1992. "Bayesian relative information measure: A tool for analyzing the outputs of general circulation models". *Journal of Geophysical Research* (in press).
- Neilson, R.P., G.A. King, J. Lenihan, and R.L. DeVelice, 1990. "The annual course of precipitation over much of the United States: Observed versus GCM simulation". In J.L. Betancourt. and A.M. MacKay, eds., *Proceedings of the Sixth Annual Pacific Climate (PACCLIM) Workshop, March 5-8, 1989*. California Department of Water Resources, Interagency Ecological Studies Program Technical Report 23, pp. 19-26.
- Peterson, D.H., ed., "Aspects of Climatic Variability in the Pacific and the western Americas". *American Geophysical Union Monograph 55*
- Revelle, R., W. Broecker, H. Craig, C.D. Keeling, and J. Smagorinsky, 1965. Appendix Y4, "Atmospheric carbon dioxide". In *Restoring the quality of our Environment, Report of the Environmental Pollution Panel*, President's Science Advisory Committee, Washington, DC.

GCM-Data Intercomparison: The Good News and The Bad

Stanley L. Grotch

ABSTRACT: General circulation models (*GCMs*) are probably the most sophisticated theoretical tools we have to simulate possible climatic effects of increasing CO₂ and other greenhouse gases. Because of tremendous social and political pressures now being raised on the issue of greenhouse warming, these models are being called upon to make predictions of possible climate change on a broad range of spatial scales. Of particular importance for regional assessments are predictions at subcontinental spatial scales. As will be illustrated here using a variety of examples, although the models do simulate “reality” very well on the “grand” scale (e.g., global, hemispheric, zonal), substantial differences are more apparent as the scale is reduced to areas particularly relevant to regional planners. It is particularly important that workers more clearly recognize the potential dangers in relying too heavily on simple summary statistics such as averages estimated over large regional scales. Many shortcomings are apparent in the model simulations of the present climate, indicating that further model improvements are needed to achieve reliable regional and seasonal projections of the future climatic conditions.

Introduction

General circulation models (*GCMs*) are being actively used to assess possible climate change due to increasing greenhouse gas concentrations. Because such simulations provide detailed climatic predictions at a wide range of scales, they are of particular interest to those making regional assessments of climatic change. It is especially important that workers using the results of such simulations be aware of some of the limitations of these results. In this study, some of the positive results from these model simulations will be shown (the *good news*) and some of the deficiencies (the *bad news*) will also be highlighted. Following an introductory section describing the nature of GCM climate simulations, the issue of the spatial scales of such simulations is examined. A comparison of the results of seven GCM simulations of the current climate and the predictions of these models for the changes due to a doubling of CO₂ is discussed. In these intercomparisons, the spatial scale over which results are compared varies from global to zonal (longitudinally averaged at a given latitude) to individual slices through the data along specified latitudes or longitudes. Finally, the dangers and pitfalls of relying on simple averages are highlighted.

Simplified Model Descriptions and CO₂ Doubling Experiments

General circulation model is the term given to numerical models that simulate the global climate by calculating the hour-by-hour evolution of the atmosphere in all three spatial dimensions based on the conservation laws for atmospheric mass: momentum, thermal energy, and water vapor. GCMs also typically include representations of surface hydrology, sea ice, cloudiness, convection, atmospheric radiation and other pertinent processes

(Washington and Parkinson 1986). Although coupled atmospheric/ocean studies have been performed for some time (Manabe and Bryan 1969), research studies are only now coupling atmospheric and more realistic ocean GCMs (*e.g.*, Manabe and Stouffer 1986), which give full treatment to ocean momentum, salinity, and thermal energy, thereby allowing study of the time rate of climatic change under different greenhouse forcings.

In CO₂ doubling experiments, two separate integrations are performed:

- A so-called “control climate”, in which conditions are assumed to simulate the present climate with atmospheric concentrations of CO₂ set at approximately current levels throughout the integration (termed the “control” or “1 × CO₂ run”).
- A second calculation, in which the atmospheric CO₂ concentration is instantly doubled and the model is run until an equilibrium state is reached (termed the “perturbed” or “2 × CO₂ run”).

The desired perturbation of any climatic variable X, (ΔX), due to a doubling of CO₂ is estimated at all gridpoints as: $\Delta X = X(2 \times CO_2) - X(1 \times CO_2)$. Typically, the Xs are the monthly, seasonally, or annually averaged gridpoint values of a particular variable (*e.g.*, surface air temperature, precipitation) for the last 3 to 10 years of each simulation.

Such simulations are termed “equilibrium” runs in distinction to “transient” integrations in which the CO₂ concentration is generally increased monotonically with time in the perturbed run. Because many more equilibrium experiments have been performed than transient runs, the intercomparisons here will analyze only equilibrium model results. This study focuses on seven equilibrium simulations that are referred to using mnemonics for the modeling groups:

CCC (Boer 1989)
CCM (Washington and Meehl 1984)
GFDL (Manabe and Wetherald 1987)
GFDL-R30 (Manabe and Wetherald 1989)
GISS (Hansen *et al.* 1984)
OSU (Schlesinger and Zhao 1989)
UKMO (Wilson and Mitchell 1987)

Further details on intercomparisons of four of these simulations may also be found in a Department of Energy report (Grotch 1988), in a forthcoming paper (Grotch and MacCracken 1991), and in the forthcoming UN/WMO report (IPCC 1990).

The models considered here were chosen because it was possible to obtain gridpoint data for comparable perturbation simulations. These models have “realistic” geography and topography, treat the seasonal cycle, and interactively represent sea ice, ground hydrology, and cloud amount and distribution. Each modeling group has made what are thought to be valid, but different, approximations and adjustments in their attempts to include the most appropriate mechanisms for CO₂ studies (*e.g.*, see Schlesinger and Mitchell 1987). Three of the models (CCC, GISS, UKMO) include the full diurnal cycle of solar radiation, and four assume diurnally averaged solar radiation (*i.e.*, a sunset at a constant zenith angle appropriate to the time of year). For purposes of this intercomparison, however, these

models are each designed to be particularly suitable for CO₂ studies and are sufficiently similar in their major characteristics for their results to be compared.

This intercomparison study is not intended to be a *beauty contest* between models, resulting in the choice of any *best* model. Such an analysis would require a much more complete comparison on many scales (both spatial and temporal), a task particularly troublesome because there are no well established case studies against which to adequately validate the models. Therefore, in many of the graphical intercomparisons, the specific model yielding a given result is not identified. Rather, the intent is to illustrate the range of results currently available and to highlight certain issues of which the non-modeler may be unaware.

The Problem of Spatial Scale

Because GCM climate simulations are very expensive, requiring substantial amounts of time on large supercomputers, there is an obvious practical incentive to reduce these costs by using as coarse a spatial grid as possible. Because of numerical stability considerations, computer time increases approximately with the inverse cube of the horizontal resolution. Until recently, the highest resolution simulations used grid spacings of about 4° in latitude by 5° in longitude (several hundred kilometers), resulting in a global grid of about 3,000 grid points (Figure 1). This resolution would appear adequate to capture the larger spatial features of climate.

However, because of concerns regarding greenhouse warming, there is considerable pressure to examine model predictions at much smaller spatial scales. When the 4°×5° grid is magnified, focusing on an area of the scale of the continental United States (as in Figure 2) or further, covering only the western states (as in Figure 3), it becomes apparent that difficulties are likely to arise using so few gridpoints for regional scale predictions. Most modelers would agree that it would be unwise to use any single (or few) gridpoints as surrogates for small scale regional climates.

Intercomparison of GCM Simulations and Historical Climate Data

In this section, seven GCM predictions of surface air temperature and precipitation for the control (or model reconstructions of current) climate are compared with two historical data sets for temperature (Oort 1983; Schutz-Gates 1971, 1972) and for precipitation (Jaeger 1976; Schutz-Gates 1971, 1972) over different spatial scales.

Table 1 presents both the December/January/February (*DJF*) and June/July/August (*JJA*) seasonally averaged and area-weighted global average temperatures. The agreement of the global averages between model simulations and the two observational data sets is generally good, and the seasonal cycle appears well simulated. For both seasons, the median of the seven simulations is within 1°C of Oort's value. If the calculated surface temperatures at individual gridpoint are cross correlated with the historical data, near-perfect correlations are obtained: 0.96-0.98. This is the *good news*. However, this good large-scale agreement provides no assurance that agreement on smaller scales will be as accurate.

Figure 1
OUTLINES OF 4° LATITUDE BY 5° LONGITUDE GRID OVER THE GLOBE

This grid of more than 3000 points appears adequate in capturing the larger scale climatic features on the global scale.

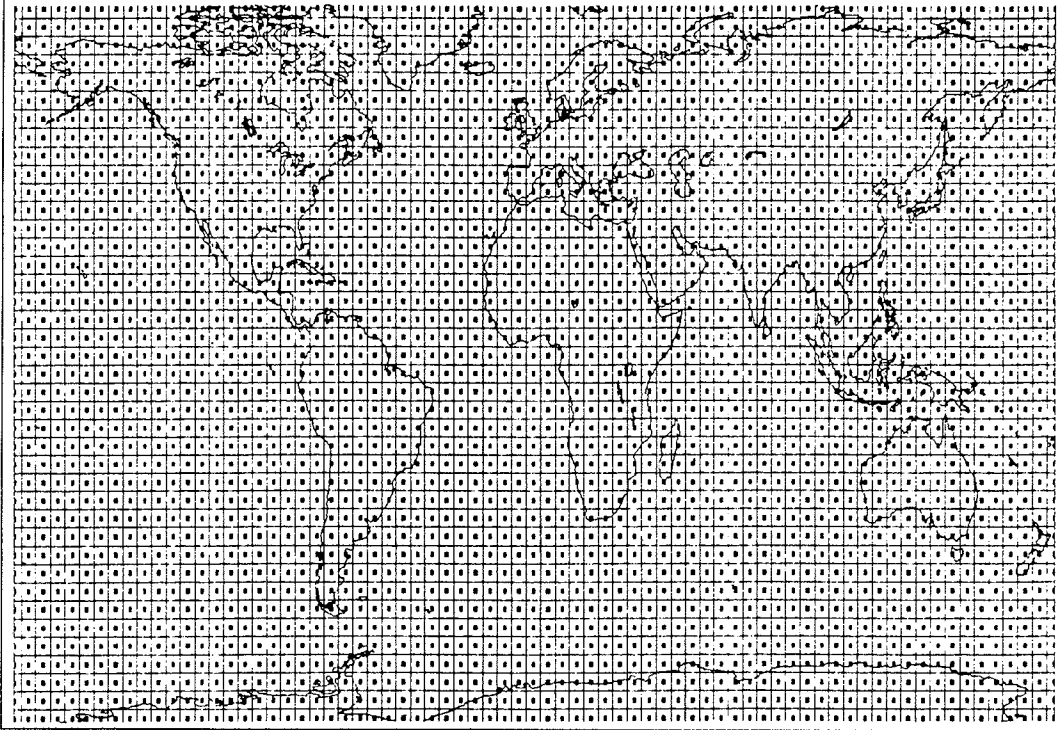


Figure 2
OUTLINES OF A 4° LATITUDE BY 5° LONGITUDE GRID
OVER THE CONTINENTAL UNITED STATES

For this area there are less than 50 points over the land areas.
The central darkened rectangle is a 1°x1° area at the center of the 4°x5° grid box.

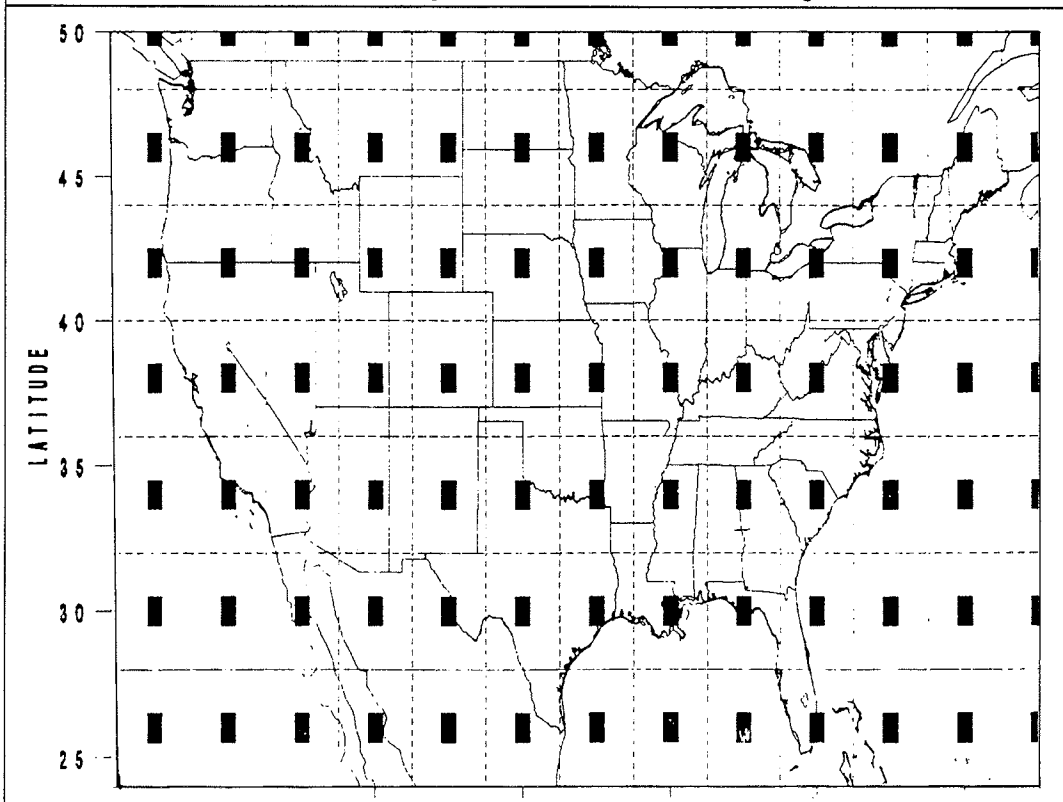


Figure 3
OUTLINES OF A 4° LATITUDE BY 5° LONGITUDE GRID
OVER THE WESTERN UNITED STATES

For the three western states, the grid is too coarse for any detailed predictions on these scales.
 The central darkened rectangle is a 1°×1° area at the center of the 4° × 5° grid box.

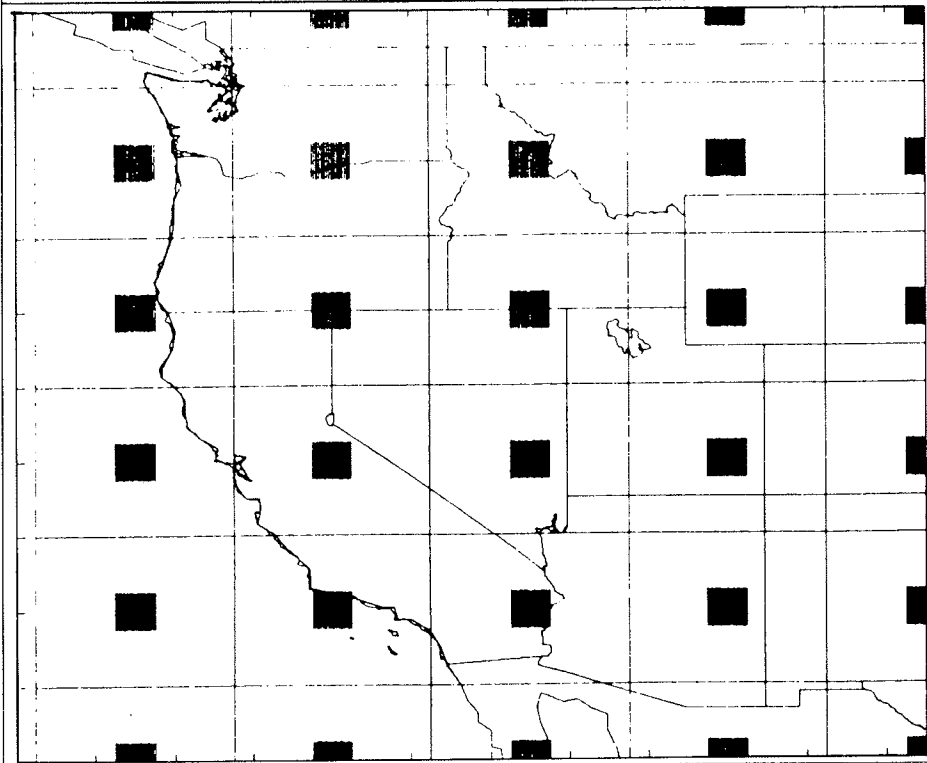


Table 1
GLOBALLY AVERAGED DJF/JJA
SEASONAL TEMPERATURES
 (°C)

Model	Dec/Jan/Feb	Jun/Jul/Aug
CCM	11.5	16.5
GFDL	12.8	17.2
GISS	12.7	15.8
OSU	14.2	17.3
UKMO	11.4	15.9
CCC	11.6	15.6
GFDL(R30)	8.1	12.8
Historical Data		
Oort	12.4	15.9
Schutz-Gates	12.2	16.1

Because latitudinal variation is often the major dominant feature of many meteorological fields, it is natural to examine model/data predictions on this basis. The most common method for intercomparison is to examine the zonally averaged values of a given variable. The zonal average is the arithmetic average of all longitudinal gridpoints at a given latitude (or latitude band). Figure 4 shows the zonally averaged DJF and JJA estimates for surface air temperature from the seven GCM simulations and compares them with the historical compilations of Oort and of Schutz and Gates. Although the general shapes of these distributions are similar, there are large differences at specific latitudes, even in these zonally averaged values. This provides a rationale for presenting model-predicted climate change as departures from the control run rather than as departures from the present climate.

For regional assessments, however, even finer resolution is needed, and in Figure 5 the latitudinal distribution of DJF and JJA surface air temperature along a specific meridian (80°W longitude) is shown. This cut, passing through the eastern United States, displays substantial differences in these simulations of the present climate. Analogous results are seen for the simulated precipitation fields generated by these GCMs. Figure 6 displays the zonal distributions for seasonally averaged control DJF precipitation (mm/day). These distributions are similar in general shape, but at many latitudes large (>100%) discrepancies result. Figure 7 shows a cut through the DJF precipitation across the United States at a latitude of 38°N in which the three highest resolution model simulations are contrasted with Jaeger's observational data. Again, although the shapes are generally similar, large percentage discrepancies arise throughout much of the United States, making such predictions quantitatively suspect on these smaller scales.

Figure 4
LATTITUDINAL DISTRIBUTIONS OF
ZONALLY AVERAGED DJF AND JJA
SURFACE AIR TEMPERATURE
SIMULATED BY 7 GCMs
COMPARED WITH THE
OORT AND SCHUTZ-GATES
OBSERVATIONAL DATA SETS

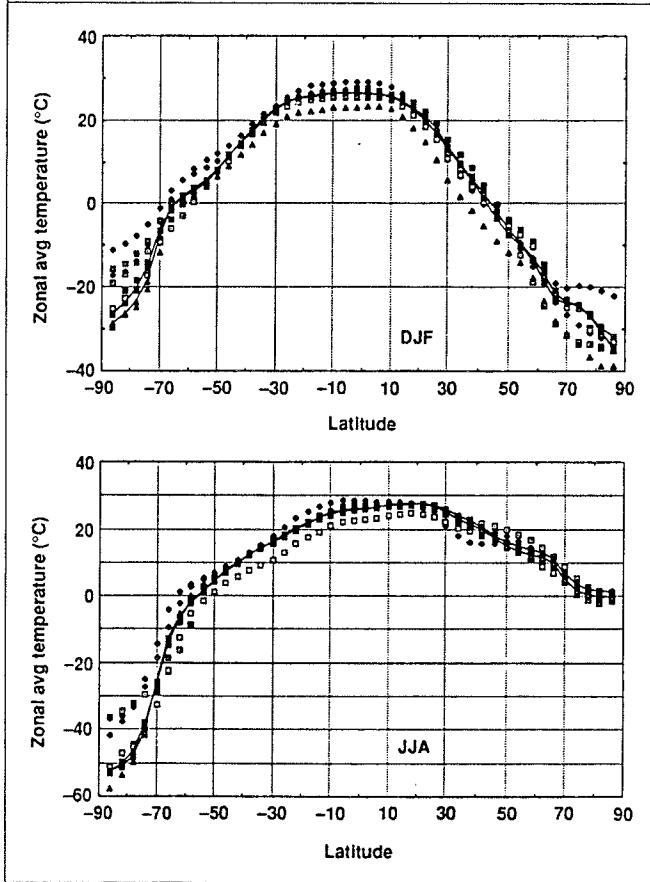
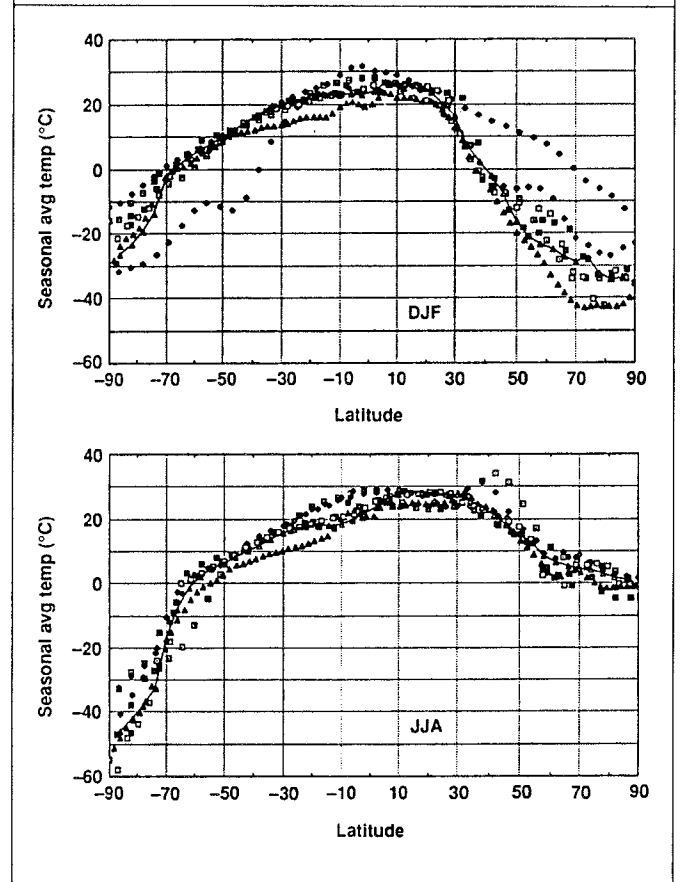


Figure 5
LATTITUDINAL DISTRIBUTIONS OF
DJF AND JJA SURFACE AIR TEMPERATURE
PREDICTED BY 7 GCMs CONTRASTED WITH OORT'S
HISTORICAL DATA ALONG THE
MERIDIAN 80° W LONGITUDE
Oort's data are represented by the solid line.



Dangers of Relying on Averages

Because the average is the single “best” number characterizing a distribution, both the climate community and particularly the general public have become beguiled by its constant application: *e.g.*, “the global average temperature is expected to rise by near $3 \pm 1.5^\circ\text{C}$ due to a doubling of CO_2 ” (National Research Council, 1982). While the average is clearly important, its indiscriminate use can be quite misleading.

It is obvious, but often overlooked, that there are an infinite number of distributions that will yield the same average. For two distributions to be truly spatially identical, it is necessary that their averages agree, but it is by no means *sufficient*. Thus, the agreement of two distributions, on average, is no guarantee whatever that the distributions are spatially the same or, in fact, necessarily even close. In fact, even if *all* of the higher moments of two distributions were to agree perfectly, they still could be *quite different* spatially.

As a trivial illustration of this fact, take all the gridpoint values predicted by a given model and mix them thoroughly, then reassign them spatially in an arbitrary manner. When

Figure 6
 ZONALLY AVERAGED DJF PRECIPITATION FOR THE CURRENT CLIMATE
 AS SIMULATED BY 7 GCMs

Although the general behavior of these curves is similar, there are large percentage differences at many latitudes.

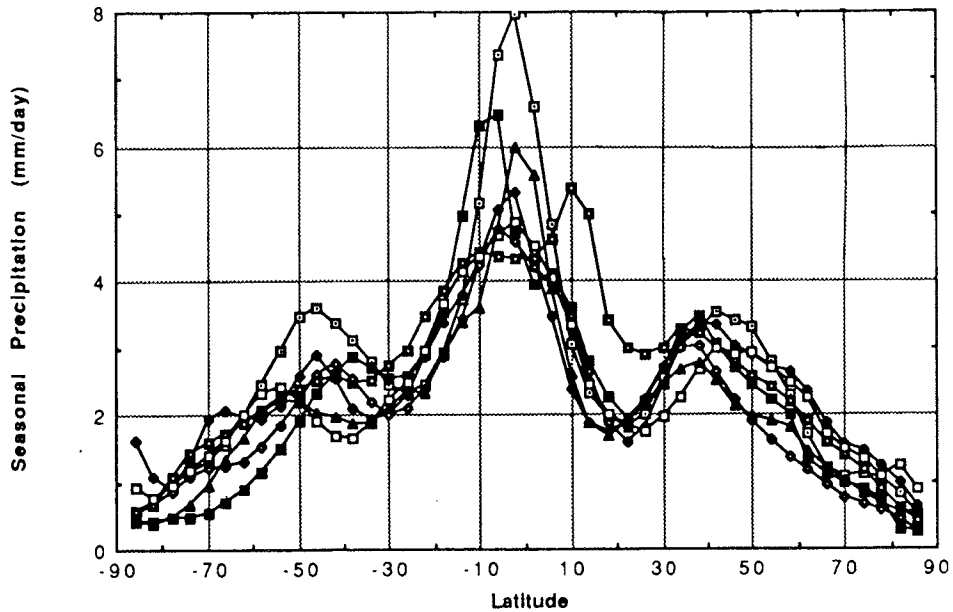
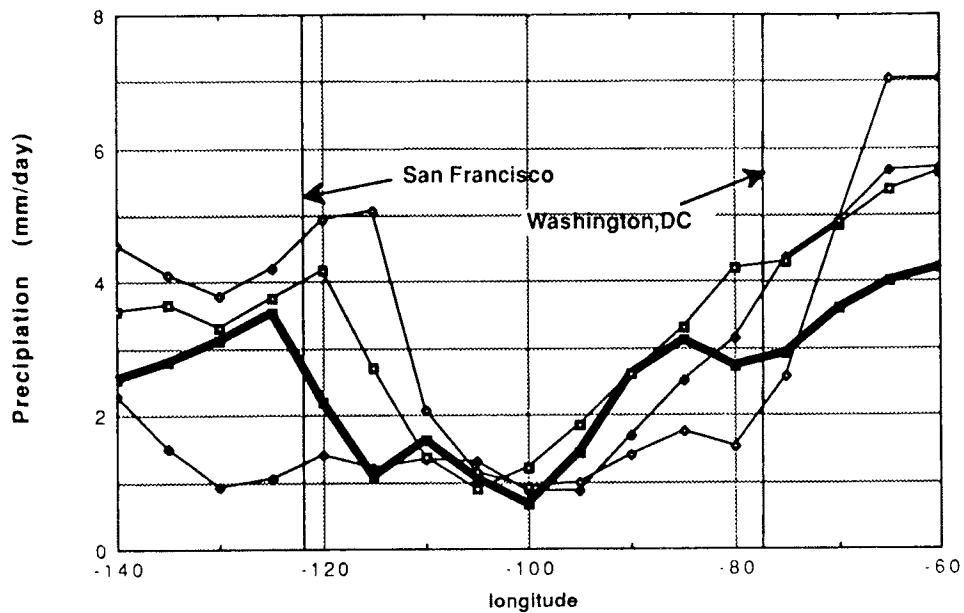


Figure 7
 LONGITUDINAL DISTRIBUTION OF SIMULATED DJF PRECIPITATION ($1 \times \text{CO}_2$) AT A
 LATITUDE OF 38°N ACROSS THE UNITED STATES

Data from three of the higher resolution models are contrasted with Jaeger's historical data (solid heavy line).



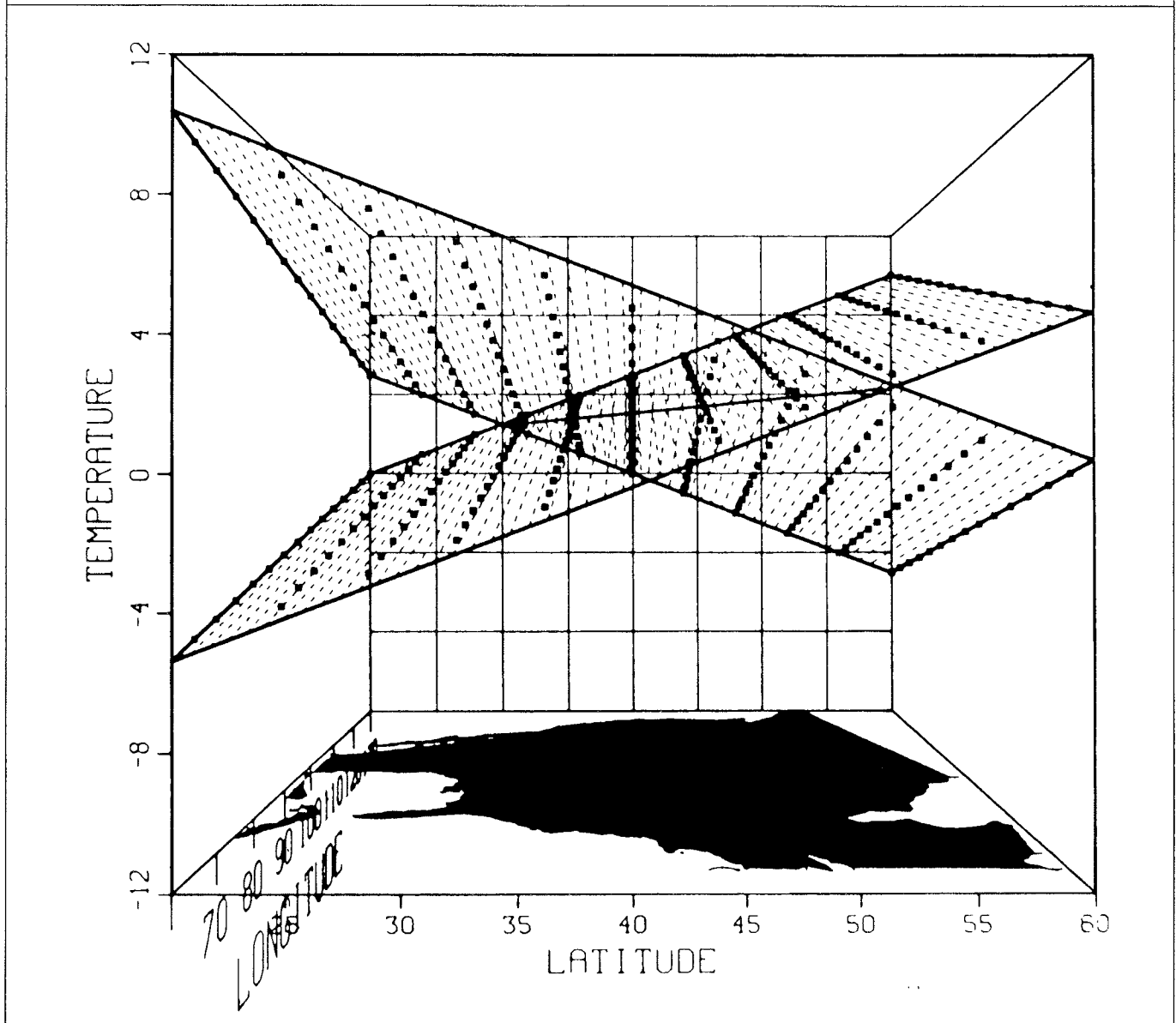
compared with the original distribution, the permuted one will produce identical averages and standard deviations; in fact, all percentiles will be identical, yet spatially the two could be entirely different. Two other examples — one hypothetical, one real — illustrate some of the pitfalls that await the unwary if simple averages are relied upon as primary measures of agreement rather than more detailed spatial distributions.

Consider first this *hypothetical* example. For a region centered over North America, two GCMs predict identical average surface temperature increases due to a doubling of CO₂: 2.50°C. Given this perfect agreement, how spatially similar are the predicted changes within this area? Where are the largest and the smallest predicted changes located? What is the average absolute or rms difference between the two predicted ΔT values over the region? For regional assessments, what are the ΔT values predicted, for example, over the mid-Atlantic states?

Other statistical characteristics of the two distributions should also be compared. In this example, assume that not only the averages of the two distributions are identical, but so are their standard deviations and, in fact, all of their higher moments. What can we now infer about the spatial distributions of these predicted values? Unfortunately, still very

Figure 8
SUPERPOSED SPATIAL DISTRIBUTIONS OF CHANGE IN TEMPERATURE OVER NORTH AMERICA
DUE TO A DOUBLING OF CO₂, AS HYPOTHETICALLY PREDICTED BY TWO MODELS

View looking west from off the Atlantic coast.



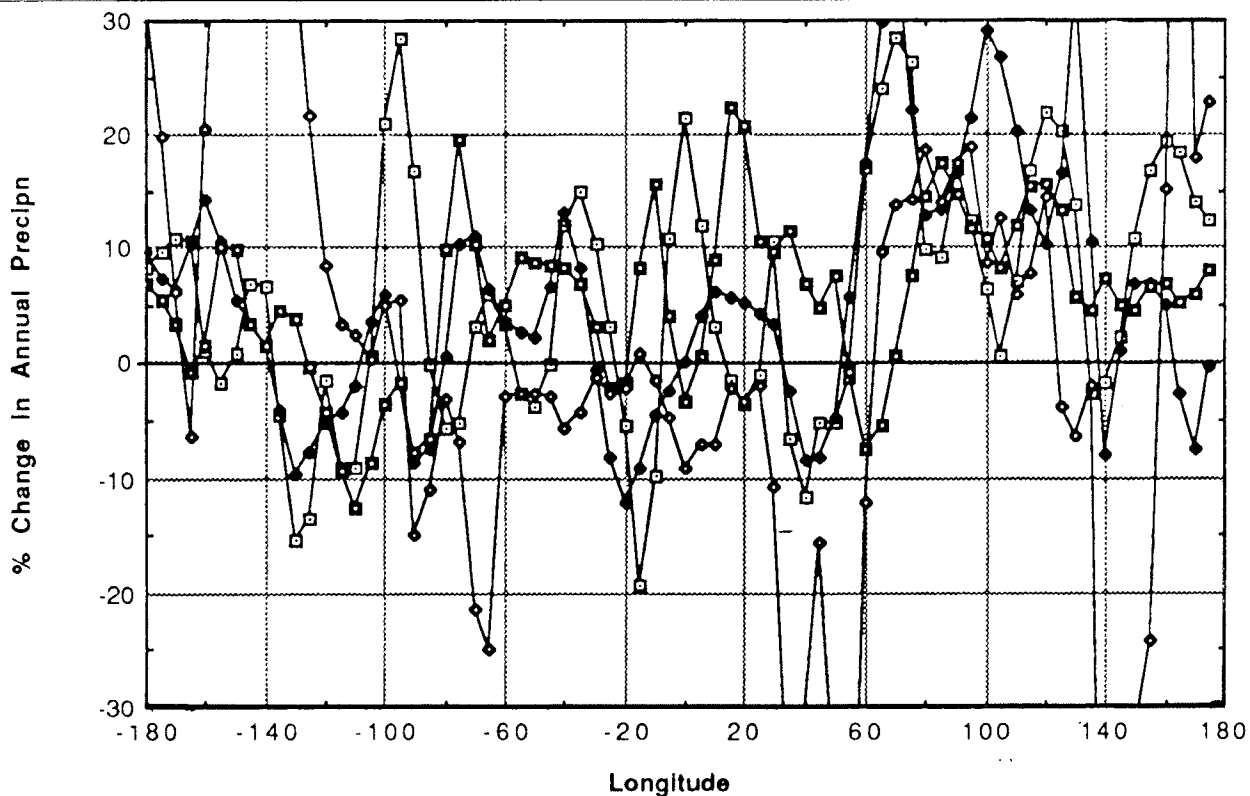
little. The two distributions could, of course, be spatially identical but, on the other hand, they could still be quite different, as shown in Figure 8 in which the two spatial distributions describing these predicted values are seen in three dimensions to both be planes. Although the two planes result in identical average ΔT values over the region, their spatial orientations are totally different.

A more appropriate quantitative measure of model agreement is a direct point-by-point comparison (only feasible when the data are on, or have been interpolated to the same grid). For the data in this example, temperature differences as large as the combined range of the two initial distributions occur. Although the two models predict identical averages over North America, there are temperature differences between the predictions that are 15°C . As is the case here, even when *all* statistical moments of two distributions agree identically, they can still be *quite different* spatially. In fact, if we were to permute all of the values at each latitude, the two predicted zonal distributions would also be identical.

As a *real* example, consider the zonally averaged predictions of these seven GCMs for the percentage change in annual precipitation after a doubling of CO_2 . Four of these models, at a latitude of 34°N , predict virtually identical zonally averaged percentage changes: 5.5%, 5.5%, 5.7%, 5.7%. The actual spatial distributions longitudinally of these predicted changes along latitude 34°N are shown in Figure 9. Although all four models predict virtually the same zonally averaged annual percentage changes in precipitation, the patterns are, in most cases, virtually uncorrelated spatially along this latitude. Once again, the fact that they are equal on average means little in describing more regional behavior.

Figure 9
LONGITUDINAL DISTRIBUTIONS OF THE PREDICTED CHANGE IN ANNUAL PRECIPITATION
AFTER A DOUBLING OF CO_2 , AS GIVEN BY 4 GCMs ALONG THE LATITUDE 34°N

These same four models predict virtually identical zonally averaged annual percentage changes in precipitation, yet most are virtually uncorrelated spatially at this latitude.



Conclusions

Due to practical concerns regarding the potential climatic effects of greenhouse gases, there are great pressures to apply the results of GCM simulations to regional assessments. Although such simulations generally agree on the larger scale averages, on smaller regional scales and for seasonal periods, there remain differences among the projected changes in temperature and precipitation for these models that are of the same order as the perturbation. The large regional discrepancies found in simulating present climate reduce our assurance in the ability of GCMs to quantitatively predict regional climate change due to increasing greenhouse gases.

One cause of the different estimates of regional and seasonal sensitivity to a doubled CO₂ concentration is almost certainly related to limitations in the quality of model simulations of the present climate. Improvement of sensitivity estimates will, therefore, require both a sustained effort to improve the climate models and investigations to determine the theoretical limits of the various time and space scales of climate predictability.

Because of the non-uniqueness of averages in describing distributions, workers should be more circumspect in relying on agreement of averages as indicators of smaller-scale agreement.

Acknowledgments

The author is grateful to the six modeling groups (led by George Boer, James Hansen, Syukuro Manabe, John Mitchell, Michael Schlesinger, and Warren Washington) for making the model results available and for their comments on an earlier report elaborating on these results.

The suggestions of my colleagues (Curt Covey, Hugh Ellsaesser, Steve Ghan, Mike MacCracken, Jerry Potter, and Karl Taylor) are especially acknowledged.

This work was performed under the auspices of the Department of Energy Atmospheric and Climate Research Division by the Lawrence Livermore National Laboratory under contract W-7405-ENG-48.

References

- Boer, G. 1989. Canadian Climate Center, Toronto, Canada. Personal communication.
- Grotch, S.L. 1988. *Regional Intercomparisons of General Circulation Model Predictions and Historical Climate Data*. TR041. U.S. Dept. of Energy. DOE/NBB-0084.
- Grotch, S.L., and M. MacCracken. 1991. "The Use of General Circulation Models to Predict Regional Climate Change". *J. of Climate* 4:386-303.
- Hansen, J., A. Lacis, D. Rind, G. Russell, P. Stone, I. Fung, R. Ruedy, and J. Lerner. 1984. "Climate Sensitivity: Analysis of Feedback Mechanisms" in *Climate Processes and Climate Sensitivity*. Ed. J.E. Hansen and T. Takahashi. Maurice Ewing Series, No. 5. American Geophysical Union. Washington, DC. pp. 130-163.

- Intergovernmental Panel on Climate Change (IPCC). 1990. *Scientific Assessment of Climate Change*. World Meteorological Organization and the United Nations Environmental Program.
- Jaeger, L. 1976. "Monatskarten des Niederschlags für die ganze Erde". *Berichte des Deutschen Wetterdienstes*, 139:1-38.
- Manabe, S., and R.J. Stouffer. 1986. "Two Stable Equilibria of a Coupled Ocean-Atmosphere Model". *J. of Climate*, 1:841-866.
- Manabe, S., and R.T. Wetherald. 1989. Personal communication.
- _____. 1987. "Large Scale Changes of Soil Wetness Induced by an Increase in Atmospheric Carbon Dioxide". *J. Atmos. Sciences*, 44:1211-1235.
- _____. 1986. "Reduction in Summer Soil Wetness Induced by an Increase in Atmospheric Carbon Dioxide". *Science*, 232:626-628.
- National Research Council. 1982. *Carbon Dioxide and Climate: A Second Assessment*. Report of the Carbon Dioxide/Climate Review Panel, National Research Council. National Academy Press. Washington, DC.
- Oort, A.H. 1983. *Global Atmospheric Circulation Statistics, 1958-1973*. National Oceanic and Atmospheric Admin. Professional Paper 14. U.S. Govt. Printing Office. Washington, DC.
- Schlesinger, M.E., and J.B. Mitchell. 1985. "Model Projections of the Equilibrium Climatic Response to Increased Carbon Dioxide" in *Projecting the Climatic Effects of Increasing Carbon Dioxide*. Ed. M.C. MacCracken and F.M. Luther. U.S. Dept. of Energy. DOE/ER-0235. Washington, DC. pp. 2-147.
- Schlesinger, M.E., and Z.C. Zhao. 1989. "Seasonal Climatic Changes Induced by Doubled CO₂ as Simulated by the OSU Atmospheric GCM/Mixed-Layer Ocean Model". *J. of Climate*, 2:459-495.
- Schutz, C., and W.L. Gates. 1972. *Global Climatic Data for Surface, 800 mb, 400 mb, July*. Rand Corporation. R-1029-ARPA. Santa Monica, CA.
- _____. 1971. *Global Climatic Data for Surface, 800 mb, 400 mb, January*. Rand Corporation. R-915-ARPA. Santa Monica, CA.
- Washington, W.M., and G.A. Meehl. 1984. "Seasonal Cycle Experiment on the Climate Sensitivity Due to a Doubling of CO₂ with an Atmospheric General Circulation Model Coupled to a Simple Mixed-Layer Ocean Model". *J. of Geophys. Research*, 89:9475-9503.
- Washington, W.M., and C.L. Parkinson. 1986. *An Introduction to Three-Dimensional Climate Modeling*. University Science Books. Mill Valley, CA
- Wilson, C.A., and J.F.W.B. Mitchell. 1987. "A Doubled CO₂ Climate Sensitivity Experiment with a Global Climate Model Including a Simple Ocean". *J. of Geophys. Research*, 92:13315-13343.

Land Surface Hydrology in a General Circulation Model: Global and Regional Fields Needed for Validation

Robert E. Dickinson and Patrick J. Kennedy

Introduction

For the last two decades most General Circulation Models (*GCMs*) have included some kind of surface hydrology submodel. The content of these submodels is becoming increasingly complex and realistic. It is still easy to identify defects in present treatments. Yet, to improve our ability to model the contribution of land hydrology to climate and climate change, we must be concerned not with just the surface hydrology submodel *per se*, but also with how it works in the overall context of the GCM.

Suppose we had a “perfect treatment” of land hydrological processes in a GCM. Incorporated into any present GCM, we would most likely obtain a simulation of the land hydrological cycle that did not appear very realistic in the light of various observational measures we might apply. The purpose of this paper is to discuss what aspects of a GCM, other than the surface parameterization, must work right for a satisfactory simulation of the land hydrological cycle to be achieved. This theme is illustrated with previously unpublished modeling simulations with the National Center for Atmospheric Research (*NCAR*) Community Climate Model (*CCM*).

It is usually difficult to judge model correctness unless the more critical aspects can be judged against independent observations. In the present context, a number of regional and global data sets are just becoming available whose use is essential for model validation. We compare these observed and model fields. The GCM simulates climate through a more-or-less detailed simulation of individual weather processes and other short time-scale atmospheric variability, including the diurnal cycle.

Modeling Framework

The Biosphere Atmosphere Transfer Scheme (*BATS*) (Dickinson 1984; Dickinson *et al.* 1986) has been developed for interfacing a detailed land model with a GCM. That is, it must provide an adequately realistic parameterization of land interactions with climate and transfer information on these interactions between the rest of the GCM and its parameterization. Whereas the physical content of parameterizations is usually given the most attention, the linkages with the rest of the model are at least as crucial for effective applications in climate modeling simulations. Programming questions such as efficiency, flexibility, and documentation are important but are not mentioned further here. Rather, we address the issue of what subset of the rich information generated by a land package should be saved for further analysis for purposes of model validation and as “hooks” for study of climate impacts.

BATS has been developed in the context of several GCMs, albeit all at the National Center for Atmospheric Research. Although it is intended to be as portable as possible, it makes some assumptions about the overlying atmosphere that limit its direct applicability to some GCMs. In particular, it assumes, for the purpose of calculating surface conditions and fluxes, that the GCM provides information on atmospheric fields within a surface-mixed layer representable through Monin-Obukhov similarity theory. This assumption requires that the lowest model gridpoint be within the first hundred meters or so of the atmosphere. The layer structure of the CCM with this point, at about 70 meters above the surface, is barely adequate for this purpose; during nighttime and polar conditions, the surface-mixed layer can, in reality, shrink to a few tens of meters, but sensible and latent fluxes are relatively weak under these conditions. Thus, without a further planetary boundary layer model, BATS is not applicable to those GCMs whose lowest atmospheric layer is "thick"; that is, about a kilometer or more in thickness.

The fields of horizontal wind, atmospheric temperature, and water vapor mixing ratio are provided from the lowest atmospheric level of the GCM. Surface pressure is an additional prognostic variable of the atmospheric model. Furthermore, the overlying column of atmosphere provides to the surface: precipitation, thermal infrared fluxes, and modification of prescribed top-of-the-atmosphere flux of solar radiation. How well GCMs generate the spatial and temporal distribution of precipitation and solar radiation may be their most serious limitation in realistically representing the surface hydrological processes.

For example, Dickinson (1989) and Shuttleworth and Dickinson (1989) note a significant excess of model incident solar radiation compared to observations in the Amazon at a field site near Manaus. They suggest this excess solar radiation as a prime candidate explanation for the simulation of excess interception by the model canopy, along with differences between the model temporal distribution of precipitation and that which occurs at a local site.

The atmospheric model we use here is the NCAR CCM, Version 1 (Williamson *et al.* 1987), which was developed from an earlier CCM0 based on an Australian model and is similar in structure to those used by Manabe at Geophysical Fluid Dynamics Laboratory. These models are pseudospectral, with spectral-space horizontal-coordinates for the hydrodynamical calculations. This approach is efficient and accurate for the wind and temperature calculation but has undesirable properties (*e.g.*, negative mixing ratios) when used for water vapor. The present study uses the rectangular (R-15) spectral truncation, which maps to about a 4.5° latitude by 7.5° longitude mesh. The vertical differencing of CCM1 (Williamson 1988) was developed to ensure conservation of energy and still provide the good simulation of the lower stratosphere given by CCM0.

The standard CCM1 includes a simple moist convective adjustment, presumed to give convective precipitation as well as precipitation from stable-layer saturation. Cloud cover is calculated. Radiation interacts with ozone, water vapor, carbon dioxide, and oxygen. Solar radiation is reflected in the atmosphere by the clouds, with optical properties a function only of model layer, and by Rayleigh scatter. In general, the treatment of clouds and their radiative interaction is much less satisfactory than the quite accurate treatment of clear-sky radiation.

The only changes we have made in the atmospheric model discussed here for use with BATS is:

- We split the solar spectrum at $0.7\mu\text{m}$ to distinguish visible and near-infrared albedo over land; and
- We use a diurnal cycle of solar radiation with surface fluxes over land calculated every 0.5-hour (the model time step), solar atmospheric heating every 3 hours, and longwave heating at the standard 12-hour frequency.

The assumption of a reduced frequency for evaluating atmospheric radiative heating has traditionally been used by most models for computational economy. It suffers from presumably small lack of energy conservation.

The BATS parameterization version 1E, has been “frozen” from further development for establishing its performance coupled to the CCM1 described above. It represents the surface over a CCM grid square as a soil partially shaded by a vegetation canopy. Soil texture is specified for each such square, and from that are inferred hydrological properties — in particular, hydraulic conductivity and soil water potential as functions of soil moisture content. The most severe hydrological limitations of the soil representations are the assumptions that precipitation and soil properties are uniform over the grid square and that soil drainage through the three layers (surface, root, and subroot zone) is only vertical. We iterate the point that, however unrealistic these assumptions may be, they can be a less severe source of error than that from inadequacies of the atmospheric model. The current unrealistic soil assumptions mentioned here should be removed in model improvements. BATS includes the dominant processes of evapotranspiration, including a standard treatment of the environmental dependence of stomatal resistance, a simple model for effective root resistance depending on soil water potential, and a treatment of evaporative losses by canopy interception. Another function of BATS and other such land parameterizations is to define the surface roughness for turbulent exchange and the surface albedo for absorption of solar radiation.

From the viewpoint of fluxes of solar radiation, the BATS canopy is viewed as a continuous distribution of absorbers. However, for other energy fluxes and energy balance as a whole, it is parameterized as a single layer.

Surface Radiative Forcing and Hydrological Response in a Model Climate Simulation

The CCM1/BATS 1E model summarized in the previous section was integrated over six annual cycles (about 10^5 time steps), a relatively modest integration with today’s computational resources. The purpose of such a control integration is to validate the model performance against observations. The simulation of atmospheric winds and temperatures for the NCAR CCMs has been shown to be reasonable in many studies. BATS does not have any major impact on these features, so we restrict ourselves here to previously unexamined questions of surface energy balance, where the verdict is not so positive.

Figure 1 shows the time series for model global average net solar radiation absorbed and thermal infrared radiation emitted, at the top of the atmosphere. Values for 4 months of Earth Radiation Budget Experiment (*ERBE*) data are indicated by \times s. From this viewpoint, the model infrared flux appears to be about 10 W m^{-2} too high, and the model solar fluxes appear to be about 15 W m^{-2} too high, corresponding to a model underestimation of global albedo by 0.03-0.04. Note, however, that the annual average *ERBE* solar fluxes apparently exceed the infrared flux by 5 W m^{-2} , so the model-absorbed solar exceeds outgoing infrared by about 10 W m^{-2} .

Possible difficulties with the model's treatment of solar radiation are further explored by examining the simulated results over a specific region, selected here to be centered over the United States. To see variations over the seasonal cycle, we average surface fields over the central United States (30° - 50° N, 80° - 105° W) and average each month over the final five years. Figure 2 summarizes radiative fluxes and evapotranspiration. The seasonal cycle of surface solar radiation over this region is an order of magnitude larger than that of net thermal infrared and so dominates the total net radiation.

Figure 3 shows similarly the model's simulated soil moisture on the surface (top 10 cm) and in the root zone (roughly 1 meter, but dependent on vegetation type) and model precipitation over the averaging region. The fourth quantity, moisture ratio, shows the root zone water variation between a field capacity (gravitational drainage of 2 mm/day) and wilting point (soil water potential of 15 hPa) normalized by this range. The soil moisture is out of phase with the precipitation, because net radiation and, hence, evapotranspiration have a larger seasonal variability (Figure 2) than does precipitation.

Figure 4 compares model runoff with observations. Model runoff is somewhat high, corresponding to the excess model precipitation. The model has two peaks, whereas the observations show a single summer peak. Some of the differences may be definitional; that is, model runoff is realized locally, whereas observations refer to runoff from major basins, which is smoothed and lagged in time relative to local runoff. However, the September peak in model runoff definitely appears unrealistic. Correspondence between model and observed precipitation is not examined here. Such an examination would have to consider both mean patterns and the discrepancies between realistic and model spatial and temporal variability of precipitation.

Figure 5 shows model versus observed surface incident solar flux for July. The model pattern is smoother than that given by observations, but otherwise it is in reasonable agreement over the western United States. However, over the eastern United States, the model shows about 20% more solar radiation than observed — an unacceptably large difference. The relative contribution of clear-sky model albedos and that of clouds to this discrepancy can be estimated from the *ERBE* satellite data (*e.g.*, Ramanathan *et al.* 1989). Figure 6, also for July, compares model clear-sky absorbed solar radiation with *ERBE* data. Both show 380 - 400 W m^{-2} across the United States, and the model values are lower than the data at higher latitudes. Hence, the model treatment of clear-sky radiation cannot explain the excess solar radiation at the surface. Consequently, this excess must result from the model clouds not reflecting enough solar radiation. Figure 7 compares the model and *ERBE* solar cloud forcing.

The model cloud forcing is generally less negative than that indicated by *ERBE*. The discrepancies are concentrated into three areas.

Figure 1
GLOBAL MONTHLY AVERAGES OF
MODEL ABSORBED
SOLAR RADIATION VERSUS
THAT OBSERVED FOR ERBE FOR
APRIL, JULY, AND OCTOBER 1985
AND JANUARY 1986

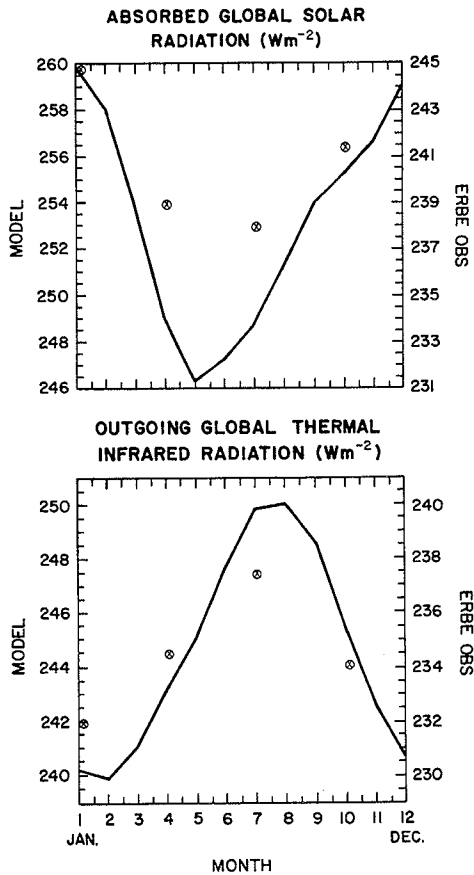


Figure 2
MONTHLY AVERAGED MODEL SURFACE RADIATION
BALANCE QUANTITIES AND EVAPOTRANSPIRATION
(Averaged Over the Indicated Box)

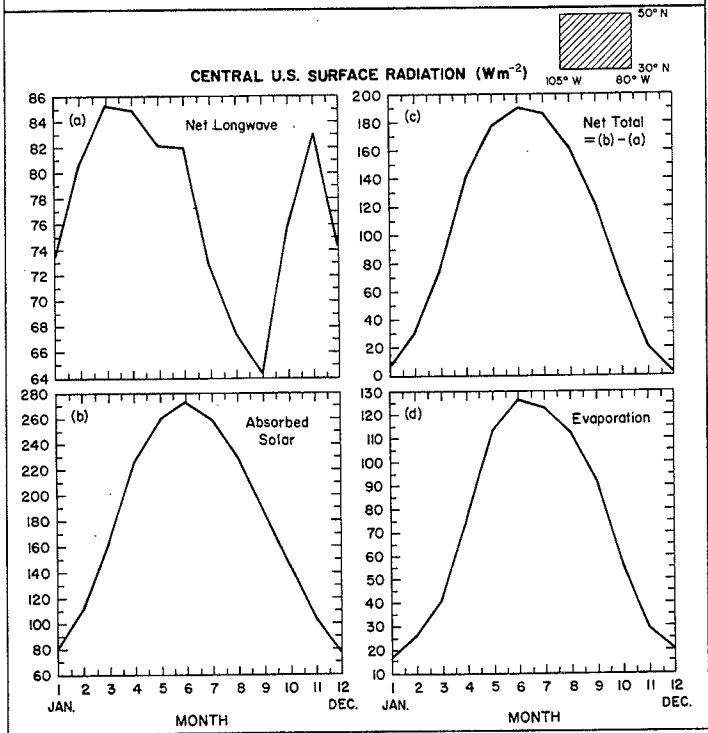
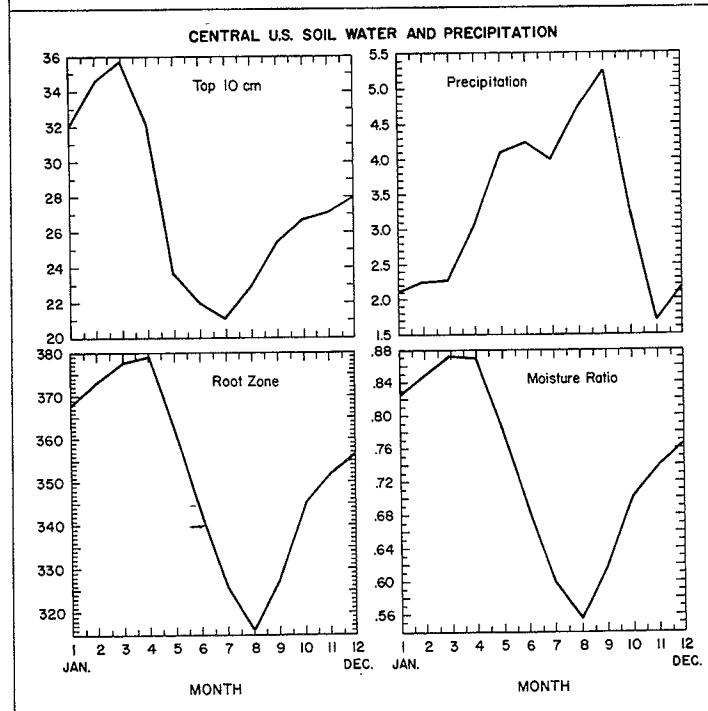


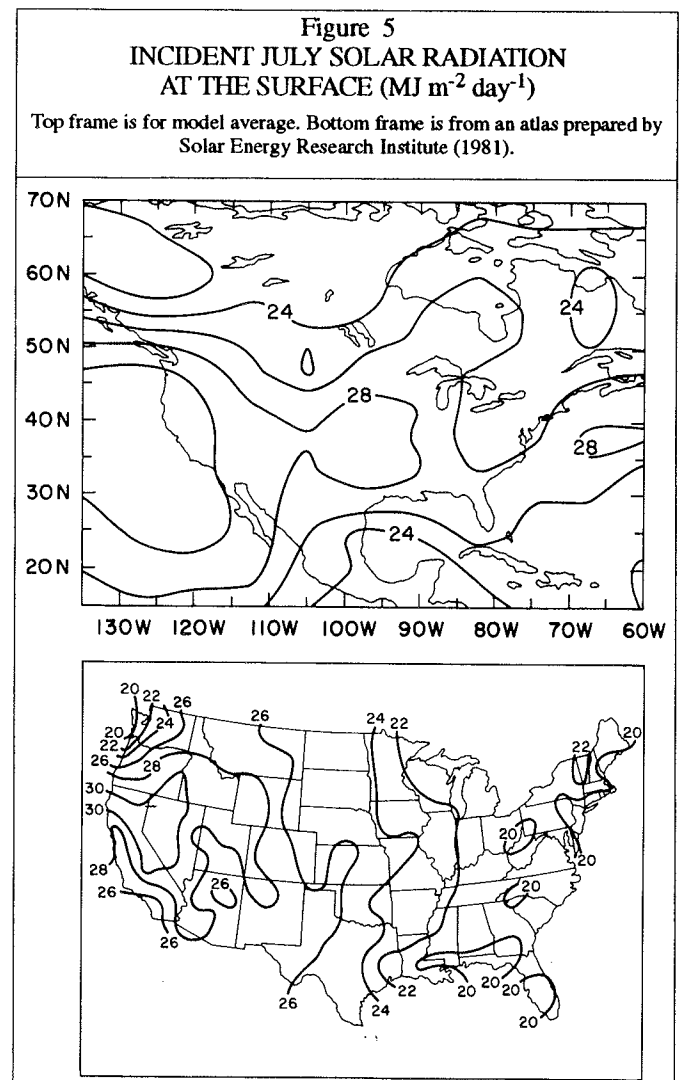
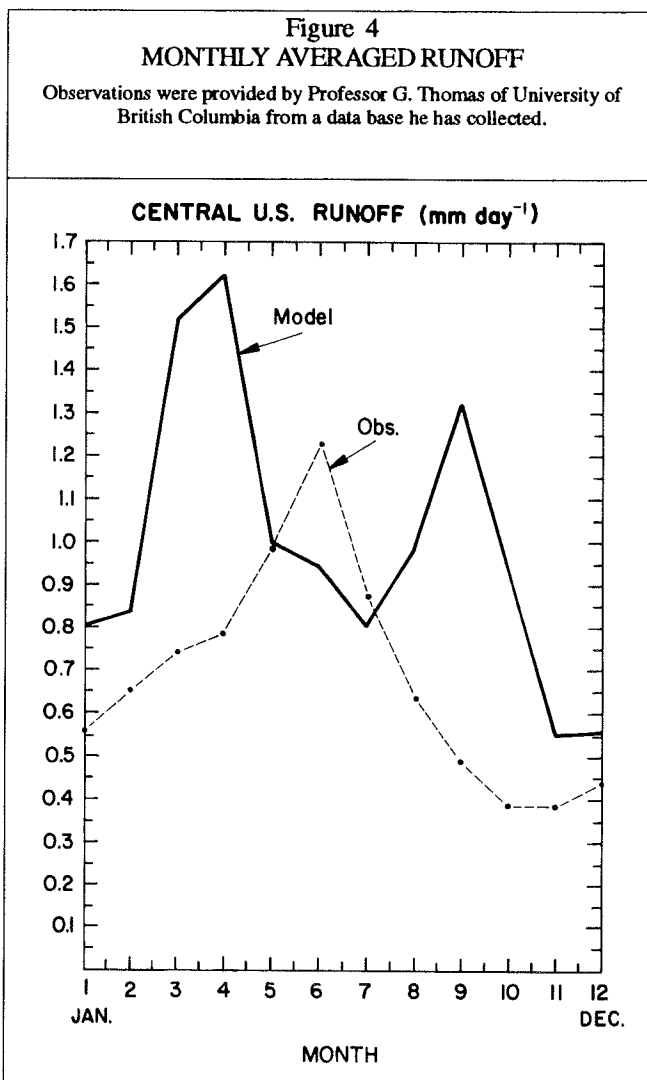
Figure 3
MONTHLY AVERAGED MODEL SOIL MOISTURE
AND PRECIPITATION
(Averaged Over the Indicated Box)



- Off the West Coast, the model shows cloud forcing between 0 and -20 W m^{-2} , whereas the data is in the range of -60 to -80 W m^{-2} . This difference is accounted for by the model's failure to reproduce the low stratus decks in that region.
- Over the eastern states, the model gives about -40 W m^{-2} , whereas the data show -60 to -80 W m^{-2} .
- Over northeastern Canada, the model shows -40 to -60 W m^{-2} and the data show -80 to -100 W m^{-2} . Evidently the model clouds over eastern North America reflect only about half as much solar radiation as is observed.

Conclusions

We argue that the surface hydrology in General Circulation Models may be limited in accuracy by shortcomings in their simulations of relevant atmospheric quantities — in particular, precipitation and surface radiation depending on cloud radiative forcing. We illustrate this possibility through an analysis of some of the output fields of a simulation



with a diurnal cycle version of the NCAR Community Climate Model. Over a global average, the model shows a small excess of absorbed solar radiation, about 10 W m^{-2} . The excess of absorbed solar radiation appears to be much larger over certain regions, including eastern North America.

Model surface radiation over the eastern United States exceeds that observed by about 20%. This excess is associated with a deficit in model cloud reflection of solar radiation as seen in a 40 W m^{-2} discrepancy in solar cloud forcing over eastern North America. Analysis of model surface energy and hydrological parameters over a box over the central states shows a close correspondence between net radiation and evapotranspiration. The seasonal cycle of soil moisture appears to be driven more by the seasonal cycle of evapotranspiration than that of precipitation. Hence, for this region at least, errors in model surface net radiation are likely to give comparable errors in all the other surface hydrological parameters.

Figure 6
 MODEL AVERAGE JULY CLEAR-SKY
 ABSORBED SOLAR RADIATION
 OVER NORTH AMERICA (top frame)
 VERSUS ERBE JULY 1985 (bottom frame)

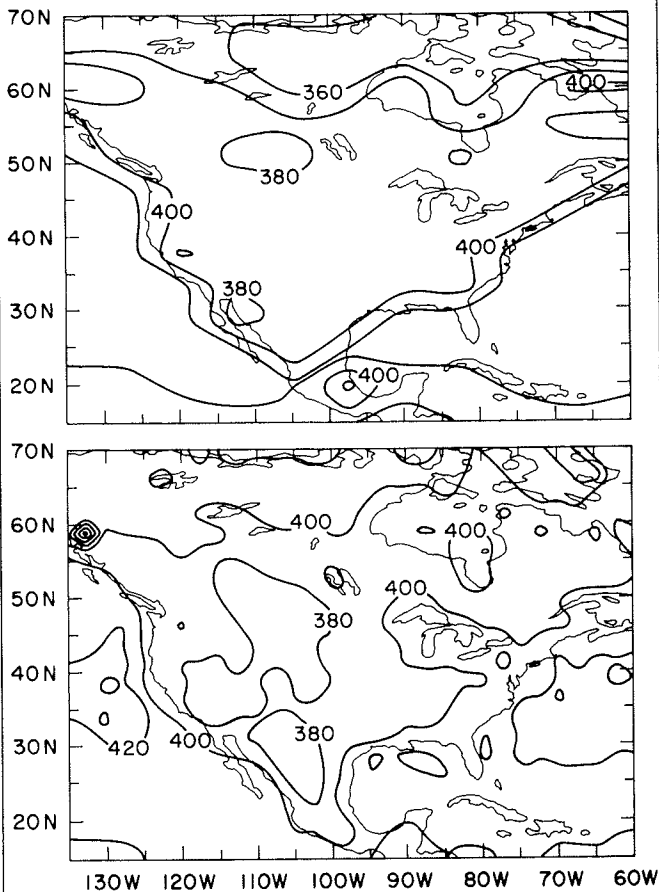
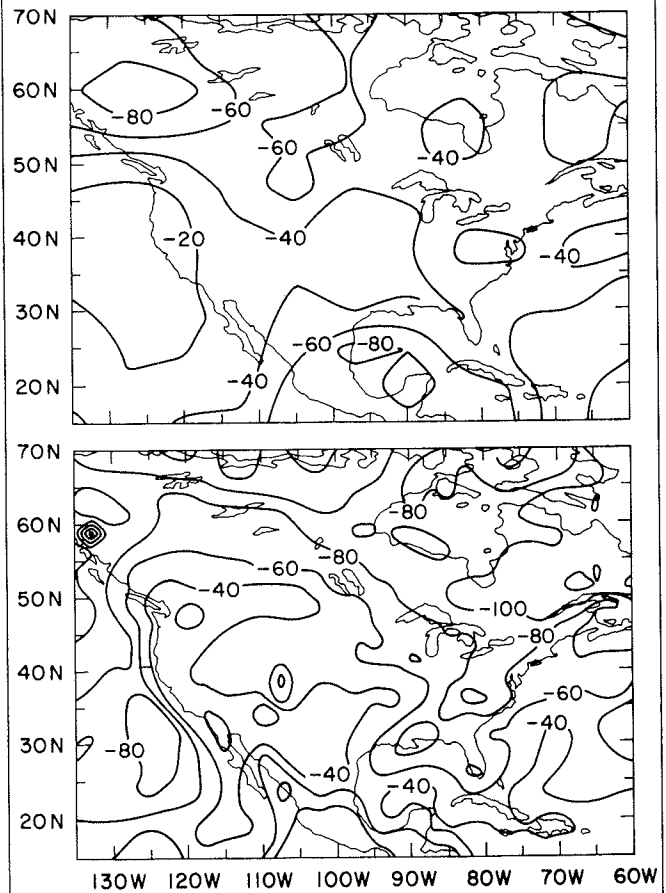


Figure 7
 MODEL AVERAGE SOLAR CLOUD FORCING OVER
 NORTH AMERICA (top frame)
 VERSUS ERBE JULY 1985 (bottom frame)

The solar energy reflected to the top of the atmosphere minus that found in the absence of clouds.



Acknowledgments

We thank G. Thomas for providing the observational runoff data shown in Figure 4; B. Briegleb for providing the ERBE data in CCM format shown in Figures 1, 6, and 7; and S. Shearer for preparing the manuscript.

We are also grateful to Kluwer Academic Publishing, The Netherlands, for granting permission to use this material.

References

- Dickinson, R.E. 1989. "Implications of Tropical Deforestation for Climate — A Comparison of Model and Observational Descriptions of Surface Energy and Hydrological Balance". *Philos. Trans. R. Soc. London, B.*, 324:423-431.
- _____. 1984. "Modeling Evapotranspiration for Three-Dimensional Global Climate Models" in *Climate Processes and Climate Sensitivity*. Geophys. Monogr. 29, Maurice Ewing Series, No. 5. American Geophysical Union. Washington, DC. pp. 58-72.
- Dickinson, R.E., A. Henderson-Sellers, P.J. Kennedy, and M.F. Wilson. 1986. *Biosphere-Atmosphere Transfer Scheme (BATS) for the NCAR Community Model*. National Center for Atmospheric Research. TN-275+STR. Boulder, CO.
- Ramanathan, R.D., R.D. Cess, E.F. Harrison, P. Minnis, B.R. Barkstrom, E. Ahmad, and D. Hartmann. 1989. "Cloud-Radiative Forcing and Climate: Results from the Earth Radiation Budget Experiment". *Science*, 243:57-63.
- Shuttleworth, J.W., and R.E. Dickinson. 1989. "Comments on 'Modelling Tropical Deforestation: A Study of GCM Land-Surface Parameterizations' by R.E. Dickinson and A. Henderson-Sellers". *Q.J.R. Meteorol. Soc.*, 115:1177-1179.
- Solar Energy Research Institute. 1981. *Solar Radiation Energy Resources Atlas of the United States*. SERI/SP-642-1037. U.S. Govt. Printing Office. Washington, DC.
- Williamson, D.L. 1988. "The Effect of Vertical Finite Difference Approximations on Simulations with the NCAR Community Climate Model". *J. of Climate*, 1(1):40-58.
- Williamson, D.L., J.T. Kiehl, V. Ramanathan, R.E. Dickinson, and J.J. Hack. 1987. *Descriptions of NCAR Community Climate Model (CCM1)*. National Center for Atmospheric Research. TN-285+STR. Boulder, CO.

Simulation and Diagnosis of Large-Scale Atmospheric Moisture and Surface Hydrology Over North America

John O. Roads, Shyh-Chin Chen, David Langley, Chih-Yue Kao,
Jordan Alpert, and Gary A. Glatzmaier

ABSTRACT: We describe a preliminary investigation into large-scale atmospheric and surface moisture variations over North America. We compare large-scale hydrologic budgets in the Los Alamos general circulation model (GCM) to observed precipitation and vertically integrated atmospheric moisture fluxes derived from the National Meteorological Center's operational analyses. The GCM faithfully simulates the integrated flux divergence and P-E differences. However, the integrated moisture content is too low, and precipitation and evaporation are too high. The model produces summertime soil moisture dryness, which supports previous studies showing increased droughts under warmer conditions.

Introduction

Radiatively active greenhouse gases have been accumulating in the earth's atmosphere due to human activity (Ramanathan 1988) as the global population has continued its exponential increase. Along with a significant increase in the global temperature, results of GCM sensitivity experiments suggest the global hydrological cycle will be intensified (Gleick 1981). That is, we expect increased precipitation and evaporation. This intensification may enlarge (or shrink) dry and wet regions. Indeed, a few GCM sensitivity experiments (*e.g.*, Manabe *et al.* 1981; Manabe and Wetherald 1980, 1986, and 1987; Manabe and Stouffer 1981;) have shown that over North America, evaporation will intensify relative to precipitation, resulting in a drier continent. This result has been supported by other studies, leading to speculation that widespread continental drought may be an inevitable byproduct of global change (*e.g.* Bolin *et al.* 1986). However, other GCM sensitivity studies (*e.g.*, Meehl and Washington 1988) have found the opposite behavior. In these other experiments, a wetter North American continent resulted from the intensified hydrological cycle. One deciding characteristic noted by Meehl and Washington (1988) was the amount of soil moisture present in the control state. Clearly, there is much to be learned in reconciling state-of-the-art GCMs to observed hydrological conditions. As stated by Meehl and Washington:

The highly parameterized hydrology in the models, lack of appropriate observed data, and complexity of hydrological processes in the real world prohibit accurate verification and/or calibration of the parameterizations in the models.

Background

In essence, we need a much better description of the observed and modeled hydrologic budgets. Consider the budget equation for the vertically integrated atmospheric water cycle:

$$\frac{\partial}{\partial t} \{q\} = E - P - \nabla \cdot \{v q\}$$

where $\{ \cdot \}$ denotes a mass weighted vertical integral, $\{ \cdot \} = \frac{1}{g} \int_0^{p_s} \cdot dp$. Since this is the

equation for the vertically integrated moisture budget, no vertical transport terms, which act to redistribute the moisture in the vertical, are present (see Boer 1986 and Boer and Sargent 1985 for an equivalent, but alternative, formulation). This equation shows that the vertically integrated moisture, or precipitable water, is increased by evaporation, decreased by precipitation, and increased by horizontal convergence. The vertically integrated moisture is also sometimes referred to as *precipitable water* or *atmospheric water storage*.

The budget equation for the land hydrology can be written in a similar fashion:

$$\frac{\partial}{\partial t} [w] = -E + P - R$$

where (\cdot) denotes a vertical (subsurface) average. This land hydrology equation shows that the vertically integrated subsurface (ground water) and land water (surface water) storage is decreased by evaporation, increased by precipitation, and decreased by runoff (streamflow and subsurface or ground water transport). Although not identical to the runoff, an indication of runoff is given by gauged streamflow records, discussed below. This land hydrology budget is a counterpart to the atmospheric moisture budget.

At intra-seasonal time scales, the surface storage terms play an important role. For example, winter snow accumulation provides spring streamflow. However, over a sufficiently long time that the storage terms are negligible, the budgets show that the integrated atmospheric moisture convergence must be equal to the runoff. Both the long-term climatological balance and the short-term storage and runoff terms will probably be affected by climate change. These budgets can easily be obtained from a GCM; development of observed budgets is more difficult.

In comparison to previous attempts to describe the hydrologic budgets using rawinsonde data (*e.g.*, Rasmusson 1977, Rosen *et al.* 1979, Peixoto and Oort 1983), we should now be able to more easily obtain (we hope) the integrated atmospheric moisture budget terms from operational objective analyses, which are tabulated on a regular grid over the globe at 12 mandatory pressure levels. Still, some effort must be expended to obtain the vertically integrated budget terms. For example, an interpolated surface pressure must first be derived. For this purpose, we are currently using the observed geopotential heights and orographic heights corresponding to a T30 spectral representation. (This resolution may have to be increased.)

Analyses of the surface pressure are also available, and the realism of our interpolation will be tested using this analyzed surface pressure in comparison to the interpolated surface pressure. Once the surface pressure is obtained, similar interpolation must be used to find

humidity and horizontal moisture transports must then be vertically integrated. This is an intensive data processing effort, since daily (there are some indications that twice daily data will be required) global values of RH (which is converted to specific humidity), T, v, and z at the 12 mandatory levels must be accessed, converted to global spherical harmonics, transformed to a physical transform grid, interpolated to find a surface value, multiplied together (on a T30 transform grid), vertically integrated, transformed to spectral space for a horizontal divergence calculation, and then converted back to physical space. Some corrections to the divergent wind component are also necessary.

Because of the global sparsity of hydrologic measurements, we are first concentrating in this study on comparisons over North America between the GCMs and observations. This, however, brings about another difficulty since GCMs have problems adequately addressing small regions. That is, the North American continent is a small region in a global GCM.

While the hydrological budgets in GCMs are internally consistent and represent most of the pertinent processes, they are distinctly different from the hydrological budgets in nature. For example, since GCMs usually employ constant depth "buckets" to simulate soil storage and since they do not have an extensive river and lake basin to store and transport water, GCMs model the runoff in a very crude fashion. If runoff occurs at any gridpoint, it is assumed to go directly to the ocean. No runoff from upstream regions is allowed to affect the local surface water balance. Other potential problems are due to the way evaporation (Dickinson *et al.* 1986), precipitation, and even the atmospheric moisture convergence (large-scale versus continuous scale) are treated in GCMs versus their behavior in nature.

Do these differences between what occurs in a GCM and nature matter? We think they might; therefore, we need to understand seasonal and interannual variability in nature and we need to develop GCMs to predict future climate scenarios. We need to know how accurately we can model the regional and large-scale hydrological budgets to determine what additional work is required in describing the surface properties of hydrology.

Observations

The observations we intend to use for this study come from many sources. Global, twice daily objective analysis data sets come from NMC (*National Meteorological Center*) and ECMWF (*European Centre for Medium Range Forecasts*) via NCAR. Major analysis changes influencing moisture fluxes occurred in 1985 at ECMWF and in May 1986 at NMC (Trenberth and Olson 1988). Hence our initial effort will concentrate on dates after May 1986. We must also continually search for any strong changes that signify analyses changes after these dates. These data can be used to compute precipitable water and moisture convergence and, as a residual, precipitation minus evaporation. If we can adequately calculate the moisture convergence, then we should have a good estimate for the P-E differences, since the atmospheric storage change is small for time scales longer than a month.

Previous studies (*e.g.*, Meko and Stockton 1984; Lins 1985) have described spatial and temporal variations of streamflow over the coterminous United States. A collection of streamflow stations suitable for climate variability studies is soon to be available for many U.S. stations from USGS (J. Landwehr and J. Slack, personal communication). We also

have available an array of Canadian stations. This streamflow data set should provide a preliminary basis for describing nature's surface water transport. A constraint on the above budgets is that over a sufficiently long time, such that storage term variability is small, atmospheric moisture convergence should be equal to surface runoff (Sargent 1989).

Precipitation data sets are available for the United States and Canada for many long-term stations from NCDC and from the Canadian Climate Center. Roads and Maisel (1990) describe some of the aspects of the U.S. data set. Standard precipitation climatologies are also available, but we intend to use temporally consistent data sets in the hope we can derive meaningful residual anomaly budget terms.

Evaporation over land can be derived as a residual from measurements of the atmospheric moisture storage and transport and precipitation. Soil moisture can be derived as a solution to a first order differential equation from the surface moisture balance. This solution will provide an unknown constant, which might be estimated from the residual evaporation and the observed potential evaporation available at many United States stations. However, these residual calculations must be scrutinized, since they are strongly dependent on errors in all the other terms. As a test of any residual calculation, we will first use GCM data where we know all budget terms accurately. Thus, the GCM data will also provide a useful test bed for making inferences about hydrologic variables that are not well observed in nature.

GCM Intercomparisons

A preliminary analysis of the annual mean atmospheric hydrologic cycles in the LANL (*Los Alamos National Laboratory*) model is shown in Figure 1. These LANL analyses are taken from 10 years of daily model data. The LANL q appears to be somewhat low in the tropical region (also see Figure 2.) The model also seems to miss many of the small-scale features near the strong topographical regions. That is, the fluxes near the high topographical regions do not appear to be very strongly modified in the GCM. The mid-latitude GCM flux also does not show the observed southwesterly flux along the eastern coasts. This may be related to weak subtropical highs that appear to dominate mid-latitude moisture flux patterns. Still, the general features of the tropical fluxes seem reasonable. Also, the divergence and convergence seem reasonable in the subtropics and tropics.

Figure 2 shows zonally integrated quantities from the LANL model. Also shown for comparison are the zonally averaged values from a preliminary analysis of the 1989 NMC objective analyses and Oort and Rasmusson (1971). Perhaps the most distinct differences between the LANL model and the observations are the relatively low values of the integrated q . This bias may be related to the cold bias in the model. Many GCMs have a cold bias, but we were somewhat surprised that minor temperature differences can affect the integrated q so strongly. Another possibility may lie in the vertical finite difference scheme present in the model, which may not faithfully represent the vertically integrated exponentially varying moisture, especially near the surface. This will be investigated further. Despite this small q , the meridional flux and flux divergence (and hence P-E difference) appear quite reasonable, suggesting a correct hydrologic cycle is achieved by the LANL model despite the lower atmospheric humidity and larger precipitation and evaporation. Another discrepancy occurs in the precipitation amounts, which are substantially higher in the LANL GCM than the raw observations would indicate (see Legates and

Figure 1
 ANNUAL AVERAGES FROM THE LANL GCM OF
 VERTICALLY INTEGRATED VALUES OF q , vq , and $\nabla \cdot vq$

q , Contour increments of 4 Kg/m^2 ;
 vq , Arrow lengths corresponding to 22.5° long represent 500 Kg/m^2
 $\nabla \cdot vq$, Contour increments represent $4 \times 10^{-5} \text{ Kg/m}^2\text{s}$

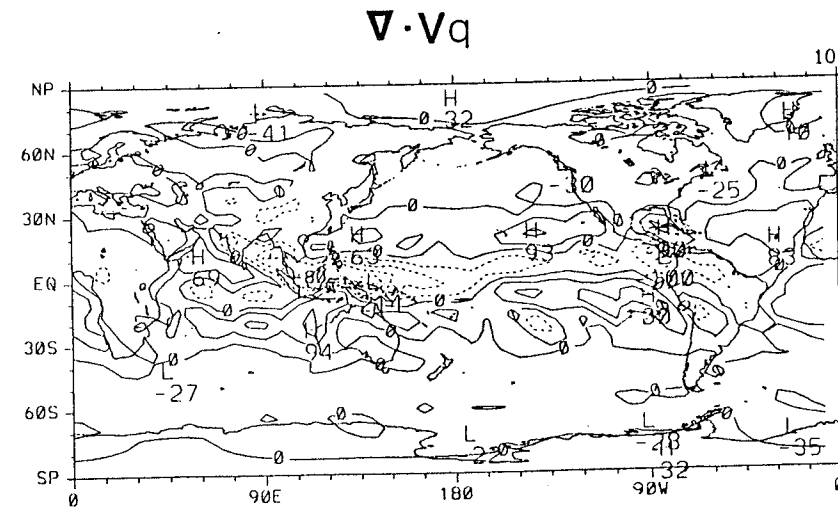
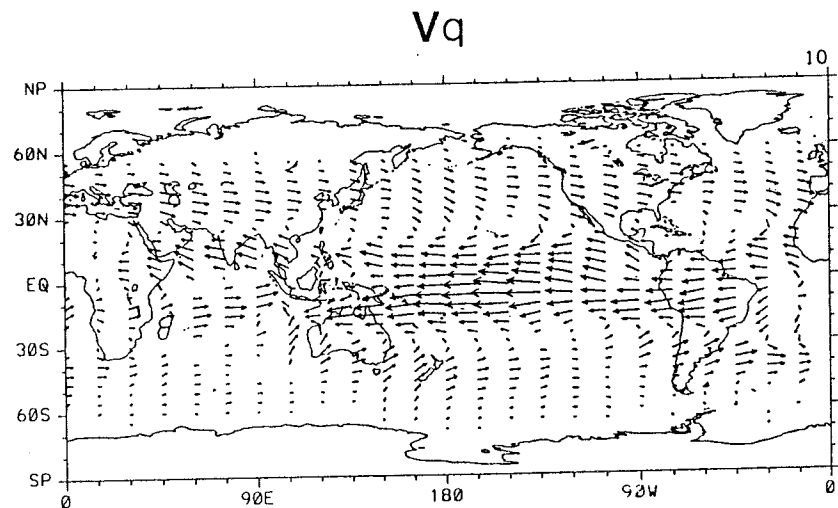
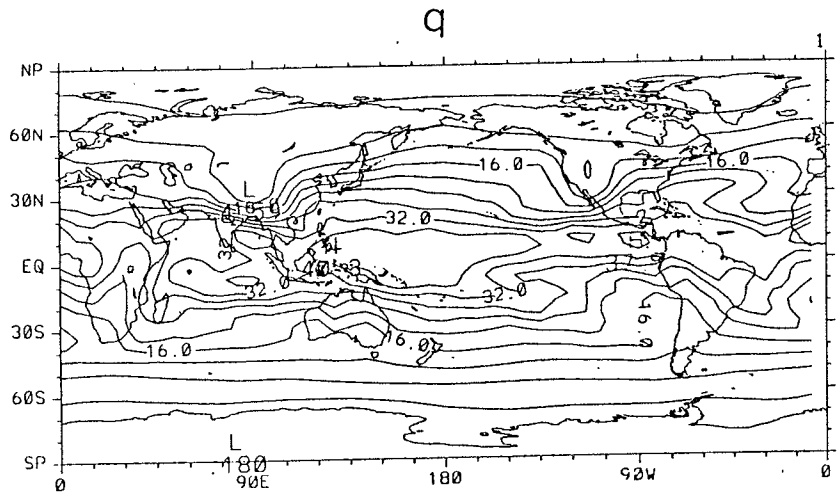
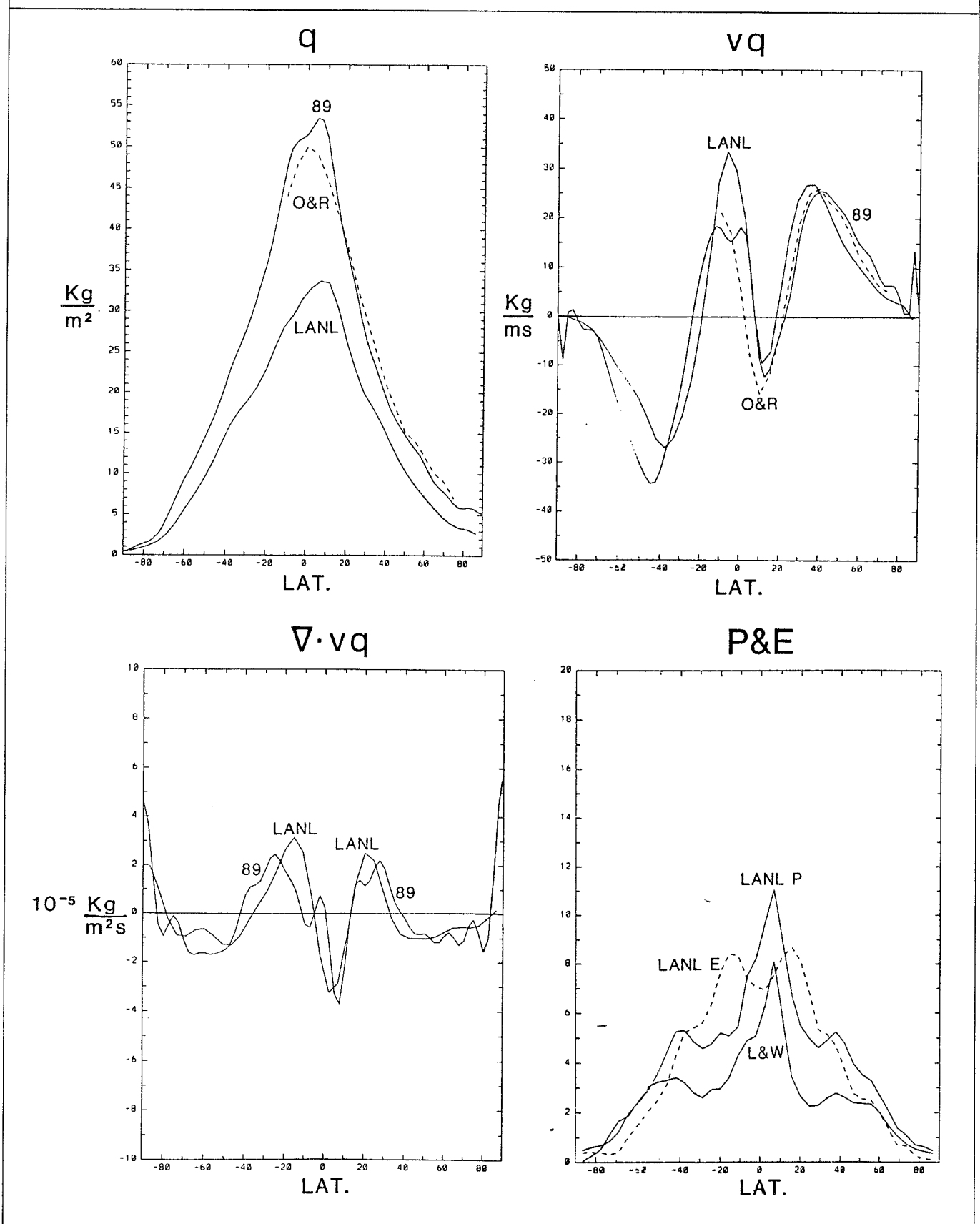


Figure 2
ZONALLY AVERAGED VALUES OF VERTICALLY INTEGRATED q , vq , and ∇ IN THE LANL MODEL
 Also shown for comparison are processed results from NMC's 1989 final analyses and from Oort and Rasmusson (1971).



Willmott 1990). This wet bias is also present in the National Meteorological Center's medium range forecast model (see Roads and Maisel 1990).

The seasonal difference in LANL atmospheric moisture q (Figure 3) is simply related to the seasonal temperature differences, although the higher resolution observations show smaller scale features related to the topography. The seasonal difference in the moisture fluxes appears to be substantially different in direction and magnitude from the observations, but the divergence patterns are similar. Again, we only have a very preliminary version of derived observations.

Figure 4 shows the seasonal differences in LANL precipitation, evaporation, and runoff over the United States. Precipitation differences are somewhat larger than observed variations, but appear to show the correct pattern of large West Coast wintertime precipitation and large summertime precipitation over the rest of the country. Evaporation contributes to part of this pattern, with the difference resulting in relatively greater streamflow in the west during the winter, relatively greater streamflow on the plains during summer, and surprisingly greater relative streamflow in the east during winter. (The observed streamflow variations will be processed to compare with the GCM.) There may be a problem due to the lack of snow in the LANL model; hence we will use this model mainly to examine interannual variability in summertime drought.

The surface water balance shows the summertime dryness that has the opposite seasonal phase to the atmospheric moisture. Although no observations or residual calculations are available yet to compare with this field, it is thought to be qualitatively realistic. This seasonal change also supports the hypothesis that warmer temperatures may result in increased droughts, at least in the LANL model.

Acknowledgments

This work was supported by U.S. Geological Survey grant 14-08-001-G1483, National Oceanic and Atmospheric Administration grant NA86-AA-D-CP104, INCOR, and Cal-space.

References

- Boer, G.J. 1986. "A Comparison of Mass and Energy Budgets from Two FGGE Datasets and a GCM". *Mon. Wea. Rev.*, 114:885-902.
- Boer, G.J., and N.E. Sargent. 1985. "Vertically Integrated Budgets of Mass and Energy for the Globe". *J. Atmos. Sci.*, 42:1592-1613.
- Bolin, B., B.R. Doos, J. Jager, R.A. Warrick (Eds.). 1986. *The Greenhouse Effect, Climate Change and Ecosystems*. Wiley, New York.
- Dickinson, R.E., A. Henderson-Sellers, P.J. Kennedy, and M.F. Wilson. 1986. *Biosphere-Atmosphere Transfer Scheme (BATS) for the NCAR Community Climate Model*. National Center for Atmospheric Research. TN-275+STR. Boulder, CO.
- Gleick, P.H. 1987. "Regional Hydrologic Consequences of Increases in Atmospheric CO₂ and Other Trace Gases". *Climatic Change*, 10:137-161.
- Legates, D.R. and C.J. Willmott. 1990. "Mean Seasonal and Spatial Variability in Gage-Corrected Global Precipitation". *J. Climatology*. Accepted.
- Lins, H.F. 1985. "Streamflow Variability in the United States: 1931-1978". *J. Clim. and Appl. Meteorol.*, 24:463-471.
- Manabe, S., and R.J. Stouffer. 1981. "Summer Dryness Due to an Increase in Atmospheric CO₂ Concentration". *Clim. Change*, 3:347-386.
- Manabe, S., and R.T. Wetherald. 1987. "Large-Scale Changes of Soil Wetness Induced by an Increase in Atmospheric Carbon Dioxide". *J. Atmos. Sci.*, 44:1211-1235.
- _____. 1986. "Reduction in Summer Soil Wetness Induced by an Increase in Atmospheric Carbon Dioxide". *Science*, 232:626-628.
- _____. 1980. "On the Distribution of Climate Change Resulting from an Increase in CO₂ Content of the Atmosphere". *J. Atmos. Sci.*, 37:99-118.
- Manabe, S., R.T. Wetherald, and R.J. Stouffer. 1981. "Summer Dryness Due to an Increase of Atmospheric CO₂ Concentration". *Climatic Change*, 3:347-386.
- Meehl, G.A., and W.M. Washington. 1988. "A Comparison of Soil-Moisture Sensitivity in Two Global Climate Models". *J. Atmos. Sci.*, 45:1476-1492.
- Meko, D.M., and C.W. Stockton. 1984. "Secular Variations in Streamflow in the Western United States". *J. Clim. and Appl. Meteor.*, 23:889-897.
- Oort, A.H., and E.M. Rasmusson. 1971. *Atmospheric Circulation Statistics*. National Oceanic and Atmospheric Admin. Professional Papers. U.S. Dept. of Commerce.
- Peixóto, J.P., and A.H. Oort. 1983. "The Atmospheric Branch of the Hydrological Cycle and Climate" in *Variations in the Global Water Budget*. Ed. A. Street-Perrott. pp.5-65.

- Ramanathan, V. 1988. "The Greenhouse Theory of Climate Change: A Test by an Inadvertent Global Experiment". *Science*, 240:293-299.
- Rasmusson, E.M. 1977. *Hydrological Application of Atmospheric Vapor-Flux Analyses*. World Meteorological Organization. Operational Report 11. Geneva, Switzerland.
- Roads, J.O., and T.N. Maisel. 1990. *Precipitation Forecasts with the National Meteorological Center's Medium-Range Forecast Model*. Submitted.
- Rosen, R.D., D.A. Salstein, and J.P. Peixóto. 1979. "Streamfunction Analysis of Interannual Variability in Large-Scale Water Vapor Flux". *Mon. Wea. Rev.*, 107:1682-1684.
- Sargent, N.E. 1989. "Inter-Annual Variability in North American Moisture Fluxes: Streamflow Records Meet Atmospheric Analyses". *14th Annual Climate Diagnostics Workshop Proceedings*. October 13-19, 1989.
- Trenberth, K.E., and J.G. Olson. 1988. *Intercomparison of NMC and ECMWF Global Analyses*. National Center for Atmospheric Research. TN-301+STR.

Toward a Rule-Based Biome Model

Ronald P. Neilson, George A. King, and Greg Koerper

ABSTRACT: Current projections of the response of the biosphere to global climatic change indicate as much as 50 to 90% spatial displacement of extratropical biomes. The mechanism of spatial shift could be dominated either by competitive displacement of northern biomes by southern biomes or by drought-induced dieback of areas susceptible to change. The current suite of global biosphere models cannot distinguish between these two processes, hence the need for a mechanistically based biome model. The first steps have been taken toward development of a rule-based, mechanistic model of regional biomes at a continental scale. The computer model is based on a suite of empirically generated conceptual models of biome distribution. With a few exceptions, the conceptual models are based on the regional water balance and the potential supply of water to vegetation from two soil layers: surface for grasses and deep for woody vegetation. The seasonality of precipitation largely determines the amount and timing of recharge of each of these soil layers and, thus, the potential mixture of vegetative life-forms that could be supported under a specific climate. The current configuration of rules accounts for the potential natural vegetation at about 94% of 1,211 climate stations over the conterminous United States. Increased temperatures, due to global warming, would: (1) reduce the supply of soil moisture over much of the United States by reducing the volume of snow and increasing winter runoff, and (2) increase the potential evapotranspiration (*PET*). Combined, these processes would likely produce widespread drought-induced dieback in the Nation's biomes. The model is in an early stage of development and will require several enhancements, including: explicit simulation of *PET*, extension to boreal and tropical biomes, a shift from steady-state to transient dynamics, and validation on other continents.

Introduction

Trace-gas-induced global climatic change has been projected to potentially shift the world's major biotic regions by hundreds of kilometers (Smith and Tirpak 1989). Under one scenario, as much as 55% of the world's terrestrial vegetation could change to a different type (Smith *et al.* in prep.; King *et al.* in prep.). Such changes could produce complicated feedbacks to the global climate, possibly exacerbating the "greenhouse effect", and would certainly produce significant ecological and economic upheavals. These projections are based, in part, on the *Holdridge life-zone* approach, which correlates the distribution of major vegetation types to annual precipitation, potential evapotranspiration, and biotemperature (Holdridge 1967).

Another global biome model (Box 1981), which is more detailed in climate parameters, is also correlational. The two approaches generally agree on the direction of mid- to high-latitude vegetation changes under $2\times\text{CO}_2$ but disagree on the sign of the change in the tropics. The tropical forests expand under the Holdridge model, but contract under the Box model (Smith *et al.* in prep.; King *et al.* in prep.). Both approaches assume a steady state; that is, they cannot simulate the transition of biomes from one type to another.

The accuracy with which these approaches predict current vegetation ranges from <50% to about 77% (Prentice 1990; Stephenson 1990). These models also do not simulate biosphere/atmosphere feedbacks. These and other limitations suggest the need for a more mechanistic approach to biome modeling — one that can be incrementally developed to

incorporate transient behavior, ecosystem productivity, trace gas emissions, and disturbance regimes (*e.g.*, wildfire).

An approach to biome modeling now being developed is more closely related to physiological plant processes. The intent is to simulate distinct life-forms or physiognomies (Beard 1978), mixtures of which produce different biomes. The model was constructed from the premise that the climate is the principal determinant of global vegetation distribution and that variations in topography, soils, disturbance regimes, and biotic interactions modify these distributions (Allen and Starr 1982, Neilson *et al.* 1989, O'Neill *et al.* 1986, Stephenson 1990, Vankat 1979, Woodward 1987). Construction of the preliminary version of the model represents a partial test of this premise. Successful classification of vegetation based exclusively on climatic information will be viewed as supportive of the premise. The present approach is limited to steady-state, potential natural vegetation. Future enhancements should include land-use considerations. Model development so far has been limited to the conterminous United States but will be extended to global vegetation in future versions.

Conceptual Development

New developments in biogeography are providing a mechanistic conceptualization of the biosphere (Bryson 1966, Neilson and Wullstein 1983, Neilson 1986, Neilson 1987, Neilson *et al.* 1989, Stephenson 1990, Woodward 1987). The model described here is based on mechanistic, conceptual models described by Neilson *et al.* (1989). These resulted from transect analyses of over 1,200 weather stations in the conterminous United States (Figure 1) and over 7,000 U.S. Geological Survey gaging stations (Quinlan *et al.* 1987, US West 1988a, US West 1988b). The approach relates the seasonality of temperature, precipitation, and runoff patterns to the physiological requirements of plants during different parts of their life cycles and seasonal cycles. Details of the approach and results are published in Neilson *et al.* (1989).

The continental transects of climate and runoff revealed regional patterns of climate and runoff seasonality that coincide with the boundaries of the major biomes of the United States (Figure 2) (Neilson *et al.* 1989). These generalizations form the basis for the model development described here and can be cast as rules for prediction of the occurrence of woody vegetation, grasslands, and deserts. Woody vegetation in the United States appears to receive enough winter precipitation to recharge a deep soil reservoir. Deep soil water is apparently required to balance the PET (*potential evapotranspiration*) during the growing season. If the amount of winter precipitation is large, a region will support a closed forest. Intermediate amounts should support a lower stature or open forest (*e.g.*, savanna or pinyon-juniper woodland); lesser amounts should support a shrubland. The amount of winter precipitation (*i.e.*, deep soil water) required is a function of growing season PET and rainfall minus runoff. Regional runoff patterns suggest that the deep soil reservoir is virtually depleted each year by transpiration and runoff.

These observations are consistent with current theory and plant physiology (Neilson *et al.* 1989, Stephenson 1990, Woodward 1987). If excess water were available in deep soil layers at the end of a growing season and ecosystems were not energy- or nutrient- limited, they should increase biomass and leaf area in subsequent seasons, thus increasing the rate of withdrawal of deep soil water. If leaf area over a landscape were so high that the rate of

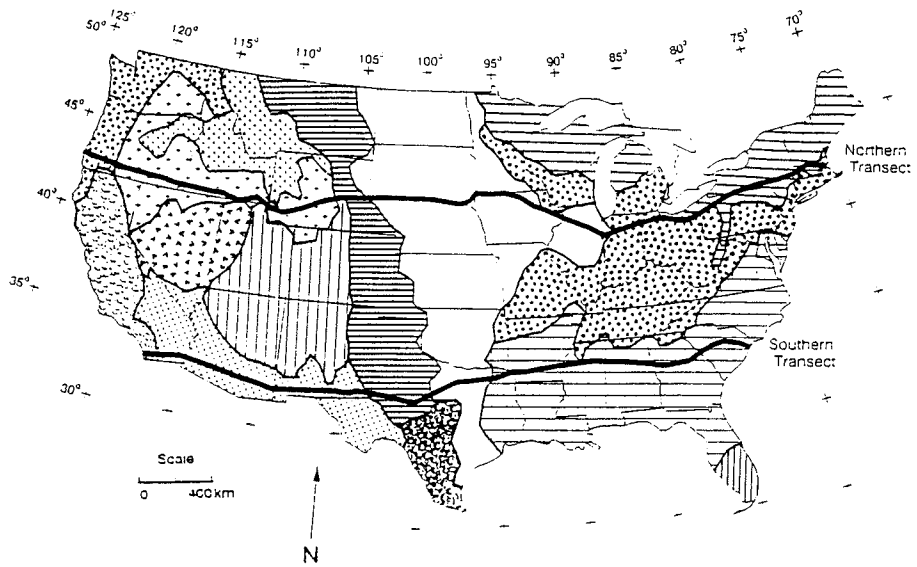
Figure 1
LOCATIONS OF WEATHER STATIONS IN THE HCN NETWORK

Conceptual models of biomes were developed from a sub-sample of these stations using transect analyses.
 The full set of stations was used to calibrate the quantitative model presented here.



Figure 2
PRINCIPAL BIOMES OF THE CONTERMINOUS UNITED STATES
 (Simplified from Dice 1943 and Küchler 1964)

Locations of two transects of the HCN network of weather stations (Figure 1) are shown.



- | | | | |
|--|---------------------------------|--|---------------------------|
| | California Vegetation | | Short Grass Prairie |
| | PNW Forests | | Tail Grass Prairie |
| | Great Basin Sage-Steppe | | South Texas Savanna |
| | Great Basin Desert Scrub | | Northern Hardwoods |
| | Northern Rocky Mountain Forests | | Eastern Deciduous Forests |
| | Southern Rocky Mountain Forests | | Southeastern Forests |
| | Southwestern Deserts | | Subtropical Forests |

water withdrawal completely depleted deep soil water, then plants would die or leaves and branches would be sloughed (Woodward 1987). Leaf area would be reduced, as would the rate of withdrawal of deep soil water. Thus, in theory, ecosystems should be in dynamic equilibrium (steady state) with the regional water balance by virtue of these intrinsic feedback processes.

While maintenance of woody vegetation appears to require deep soil water, maintenance of grasses appears to require sufficient surface soil moisture during growth and reproduction, usually the spring to summer months. Mixtures of the two life-forms can occur if there is enough moisture in the appropriate soil layers during the growing season and if interference by one life-form does not preclude existence of the other. Grasslands can occur if the woody canopy is open enough to allow high light penetration to the soil surface and if there is a sufficient supply of surface soil moisture during the active growing season of grasses, generally spring (Neilson 1987, Neilson *et al.* 1989). This implies a sufficiently low level of deep soil water that a closed forest would be precluded from the site. If spring rains are accompanied by high midsummer rains, surface soil will remain moist and a large stature grassland should be supported (*e.g.*, the tall grass prairie). If both winters and springs are quite dry, maintenance of both woody vegetation and grasses is hindered, and a desert may be expected. High midsummer rains in such a desert area can support a low-stature grassland, as in the Chihuahuan and Sonoran deserts of the Southwest (Neilson 1986, Neilson 1987).

A few biome boundaries in the United States appear to be directly controlled by cold temperature rather than by water balance. The most prominent of these are:

- The boundary of the temperate forests with the boreal forest (Burke *et al.* 1976).
- Possibly the boundary between the Southeast pines and hardwoods with the oak-hickory forest to the north (Neilson *et al.* 1989).

The current configuration of our biome model does not address these boundaries.

The model is being developed in stages that will progress from empirical and correlational to simulation of water balance and thermal constraints. The empirical rules described here are generally adequate to define most dominant vegetation types in the conterminous United States. In our model, threshold values of precipitation amounts during different seasons determine transitions between different life-forms, as described above. This configuration addresses the *supply* side of the water balance. The *demand* function, PET, is assumed to be fixed and is not directly factored into the rules. Given the assumption of fixed PET, the current configuration of the rules cannot be used to assess future climate effects. This initial version of the model was constrained by the unavailability of data for the physically based calculation of PET at large spatial scales. PET will be incorporated in later versions.

The rules allow mixtures of life-forms, such as trees and grasses, if the canopy is open. These mixtures can produce complicated biotic interactions and disturbance regimes. For example, the eastern deciduous forest is characterized by both wind and fire disturbances, with wind perhaps the most important (Runkle 1985). However, the adjacent prairie supports a natural, high-frequency fire regime (Abrams *et al.* 1986, Vankat 1979). If the

tree canopy is open, such that a well developed grass layer forms, woody vegetation is at risk from fire. The presence of high grass biomass also places woody vegetation at risk from herbivores and from competition for both light and water between shrub seedlings and rapidly growing grasses. Under these conditions, strictly climatic rules for prediction of biome physiognomy will not suffice. Secondary influences from disturbance and biotic interactions are important and can remove one or more climatically favored life-forms (Abrams *et al.* 1986, Vankat 1979). Therefore, under certain climatic conditions where specific mixtures are favored, secondary rules are invoked to modulate the biome physiognomy. Variations in soil infiltration rates, water-holding capacity, and nutrient status will also require secondary rules.

The demand function — PET minus growing season rainfall — will determine the amount of supplemental soil water required by different life-forms during different seasons in future versions of the model. Enhanced versions of the model will be operable under future climate. Additional enhancements will include dynamic simulation of regional water balance, using an energy balance approach with vegetation and leaf area acting as conduits between the soil and the atmosphere (Federer 1982, Woodward 1987). Model development and calibration are being achieved using the site-specific monthly data from the 1211-station HCN (*Historical Climatology Network*) (Figure 1, Quinlan *et al.* 1987). Once calibrated, the model will be operated on a distributed climate over a dense grid.

Model Description

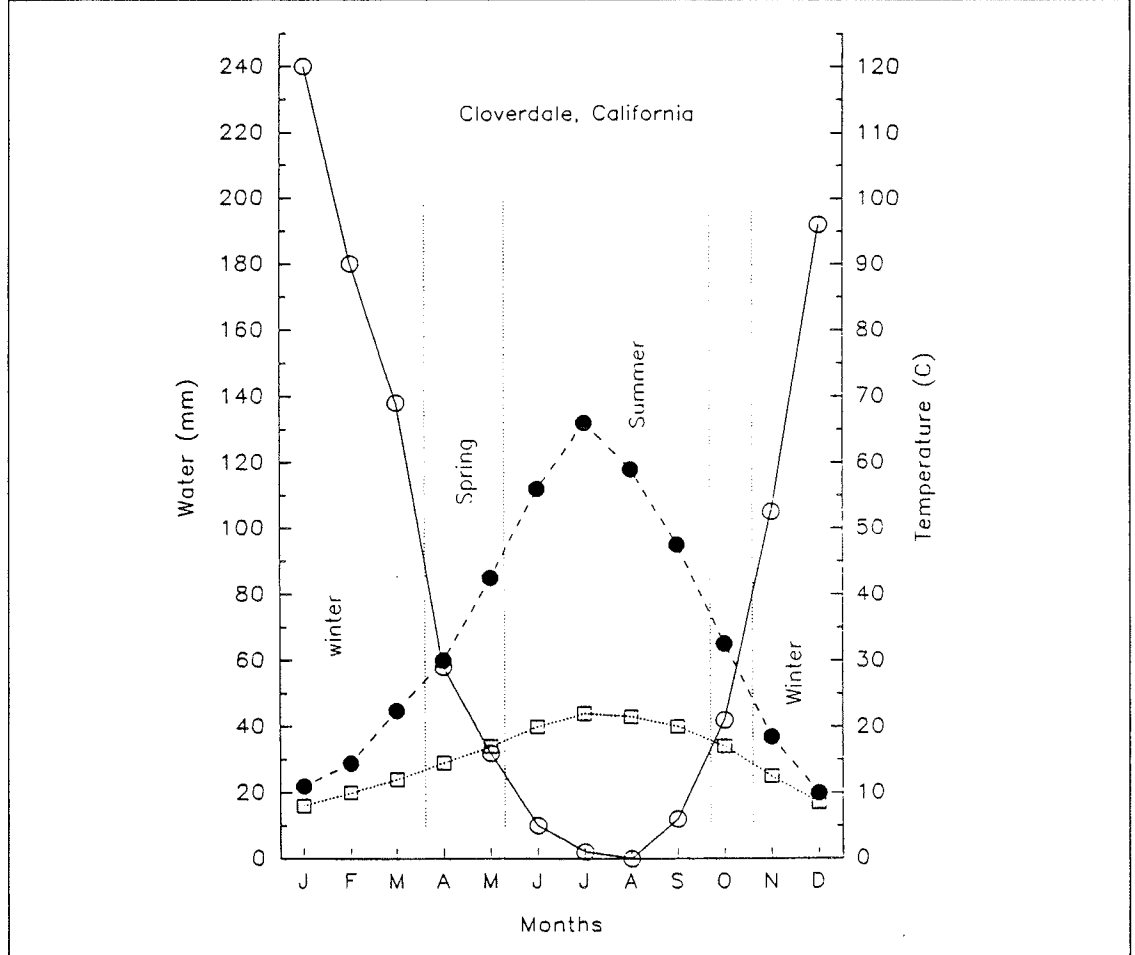
The model was constructed as a set of rules based on the conceptual models of Neilson *et al.* (1989). The entire HCN was used to calibrate the rules. Each station was pre-classified to a specific biome based on a map modified from Kùchler (1964) and Dice (1943). The stations were then processed through the rule-base and classified accordingly. Accuracy was determined by comparison between pre- and post-classifications. Parameter adjustment and calibration were dependent on visual interpretation of the mapped residuals. Error in classification can arise from either the pre-classification or the rule-based classification. A careful analysis of the residuals is necessary to determine the source of the error.

The most unique feature of the model is the temperature-based definition of seasons. Winter, spring, and summer are the principal seasons considered. Temperature thresholds, input as parameters, were used to define the beginning and end of the seasons (Figure 3). Therefore, the length of seasons automatically scales with latitude, altitude, and continentality. A map of precipitation during any one season would not represent precipitation amounts over the same period at all map locations.

The beginning and end of winter are defined from both hydrologic and biotic perspectives. In temperate zone summers, PET is generally high enough that incident precipitation does not infiltrate to deep soil layers, but either runs off directly or is evapotranspired from vegetation surfaces and surface soil layers (Major 1963, Thornthwaite 1948, Thornthwaite and Mather 1955). In cooler months, PET is low enough that incident precipitation can infiltrate to deep soil layers. Accumulated snow will also infiltrate or run off as it melts. Thus, we define a temperature threshold above which precipitation cannot reach deep soil layers and below which it can. The infiltration period defines winter in temperate latitudes. The threshold also carries a biotic importance in that it closely relates to the timing of dormancy onset and release in plants.

Figure 3
 EXAMPLE OF RULE-BASED PARTITIONING OF THE SEASONS

Precipitation = Open Circles; Temperature = Open Squares; Potential Evapotranspiration = Closed Circles
 Vertical dotted lines indicate locations of temperature thresholds used in the model to delineate seasonal transitions. Temperature thresholds are used to define the beginning and end of seasons for each weather station. Within each season, precipitation amounts are accumulated for seasonal totals or examined in terms of precipitation per month. Different rainfall amounts within the different seasons are used by the rule-base to differentiate between different life-forms that would potentially be supported by that climate.



Spring is viewed from the hydrologic perspective as the period over which the surface soil layer can be depleted. This period is critical for seedling establishment of woody species and for completion of the life cycles of grasses and ephemerals. In the temperate zone, the surface soil will dry rapidly in the absence of spring rains, precluding a major grassland development. In northern states under these rules, winter can extend to quite late in the year and spring can extend through most of the growing season, with little to no summer.

Summer is generally the period of greatest water stress. If spring is wet enough, grasses can complete their life cycles before critical mid-summer drought stress (Vankat 1979). However, if summers are also wet, different grass species can continue to grow, producing a mixed or tall grass environment.

There are two classes of parameters in the model:

- Temperature thresholds that define the beginning and ending of seasons.
- Precipitation thresholds within seasons that constrain the life-forms dependent on that season.

Figure 4 is a model flow chart showing the decision tree applied to each meteorological record of monthly temperature and precipitation. Winter precipitation thresholds are configured as absolute amounts, since the timing of precipitation is not critical. That is, of all the accumulated precipitation during the winter, a fixed fraction is assumed to infiltrate to deep soil layers at some time during winter, with the remainder being returned to the atmosphere (evaporation, sublimation) or routed to surface water (runoff). However, during spring and summer, the supply of water (precipitation) and demand for water (evapotranspiration) are essentially simultaneous when viewed from a monthly time-step. Therefore, precipitation thresholds during spring and summer are defined in units of millimeters per month.

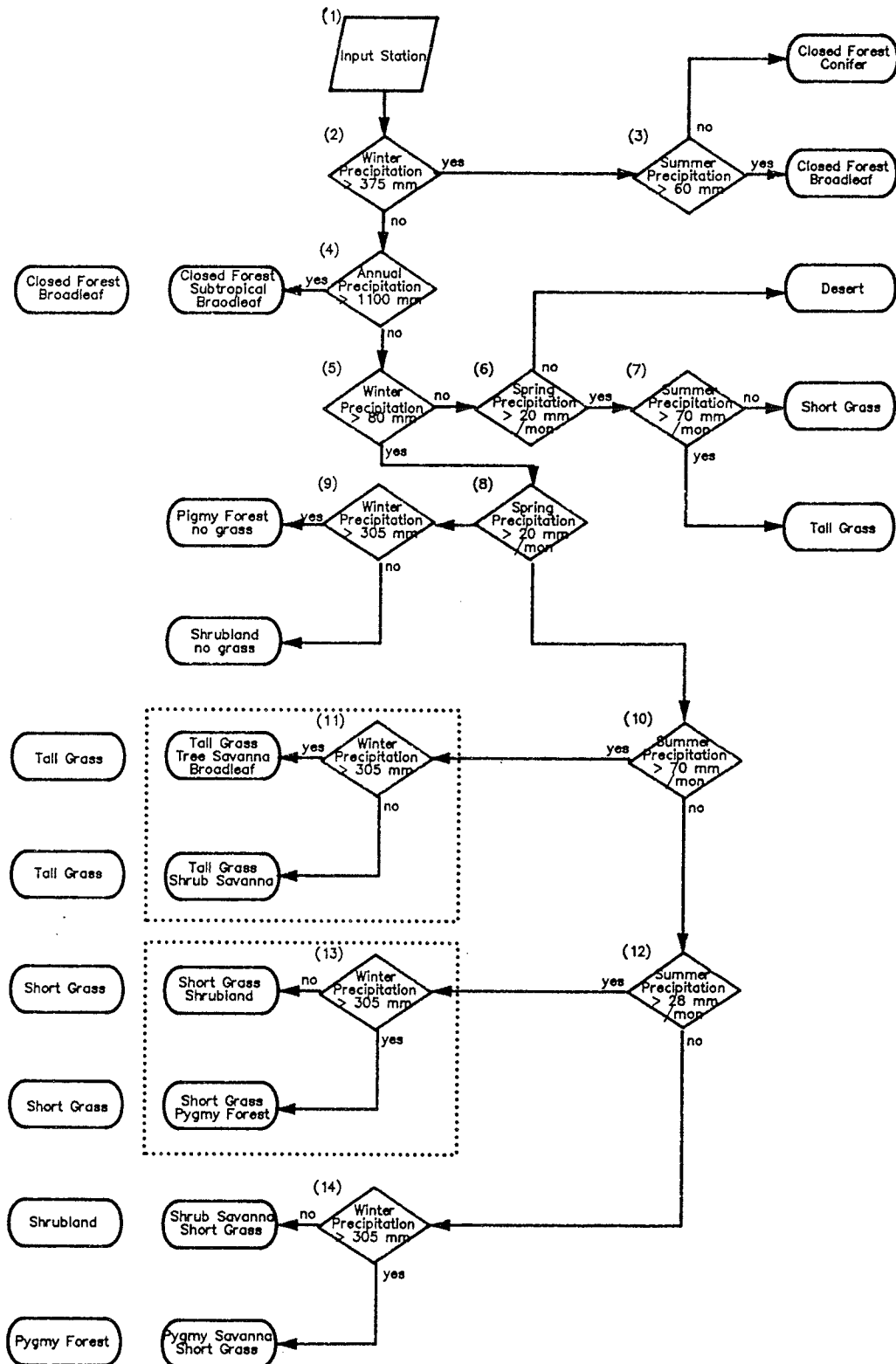
The rules are equivalent to a dichotomous key with simple yes/no decisions determining the trajectory through the rules and the ultimate declaration of biome type for a station (or cell, if applied to a full grid). The flow chart is arranged such that all winter decisions are in the first column of diamond shapes, followed by a column of spring decisions and a column of summer decisions. The decisions enclosed by dashed lines (rules 11 and 13) are implied rather than explicitly coded rules in the current configuration. The implied rules arise from assuming the application of secondary biome rules for biotic interaction and disturbance regimes. The bubbles to the left of the flowchart are the simplified classifications applied at the termination of the adjacent rule. They indicate the influence of the secondary, implied rules accounting for fire and biotic interactions. For example, a mixture of open-canopy, deciduous trees with tall grass prairie is directly classified as tall grass prairie. Similarly, all Pygmy forests (pinyon-juniper woodland), with or without grass, are classified as Pygmy forest. Future versions of the model will retain all such mixtures and distinctions.

The calibrated threshold separating closed forest from non-closed forest is 375 mm of winter precipitation (rule 2). The amount of summer precipitation per month (rule 3) separates broadleaf from conifer forests. The physiological inference is that broadleaf trees cannot withstand the degree of mid-summer vapor-pressure stress across the leaf surface that conifers can withstand (Marshall and Waring 1984, Neilson *et al.* 1989, Running 1975, Waring and Franklin 1979).

The current configuration of the model becomes inadequate as the stations approach subtropical climates. Rule 4 is a temporary proxy for a set of rules that will deal with subtropical climates. As you approach the Florida peninsula, winters become ever shorter and eventually nonexistent as defined by the temperature thresholds. Thus, precipitation at these stations during winter is not sufficient to support a forest, a clear artifact of the rules. As the growing season becomes longer, the infiltration period of winter becomes shorter. Under these situations, infiltration can still occur if the amount of rainfall more than compensates for a high PET. This does occur in forested areas in the subtropical climates of the southeastern United States and elsewhere (Neilson *et al.* 1989). However, implementation of such a rule must await a future version of the model that incorporates physically based PET calculations. A workable place-holder is a threshold for annual precipitation of about 1100 mm, given that winter precipitation is below a closed-forest threshold (rule 4). This correctly classifies closed-forest stations in the far southeastern United States, yet does not interfere with appropriate winter rule-based decisions in more northerly latitudes.

Figure 4
FLOW CHART OF THE RULE-BASE

Monthly mean temperature and monthly total precipitation are input for each station.
Seasons are defined as in Figure 3, and precipitation amounts are linearly interpolated for each season from the monthly data.
The rule -base is a dichotomous key that classifies each station as to the potential natural vegetation based on climate. The enclosed rules (11 and 12, dashed lines) indicate implied, secondary rules whereby disturbance regimes and biotic interactions are inferred to constrain one or more life-forms from a dominant expression in the mixture of life-forms.



After partitioning the high winter precipitation (*i.e.*, closed-forest stations), rule 5 selects sites with winter precipitation less than 80 mm. These stations are ultimately classified as desert or grassland based on spring precipitation (rule 6, 20 mm/mo) and tall or short grass based on summer precipitation (rule 7, 70 mm/mo).

The remaining stations will be classified as either shrublands, open forest (savanna), or grasslands potentially supporting woody species. Shrubland and open forest are distinguished depending on whether winter rains are above or below 305 mm (rules 9, 11, 13, 14). Each type (shrub or tree) can be broadleaf or microphyllous (small leaf), depending on the level of summer rains (rules 10, 12), reflecting again the inferred vapor-pressure gradient across the leaf surface. If summer rains are sufficient to support a broadleaf type (rule 10), the result is either a broadleaf, tall-grass savanna or tall-grass shrub savanna. In either case, secondary rules are invoked to classify these sites as tall grass prairie, with the principal mechanism for grass dominance assumed to be fire.

Given sufficient winter rain to support shrubs or open forest (rule 5), but less than 70 mm/mo of summer rain (rule 10), only a xeromorphic leaf structure can be supported. The tree form will be conifer and could be a xeric conifer savanna, such as ponderosa pine or a smaller stature but more dense pygmy forest of pinyon pine and juniper. In either case, the conifer leaf area is comparatively low. If only the shrub form can be supported (rule 14), the shrubs would be microphyllous. If summer rain is more than 28 mm/mo and spring rain more than 20 mm/mo (rule 8), then a well developed short grass community can be supported. Under these conditions, secondary rules are again invoked to remove the woody component (rule 13), and the communities are classified as short grass. Below 28 mm/mo of summer rain, the grassland is of lower biomass, weakening the secondary rules and resulting in either a shrub or pygmy forest savanna, depending on winter rain (rule 14).

Model Calibration

The model parameters were adjusted to provide an optimal fit to the specified biome boundaries. This was accomplished iteratively by visual examination of the residuals and calculation of percent correct classification. Two classes of parameters require calibration:

- Thermal constraints controlling the beginning and end of seasons.
- Precipitation thresholds within seasons for different life-forms.

These must initially be calibrated in tandem, with sensitivity of both classes being examined. However, once the thermal thresholds are set, primary calibration is with the precipitation thresholds. Future versions of the model that incorporate PET will use the PET-minus-precipitation estimates in conjunction with thermal information to control seasonal timing and length.

Most rules exhibit one or more “balance” points. That is, increasing or decreasing the value of a parameter may continue to increase the correct classification of a particular biome, but there will be a point above or below which further adjustment occurs at the expense of correct classification in other biomes. The parameters were adjusted close to these balance points. Some parameters were clearly more sensitive than others, but we have not attempted a formal sensitivity analysis.

The site-specific accuracy of the calibration was 79%. Highest success was 94% in the eastern United States forests and lowest was 0% for the 11 grassland stations in the central valley of California (Figure 5, Table 1). The current model does not subdivide the eastern forest into the three subsections. When these rules are implemented, errors in classification undoubtedly will occur near the ecotones. A few sites near the border between the northern hardwoods and the boreal forest were classified as conifer, a reasonable occurrence. The mixed forests of the Rocky Mountains were only predicted at 19% accuracy (28% northern Rockies, 12% southern Rockies (Table 1). The next lowest success was 70% for the tall grass prairie; the remaining biomes were predicted at better than 80% accuracy.

Closer examination of the residuals reveals that the model is more accurate than these indications, since pre-classification error is incorporated in the results. The California grasslands were predicted as conifer forest (45%), shrubland (36%), and pinyon-juniper (*P-J*) woodland (18%). Given the wet winters and very dry summers, these predictions may be quite reasonable. The conifer forest and P-J woodland stations cluster in the north end of the valley and at the boundaries with the neighboring conifer forests. These could be accurate classifications given the potential inaccuracies of the pre-classification biome map. A shrubland classification for the remaining sites may also be acceptable.

Remember that the rule-based classifications have been simplified to indicate only the dominant life-form, even if a mixture is actually being selected (Figure 4). The shrubland classification in the current configuration of rules is actually a mixture of shrub and short grass life-forms (rule 14). Climatically, the mixed shrub/grass classification for the central valley is quite reasonable; however, the relative mix of shrubs and grass is likely inaccurate in that the model does not yet account for the unusually long spring period over which grass biomass would build. Given sufficient grass biomass, the natural and anthropogenic influence of fire could have rendered the valley more of a monotypic grassland (Vankat 1979). Other possibilities for a lack of shrubs in the central valley include: (1) the presence of fine surface soils that might hinder percolation of deep soil water, and (2) the lack of sufficient summer rain usually necessary for establishment of shrubs (Neilson 1986).

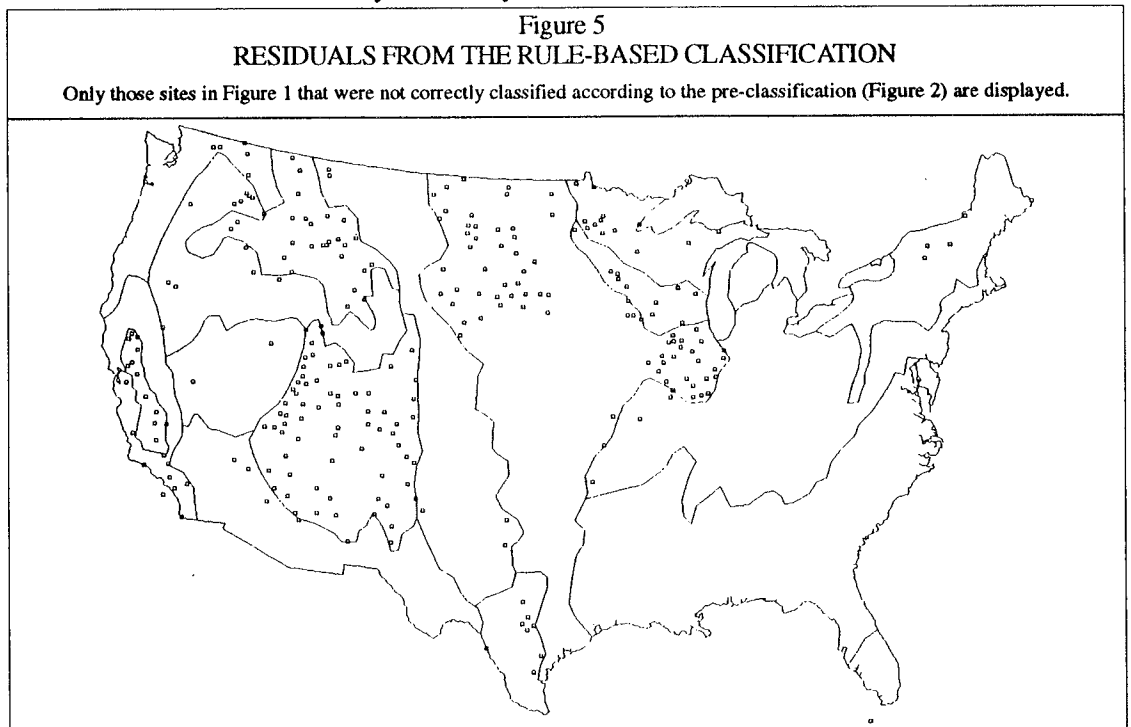


Table 1
SUMMARY OF CLASSIFICATIONS

Entries are percentages.

Bold numbers correspond to groupings of similar biomes. Italics highlight the correct classification category.

Numbers in parentheses are sample sizes and percentages if the northern mixed grass prairie of Küchler (1964?) is considered short grass prairie as determined by the rule-base. The current configuration of rules does not explicitly attempt to distinguish mixed grass as intermediate between short and tall grass.

	Number of Weather Stations	Conifer Forest	Shrub- land	South- west Deserts	Pinyon- Juniper	Short Grass	Tall Grass	Broad- leaf Forest
Conifer Forests	91	82	9		8	1		
Northwest	58	<i>91</i>	2		5	2		
Southwest	33	<i>67</i>	21		12			
California Grassland	11	45	36		18	<i>0</i>		
Shrubland	78	12	81	1	5	1		
Northern Great Basin	63	14	<i>79</i>		6			
Southern Great Basin	15		<i>87</i>	7		7		
Southwest Deserts	34		12	88				
Mixed Forest	114	15	53	2	11	16	2	
Northern Rockies	36	28	39		11	22		
Southern Rockies	78	9	59	5	<i>12</i>	13	3	
Short Grass Prairie	81		2	2		<i>84</i>	11	
<i>Central</i>	(122) 67		3	1		(89) <i>93</i>	3	
South Texas Savanna	(108) 14			7		(95) <i>43</i>	50	
Tall Grass Prairie	242					17	70	13
	(201)					(0)	(84)	(16)
Broadleaf Forests	560	1		<1			4	94
Northern Hardwood	129	6					8	<i>86</i>
Deciduous Forest	234						6	<i>94</i>
Southeast Forest	189							<i>100</i>
Subtropical Forest	8			12				<i>88</i>
Total	1211	79						
		(82)						
Total (Drop Rocky Mountains)	1097	85						
		(88)						
Total (Accept Rockies, California, and Mixed Grass as Correct)	1211	94						

Both the northern and southern Rocky Mountain regions were poorly predicted. The over-simplistic pre-classification into one category each — conifers in the north and pinyon-juniper in the south — does not capture the vertical zonation of vegetation in these regions. Most of the weather stations in this highly dissected terrain occur in valley bottoms often dominated by shrubland or grassland (Küchler 1964, Vankat 1979). Classifications for the northern Rocky Mountains include conifer (28%), pinyon-juniper (11%), shrubland (39%), and short grass (22%). The southern Rocky Mountains are warmer, more xeric in winter, and wetter in summer, with conifer (9%), pinyon-juniper (12%), shrubland (59%), desert (5%), short grass (13%), and tall grass (3%). We examined most of these stations individually and concluded that these classifications are generally accurate. If the Rocky Mountain rule-based classifications are accepted as correct, model performance shifts from 79% to 90% overall. If the Rocky Mountains are removed from the classification, the performance is 85% (Table 1).

A third set of residual mis-classifications stems from 17% of the tall grass prairie stations being classified as short grass prairie. These stations are in a region in the northern plains designated by Küchler (1964) as mixed grass, a life-form for which we have not written a rule. Thus, our pre-classification as either short or tall grass is arbitrary. If these stations are accepted as correctly classified, performance of the model in the tall grass shifts from 70% to 84%, and the overall rating increases from 79% to 82%. If the mixed grass is accepted but both the Rockies and the central valley are excluded, accuracy of the model is 88%. If both the Rocky Mountains and the mixed grass classifications are accepted, the overall accuracy shifts to 93%. If the central valley classifications are also accepted, the overall accuracy is 94%.

The remaining cluster of residuals occurs where much of the prairie peninsula is classified as broadleaf forest rather than grassland. Classification of the prairie peninsula has been a particular challenge to biogeographers and climatologists (Borchert 1950, Corcoran 1982, Küchler 1972, Manogaran 1983, Transeau 1935). There is considerable debate as to whether the prairie peninsula is climatically determined or whether man historically induced the prairie through fire (Vankat 1979). Fires clearly play a major role in reducing the dominance of woody vegetation. However, a climatic classification of the prairie peninsula, based on a moisture index of Thornthwaite, indicates that the region is climatically unique (Manogaran 1983). The current configuration of the rule-base lacks the PET calculations necessary to reflect this unique climatology. The next version will incorporate the PET calculations.

The prairie peninsula also occurs at the convergence of two air mass gradients (Bryson 1966). As a consequence, regional rainfall gradients are relatively shallow (Neilson *et al.* 1989) and should exhibit considerable year-to-year variability. We tested the sensitivity of the prairie-forest border to small changes in the winter rainfall threshold. The prairie peninsula was most sensitive to these changes; the border locations to the north and south were more stable. It is possible that year-to-year variability of weather patterns produces extreme years that preclude long-term maintenance of forest in the prairie peninsula. We expect the model rendition of the prairie peninsula will improve with future enhancements.

Future Model Development

The primary limitation of the current configuration of the model is that it simulates only the *supply* side of the water balance. The next enhancement will be to include the *demand* side as driven by PET. Precipitation thresholds will be reevaluated as a function of seasonal PET and seasonal rainfall supply. Within the water balance thresholds for each life-form, water balance will be treated as a continuum and calculated using energy balance equations, allowing a prediction of leaf area as well as life-form (Woodward 1987). Regional information on soil water holding capacity and texture will be required to fine-tune the regional water balance estimates. The continued use of thresholds in the model recognizes the use of thresholds in defining physiognomic distinctions. It may be possible in the future to loosen this constraint and treat life-form physiognomies as a continuum. Grass physiognomy extends toward large and woody, as in bamboo, and woody plants extend toward small ephemerals, as in many semi-arid species.

With the incorporation of PET, the model will be complete enough for a preliminary estimate of 2×CO₂ impacts on biome distribution over the conterminous United States.

Qualitative estimates have been made based on the conceptual precursor to this model (Neilson *et al.* 1989). Biome boundaries are expected to shift several degrees of latitude and hundreds of meters of elevation.

Temperature constraints will also be added to the model to differentiate the mixed forests of the southeastern United States from the eastern deciduous forest and the temperate forest from the boreal forest (Figure 2). The model will also be extended to both boreal and tropical regions. These extensions will require very different kinds of rules than those developed for temperate zone biomes. For example, the current, thermally defined summer shortens with increasing latitude and disappears at about the latitude of the boreal forest. Likewise, the thermally defined winter does not occur in the subtropics, *i.e.*, the vicinity of Florida. Transect analyses, as applied in the United States (Neilson *et al.* 1989), will be extended to other parts of the world to assist in formulation of additional rules.

Calibration of the model with regard to secondary rules, those invoking fire and biotic interactions, will require continuing investigation. Since the natural environment expresses the influence of these processes, it is particularly difficult to assign thresholds that adequately constrain biomes in the absence of secondary rules. For example, the winter precipitation threshold below which shrubs cannot be supported is currently set at 80 mm (rule 5, Figure 4). This produces shrubland in the Great Basin and desert in the Southwest. It also produces shrubland throughout the Great Plains. The simultaneous presence of grassland in the plains invokes the secondary rules to shift the biome classification to grassland. If the winter threshold (rule 5) is set to 200 mm, fewer plains sites are attributed a shrub component, but the Great Basin becomes a desert. The Great Basin is characterized by a series of parallel mountain ranges separated by narrow valleys wherein the shrublands occur. The mountains collect winter precipitation, which can run off and infiltrate to deep soil layers in adjacent alluvial fans (Schlesinger and Jones 1984), providing greater deep soil water for support of shrubland than incident precipitation alone. Thus, we are left with a choice for secondary rules:

- Invoke fire in the plains to remove shrubs, or
- Invoke “run on” in the Great Basin to augment deep soil water and support shrubs.

The first option is used now, but there is little information as to the comparative degree to which these processes control shrubland distribution.

The model could be described as a demographic rather than an ecosystem model, since it simulates life-form (Beard 1978) but does not address nutrient dynamics (O’Neill *et al.* 1986). Alternative approaches to simulation of productivity and nutrient dynamics will be explored (*e.g.*, Jarvis and Leverenz 1983). Once the model incorporates an energy balance approach to determining the life-form thresholds, water flux through the ecosystems will be directly calculated. This information, coupled with water-use efficiency and energy-use efficiency parameters (Landsberg and McMurtrie 1985, Linder 1985, Montieth 1977, Tucker *et al.* 1986) should allow estimates of potential primary productivity. Potential productivity could be modulated by nutrient-use efficiency and soil nitrogen estimates (Prescott *et al.* 1989, Vitousek 1984). Decomposition rates could be parameterized as functions of temperature and moisture (Meentemeyer 1978).

Increased levels of CO₂ are known to increase productivity and water-use efficiency in many plants (Strain and Cure 1985). The potential importance of these effects at landscape and biome scales is under debate. If these effects are significant at a regional scale, then the impacts of climatic change could be considerably ameliorated, assuming the gradually increasing influence of direct effects of CO₂ is not preceded by adverse climatic effects of increasing trace gases, such as widespread drought. Also, even if direct effects prove important over a wide array of plants, it is not clear how much influence plant-scale water balance, modulated by the stomata, has over landscape-scale water balance. The latter appears to be largely driven by radiation and modulated by root density and depth and by leaf area (Federer 1982, Jarvis and McNaughton 1986). Clearly, stomatal processes will control rates of drying; however, the accurate simulation of drying curves may not be important at time steps of one month (Cowan 1965).

A particularly important enhancement to the model will be to move from steady state to transient dynamics. The potential spatial redistribution of biomes could be mediated by major diebacks or declines in some areas and advances in others (Neilson *et al.* 1989, Solomon 1986, Overpeck *et al.* 1990). Simulation of these dynamics will require both demographic and ecosystem processes. Dispersal of important tree types is expected to lag considerably behind the rapidity of climatic change and potential movement of boundaries (Davis 1986, Smith and Tirpak 1989). It will be important to incorporate functional categories of seed dispersal in the life-history characterizations (Beard 1978). As extra-tropical forests shift toward the poles, large areas of their current distributions could undergo severe, drought-induced decline and dieback (Neilson *et al.* 1989, Overpeck *et al.* 1990). These would be susceptible to fire. The release of CO₂ into the atmosphere from these fires and subsequent decay of the remaining dead biomass could produce a positive feedback to the "greenhouse effect" (Neilson *et al.* in prep.). The regrowth of burned landscapes and the potential expansion of the tropics could ameliorate this CO₂ pulse to some extent. We have begun modeling these processes and will incorporate these dynamics into future versions of the model.

Simulation of transient dynamics could also be necessary for accurate delineation of some biome boundaries. Sensitivity analyses on the winter precipitation parameter separating closed from open forest (375 mm), indicates the eastern extent of the prairie peninsula is quite sensitive to this parameter. Year-to-year variability of rainfall could be shifting this climatic transition considerably (Coupland 1958, Küchler 1972). Even though the average climate of the prairie peninsula may be suitable for forest establishment and growth, the extremes due to natural climatic variability could preclude their long-term viability in the region.

As model development continues, calibration and validation will be increasingly important. Although the focus has been on enhancements to the model, it is apparent that the calibration is very dependent on accuracy of the pre-classification. In the Rocky Mountains, for example, correct model calibration will require a much higher spatial resolution of biome type than needed for less mountainous terrain. Literature and existing maps will be useful in this endeavor. However, satellite technology has the potential to provide this classification at a comparatively high resolution (Tucker *et al.* 1985). Remote classification of vegetation should be a high priority for all the world's vegetation.

Three approaches to model validation will be explored:

- Implementation on another continent.
- Simulation of paleoclimates (Webb *et al.* 1990).
- Rescaling the model to a smaller, but heterogeneous extent.

We will attempt to validate the model through extension to other continents, attempts to reconstruct past vegetation, and attempts to rescale the model. Since the model is physically driven and is purported to be mechanistically based, it should apply at any scale of resolution. Thus, application to a heterogeneous watershed such as the Colorado drainage would be an interesting test of the model.

Conclusions

The initial stage of development of a rule-based, mechanistic model of vegetative life-form distribution has been described. Different life-form mixtures deduced from the rules produce different biomes, with demonstrated prediction potential of up to 94% accuracy. The current configuration of rules is based entirely on the seasonal patterns of regional water balance and the relation of these patterns to different plant life-forms. The apparent success of the model makes two important points.

- Regional water balance does appear to be a critical climatic mechanism determining plant distributions.
- Success of the model, even when the demand side of regional water balance (PET) was not directly considered, implies that on regional scales water balance is currently in equilibrium with the vegetation.

It follows that the atmospheric demand for water (PET) is in balance with the supply of water through transpiration. The regional rate of transpiration, according to theory (Woodward 1987), should be related to the amount of leaf area (biomass) over that region. The amount of leaf area over a region should be a direct result of ecosystem feedback processes that select for a specific leaf area as a function of water supply and atmospheric demand. The implication is that ecosystems are precariously balanced with respect to regional water balance and that a rapid change in either supply or demand for water could produce a catastrophic response from regional vegetation.

Being mechanistic in concept, future model enhancements to incorporate ecosystem and spatial demographic processes with temporal dynamics should be relatively straightforward, albeit challenging to implement. The value of these efforts, particularly when coupled with global atmosphere models and land-use characteristics, should be realized in a much improved predictive potential of global change and biosphere/atmosphere feedbacks.

References

- Abrams, M.D., A.K. Knapp, and L.C. Hulbert. 1986. "A Ten-Year Record of Aboveground Biomass in a Kansas Tallgrass Prairie: Effect of Fire and Topographic Position". *Amer. J. Bot.*, 73(10):1509-1510.

- Beard, J.S. 1978. "The Physiognomic Approach" in *Classification of Plant Communities*. Ed. Robert H. Whittaker. The Hague, Netherlands.
- Borchert, J.R. 1950. "The Climate of the Central North American Grassland". *Annals of the Association of American Geographers*, 15(1):1-38.
- Box, E.O. 1981. *Macroclimate and Plant Forms: An Introduction to Predictive Modeling in Phytogeography*. Dr. W. Junk Publishers. The Hague.
- Bryson, R.A. 1966. "Air Masses, Streamlines, and the Boreal Forest". *Geographical Bulletin* 8(3):228-269.
- Burke, M. J., L.V. Gusta, H.A. Quamme, C.J. Weiser, and P.H. Li. 1976. "Freezing Injury in Plants". *Annual Review of Plant Physiology*, 27:507-528.
- Corcoran, W.T. 1982. "Moisture Stress, Mid-Tropospheric Pressure Patterns, and the Forest/Grassland Transition in the South Central States". *Physical Geography* 3(2):148-159.
- Coupland, R.T. 1958. "The Effects of Fluctuations in Weather upon the Grasslands of the Great Plains". *The Botanical Review*, 23(5):273-317.
- Cowan, I.R. 1965. "Transport of Water in the Soil-Plant-Atmosphere System". *J. Applied Ecology*, 2:221-239.
- Davis, M.B. 1986. "Lags in the Response of Forest Vegetation to Climatic Change" in *Climate-Vegetation Interactions*. Ed. C. Rosenzweig and R. Dickson. OIES-UCAR, Boulder, CO.
- Dice, L.R. 1943. *The Biotic Provinces of North America*. University of Michigan Press. Ann Arbor. pp. 1-79.
- Federer, C.A. 1982. "Transpirational Supply and Demand: Plant, Soil, and Atmospheric Effects Evaluated by Simulation". *Water Resources Research*, 18(2):355-362.
- Jarvis, P.G., and J.W. Leverenz. 1983. "Introduction: Temperate Forest" in *Productivity of Temperate, Deciduous, and Evergreen Forests*. *Encyclopedia of Plant Physiology*. Springer-Verlag. Berlin. pp. 243-280.
- Jarvis, P.G., and K.G. McNaughton. 1986. "Stomatal Control of Transpiration: Scaling Up from Leaf to Region". *Advances in Ecological Research*, 15:1-49.
- Küchler, A.W. 1972. "The Oscillations of the Mixed Prairie in Kansas". *Erdkunde, Archiv für wissenschaftliche Geographie*, 26:120-129.
- _____. 1964. *The Potential Natural Vegetation of the Conterminous United States*. American Geographical Society Special Publication No. 36.
- Landsberg, J.J., and R. McMurtrie. 1985. "Models Based on Physiology as Tools for Research and Forest Management" in *Research for Forest Management*. Ed. J.J. Landsberg and W. Parsons. Proceedings of a Conference Organized by the Division of Forest Research, CSIRO, May 21-25, 1984. Canberra, Australia.
- Linder, S. 1985. "Potential and Actual Production in Australian Forest Stands" in *Research for Forest Management*. Ed. J.J. Landsberg and W. Parsons. CSIRO, Australia.

- Major, J. 1963. "A Climatic Index to Vascular Plant Activity". *Ecology*, 44:485-498.
- Manogaran, C. 1983. "The Prairie Peninsula: A Climatic Perspective". *Physical Geography*, 4(2):153-166.
- Marshall, J.D., and R.H. Waring. 1984. "Conifers and Broadleaf Species: Stomatal Sensitivity Differs in Western Oregon". *Can. J. For. Res.*, 14:905-908.
- Meentemeyer, V. 1978. "Macroclimate and Lignin Control of Litter Decomposition Rates". *Ecology*, 59(3):465-472.
- Monteith, J.L. 1977. "Climate and the Efficiency of Crop Production in Britain". *Phil. Trans. R. Soc. Lond. B.*, 281:277-294.
- Neilson, R.P. 1987. "Biotic Regionalization and Climatic Controls in Western North America". *Vegetatio*, 70:135-147.
- _____. 1986. "High-Resolution Climatic Analysis and Southwest Biogeography". *Science*, 232:27-34.
- Neilson, R.P., G.A. King, R.L. DeVelice, J. Lenihan, D. Marks, J. Dolph, B. Campbell, and G. Glick. 1989. *Sensitivity of Ecological Landscapes and Regions to Global Climate Change*. U.S. Environmental Protection Agency, Environmental Research Laboratory, Corvallis, OR.
- Neilson, R.P., and L.H. Wullstein. 1983. "Biogeography of Two Southwest American Oaks in Relation to Atmospheric Dynamics". *J. of Biogeography*, 10:275-297.
- O'Neill, R.V., D.L. DeAngelis, J.B. Waide, and T.F.H. Allen. 1986. "A Hierarchical Concept of Ecosystems" in *Monographs in Population Biology*. Ed. R.M. May. Princeton University Press. Princeton, NJ.
- Overpeck, J.T., D. Rind, and R. Goldberg. 1990. "Climate-Induced Changes in Forest Disturbance and Vegetation". *Nature*, 343:51-51.
- Prentice, K.C. 1990. "Bioclimatic Distribution of Vegetation for GCM Studies". *J. Geo. Res.* 95:11811-11830.
- Prescott, C.E., J.P. Corbin, and D. Parkinson. 1989. "Biomass, Productivity, and Nutrient-Use Efficiency of Aboveground Vegetation in Four Rocky Mountain Coniferous Forests". *Can. J. Res.*, 19:309-317.
- Quinlan, F.T., T.R. Karl, and C.N. Williams, Jr. 1987. *United States Historical Climatology Network (HCN) Serial Temperature and Precipitation Data*. Carbon Dioxide Information Analysis Center, NDP-019. Oak Ridge National Laboratory. Oak Ridge, TN.
- Runkle, J.R. 1985 "Disturbance Regimes in Temperate Forests" in *The Ecology of Natural Disturbance and Patch Dynamics*. Ed. S.T.A. Pickett and P.S. White.
- Running, S.W. 1975. "Environmental Control of Leaf Water and Conductance in Conifers". *Can. J. Res. For. Res.*, 6:104-112.
- Schlesinger, W.H., and C.S. Jones. 1984. "The Comparative Importance of Overland Runoff and Mean Annual Rainfall to Shrub Communities of the Mojave Desert". *Bot. Gaz.*, 145(1):116-124.

- Smith, J.B., and D. Tirpak (eds.). 1989. *The Potential Effects of Global Climate Change on the United States*. Report to Congress. U.S. Environmental Protection Agency. EPA-230-05-89-050. Washington, DC.
- Solomon, D.M. 1986. "Transient Response of Forests to CO₂-Induced Climate Change: Simulation Modeling Experiments in Eastern North America". *Oecologia*, 68:567-579.
- Stephenson, N.L. 1990. "Climatic Control of Vegetation Distribution: The Role of the Water Balance". *American Naturalist*, 135:649-670.
- Strain, B.R. and J.D. Cure. 1985. *Direct Effects of Increasing Carbon Dioxide on Vegetation*. U.S. Dept. of Energy, Carbon Dioxide Research Division DOE/ER-0238. Washington, DC.
- Thornthwaite, C.W. 1948. "An Approach Toward a Rational Classification of Climate". *Geographical Review*, 38:55-94.
- Thornthwaite, C.W., and J.R. Mather. 1955. *The Water Balance*. Publications in Climatology, Vol. VIII, No. 1. Drexel Institute of Technology. Centerton, NJ.
- Transeau, E.N. 1935. "The Prairie Peninsula". *Ecology*, 16(3):423-439.
- Tucker, C.J., I.Y. Fung, C.D. Keeling, and R.H. Gammon. 1986. "Relationship Between Atmospheric CO₂ Variations and a Satellite-Derived Vegetation Index". *Nature*, 319:195-199.
- Tucker, C.J., J.R.G. Townshend, and T.E. Goff. 1985. "African Land-Cover Classification Using Satellite Data". *Science*, 227:369-375.
- US WEST. 1988a. *Climatedata User's Manual: TD3200 Summary of the Day — Cooperative Observer Network*. US WEST Optical Publishing. Denver, CO.
- US WEST. 1988b. *Hydrodata User's Manual: USGS Daily and Peak Values, Version 2.0*. US WEST Optical Publishing. Denver, CO.
- Vankat, J.L. 1979. *The Natural Vegetation of North America*. John Wiley and Sons. New York.
- Vitousek, P.M. 1984. "Litterfall, Nutrient Cycling, and Nutrient Limitation in Tropical Forests". *Ecology*, 65(1):285-298.
- Waring, R.H., and J.F. Franklin. 1979. "Evergreen Coniferous Forests of the Pacific Northwest". *Science* 204:1380-1386.
- Webb, T.III, P.J. Bartlein, and J.E. Kutzbach. 1990. "Climatic Change in Eastern North America During the Past 18,000 Years: Comparisons of Pollen Data with Model Results" in *North America and Adjacent Oceans During the Last Deglaciation*. Ed. W.F. Ruddiman, and H.E. Wright. Geology of North America. Geological Society of America. Boulder, CO.
- Woodward, F.I. 1987. *Climate and Plant Distribution*. Cambridge University Press. London, England.

Skill of Monthly Forecasts during the Northern Hemisphere Summer

Kingtse C. Mo

ABSTRACT: We have performed GCM experiments using the National Meteorological Center's Medium Range Forecasting (MRF) model to study the skill of monthly forecasts during the Northern Hemisphere summer and to test the impact of sea surface temperature anomalies (SSTAs) on such forecasts. The daily skill varies a great deal. The skillful daily forecasts last from 5 to 8 days for the Southern Hemisphere and from 6 to 8 days for the Northern Hemisphere. SSTAs have positive impact on the forecasts in the tropics and surface variables, but the impact of tropical SSTAs on the extra-tropical circulations is, in general, positive but small. Overall, the initial conditions play a more important role than SSTAs in determining the forecast skill.

Description of Experiments

All experiments were done using the National Meteorological Center's spectral model of 1989 (NMC Staff 1988, Kanamitsu *et al.* 1990), which is the same as the current MRF (Medium Range Forecasting) model except that the horizontal resolution is T40 (320 km) instead of T80.

We performed two sets of experiments. The first set (SSTA) consisted of 30-day forecasts with sea surface temperature anomalies fixed at the initial date during the integration. For the summer of 1987, 1988, and 1989, three experiments were made using three different initial conditions around May 22, separated by one day. The second set of experiments (CSST) used the same initial conditions as the first set, but was run with climatological SST. We have 18 experiments in total.

All data presented here and initial conditions for the model experiments were derived from NMC analyses. Sea surface temperatures used were obtained from the NMC real-time global SST analysis (Reynolds, 1988). The SST climatology was that of Alexander and Mobley (1974). The June "climatology" of the model was obtained from the ensemble average of the nine 30-day means for all CSST experiments.

Skill of the 30-Day Mean Forecasts

Table 1 contains the extra-tropical anomaly correlations (AC), the root mean square (RMS) errors, and the correlation coefficients for the anomaly (CCA) as defined in Miyakoda *et al.* (1986) for 30-day mean 500 mb heights for each individual forecast as well as the ensemble means. Evaluations were done for the Northern Hemisphere (30N-90N), and Southern Hemisphere (30S-90S) separately. In general, the Northern Hemisphere CCA number is higher than the anomaly correlation for the same forecast, indicating some skill in predicting the domain-averaged anomalies. The skill varies considerably from one experiment to another. The inter-annual variability in the skill is much greater than that introduced by the slight shift of the initial conditions or the SSTAs.

Table 1
ANOMALY CORRELATIONS,
CORRELATION COEFFICIENTS FOR THE ANOMALY, AND
RMS ERRORS FOR 30-DAY MEAN 500 mb HEIGHTS

Extra-Tropical Northern Hemisphere (30N-90N)						
Initial Date	AC*100		CCA*100		RMS Error (m)	
	SSTA	CSST	SSTA	CSST	SSTA	CSST
5/22/87	16	30	34	49	35	51
5/23/87	28	32	46	42	50	47
5/24/87	32	29	42	45	57	49
Ensemble	24	31	39	50	51	47
5/21/88	59	50	71	64	38	42
5/22/88	41	24	56	47	47	47
5/23/88	65	31	75	52	32	46
Ensemble	60	42	71	60	34	38
5/21/89	6	- 7	22	20	52	52
5/22/89	- 3	-12	14	23	53	60
5/23/89	2	10	28	37	52	70
Ensemble	7	2	26	31	48	54
Extra-Tropical Southern Hemisphere (30S-90S)						
Initial Date	AC*100		CCA*100		RMS Error (m)	
	SSTA	CSST	SSTA	CSST	SSTA	CSST
5/22/87	38	41	38	20	54	57
5/23/87	37	45	25	44	48	60
5/24/87	45	39	44	22	55	54
Ensemble	48	43	45	25	47	56
5/21/88	37	39	37	33	65	68
5/22/88	52	33	52	28	64	71
5/23/88	42	53	42	43	59	69
Ensemble	50	46	50	37	59	66
5/21/89	75	54	74	52	52	52
5/22/89	66	51	67	52	53	60
5/23/89	42	54	44	12	52	70
Ensemble	72	40	75	42	48	54

The Southern Hemisphere forecasts are consistently more skillful than those for the Northern Hemisphere, perhaps because winter is more predictable. All Southern Hemisphere forecasts with SSTAs are skillful or nearly so, but only the 1988 Northern Hemisphere forecast can be considered skillful. June 1988 was marked as a cold ENSO event. It was also the month that the heat wave and drought in the midwestern United States peaked. The flow pattern during this month was quasi-stationary. In general, the model is more skillful in predicting persistent flow regimes.

Experiments using CSST do not reduce skill significantly. The spread among three SSTA forecasts for a given year is as large as the difference in skill due to the SST anomalies.

Skill of Daily Forecasts

Figure 1 shows the anomaly correlations for daily ensemble means of the 500-mb anomalies for the CSST and SSTA experiments for the Northern Hemisphere and Southern Hemisphere. The forecast is considered skillful if the anomaly correlation is greater than 0.6. The evolution of the daily skill varies a great deal from case to case. The daily forecasts are skillful for 5 to 8 days in the Southern Hemisphere and for 6 to 9 days in the Northern Hemisphere.

Our results agree with findings of Palmer and Owen (1986) that, in general, there are no significant differences in skill for experiments with and without SSTAs for the first 10 days and that beyond the first 10 days, the SSTA experiments are better than CSST experiments. After the first 10 days, however, the anomaly correlations drop to 0.2 to 0.3. This means the forecasts have deteriorated to the point of having little or no skill, so the improvement from knowing SSTAs may not be very useful.

To study the skill scores for forecasts in the tropics, we turned to the 200 mb stream functions. Figure 2 shows the anomaly correlations for daily ensemble means in the tropics (30N -30S) for SSTA and CSST experiments. The dashed lines represent the 95% confidence intervals for daily ACs for the SSTA experiments and full lines with circles are the daily AC after correcting the systematic errors. The systematic error is defined as the difference between the model climatology and the CAC climatology based on NMC analyses. The ACs of the SSTA experiments are clearly higher than those of CSST experiments throughout the 30 days of the forecasts. After 10 days, the model starts to drift toward its own climatology. The correction of systematic error will help forecasts in the tropics.

Discussion

In general, the model produces useful forecasts up to 7 days. After that, the model starts to drift to its own climatology. For the 30-day means, the model is able to produce reasonable rotational part of the flow. The main jetstreams in both hemispheres are reasonably simulated. The major deficiency is in the tropics.

Figure 3 gives the 200-mb divergence for June climatology based on the NMC analyses and for the model's climatology. The model reproduces the major areas of convection over the land masses in the Northern Hemisphere over central America, Africa, and the Indonesian maritime continent and summer monsoon. However the magnitudes of the divergence associated with the tropical convection and associated convergence are significantly underestimated. The model fails to simulate the strength of convection in the western and central Pacific. This failure occurs in the first 3 days of the simulation, and this may have affected the extratropical forecasts during the warm ENSO event.

Shukla and Fennessy (1988) suggested that a correctly simulated heating mechanism is essential for a successful prediction. If the model cannot transfer the message of the SSTAs to the corresponding heating field, then the extra-tropical forecasts will not benefit from the additional information associated with the SSTAs. If the model simulates the convection associated with SSTAs correctly, the impact of SSTAs will still take a few days to affect the extra-tropical circulation. For this reason, we do not see large differences

Figure 1
ANOMALY CORRELATION FOR DAILY ENSEMBLE FORECASTS OF THE
500-MB EXPERIMENTS FOR THE NORTHERN HEMISPHERE AND SOUTHERN HEMISPHERE

Solid Line = CSST Experiments
 Solid Line and Circles = SSTA Experiments
 Dashed Line = 95% Confidence Level for CSST Experiments

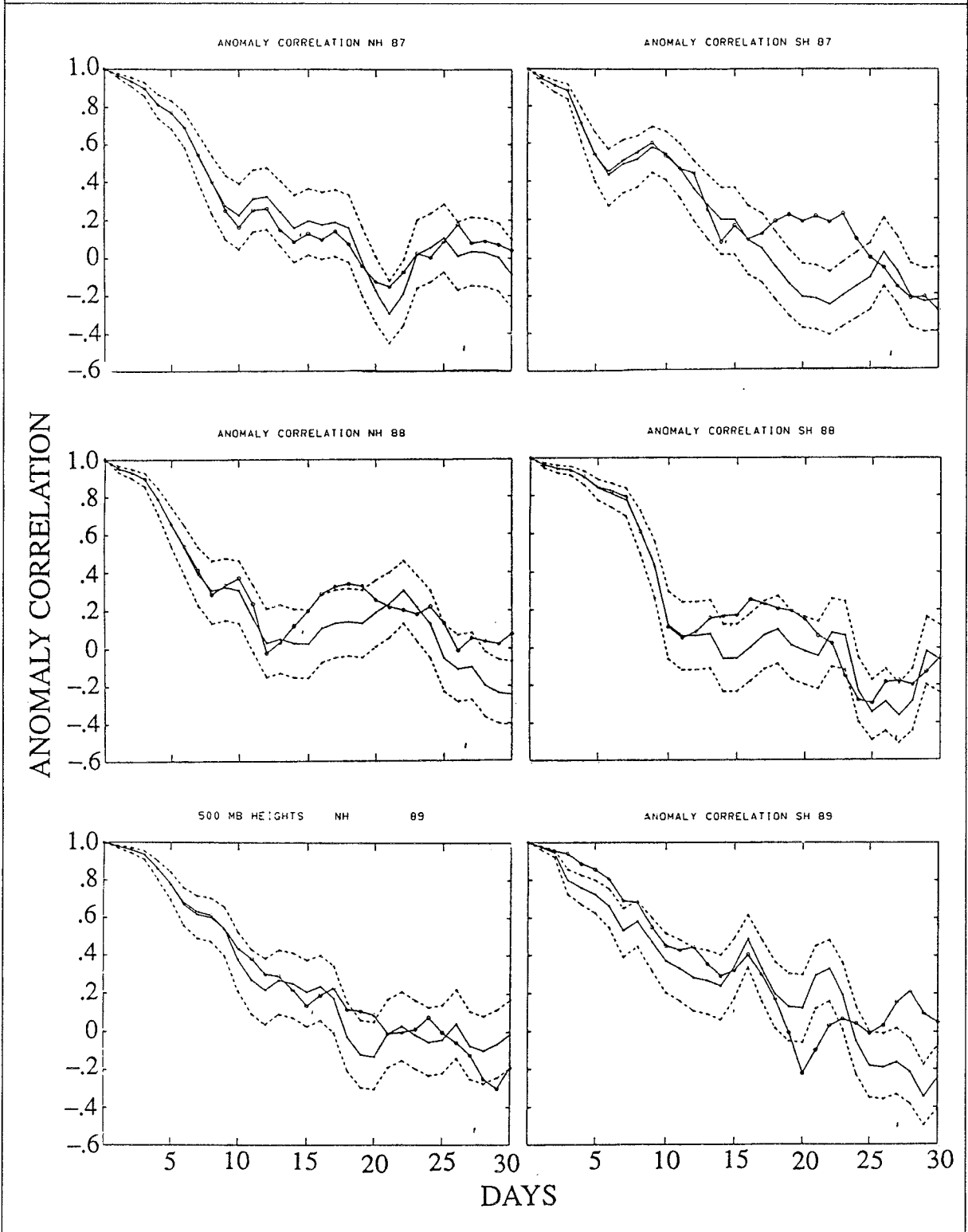


Figure 2
ANOMALY CORRELATION FOR
DAILY ENSEMBLE FORECASTS OF THE
TROPICAL 200-MB STREAM FUNCTIONS

Solid Line=SSTA Experiments
 Solid Line and Circles=SSTA Experiments After Systematic Error Correction
 Dashed Line=95% Confidence Level for SSTA Experiments
 Dashed Line and Circles=CSST Experiments

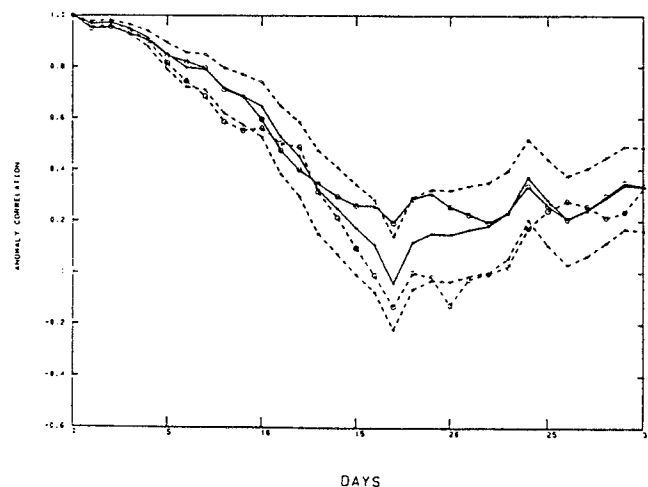
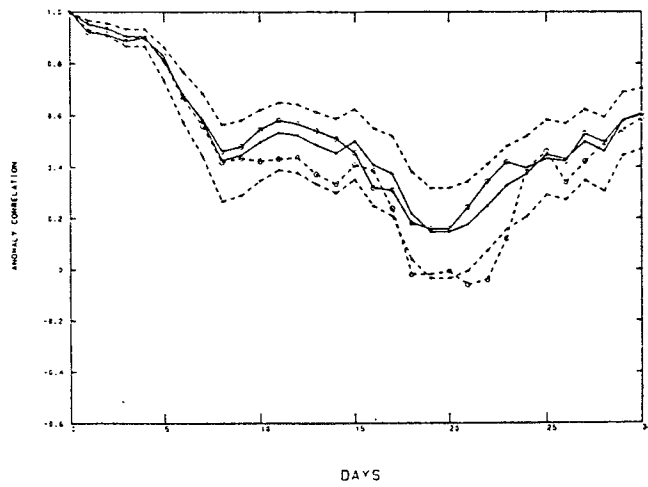
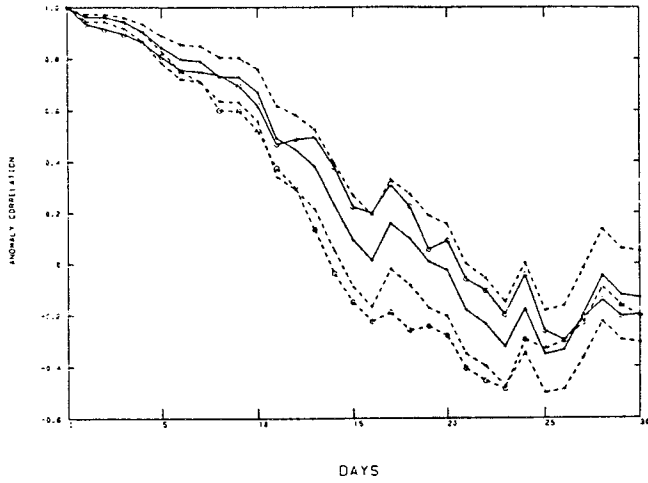
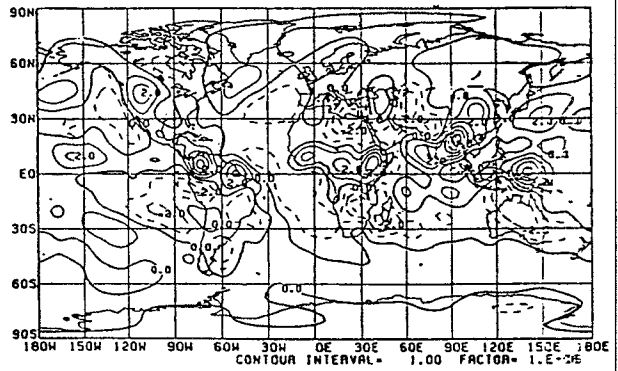
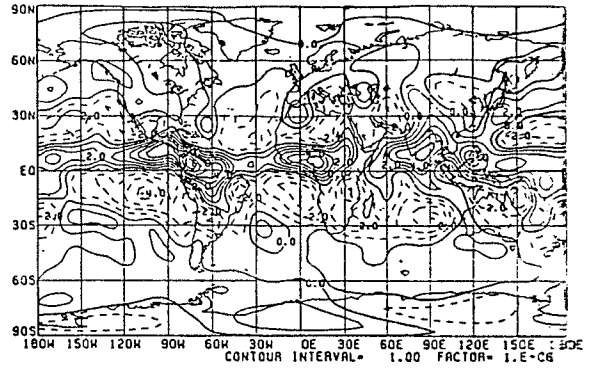


Figure 3
200-MB DIVERGENCE FOR THE
CAC CLIMATOLOGY (1986-1989) AND
FOR THE MODEL'S CLIMATOLOGY

Contour Interval = 1.E-06/second



between experiments with and without SSTAs for the first 10 days. During that time, the transient eddies and the interaction between middle scale waves and planetary waves determine the outcome of forecasts (Tracton 1990).

Overall, the interannual variability in initial conditions plays a more important role than the variations of the boundary forcing in determining the forecast skill of monthly forecasts. Palmer (1988), O'lenic and Livezey (1989), and many others have suggested that the skill of extended range forecasts is regime-dependent. If the initial flow is in a rather stable regime, then the forecasts are likely to have higher skill. This may explain why initial conditions are more crucial than the SSTAs in determining the outcome of forecasts.

References

- Alexander, R.C. and R.C. Mobley. 1974. *Monthly Averaged Sea Surface Temperatures and Ice Pack Limited on a 1 Degree Global Grid*. Rand Corp. R-1310 ARPA. 1974.
- Kanamitsu, M., K.C. Mo, and E. Kalnay. 1990. "Annual Cycle Integration of the NMC Medium Range Forecasting Model". *Mon. Wea. Rev.* 118:2543-2567.
- Miyakoda, K., J. Sirutis, and J. Ploshay. 1986. "One Month Forecast Experiments Without Anomaly Boundary Forcing". *Mon. Wea. Rev.*, 110:2363-2401.
- NMC Staff. 1988. *Documentation of the Research Version of the NMC Medium Range Forecasting Model*. National Oceanic and Atmospheric Admin., NMC Division. Washington, DC.
- O'lenic, E.A. and R. Livezey. 1989. "Relationships Between Systematic Errors in Medium Range Numerical Forecasts and Some of the Principal Modes of Low Frequency Variability of the Northern Hemisphere 700 mb Circulation". *Mon. Wea. Rev.*, 117:1262-1280.
- Palmer, T.N. 1988. "Medium and Extended Range Predictability and Stability of the Pacific/North American Mode". *Quart. J. Roy. Meteor. Soc.*, 114:691-713.
- Palmer, T.N. and J.A. Owen. 1986. "Forecast and Sensitivity Experiments on the UK Meteorological Office GCM with El Niño SST Anomalies". *Proceedings of the Workshop on Comparison of Simulations by Numerical Models of the Sensitivity of the Atmospheric Circulation to Sea Surface Temperature Anomalies*. World Meteorological Organization, TD 138:81-94.
- Reynolds, R.W. 1988. "A Real Time Global Sea Surface Temperature Analysis". *J. Climate*, 1:75-86.
- Shukla, J. and M.J. Fennessy. 1988. "Prediction of Time Mean Atmospheric Circulation and Rainfall Influence of Pacific SST Anomaly". *J. Atmos. Sci.*, 45:9-40.
- Tracton, M.S. 1990. "Predictability and Its Relationship to Scale Interaction Processes in Blocking". *Mon. Wea. Rev.* 118:1666-1695.

Wind Climate Trends in the Pacific Northwest and the Implications to Renewable Energy Supply

John E. Wade and Kelly T. Redmond

Abstract: This paper examines the influence of wind climate variations on new Pacific Northwest renewable energy sources. Wind represents a potentially valuable supplemental source of energy in the region. Hydroelectric provides about 85% of the region's electrical energy. Wind climate variation was found to have significant impact on availability of both energy sources. Since 1976, weaker winds were noted both at the surface and at higher levels in the atmosphere. The weaker winds were associated with up to an estimated 19% less wind energy available at some sites and 15% reduction in streamflow (measured at The Dalles on the Columbia River). The recent period of weaker winds may be associated with a stronger North Pacific Low in the last decade. This would result in winter storms more often being deflected farther north, to Canada. Also, in the last dozen years, lower SOI values were common. Other investigators have found low SOI to be associated with drier conditions in the Pacific Northwest.

Introduction

An implicit assumption in energy planning is that future climate will be similar to past climate. This assumption is often incorrect, but utilities have found there is little risk in assuming a steady-state climate. Planners use 30-year means, standard deviations, and ranges about the means to determine possible future climate variations. Normally, climate changes encountered will be within the variations described by these 30-year statistics.

In the past, utilities on the West Coast have operated with large reserve capacity. This reserve capacity and the flexibility of purchasing additional power from Canada and through interties have made energy planning somewhat insensitive to climate variation outside climate "normals". However, the prospect of global climate change may increase the vulnerability of energy planning to climate change. Utilities systems, particularly in the southwestern United States, are operating with smaller reserve capacity. New capacity additions are experiencing delays, and some transmission systems are approaching their limits. The combination of western United States utilities operating closer to the margin and the possibility of climate changes outside those in the past 10,000 years suggest challenges ahead for energy planners.

Most discussion about the influence of climate change on energy planning is focused on the demand side. Warm climate increases air conditioning and irrigation energy demand and reduces winter heating demand. Cool climate increases winter heating and reduces summer cooling demand. In the western United States, and particularly in the northwest, climate also has an important impact on energy supply. About 85% of the northwest's electrical energy is supplied by hydroelectric power. Hydroelectric energy supply is climate-dependent, as are wind and solar, two supplemental energy sources.

This paper discusses the sensitivity of wind and hydroelectric energy supply to climate change.

Background

The investigation began as an attempt to determine how representative the wind climate for 1976-1983 was of a 30-year period (see Wade *et al.* 1986). (Thirty years represents the lifetime of wind turbine generator blades.) The study used surface wind data at several locations on the Oregon Coast and upper air data at Medford and Salem, Oregon. Winds measured along the coast were about 16% weaker than the 35-year mean. A consistent trend of below-average winds, both at the surface and higher levels in the atmosphere, were found in western Oregon, confirming earlier results by Redmond (1985). These findings were important for wind energy, because a 16% reduction in wind speed means a 42% reduction in available energy, due to the cubic relationship between wind speed and energy. The reduction in amount of energy produced by a turbine will be less, because a wind turbine cannot use all the energy available in the wind.

Wind is an important supplemental source of energy, but still makes up less than 1,400 megawatts of available capacity, compared to more than 45,000 megawatts of hydroelectric capacity in the western United States. The snow that falls in the mountains is carried in by winter storms. Weaker winds aloft are associated with weaker and less frequent storms and less snowpack. Less snowpack results in less hydroelectric energy. Subsequent studies (Wade *et al.* 1987 and 1989) found this trend of weaker wind circulation over the entire Pacific Northwest.

Method

The approach used was to determine the extent to which the winds measured from 1976 to 1987 represent the long-term wind climate (*i.e.*, a 30-year period). The years 1976-1987 represent the period over which wind data have been collected for Bonneville Power Administration's regional wind energy assessment.

Surface and upper air data were examined for the entire Pacific Northwest. For surface data, only sites with a long-term wind history at one anemometer height were considered. Few records went back before the 1950s because anemometer heights have varied so much. (In the 1960s, many airports selected 20 feet as an ideal anemometer height.) Upper air wind variations were examined at the seven Pacific Northwest upper air observing locations. Upper wind levels examined were for 850 mb (about 5,000 feet above mean sea level, or *msl*), 700 mb (near 10,000 feet *msl*), and 500 mb (about 35,000 feet *msl*). Upper air data have been collected via balloon soundings twice a day for the last 40 years.

A statistical model was developed to reconstruct the wind record at three wind energy survey sites with continuous data since 1976. Winds at these sites were correlated to nearby surface or upper air wind measurements at locations with 30 years' of data to reconstruct a wind record. Normalized departures from the mean for 1976-1987 for the wind energy survey site were correlated to normalized departures at the predictor long-term reference site.

To estimate the implication of long-term variations in wind speed to energy output, three types of wind turbines were used to compare projected output for 1976-1987 to projected output before 1976. The average percent difference in annual energy output for the three turbines was used to assess energy implications of wind climate variations over time.

Long-Term Trends in Wind Speed in the Pacific Northwest

Five long-term National Weather Service surface wind sites in the Pacific Northwest were examined for annual wind speed variation at surface anemometer height (Table 1). Sites were chosen because anemometer height at each of them remained stable for a relatively long period. All sites show a recent small decrease in mean annual wind speed. Changes in local roughness may also account for some of the recent wind speed decreases evident in Table 1. While it is possible to adjust wind data for changes in height, it is more difficult to correct for changes in surface roughness and exposure.

Table 1
MEAN ANNUAL SURFACE WIND SPEED,
STANDARD DEVIATION, AND PERCENT CHANGE SINCE 1976
(in miles per hour)

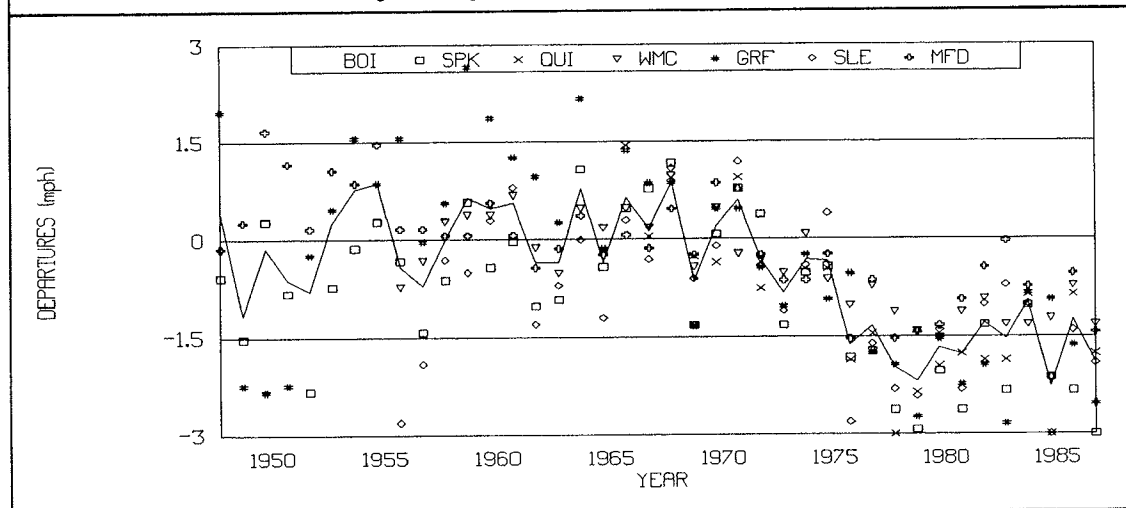
	Seattle- Tacoma WA	Pocatello ID	No. Bend OR	Salem OR	Medford OR
Period	1960-1987	1960-1987	1960-1987	1960-1987	1960-1987
Mean before 1976	8.5	10.0	8.5	7.2	4.9
Standard Deviation before 1976	0.9	0.6	0.4	0.4	0.3
Mean, 1976-1987	8.3	9.7	8.1	6.5	4.8
Standard Deviation, 1976-1987	0.2	0.3	0.3	0.4	0.2
Percent Change	-2.4	-3.0	-5.9	-9.2	-1.2

NOTE: Seattle-Tacoma: Moved 2,800 feet southwest of previous site from 1/1/60 to 12/2/69.
Pocatello: Began recording at 20 feet 8/6/60.
North Bend: 20 feet 1/60-12/87.
Salem: 20 feet since 2/59.
Medford: 20 feet since 5/59.

Winds aloft provide wind speed measurements over time at constant height and pressure levels. Figure 1 shows annual wind speeds for the seven National Weather Service upper air sites at the 850 millibar level. The figure shows distinctly weaker winds over the last 11 years than were measured previously. This was also evident at other pressure levels (700 and 500 mb).

Figure 1
ANNUAL VARIATION OF WIND SPEED AT THE
850-MILLIBAR LEVEL AT SEVEN PACIFIC NORTHWEST LOCATIONS

Winds are given as departures (in mph) from the mean before 1976.



To evaluate the association between wind climate variation and hydroelectric energy supply, the modified streamflow for January through July at The Dalles was compared to winter 850-millibar winds at Spokane, Washington. Normalized departures from the mean for the period 1949 to 1987 were plotted for both time series. The Dalles is the second to last dam on the Columbia River, and Spokane is the upper air site nearest the most important part of the Columbia River watershed.

At the 850-mb level, the decrease in wind speed over 1976-1987 was similar at all seven upper air sites (Table 2). Since many of the best potential wind energy development sites are at high elevations, results in Table 2 are of considerable interest. We would expect wind measurements at sites on well exposed ridgetops to be closely related to measurements in the free air at about 5,000 feet msl (1,500 meters). Winter showed the most evidence of recent weaker winds at sites. Summer had the least evidence of weaker winds aloft.

Site	Percent Departure From:	
	All Years Before 1976	1966-1975 Mean
Quillayute, WA	-10%	-10%
Spokane, WA	-11%	-13%
Boise, ID	-11%	-11%
Great Falls, MT	-11%	- 9%
Salem, OR	- 9%	-11%
Medford, OR	-11%	- 9%
Winnemucca, NV	11%	-11%

Reconstructing Wind Energy Potential Before 1976

For the Cape Blanco wind energy site, we used wind data at North Bend Airport as a long-term reference. North Bend is also along the coast, but is about 50 miles north of Cape Blanco. The energy output for the most recent period at Cape Blanco was estimated to have decreased by 6%, which is similar to the wind speed deficit (Table 3). Much of the stronger wind during the reconstructed period at Cape Blanco would have been outside the operating range of the three representative wind turbines. Data used to reconstruct the Kennewick winds prior to 1976 were the 850-mb winds at Spokane. The Kennewick anemometer site is at elevation 2,200 feet. Data in Table 3 suggest wind speeds at Kennewick were stronger before 1976 by about 11% ($\pm 5\%$). Estimated average annual energy output of the three wind turbines would be 14% lower than what we estimate would have been available before 1976. At Pequop Summit, wind speeds were estimated to be 14% stronger before 1976 than after. An average of 19% more annual energy output would have been available with wind speeds estimated before 1976. The predictor information for Pequop Summit, at 7,500 feet, consisted of the Winnemucca 850 mb winds.

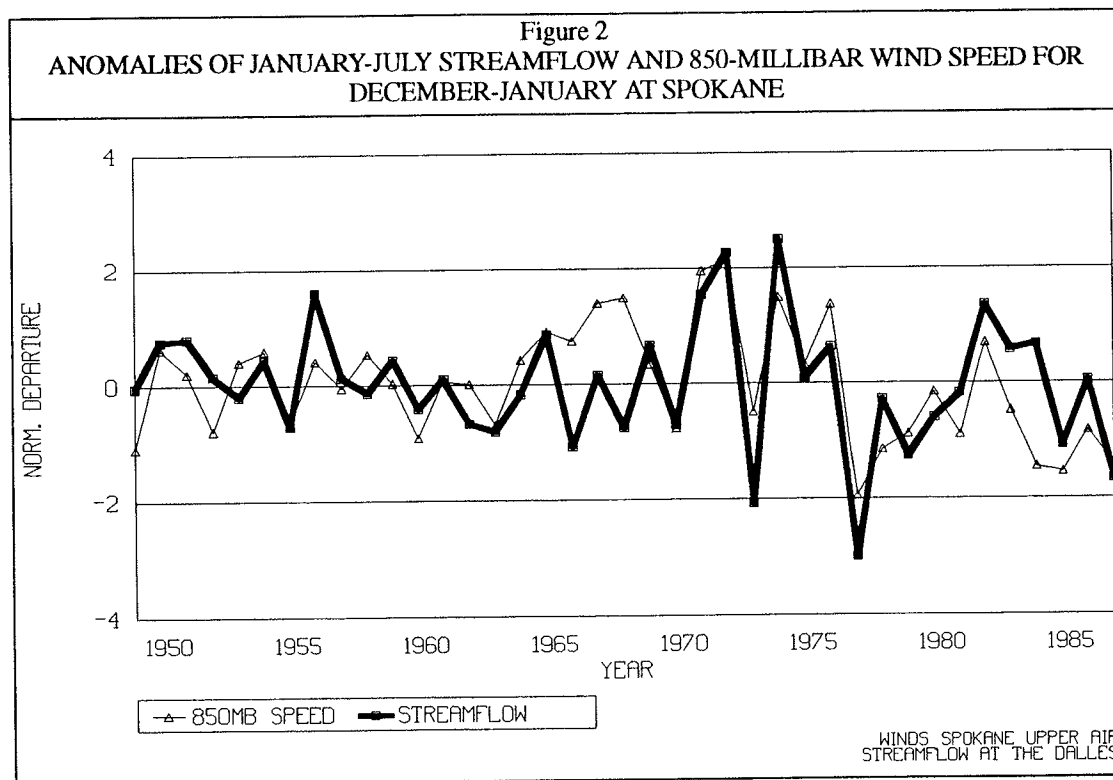
Wind Energy Site/ Reference Site	Velocity 1976-1987 (mph)	Velocity 1950-1976 (mph)	Percent Speed Difference	Percent Energy Difference
Cape Blanco	18.7	20.0	-6.5 \pm 4.2	- 6
North Bend	7.9	8.7	-9.2	
Kennewick	15.4	17.3	-11 \pm 4.9	-14
Spokane 850 mb	14.6	6.7	-13	
Pequop Summit	15.4	17.9	-14 \pm 4.5	-19
Winnemucca 850 mb	9.4	10.6	-11	

Relationship of Wind Climate to Hydroelectric Supply

Wind climate variations are associated with variations in another source of renewable energy — hydroelectricity. Although most precipitation in this region occurs from November through March, peak streamflow is during the spring and early summer, when snow melts in the mountains. The amount of January through July streamflow determines how much energy Bonneville Power Administration will have to supply Pacific Northwest customers. Flow exceeding 90 million acre-feet (about 90% of average) can be sold to other utilities in the western United States.

Figure 2 shows a comparison of the strength of winter winds at 850 mb to January-July streamflow at The Dalles. Weaker winter winds are associated with lower streamflow. These results support earlier work by Cayan and Peterson (1989) who found that effects of large-scale circulation anomalies can be detected in the variation of streamflow in the western United States. They found these circulation anomalies most evident in winter, when atmospheric circulation was most variable. When the North Pacific Low is strong, storms tend to be carried northward into British Columbia, so the Pacific Northwest is dry. When the low is weak, the jet stream carries ample moisture over the Pacific Northwest, resulting in high streamflow.

Redmond and Koch (1990) and Wade *et al.* (1989) noted that the Southern Oscillation index (used to identify El Niño events) is also related to streamflow and winter precipitation in the Pacific Northwest. High SOI values are related to high precipitation and higher streamflow. Since 1976, when weaker winds have prevailed in the Pacific Northwest, the SOI has been lower and the North Pacific Low has been stronger. At the same time, January-July streamflow for 1977 through 1987 has been about 15% lower than for the previous 11 years (1966-1976), when high SOI and weaker North Pacific Lows were more frequent.



Conclusions

- Winds measured in the Pacific Northwest from 1976 through 1987 were weaker than those measured before 1976 at many surface and all upper air locations.
- Estimates of wind energy availability based on the winds measured since 1976 will be conservative for most of the region. For the three wind energy sites with over a decade of wind data the estimated decrease in annual energy output for the past eleven years varied between 6 and 19%.
- The results of this investigation suggest that weaker winds aloft in the winter months in the Northwest are associated with reduced streamflow on the Columbia River during the January to July runoff period.
- The January to July streamflow for 1977 through 1987 has been about 15% lower than for the previous 11 years (1966-1976) when high SOI values and weaker North Pacific Lows were more frequent.
- Climate change that would result in a weakening of the prevailing westerly flow in the winter and spring months will influence the supply of hydroelectric energy in the Pacific Northwest.

Acknowledgments

The research described in this paper was performed by the authors while associated with Oregon State University and supported by a contract from the Bonneville Power Administration.

References

- Cayan, D.R. and D.H. Peterson. 1989. "The Influence of the North Pacific Atmospheric Circulation on Streamflow in the West" in *Aspects of Climate Variability in the Pacific and the Western Americas*. Ed. D.H. Peterson. *Geophysical Monograph*, 55:375-397.
- Redmond, K. 1985. *Wind Speed Trends in Southern Coastal Oregon*. Wind Resource Assessment Laboratory Report. Corvallis, OR.
- Redmond, K. and R. Koch. 1989. "Western Surface Climate and Streamflow and the El Niño/Southern Oscillation" in *Proceedings of the 1990 ASCE National Conference on Hydraulic Engineering and International Symposium on the Hydraulics/Hydrology of Arid Lands*. San Diego, CA, July 30-August 3. p.567-572.
- Wade, J.E., R.W. Baker, W.G. Butler, and A. Duncan. 1986. "The Meteorological Aspects of a Windfarm Feasibility Study" in *Proceedings of the ASME Wind Energy Symposium*. New Orleans, LA.
- Wade, J.E., R.W. Baker, and S.N. Walker. 1989. *Regional Wind Energy Assessment Report*. Bonneville Power Administration. Report 89-33. Portland, OR.
- Wade, J.E., K. Redmond, and P.C. Klingeman. 1989. *The Effects of Climate Change on Energy Planning and Operations in the Pacific Northwest*. Bonneville Power Administration. Report 89-29. Portland, OR.
- Wade, J.E., R.J. Wittrup, K. Redmond, and J.R. Buckley. 1987. *Climate Change in the Pacific Northwest and Its Impact on Energy Planning: A Preliminary Report of Findings*. Bonneville Power Administration. Report 87-26. Portland, OR.

Climate Variability and Crater Lake Water Levels

Kelly T. Redmond

Abstract: Crater Lake has fluctuated in elevation by 5 meters during the 20th Century. Reasons for these fluctuations were investigated as part of a long-term study of the Crater Lake ecosystem. Lake level changes were found to be closely related to precipitation variations. The lake can be thought of as acting as both a giant precipitation gage and as a large evaporation "pan". Winter snowfall variations are related to variations in the Southern Oscillation Index. Crater Lake offers a unique combination of simple geometry and hydrology, and a long record of supporting data, available nowhere else in the world for a caldera lake.

Introduction

An apparent decrease was noted in the exceptional clarity of Crater Lake, in Oregon, during the late 1970s and early 1980s. In 1982, Congress mandated a 10-year study of the physical, chemical, and biological characteristics of the lake and its environment. The goals were to:

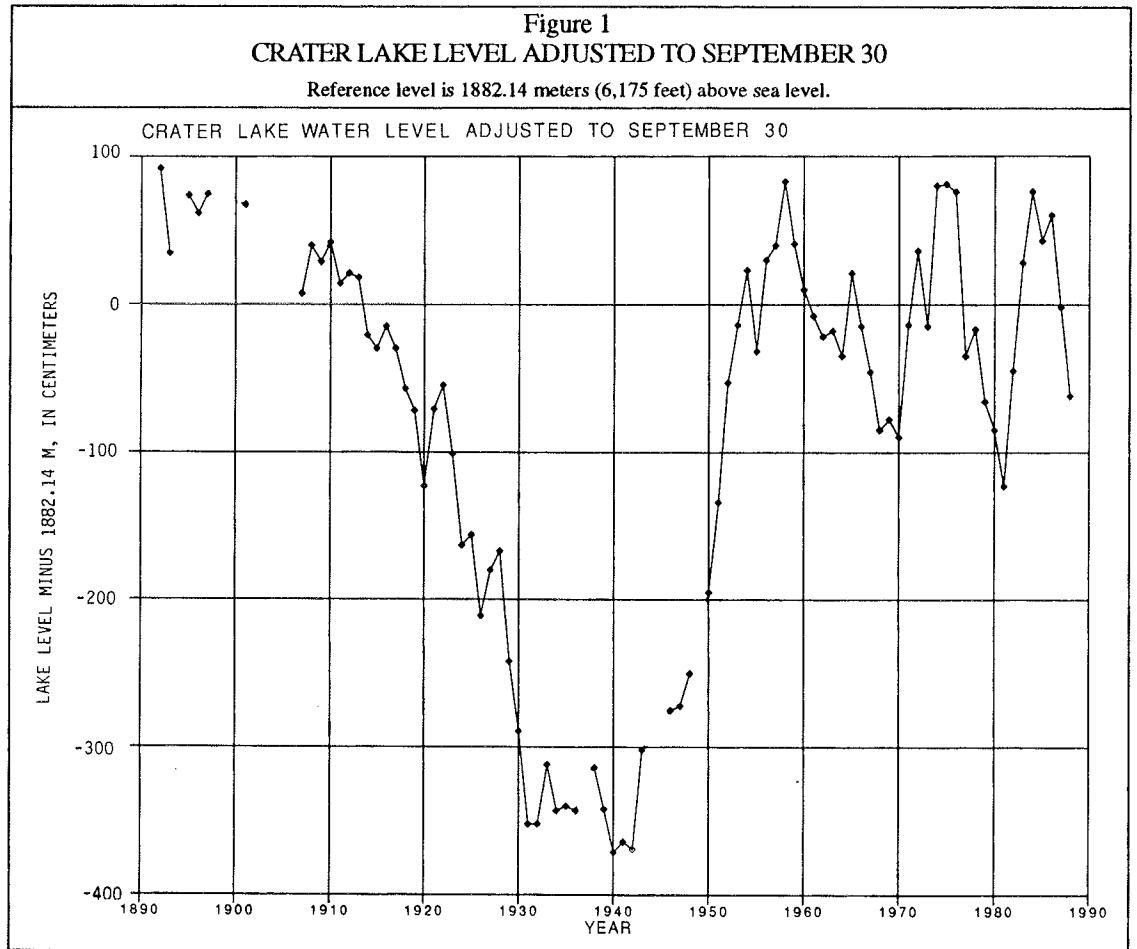
- » *Develop a reliable data base for future use.*
- » *Develop a better understanding of the behavior of the lake and surrounding areas.*
- » *Establish a long-term monitoring program.*

The program was directed by Gary Larson of the Cooperative Park Studies Unit in the College of Forestry at Oregon State University (Larson 1990). Other dimensions of this limnological investigation addressed the paleohistory of the lake, the chemistry of the lake and springs that feed it, a series of deep dives in manned submersibles to search for hydrothermal activity, and interactions among biological communities in the lake and their relationship to the external environment.

The surface elevation of Crater Lake has varied over a range of about 5 meters during the 20th Century (Figure 1). The most prominent feature in this record is an extended period of low water during the 1930s. More modest fluctuations of 1 or 2 meters have occurred during the past three decades. The primary purpose of this work was to explain these variations.

Physical Setting

Crater Lake lies in a caldera atop the gentle crest of the Cascade Range and is surrounded by steep cliffs. Water surface is at elevation 1882.14 meters (6,175 feet). The rim has an average elevation of 2100 meters, with high points to 2500 m. The rim and the lake surface are above the surrounding landscape, which has an average altitude near 1500 m. The lake is nearly circular, with a surface area of 53 square kilometers. The lake occupies 78.5



percent of its own drainage basin. Crater Lake is the seventh deepest lake in the world, with the deepest point at 589 m. No streams spill over the rim, and none leave the lake. Water enters and exits almost entirely through seepage and evaporation, with a small contribution from blowing snow.

Data

Daily weather measurements have been made since 1931 at park headquarters (elevation 2173 m) 2 km from the southwest side of the lake. Water level and temperature have been measured daily throughout the year by automated equipment on the northeast side of the lake since 1961, with sporadic readings since the late 1800s. These readings, referenced to a pin in a rock, are mostly from the warmer months, since access is difficult and dangerous in winter.

Climate

Crater Lake shares the general climate of the Pacific Northwest. Winters are very wet and summers are very dry. Measurable precipitation occurs less than 10 percent of the days in July, 60 percent of the days in January, and 140 days a year, on average. Park headquarters receives 167 centimeters of precipitation annually, mostly as snow. The park sits astride a sharp climatic divide. Storage gages show annual precipitation decreases across the lake from about 200 cm on the southwest rim to about 100 cm on the northeast rim.

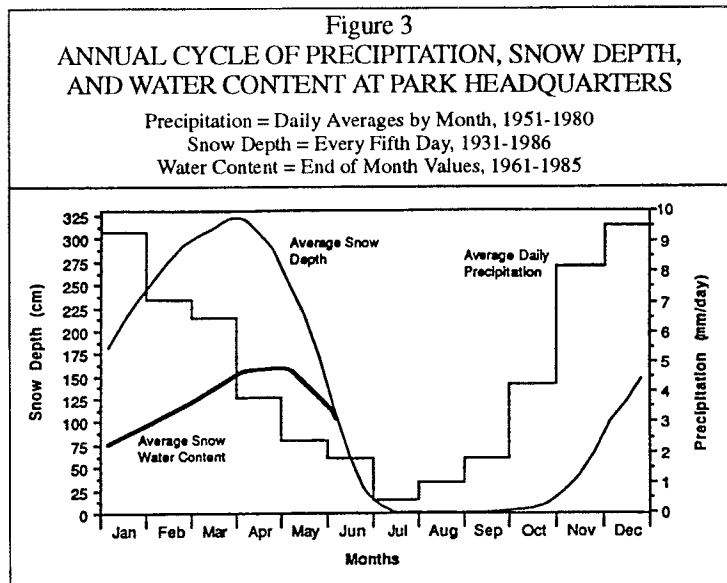
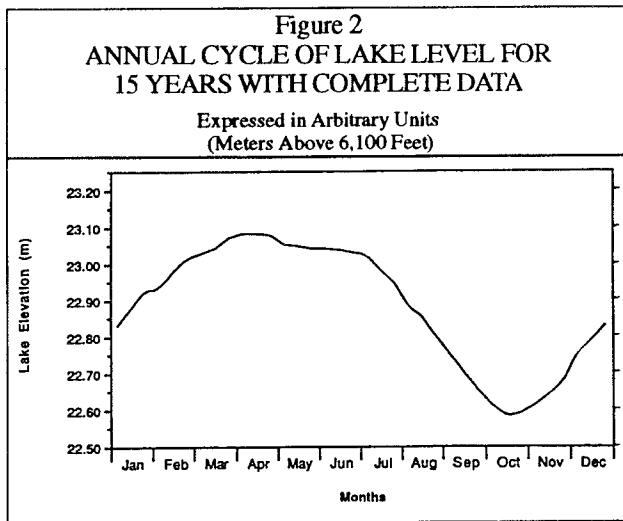
Annual snowfall at park headquarters is 1306 cm. Snow begins to accumulate in early November, reaching an average depth of 325 cm near the end of March, with an average water content of 160 cm at park headquarters.

Through most of the year, average air temperature is lower than that of the water surface, which ranges from 4 to 5°C from March through May to about 15°C in August.

Lake Water Budget

The lake rises and falls about half a meter annually, with a broad peak in late April and a minimum in late October (Figure 2). Lake level rises sharply as the winter precipitation begins in October. Much of this rise is from direct precipitation on the lake. After the peak of the wet season, the lake stays high. By June, even though precipitation declines greatly, the lake typically has fallen very little. Melting of the copious snowpack supplies most of this water.

After the last of the snow has melted, usually around July 1, the lake begins to drop steadily toward its autumn minimum (Figures 2 and 3). The rate of seepage appears to be constant throughout the year (Redmond 1990), with the difference between precipitation and evaporation responsible for most temporal variations in the rate of change of lake surface elevation.



Climatic Variations and Lake Level

Decadal fluctuations in the water flux across the lake/air interface are assumed to be the primary reason for lake level changes. Variability in either precipitation or evaporation, or both, could account for changes in this flux on annual time scales. Because the time series of annual evaporation is more difficult to construct, initial investigations focused on whether precipitation variations alone could account for year-to-year lake level changes.

Most precipitation in western Oregon results from travelling synoptic-scale disturbances, with a considerable percentage falling from stratiform clouds. Precipitation amounts thus tend to be quite well correlated in space, at annual, seasonal, monthly, and in many cases

even daily time scales. Although precipitation recorded at park headquarters is not necessarily equal to the lake basin average precipitation, the ratio between the two should be fairly constant.

The relationship between annual water year (October-September) precipitation at park headquarters and the lake level change from one September 30 to the next can be expressed as:

$$LLC = -246.5 + 1.457*PHQ \quad (r^2 = 0.915)$$

where *LLC* is the lake level change (cm) and *PHQ* is park headquarters precipitation (cm).

The relationship is based on years since the gaging station was installed. A strong association exists between precipitation and lake level changes.

Because the precipitation record at park headquarters only begins in 1931, nearby stations were used to estimate water year precipitation for prior years. Because of its long record, Roseburg, 105 kilometers to the west and 1800 meters lower in elevation, was selected. The correlation in water year precipitation between the two locations from 1931 to 1987 is $r=0.79$. The Roseburg record was used to reconstruct Crater Lake precipitation back to 1890.

Lake levels were then reconstructed from the observed plus reconstructed precipitation record for park headquarters. The method was:

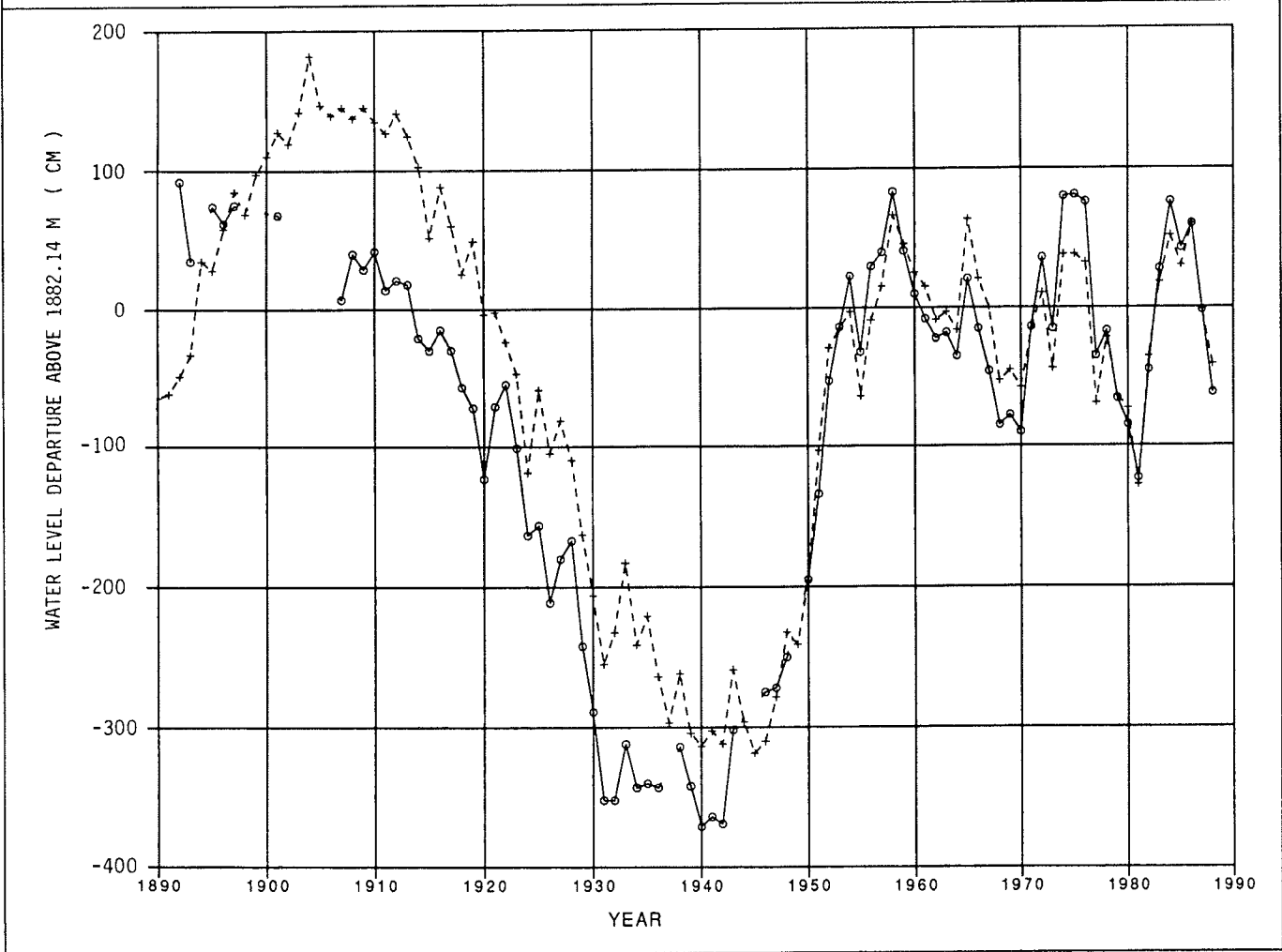
- Begin with the known level at a recent date (here, September 30, 1986).
- Use the regression relationship (above) with Crater Lake precipitation (observed or estimated) to estimate the annual change in lake level.
- Subtract this change from the current level to obtain an estimate of the previous year's level.
- Repeat this process each year, stepping backward in time.

The lake level as reconstructed by this process is shown in Figure 4, along with the observed levels. The rate of decline in lake level during the 1920s is well simulated, as is the rapid lake level rise around 1950. As can be seen, a poor estimate of lake level change in any given year will appear as a constant difference from observed lake level until counterbalanced by another equal estimation error of the opposite sign.

Crater Lake was closed during much of World War II, and monthly precipitation values for several years (1942-1946) have been estimated from nearby sites. Apparently precipitation for one or more of the years 1944-1946 was not well estimated, or the ratio of basin-averaged precipitation to headquarters precipitation differed in those years. The effect is that lake level is overestimated by about a meter for all earlier years back to about 1905. A change in location is noted at the Roseburg site in 1905, so perhaps the record there is not homogeneous. This matter was not explored further. Since 1950, lake level variations are simulated well by precipitation variations alone.

The extended period of low water in the 1930s is also reflected in other streamflow and lake level records in the vicinity.

Figure 4
RECONSTRUCTED AND OBSERVED LAKE LEVEL ON SEPTEMBER 30,
ESTIMATING FORWARD AND BACKWARD FROM SEPTEMBER 30, 1986
 Based on Crater Lake precipitation measured since 1931 and estimated from Roseburg for prior period.
 Reconstructed + Observed o



Residuals from the regression equation between LLC and PHQ were examined for evidence of a stage/seepage relationship. No indication was found that more seepage occurs when the lake is high than when it is low. This is not surprising, given that the fractional change in depth this century has been less than one percent of the total depth.

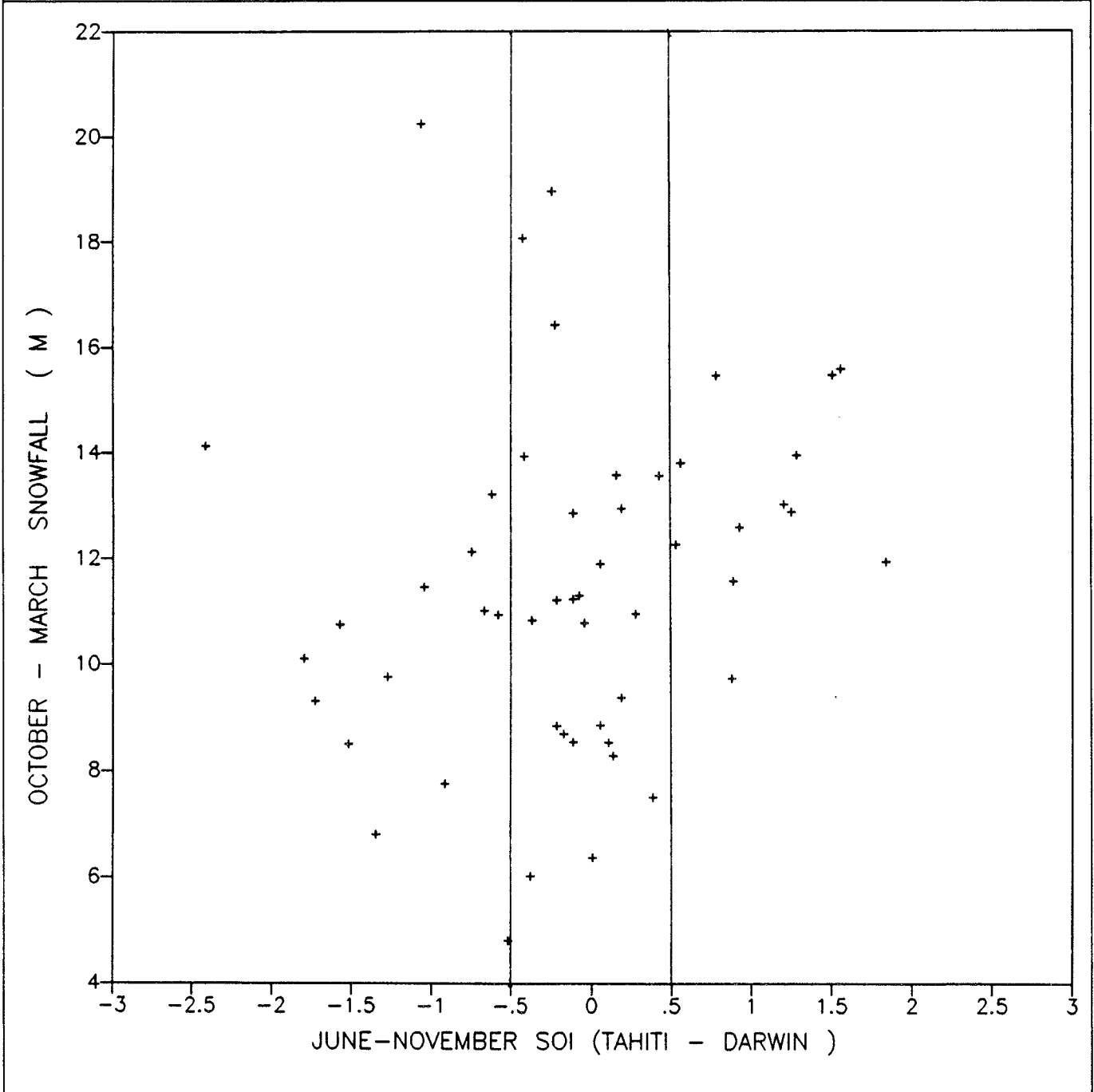
Crater Lake and El Niño/Southern Oscillation

Other work (Redmond and Koch 1990) has shown that precipitation in the Pacific Northwest and in the Desert Southwest has a strong association with the Southern Oscillation Index (SOI), which in turn is closely related to occurrence of El Niño or its “anti-El Niño” counterpart. The SOI consists of the standardized difference in sea level pressure at Tahiti minus Darwin, Australia. Negative SOI (“El Niño”) is associated with wet winters in the southwestern United States and dry, warm winters in the northwest; positive SOI is associated with the reverse. Furthermore, the strongest correlations are found when SOI values lead climate variables by 4 months. Low precipitation and warm temperatures imply less snowfall.

Figure 5 is a scatter plot for 52 years of October-March snowfall against previous June-November average SOI. Years with 6-month SOI values exceeding 0.5 receive an average of 13.2 meters of snow during these 6 months, compared with 10.8 meters in years with average SOI values below -0.50 ($P < 0.05$). Crater Lake is somewhat south of the area of maximum correlation between SOI and winter precipitation found by Redmond and Koch (1990), located in the Puget Sound and northern Cascades region.

Figure 5
 RELATIONSHIP BETWEEN JUNE-NOVEMBER SOUTHERN OSCILLATION INDEX
 AND OCTOBER-MARCH SNOWFALL AT PARK HEADQUARTERS
 1933-34 THROUGH 1988-89 (EXCEPT 1942-43 TO 1945-46)

Vertical lines indicate SOI values of +0.50 and -0.50.



Summary and Discussion

Elevation of the Crater Lake water surface has fluctuated by about 5 meters this century. Changes are controlled primarily by variations in evaporation and precipitation. Year-to-year changes in the lake level are closely associated with precipitation variations. Fluctuations in annual evaporation are, thus, not as important, or else evaporation variations are related to precipitation variations.

Since precipitation occurs in winter and evaporation has been assumed by previous workers (e.g., Phillips 1968, Simpson 1970) to occur primarily in summer, at first glance it might be expected that precipitation will be poorly correlated with evaporation. However, intriguing evidence from various phases of the present work indicates considerable evaporation may be occurring in the cooler portions of the year and on cooler days during the warm portion of the year.

Physical considerations show this to be plausible (Derecki 1981). In winter, vertical stability is much lower (the lake almost never freezes and is thus almost warmer than the overlying air), wind speeds are higher, and relative humidity averages near 60 percent in the free air (over nearby Medford), all of which promote evaporation. Future work will explore this further. For these purposes, Crater Lake can be essentially considered to act as a large evaporation pan.

Additional evidence has been presented showing winter snowpack variations are related to variations in the Southern Oscillation Index.

References

- Derecki, J.A. 1981. "Stability Effects on Great Lakes Evaporation". *J. Great Lakes, Res.*, 7:357-362.
- Larson, G.L. 1990. "Status of the Ten-Year Limnological Study of Crater Lake, Crater Lake National Park" in *Crater Lake: An Ecosystem Study*. Ed. E.T. Drake, G.L. Larson, J. Dymond, and B. Collier. Pacific Division, AAAS, California Academy of Sciences. San Francisco. pp. 7-18.
- Phillips, K.N. 1968. *Hydrology of Crater, East, and Davis Lakes, Oregon*. U.S. Geological Survey. Water Supply Paper 1859-E.
- Redmond, K.T. 1990. "Crater Lake Climate and Lake Level Variability" in *Crater Lake: An Ecosystem Study*. Ed. E.T. Drake, G.L. Larson, J. Dymond, and B. Collier. Pacific Division, AAAS, California Academy of Sciences. San Francisco. pp. 127-142.
- Redmond, K.T. and R.W. Koch, 1990. "Western Surface Climate and Streamflow and the El Niño/ Southern Oscillation" in *Proceedings of ASCE International Symposium on the Hydraulics/ Hydrology of Arid Lands*. San Diego, CA, July 30 to August 3. pp 567-572.
- Simpson, H.J. 1970. "Tritium in Crater Lake, Oregon". *Jour. Geophys. Res.*, 75: 5195-5207.

The Influence of Seasonal Precipitation and Temperature Variations on Runoff in California and Southwestern Oregon

Larry G. Riddle, Daniel R. Cayan, and Edward Aguado

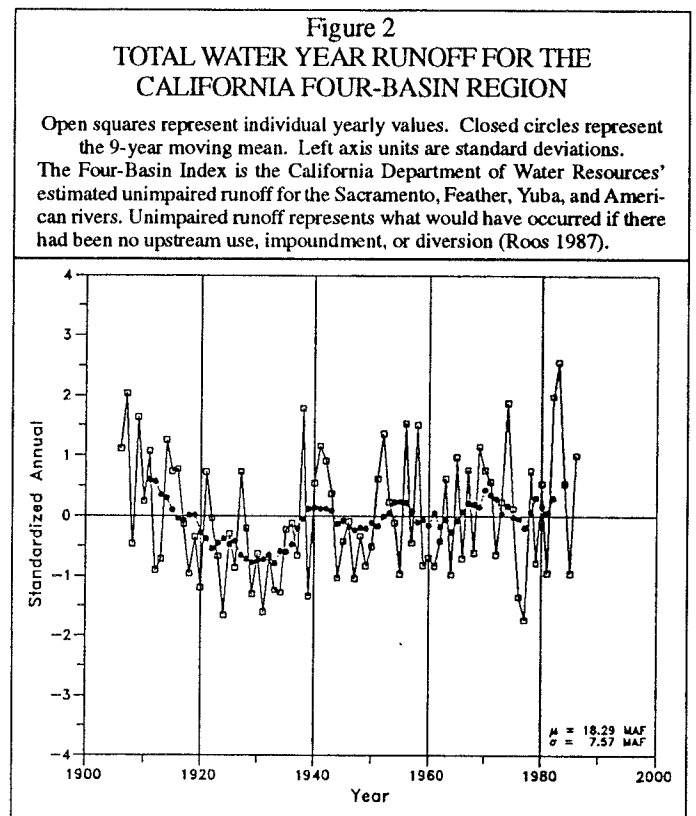
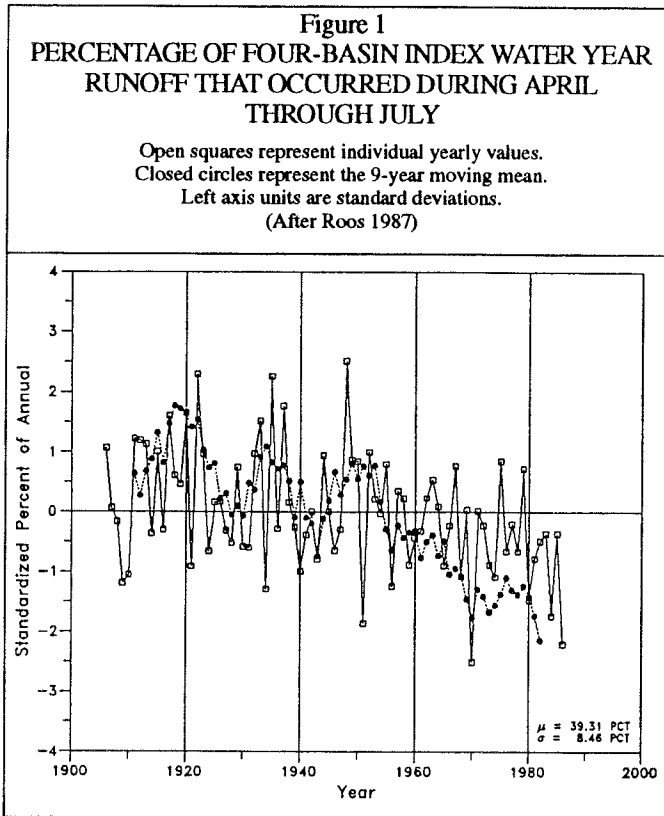
ABSTRACT: There is considerable seasonal-to-interannual variability in the runoff of major watersheds in the Sierra Nevada, Coastal, and Cascade ranges of California and southwestern Oregon. This variability is reflected in both the amount and timing of runoff. This study examines that variability using long historical streamflow records and seasonal mean temperature and precipitation. Both measured seasonal and fractional seasonal runoff are examined in sets of primary and secondary basins at low, moderate, and high elevations. Linear regression models are derived for the primary basins using a training period of 37 water years to determine the relationship between precipitation, air temperature, and runoff in the various seasons. Model-predicted runoff for the training period and a second 37-year independent test period are compared to observed runoff during those periods. Analysis shows seasonal precipitation and temperature will normally explain at least 60% of the seasonal runoff variation during both periods. Using the primary basin models to predict secondary basin runoff is achieved with little loss of skill. Precipitation is the only significant predictor for both amount and timing of runoff in the low elevation basins. As elevation increases, the models rely more and more on temperature to explain amount and timing of runoff.

Introduction

There is considerable interannual variation in annual and seasonal runoff in the Sierra Nevada, Coastal, and Cascade ranges of California and southwestern Oregon. The coefficient of variation (*CV*) for annual runoff is: Smith River, 63; Cosumnes River, 112; and upper San Joaquin River, 82.

Because of this variability, the seasonal timing of runoff and the magnitude of peak annual streamflow also vary considerably over time and are not well related to magnitude of total water year runoff. (A water year is from October 1 through September 30.) Of particular importance is an apparent decline in spring and early summer runoff from the Sierra Nevada, first observed by Roos (1987) and colleagues at the California Department of Water Resources. While measured water-year (*WY*) and April-July (*AMJJ*) runoff have increased, the *AMJJ/WY* fractional runoff has decreased by about 10% over nearly 80 years of record. Figure 1 reveals this trend since about 1950 in the Sacramento basin. At the same time, there has been no trend in the magnitude of annual runoff (Figure 2).

Further inspection shows that many streams in the West, from the John Day in north-central Oregon to the Kern in Southern California, have similar significant declines in spring/early summer fractional runoff. The cause is complex, involving both precipitation and temperature. For many basins, the fractional spring/early summer runoff is affected by climatic behavior across all the seasons. In the Sierra Nevada, the decreased *AMJJ* fraction appears to have been produced by increased precipitation in late-summer, fall, and winter, with decreased precipitation in spring. In addition, temperature along the west coast has increased during the non-summer seasons, enhancing earlier runoff and possibly



evapotranspiration in spring, although no change was observed that is not consistent with natural variation.

The trend toward earlier runoff may negatively affect agriculture, California's major consumer of water (Kahrl 1978), especially in the Central Valley. More than 80% of the region's precipitation occurs during November through March (the cool season), with total precipitation increasing with both latitude (from south to north) and elevation (from low to high). The high elevation reporting stations normally accumulate from 400% to 500% more precipitation than at nearby low elevation stations, most of it as snow (Lydolph 1985). Although the majority of west coast precipitation occurs during winter, it is not needed for irrigation until the height of the growing season, spring and early summer (AMJJ).

California depends on the Sierra Nevada snowpack to store winter precipitation until it is needed during the growing season (Rooney 1969). About half of the Sierra Nevada snow storage area is in moderate elevation basins that are extremely sensitive to temperature (Roos 1989). Thus, it is important to determine how variation in timing is affected by climate variation.

California's mean annual precipitation is about 247 km³, of which 146 km³ (59%) is lost to nonagricultural evapotranspiration and 87 km³ (35%) eventually becomes runoff. The remaining 6% is consumed primarily by soil moisture and ground water recharge. Slightly more than half the runoff (46 km³) is consumed by the people of California. The largest use is for agriculture, accounting for 39 km³ or 85% of the consumptive use (Kahrl 1978).

In years with below average runoff, the human-use fraction increases dramatically, even though consumption may decrease in absolute terms. Equal in importance to the amount of flow is the character (timing and uniformity) of the flow. If a larger fraction of the runoff

occurs earlier in the water year, more emphasis must be placed on Sierra Nevada reservoirs as storage for agricultural water. These reservoirs are multipurpose facilities (agriculture, flood control, and recreation), and it is difficult to balance the conflicting demands of agriculture (requiring full reservoirs for irrigation) and flood control (maximizing storage capacity to absorb storm and snowmelt surges).

Climate is one decisive factor in determining quantity and character of streamflow (Bruce and Clark 1966). The other is basin elevation (Cayan and Peterson 1989). Water managers would benefit from a better understanding of how climate (specifically precipitation and temperature) and elevation affect the phasing of runoff. This study examines the dependence on temperature and precipitation of seasonal runoff and the seasonal fraction of water year runoff in California and southwestern Oregon. For comparison, three pairs of low, moderate, and high elevation streams are considered. Questions addressed are:

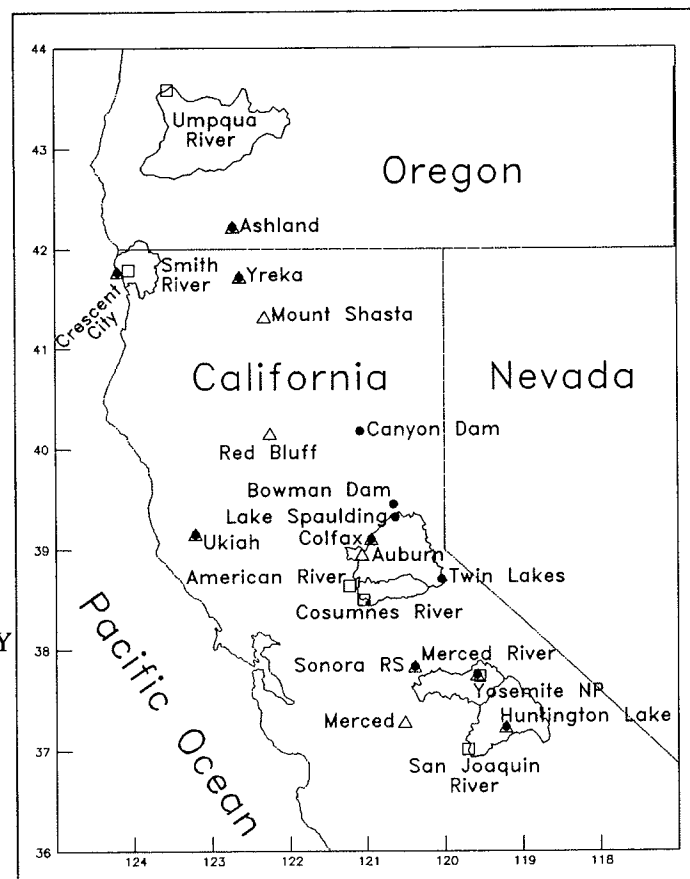
- How is seasonal variation in runoff affected by fluctuations in seasonal temperature and precipitation?
- How is the seasonal fraction of total water year runoff affected by fluctuations in seasonal temperature and precipitation?

Data and Methodology

The study area runs from the south-central Sierra Nevada Mountains near Fresno, California, northwestward to the inter-montane region around Roseburg, Oregon (Figure 3).

Figure 3
LOCATIONS OF PRIMARY AND SECONDARY RIVER BASINS USED IN THIS STUDY

Open squares show river gaging stations.
Open triangles show temperature stations.
Closed circles are precipitation stations.



From this region, three pairs of primary and secondary river basins were selected for study. Basin pairs consist of a primary and secondary basin for each of three mean elevation ranges:

Low – Smith and Umpqua (less than 1000 meters),

Moderate – Cosumnes and American (1000 to 2000 meters)

High – Upper San Joaquin and Merced (greater than 2000 meters).

Statistical models relating primary basin runoff to regionally averaged air temperature and precipitation are obtained through multiple linear regression. The resulting models are verified by applying them to the secondary basins. Data used are monthly and seasonal streamflow for the six primary and secondary basins (Table 1) and seasonal mean regional precipitation and temperature anomalies derived from long-term National Weather Service and cooperative stations for the three primary basins (Table 2).

Streamflow records used cover water years 1913 through 1986 except for the Merced River, where the record does not begin until 1916, and the Smith River, where the record begins in 1932. Streamflow data were extracted from U.S. Geological Survey daily streamflow data on the EarthInfo, Inc. (formerly USWest Optical Publishing) *HYDRO-DATA CD-ROM Volume 2.0*, using the USWest software. Unimpaired streamflow for the upper San Joaquin River was obtained from the California Department of Water Resources.

Monthly total precipitation and mean temperature anomalies were used to make seasonal totals and averages for the primary basins. Precipitation data for 1980 and earlier are from the California Department of Water Resources. Precipitation data for 1981 through 1986 are from National Climatic Data Center, NOAA via EarthInfo, Inc. *CLIMATEDATA CD-ROM Volume 2.01* and EarthInfo software. Temperature data were provided by J. Goodridge, former climatologist for the California Department of Water Resources.

Care must be exercised in the selection of climatic data sets, because changes in instrument location or surroundings can contaminate natural variability. Most stations with long records have undergone some change (Cayan and Douglas 1984). Stations used in this study were selected on the basis of length of record, location, elevation, compatibility with surrounding stations, and absence of any apparent “step-function” changes in long-term trends.

Four precipitation and four temperature stations (Table 2) were selected for each primary basin. Co-located temperature and precipitation stations were chosen when available, usually in the lower elevations, since high elevation temperature stations are not as common as high elevation precipitation stations.

Monthly mean streamflow, total precipitation, and air temperature anomalies were graphed as time-series curves after being passed through a 109-month (equivalent 9-year) Gaussian low-pass filter to illustrate long-term trends (Figures 4 and 5). Several stations were rejected on the basis of having trends or step functions, but four stations from each primary basin were identified where the low frequency variability appeared natural.

Table 1
PRIMARY AND SECONDARY RIVERS USED IN THIS STUDY

Units for monthly and annual streamflow means are cubic meters per second.
"CoVar" is the dimensionless coefficient of variation (standard deviation divided by the mean and multiplied by 100).
"Percent" is the percent of annual runoff occurring in that month.

Cosumnes River at Michigan Bar

Mean Basin Elevation:	1121m			Area:	1388 km				Location:	38.50N 121.04W			
Period:	1908-1987			Gauge Elevation:	51m				Agency:	USGS			
	O	N	D	J	F	M	A	M	J	J	A	S	Annual
Mean	0.9	4.3	12.9	25.7	34.1	33.6	31.3	19.9	7.2	1.7	0.6	0.4	14.4
CoVar	137.5	220.3	166.7	117.5	91.5	79.2	69.9	70.2	83.9	94.9	100.0	114.3	112.2
Percent	0.23	0.53	2.51	7.48	14.90	19.76	19.45	18.17	11.50	4.18	0.97	0.33	

American River at Fair Oaks

Mean Basin Elevation:	1433m			Area:	4890 km				Location:	38.64N 121.23W			
Period:	1905-1986			Gauge Elevation:	22m				Agency:	USGS			
	O	N	D	J	F	M	A	M	J	J	A	S	Annual
Mean	28.0	51.9	92.4	140.5	167.0	174.7	194.2	198.0	131.2	59.7	37.2	30.8	108.8
CoVar	93.5	130.4	117.3	103.6	81.6	71.5	57.6	59.3	71.7	76.1	102.3	109.2	89.5
Percent	2.36	2.14	3.98	7.08	10.76	12.79	13.38	14.87	15.16	10.05	4.58	2.85	

San Joaquin River (Estimated Unimpaired Flow)

Mean Basin Elevation:	2286m			Area:	3354 km				Location:	37.01N 119.70W			
Period:	1901-1988			Gauge Elevation:					Agency:	CalDWR			
	O	N	D	J	F	M	A	M	J	J	A	S	Annual
Mean	10.7	16.0	26.6	37.8	51.3	67.8	117.3	207.4	196.0	86.2	27.8	12.3	71.4
CoVar	95.2	105.0	123.0	96.2	76.8	61.0	42.8	43.2	59.0	91.0	88.3	97.0	81.5
Percent	1.43	1.25	1.87	3.11	4.41	5.99	7.91	13.69	24.19	22.86	10.05	3.24	

Merced River at Happy Isles Bridge, Yosemite NP

Mean Basin Elevation:	2743m			Area:	469 km				Location:	37.73N 119.56W			
Period:	1916-1987			Gauge Elevation:	1224m				Agency:	USGS			
	O	N	D	J	F	M	A	M	J	J	A	S	Annual
Mean	1.1	1.8	2.5	2.3	3.0	5.0	15.1	36.2	35.4	13.1	3.2	1.3	10.0
CoVar	133.3	169.8	155.1	91.4	72.6	50.6	38.7	36.4	54.0	88.8	108.8	140.0	95.0
Percent	1.06	0.92	1.49	2.10	1.91	2.50	4.20	12.56	30.17	29.49	10.93	2.67	

Smith River at Crescent City

Mean Basin Elevation:	457m			Area:	1577 km				Location:	41.79N 124.05W			
Period:	1932-1987			Gauge Elevation:	27m				Agency:	USGS			
	O	N	D	J	F	M	A	M	J	J	A	S	Annual
Mean	32.3	140.8	220.8	243.9	221.3	187.2	124.6	79.2	34.2	15.0	9.6	9.8	109.9
CoVar	153.1	86.3	65.7	59.0	51.0	47.9	51.8	55.2	59.3	36.2	27.1	65.4	63.2
Percent	0.75	2.45	10.68	16.74	18.50	16.78	14.19	9.45	6.00	2.60	1.13	0.73	

Umpqua River at Elkton

Mean Basin Elevation:	756m			Area:	9539 km				Location:	43.59N 123.55W			
Period:	1906-1987			Gauge Elevation:	28m				Agency:	USGS			
	O	N	D	J	F	M	A	M	J	J	A	S	Annual
Mean	54.9	206.1	383.6	452.2	438.9	350.6	271.8	183.7	106.4	49.4	33.4	34.2	213.8
CoVar	85.5	79.4	70.9	54.5	44.6	44.4	41.6	44.3	48.9	41.5	20.4	29.2	50.4
Percent	1.33	2.14	8.03	14.96	17.63	17.11	13.67	10.60	7.16	4.15	1.93	1.30	

Table 2
PRECIPITATION AND TEMPERATURE STATIONS
USED IN THIS STUDY

Elevations are in meters.

Station	Elev	Precipitation	Temperature
Smith Basin			
Ashland, Oregon	533	1879-1986	1889-1986
Crescent City	12	1885-1986	1894-1988
Ukiah	190	1876-1986	1892-1988
Yreka	802	1871-1986	1914-1988
Cosumnes Basin			
Auburn	500		1871-1988
Bowman Dam	1630	1871-1986	
Canyon Dam	1388	1907-1986	
Colfax	737	1869-1986	1870-1988
Lake Spaulding	1572	1894-1986	
Mount Shasta	1094		1906-1988
Red Bluff	104		1872-1988
San Joaquin			
Huntington Lake	2140	1912-1986	1916-1988
Merced	51		1872-1988
Sonora RS	532	1887-1986	1906-1988
Twin Lakes	2386	1919-1986	
Yosemite NP Hq	1215	1903-1986	1905-1989

Figure 4
109-MONTH GAUSSIAN LOW-PASS FILTERED
PRECIPITATION RECORDS FOR THE
FOUR STATIONS USED TO CONSTRUCT THE
SOUTHERN SIERRA NEVADA
MEAN BASIN PRECIPITATION DATA AND THE
CONSTRUCTED MEAN

Note the coherency of the records.

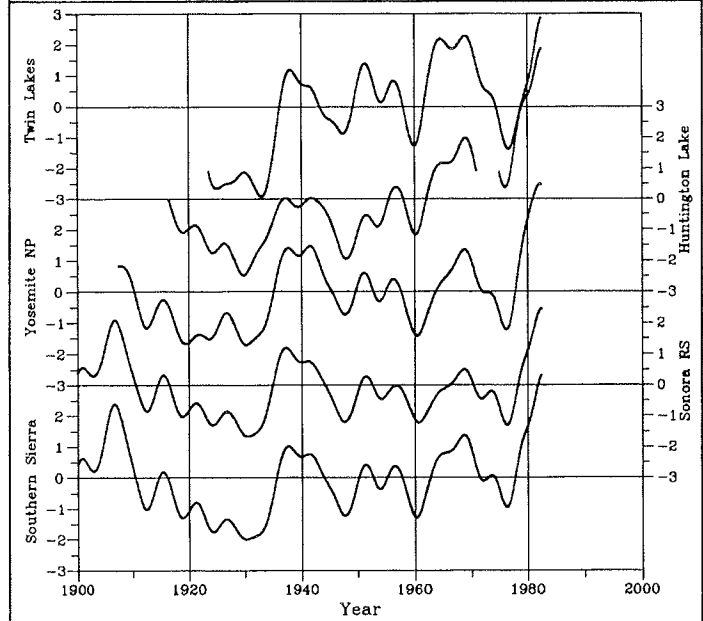
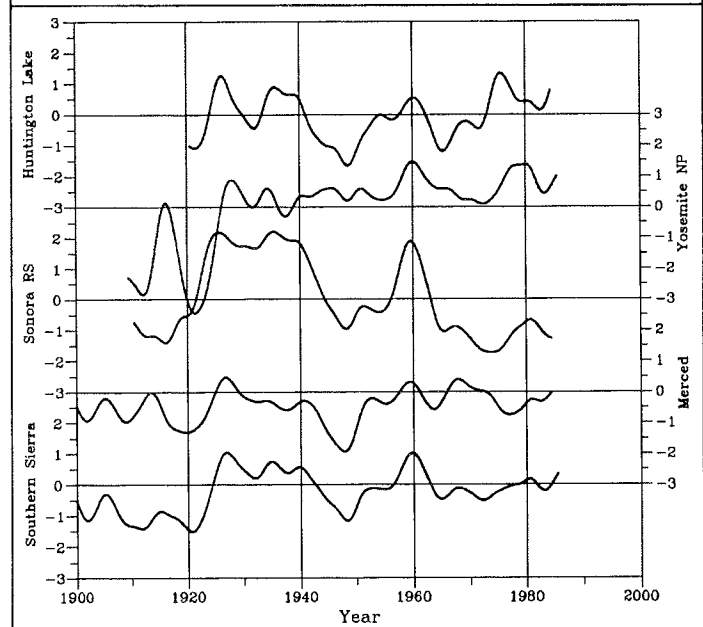


Figure 5
TEMPERATURE STATIONS USED IN THE
SOUTHERN SIERRA NEVADA
MEAN BASIN TEMPERATURE DATA



To produce basin averages, the four stations for each parameter for each basin were averaged together to represent regional conditions. The procedure used to average the monthly data is:

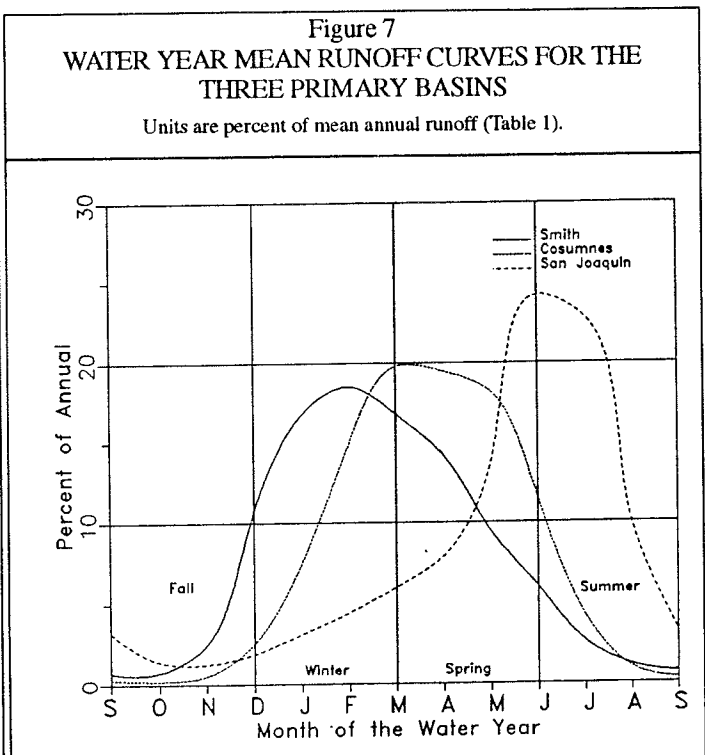
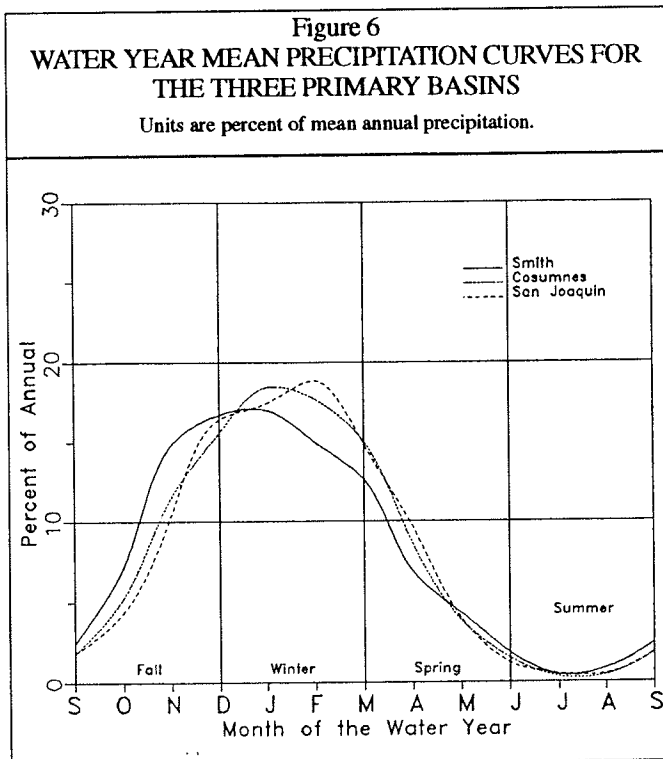
$$\bar{X} = \left[\sum_{i=1}^n \frac{X_i}{\sigma_i} \right] \cdot \frac{1}{n} \cdot \left[\left(\sum_{j=1}^m \sigma_j^2 \right) / m \right]^{\frac{1}{2}} \quad (1)$$

where: X = the individual station total measured precipitation or mean monthly temperature anomaly,
 Sigma = the standard deviation for that month for that station,
 n = the number of stations with data for the particular month and year,
 m = the total number of stations.

Equation 1 was designed to retain the level of natural variability for all stations, even when data for one or more station was missing.

To better tune to the runoff annual cycle in the western United States, seasons used in this study do not coincide with the traditional, climatically defined seasons. NDJ (*November, December, January*) is the first season of the adjusted runoff cycle used. NDJ is the period in which early winter precipitation occurs, a 3-month interval of increasing precipitation that culminates in the long-term mean precipitation peak (Figure 6). Only low elevation basins (with little or no snow accumulation) experience significant runoff during this period, and none reaches peak flow (Figure 7).

The second season is FMA (*February, March, April*). By the first week of February, late winter precipitation is normally peaking or has peaked throughout the region and started to decline. Low and moderate elevation basin streamflows build rapidly, reach their peak, and start to decline, while streamflow in high elevation basins is still slowly increasing.



During the third season, MJJ (*May, June, July*), precipitation continues to decline and reaches minimum at the end of the season. Low elevation streamflow continues the steady decline begun in mid-FMA. Moderate elevation streamflow continues the slow decline begun in the latter part of FMA, then decreases swiftly in June and July. High elevation streamflow makes an abrupt increase in early MJJ and peaks in the latter part of the season.

The final season, ASO (*August, September, October*), begins at the point of minimum precipitation for the entire region. Precipitation increases very little during this season. Minimum streamflow for low and moderate elevation basins is during ASO. Streamflow in high elevation basins is at or near its peak in August, but then decrease precipitously and reaches its minimum at the transition from ASO to NDJ.

Streamflow Analysis: The Influence of Temperature and Precipitation

Linear statistical models of runoff or seasonal fractional runoff were derived from precipitation, temperature, and initial fall streamflow using multiple regression. In this method, which employs the backward stepwise regression technique, several independent variables are run through multiple elimination steps. During each step, the independent predictor having the lowest confidence level is discarded and the ability to predict the dependent variable and remaining predictor confidence levels is recomputed. This is repeated until the confidence levels of all remaining predictors are above some preselected critical value. The minimum confidence level used for building the runoff models in this study was 0.95.

Predictors were seasonal precipitation and air temperature (ASO, NDJ, FMA, and MJJ) and October runoff (an indicator of base flow at the beginning of the wet season). Dependent variables for the first set of model runs were the runoff totals in each of three seasons (NDJ, FMA, and MJJ) for each of the three primary river basins (Smith, Cosumnes, and upper San Joaquin). For the second set of model runs, dependent variables were the seasonal runoff totals as a fraction of annual runoff.

To test the validity of the models against independent data, a training period consisting of the 37 water years, 1950 to 1986, was used to derive the models, and an equal length period, 1913 (or beginning of record) to 1949, was used as a test period. Three secondary basins (Umpqua, American, and Merced) were selected for their elevational and geographic resemblance to the primary basins. The models for the primary basins were then used to predict seasonal runoff for two periods (1913-1949 and 1950-1986) for the primary and secondary basins. Observed runoff (the independent variable) was correlated with predicted runoff (the dependent variable) by simple linear regression.

It is worth noting that the simple linear regression analysis routine (with one independent and one dependent variable) used to test the level of correlation between predicted and observed runoff or fractional runoff standardizes the variables prior to regression, obviating disparities in runoff magnitude between the primary and secondary basins. Models designed for operational prediction of runoff or fractional runoff would have to have provisions for adjusting the coefficients before they could be applied to the secondary basins.

Correlation coefficients (as a percent of variance of the seasonal anomalies) for the regression models are presented in Table 3. The average skill score for the measured runoff models (expressed as coefficients of determination, R^2) for all primary basins in all seasons was 0.76 for the training period (1950-1986) and 0.66 for the test period (1913-1949). The average score for seasonal fractional runoff models for all primary basins in all seasons was 0.74 for the training period and 0.58 for the test period. For the secondary basins, measured runoff scores were 0.60 for the training period and 0.54 for the test period. Secondary basin seasonal fractional runoff models scored 0.54 for the training period and 0.48 for the test period. The average change in skill score from the primary to the secondary basins for measured runoff models was -0.16 for the training period and -0.12 for the test period. Seasonal fractional runoff lost -0.20 for the training period and -0.10 for the test period.

Basin	Water Years	Measured Runoff				Fractional Runoff			
		NDJ	FMA	MJJ	Mean	NDJ	FMA	MJJ	Mean
Smith	50-86	0.85	0.79	0.40	0.68	0.85	0.86	0.51	0.74
	13-49	0.82	0.66	0.30	0.59	0.59	0.73	0.40	0.57
Cosumnes	50-86	0.61	0.88	0.74	0.74	0.70	0.76	0.76	0.74
	13-49	0.69	0.64	0.74	0.69	0.63	0.63	0.67	0.64
San Joaquin	50-86	0.84	0.90	0.92	0.85	0.78	0.70	0.73	0.74
	13-49	0.62	0.69	0.77	0.69	0.41	0.65	0.55	0.54
Umpqua	50-86	0.72	0.53	0.28	0.51	0.71	0.65	0.43	0.60
	13-49	0.60	0.43	0.16	0.37	0.40	0.47	0.29	0.39
American	50-86	0.58	0.84	0.62	0.68	0.58	0.34	0.23	0.38
	13-49	0.81	0.60	0.71	0.71	0.56	0.56	0.68	0.60
Merced	50-86	0.55	0.33	0.93	0.60	0.61	0.61	0.67	0.63
	13-49	0.30	0.50	0.84	0.55	0.21	0.62	0.53	0.45
Smith/Umpqua δR^2	50-86	-0.13	-0.26	-0.12	-0.17	-0.14	-0.21	-0.08	-0.14
	13-49	-0.22	-0.23	-0.14	-0.22	-0.19	-0.26	-0.11	-0.18
Cosumes/American δR^2	50-86	-0.03	-0.04	-0.12	-0.06	-0.12	-0.42	-0.53	-0.36
	13-49	0.12	-0.04	-0.03	0.02	-0.07	-0.07	0.01	-0.04
SanJoaquin/Merced δR^2	50-86	-0.29	-0.57	0.01	-0.25	-0.17	-0.09	-0.06	-0.11
	13-49	-0.32	-0.19	0.07	-0.14	-0.20	-0.03	-0.02	-0.09

It is interesting that the season with the highest skill score for each basin is closely related to the mean elevation and season of peak streamflow for that basin. The higher the mean elevation, the later peak streamflow and highest skill score occurred. In all basins except the American, the training period skill scores were higher than those of the test period. The reversal in the American River basin is probably due to steady and extensive increases in impoundment and diversion during the last 50 years.

The models explained about 75% of the variance in measured and fractional streamflow during the training period and 60% for the test period. Skill scores for fractional runoff (a complicated parameter, since fractional runoff can see both forward and backward within the water year) were almost as high as those of measured runoff. The relatively small decrease in skill scores from the primary to secondary basins indicates the phenomena controlling streamflow are coherent at a regional scale.

It is emphasized that the intent of these models is a climatic analysis of the effect of regional-scale temperature and precipitation on runoff and not to maximize prediction of runoff variance. Effects of biotic associations or watershed structure, such as soil type, amount, slope, etc., are not accounted for. However, regression models of this type do constitute the primary method of water supply forecasting by the National Weather Service and Soil Conservation Service for watersheds in the western United States. As shown in Table 3, this technique accounts for a major portion of seasonal variance and holds up well on independent data samples.

Measured Runoff Models

Table 4 and Figure 8 illustrate the relationship between each of the independent variables and measured seasonal runoff. At low elevations (represented by the Smith River) the only independent variables significantly related to streamflow at the 0.95 confidence level were precipitation the same season and, in NDJ and MJJ, precipitation the previous season. Temperature was not related to observed runoff in this basin for any season. For NDJ and FMA, same-season precipitation was strongly correlated with streamflow, with a beta coefficient of 0.92 for NDJ and 0.89 for FMA. This implies that most precipitation is not stored within the basin for long periods. This fact, coupled with the low elevation of the basin, suggests that precipitation falls largely as rain or as snowfall that melts soon after it falls.

Over the Cosumnes basin, representing moderate elevations, same-season precipitation is also the most important independent variable for runoff for NDJ and FMA streamflow, although the beta coefficients are less than those of the Smith River basin. For FMA and MJJ, seasonal streamflow is also related to precipitation accumulated in the two preceding seasons, with the highest beta coefficients going to NDJ and FMA, the cool, wet seasons. For MJJ, precipitation for the preceding seasons has a greater impact than does same-sea-

Basin	Season	Oct SF	Precipitation				Temperature Anomaly			
			ASO	NDJ	FMA	MJJ	ASO	NDJ	FMA	MJJ
Smith	NDJ		.15	.92						
	FMA					.89				
	MJJ					.34		.47		
	NDJ%					.82		-.34		-.20
	FMA%			-.25		-.74		.57		
	MJJ%					-.57				.46
Cosumnes	NDJ					.78				
	FMA			.14		.42		.71		-.15
	MJJ					.33		.45		.22
	NDJ%					.66		-.53		
	FMA%					-.39		.69		.31
	MJJ%		.46	-.64	-.43					-.62
San Joaquin	NDJ			.29		.91				.20
	FMA					.57		.79		-.14
	MJJ					.52		.64		-.18
	NDJ%			.35		.69		-.63		.27
	FMA%					-.25				.58
	MJJ%			-.39	-.32	.46		.34		-.37

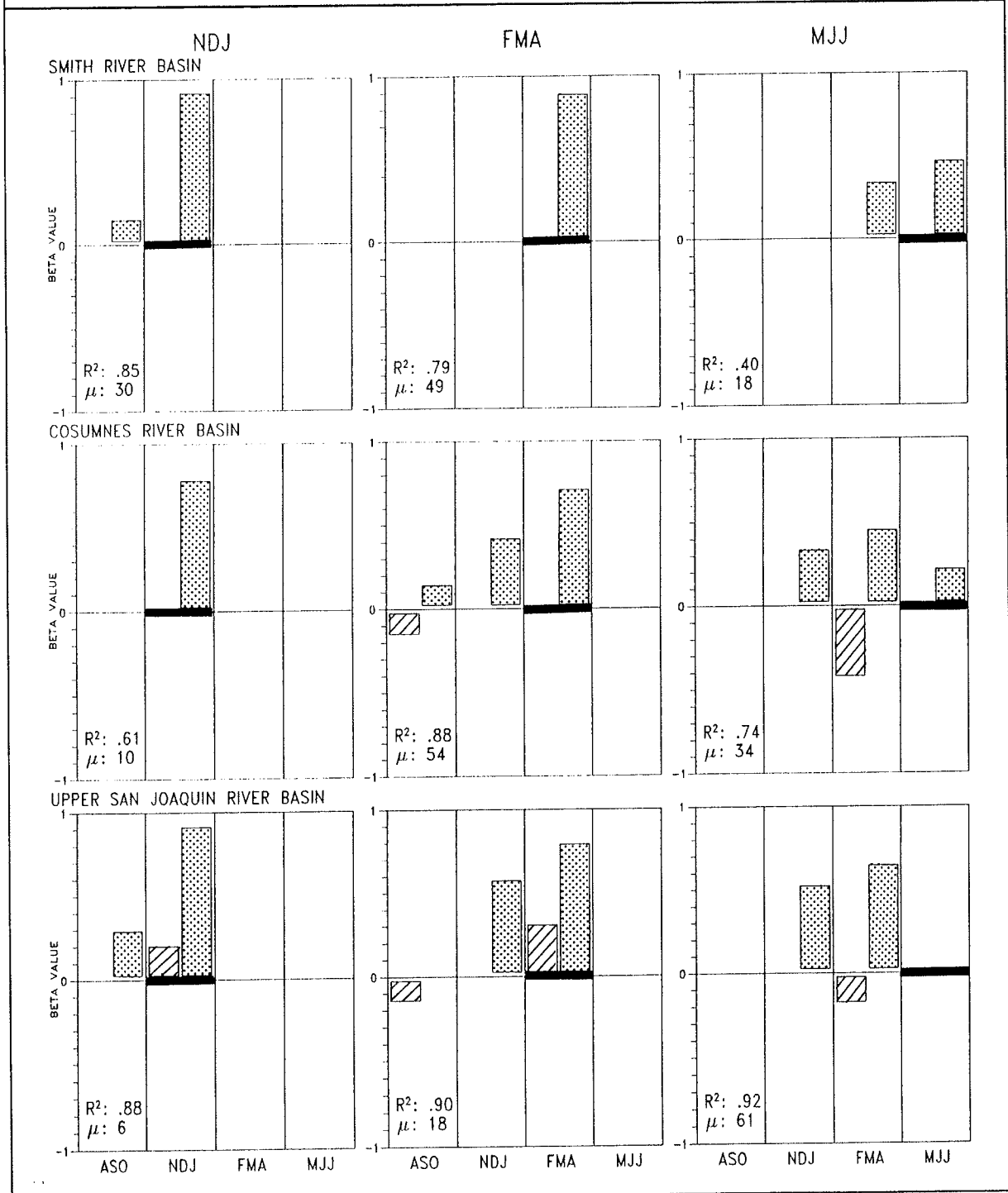
son precipitation. MJJ streamflow is negatively correlated with the previous season's temperature with about the same weight as the previous season's precipitation (-0.42 versus 0.45), but with the opposite sign. A viable explanation for this is that negative FMA temperature anomalies retard late winter/early spring snowmelt, leading to an increased fraction of annual runoff during late spring/early summer.

Figure 8
BETA COEFFICIENTS FOR THE MEASURED SEASONAL RUNOFF MODELS

The beta coefficient is an index of the relative importance of predictor variables (Clark and Hosking 1986).

Dotted bars represent the precipitation beta coefficients. Hatched bars represent temperature beta coefficients.

The coefficient of determination of the model for the training period and the percentage of annual runoff occurring during that season are listed in the lower left corner of each graph.



For the upper San Joaquin basin, representing high elevations, the measured runoff models are remarkably similar in all seasons, with an almost total dependence on wet season predictors. The NDJ model (where FMA precipitation and temperature have not yet occurred) relies heavily on same-season precipitation, with slight influence by same-season temperature and preceding season precipitation. In models that do know about the FMA predictors (FMA and MJJ), precipitation in NDJ and FMA is responsible for the vast majority of the variance accounted for, with about the same proportions in both seasons. FMA temperature is the next most significant predictor, changing its sign from positive in FMA to negative in MJJ. This reflects the importance of late winter temperature in enhancing or retarding late winter runoff. MJJ high elevation measured runoff was the only model that placed no reliance on same-season predictors. MJJ accounts for 61% of the mean annual runoff in the upper San Joaquin. Any MJJ precipitation or temperature signals are lost in the overwhelming volume of wet season signals.

Looking at the measured runoff models by season, across the basins, shows the influence of elevation in determining runoff. NDJ, with little precipitation in the preceding season, relies heavily on same-season precipitation, with no temperature influence except in the highest basins. FMA relies solely on same-season precipitation in the low elevation basins, but relies increasingly on preceding season precipitation and temperature in general as elevation increases. The MJJ models change greatly as elevation increases, with a shift in significance of precipitation predictors to earlier in the water year. Temperature also increases in importance.

Fractional Runoff Models

Fractional runoff models (Table 4 and Figure 9) can see the entire water year, so they rely on more predictors but assign each predictor less weight. Precipitation is normally more significant than temperature, always positively correlated in-season, and normally negatively correlated out-of-season. As with the measured runoff models, temperature is not important at low elevations but becomes increasingly more important as elevation increases.

In the low elevation models, precipitation is the only significant predictor, with NDJ (accounting for about half the total mean annual precipitation) always being the single most important predictor. In FMA and MJJ, in-season precipitation is predictably the second most influential predictor. MJJ is interesting in that it is positively correlated to in-season precipitation, negatively correlated to NDJ precipitation, but not significantly correlated at all with FMA precipitation. This lack of correlation is not due to a lack of influence (about 37% of mean annual precipitation is accumulated in FMA) but is because FMA precipitation is as likely to hinder MJJ fractional runoff (especially during warm winters) as it is to help (as it would in cooler winters, when some snowpack storage delay is likely).

The moderate elevation fractional runoff models for NDJ and FMA are fairly simple. The single most important predictor (always positive) is same-season precipitation. The second most influential predictor (always negative) is precipitation in the other of the two wet seasons (FMA during NDJ and *vice versa*). In the FMA model, temperature for FMA and MJJ both appear as positively correlated predictors but of minor importance. As in the low elevation models, MJJ is the most interesting. FMA precipitation is again absent from the

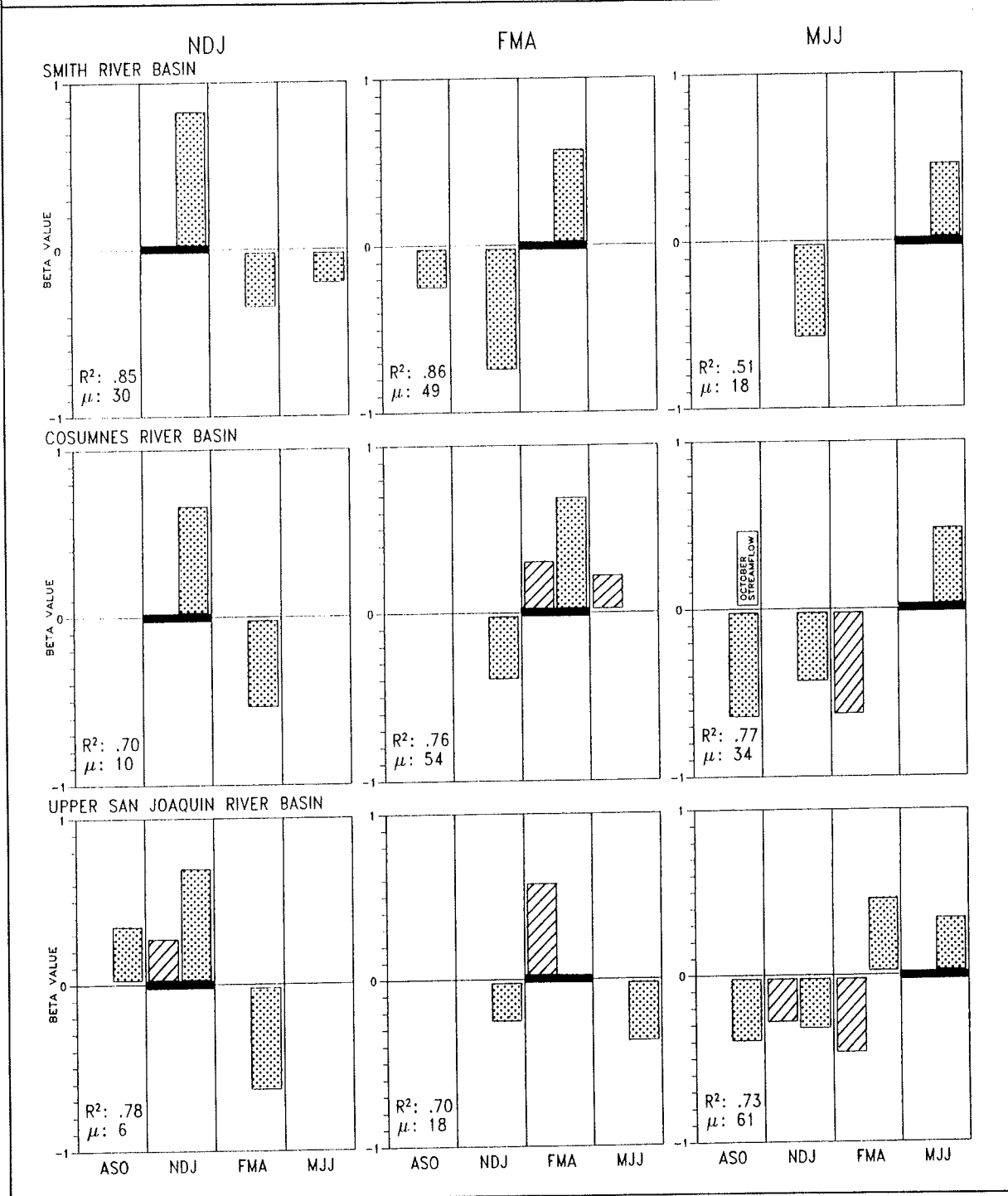
Figure 9

BETA COEFFICIENTS FOR THE FRACTIONAL SEASONAL RUNOFF MODELS

The beta coefficient is an index of the relative importance of predictor variables (Clark and Hosking 1986).

Dotted bars represent the precipitation beta coefficients. Hatched bars represent temperature beta coefficients.

The coefficient of determination of the model for the training period and the percentage of annual runoff occurring during that season are listed in the lower left corner of each graph.



surviving predictors, for the reason discussed above. ASO precipitation and FMA temperature (both negatively correlated) are of about equal importance as the most influential predictors. The strong correlation of high ASO precipitation and low MJJ fractional runoff (which also appears in the high elevation basin) may be an indicator that something frequently occurs in fall that is prejudicial to spring runoff (perhaps an early wet season followed by a persistent coastal ridge). The FMA temperature correlation (which also appears at higher elevations) is similar to that of the measured runoff models. This indicates the temperature sensitivity of the moderate and high elevation basins. Pre-wet season streamflow makes its only appearance, positively correlated. This probably means that, when October streamflow is higher than normal, base flow throughout the water year will be higher than normal, decreasing the importance of wet season precipitation as a contributor to total runoff.

The most significant differences between the high elevation fractional runoff models and the low and moderate elevation models are:

- The shift from MJJ to FMA of the lack of FMA precipitation in the model, and
- The appearance of two positive precipitation predictors in a single model.

In the high elevation models, FMA is the season where FMA precipitation can help as much as hinder runoff, causing it to lack significance and drop out of the model. This ambivalence is reflected in the FMA model skill score of 0.70, the lowest of any of the high elevation models. This is the only model, measured or fractional, without any positive precipitation predictors. The NDJ and MJJ models, the only fractional runoff models with two positive precipitation predictors, illustrate the blurring effect temperature can have on in-season/out-of-season precipitation. In the high elevation basins, where most wet season precipitation falls as snow, the quantity and timing of precipitation is not as important as is temperature.

Summary and Conclusions

Regression results indicate the ability of seasonal mean precipitation and temperature in determining seasonal runoff in low, moderate, and high elevation basins in central and northern California. The models derived from data over the training period (1950-1986) were validated using independent data from the test period (1913-1949) and also by applying each model, without modification, to a nearby sister basin with similar elevation and geography. In general, more than half of seasonal streamflow variation was accounted for.

It is interesting that highest (San Joaquin basin measured streamflow) and lowest (Smith basin measured streamflow) scores during the training period occurred during the same season — May, June, July. MJJ is the largest single season contributor to annual runoff for high elevation basins (where most wet season precipitation falls as snow) and the smallest contributor of the three seasons modeled for low elevation basins (where most precipitation falls as rain). Influence of the predictor variables depended to a large extent

on elevation of the basins, emphasizing the importance of snow as a storage medium for wet season precipitation in the higher basins.

For low elevation basins, precipitation is the only significant predictor. For measured runoff in these coastal streams, the only important indicators were same-season and preceding-season precipitation, with the same-season precipitation always being the most important predictor. Fractional runoff models always selected NDJ precipitation as the most important predictor, with same-season precipitation (in the case of FMA and MJJ) being the second most important. About half of the low elevation precipitation falls during NDJ. Temperature and base flow at the beginning of the water year were not significant (at the 0.95 significance level). This illustrates the immediate nature of low elevation basin streamflow (*i.e.*, when precipitation falls, runoff occurs).

In the mid-level basin models, precipitation is still the most significant predictor (as in almost all the models), but temperature has started to exert its influence. Measured runoff models, except NDJ, can see two preceding seasons' precipitation. NDJ precipitation is felt so strongly in-season that all other predictors, precipitation and temperature, lack significance at the 0.95 confidence level. In both FMA and MJJ, the FMA precipitation is the most significant predictor. Fractional runoff precipitation is similar to low elevation models, but with decreased reliance on NDJ precipitation in all seasons. This decrease in importance is due to an increase in the fraction of NDJ precipitation falling as snow. Temperature was not an influence on runoff during NDJ, was of only secondary importance during FMA, and was quite important during MJJ. This was true for both measured and fractional runoff, with in-season temperature important only for FMA fractional runoff. Temperature would probably be a more important contributor, with consequently improved skill scores, if a method for measuring individual storm temperature profiles could be devised. Temperatures used in this study are monthly mean anomalies. The height of the freezing level and variations in the lapse rate during individual storms are thought to play a more important role in the mid-level basin than in any other basin; however, the freezing level is only poorly represented by monthly mean temperature, and the lapse rate is not represented at all. The mid-level basin MJJ fractional runoff was the only model in which October streamflow survived stepwise elimination, and then it was only a minor contributor.

In high elevation basins, precipitation continues to be the most significant predictor except in FMA fractional runoff, which is the only model of any type, at any elevation, and in any season where mean monthly temperature is the most significant predictor. High elevation FMA precipitation is primarily snow and is as likely to contribute to MJJ runoff (if the temperature is cold) as FMA (if the temperature is warm), accounting for the importance of FMA temperature. Measured runoff precipitation is similar to moderate elevation precipitation, although it can only see two precipitation predictors at a time. Fractional runoff also closely resembles the moderate elevation models except FMA. Temperature, for the first time, was a contributor in all seasons for both measured and fractional runoff. The high elevation basin, with its increased precipitation and greater ability to store precipitation of any season as snow, has the greatest ability to remember preceding season precipitation. It also has the greatest dependence on monthly and seasonal mean temperatures. The difference of a few degrees in seasonal mean temperature can cause significant shifts in the timing of maximum streamflow. The model results show that this, along with

the timing of precipitation, accounts for at least half of fractional runoff variation in the Sierra Nevada range.

Precipitation is always positively correlated in all the measured streamflow models, at all elevations. In the fractional runoff models, same-season precipitation is always positively correlated and out-of-season is always negatively correlated, except for the high elevation basins, where most precipitation falls as snow.

Acknowledgments

We thank Maurice Roos and Gary Hester of the California Department of Water Resources for streamflow and precipitation data and for valuable insight discussions. James Goodridge provided the temperature data and an exhaustive evaluation of the quality of those records. We thank the organizers and sponsors of the Pacific Climate (PACCLIM) Workshop, and particularly Julio Betancourt and Dave Peterson of the USGS. Support was provided by the University of California Water Resources Center, the Scripps Institution of Oceanography Experimental Forecast Center, and the State of California, Department of Water Resources through the Division of Flood Forecasting.

References

- Bruce, J.P., and R.H. Clark. 1966. *Introduction to Hydrometeorology*. Pergamon Press.
- Cayan, D.R., and A.V. Douglas. 1984. "Urban Influences on Surface Temperatures in the Southwestern United States During Recent Decades". *J. of Climate and Applied Meteorology*, 23.
- Cayan, D.R., and D.H. Peterson. 1989. "The Influence of North Pacific Atmospheric Circulation on Streamflow in the West" in *Aspects of Climate Variability in the Pacific and the Western Americas*. Ed. D.H. Peterson. American Geophysical Union Geophysical Monograph, 55.
- Clark, W.A.V., and P.L. Hosking. 1986. *Statistical Methods for Geographers*. John Wiley and Sons.
- Kahrl, W.L. (Ed.). 1978. *California Water Atlas*. State of California.
- Lydolph, P.E. 1985. *The Climate of the Earth*. Rowman and Allanheld. Totawa, NJ.
- Rooney, J. 1969. "The Economic and Social Implications of Snow and Ice" in *Introduction to Geographical Hydrology*. Ed. R.J. Chorley. Methuen and Co. London.
- Roos, M. 1989. "Possible Climate Change and Its Impact on Water Supply in California" presented at Oceans '89 Conference, Seattle, WA, September 20, 1989.
- _____. 1987. "Possible Changes in California Snowmelt Runoff Patterns". *Proceedings of the 4th Pacific Climate Workshop (PACCLIM)*. Pacific Grove, CA, March 22-26, 1987.

“Cool” vs. “Warm” Winter Precipitation and Its Effect on Streamflow in California

Daniel R. Cayan

Abstract: Precipitation is a difficult variable to understand and predict. In this study, monthly precipitation in California is divided into two classes according to the monthly temperature to better diagnose the atmospheric circulation that causes precipitation, and to illustrate how temperature compounds the precipitation to runoff process.

Background: Monthly Precipitation in the West

Precipitation occurs episodically, and, in many West Coast locations, the majority of precipitation is received in a few winter storms. For example, at Sacramento, only 186 of 1,512 winter (November-March) days received 0.25 inches or more of precipitation within a 10-year census (U.S. Dept. of Commerce 1963). To smooth this sporadic nature, monthly aggregates or averages of the precipitation are often employed (*e.g.*, Englehart and Douglas 1985), but even averaging over time and space does not remove its noisy temporal behavior, as there is little correlation of precipitation from one month to the next.

To explain monthly precipitation anomalies, they have been correlated to large-scale atmospheric circulation. Traditionally, it has been approximated that atmospheric flow patterns responsible for heavy and light precipitation in California are mirror images (*e.g.*, Weare and Hoeschele 1983; Cayan and Roads 1984; Klein and Bloom 1987). Specifically, anomalously low atmospheric pressure lying off the California coast is conducive to enhanced southwesterly flow, which makes for active storms, stronger winds, and greater moisture flow into the state, while anomalously high pressure is associated with lack of storms and dry conditions.

This description generally applies to most near-coastal basins along the Pacific Coast of North America, as was shown by correlations of winter sea level pressure (*SLP*) with December-August streamflow anomalies (Cayan and Peterson 1988). However, it is well known that a variety of synoptic patterns result in precipitation (Weaver 1962, Enzel *et al.* 1989). Furthermore, inspection of the flow patterns for heavy and light California winter precipitation episodes indicates substantial differences between patterns for the two cases. (Recall that heavy precipitation is favored by negative anomalies of *SLP* or 700 mb geopotential height centered offshore of Northern California, while light precipitation is associated with positive anomalies in this region.)

A comparison of composite flow patterns for heavy vs. light precipitation suggests that both cases have a strong regional signature, along the lines of the correlations mentioned above, but there is a stronger remote “teleconnected” signal for light conditions than for heavy. This is confirmed by teleconnection statistics for positive vs. negative 700 mb height anomalies off the West Coast at 40°N 130°W from the Wagner and Maisel (1988) atlas — there are significant anomaly probabilities upstream and downstream from the

positive anomaly center and a lack of significant probabilities in remote regions from the negative anomaly center.

Overall, taking all California monthly precipitation cases together, a simple correlation with 700 mb heights accounts for roughly 40-60% of the monthly precipitation variance in winter for Northern and Central California; consideration of the light and heavy cases individually appears to add more detail. A further cut of monthly precipitation in terms of monthly temperature provides more insight into the causal atmospheric flow patterns and into the effects on the surface hydrology.

Data

Winter precipitation was stratified into “warm” and “cool” groups on the basis of regional monthly temperature anomalies averaged over the two climate divisions: Sacramento drainage and San Joaquin drainage. Divisional temperatures are thought to be adequate because the anomalous temperature has broad scales. This discrimination divides the observed record of heavier-than-normal precipitation into two almost equally likely classes because monthly temperature and precipitation are nearly uncorrelated during winter along the West Coast and in California in particular.

In carrying out this study, we also used daily temperature and precipitation from the EARTHINFO, Inc., CLIMATEDATA CDROM, and from the National Oceanic and Atmospheric Administration daily weather map series. Streamflow data were obtained from the U.S. Geological Survey via an EARTHINFO, Inc., HYDRODATA CDROM. Atmospheric circulation is represented by the monthly gridded sea level pressure set (Trenbert and Paolino 1980), which begins in 1899, and twice daily 700 mb height analyses, also gridded, which begin in 1947.

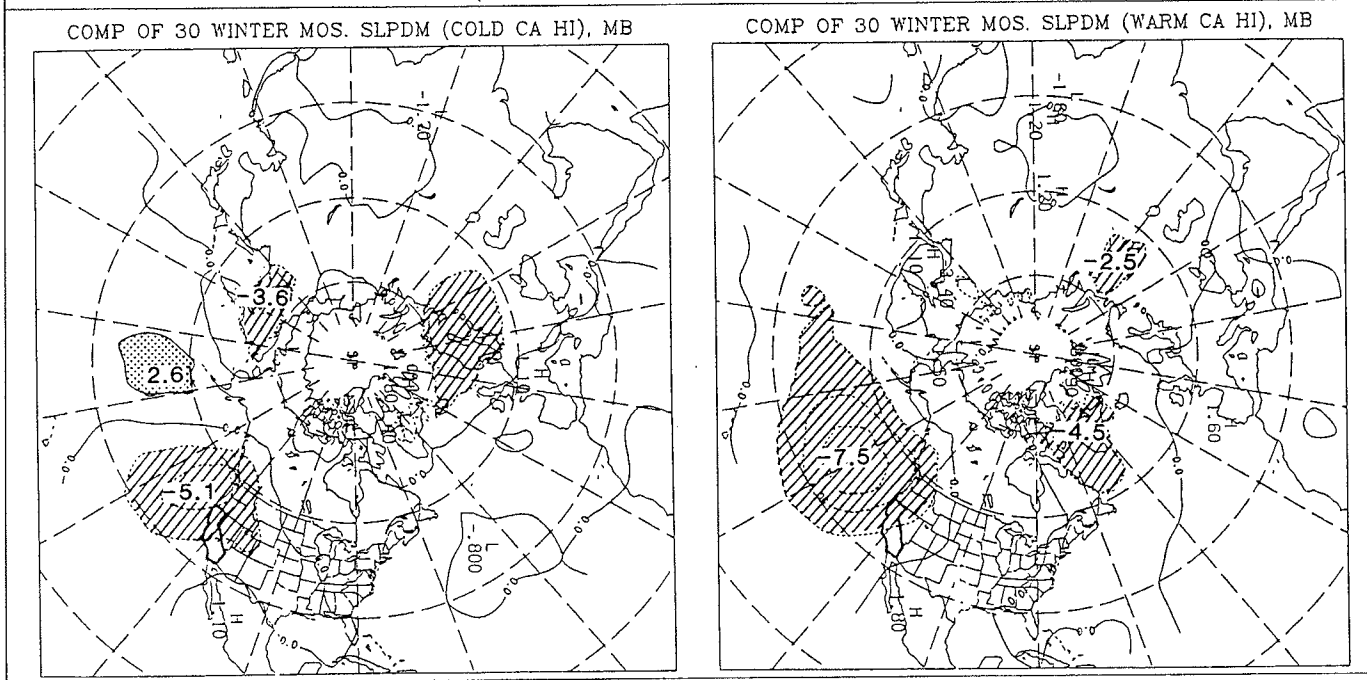
Cool vs. Warm Precipitation: The Link to Atmospheric Circulation

There are two major reasons for considering temperature in association with precipitation. The first is that the anomalous temperature may provide a means for better identifying distinct precipitation-bearing atmospheric circulation types. For example, Figure 1 compares a composite of SLP (*sea level pressure*) anomalies for the 30 wettest cool winter months (climate divisional averages) with one for the 30 wettest warm winter months from a ranking of temperature and precipitation for November-March from 1899 through 1986. SLP is used here because it has a longer record than the upper level geopotential height, allowing more extreme cases.

In both composites, there is a prominent negative SLP anomaly center northwest of California, but the cool/wet pattern is confined to the region east of about 150°W, with a positive anomaly center to the west centered at about 40°N 170°W. The warm/wet pattern has a much larger negative anomaly center, which occupies most of the eastern North Pacific basin, and no significant positive anomalies to its west.

In synoptic terms, the cool/wet pattern suggests a higher amplitude flow across the North Pacific, with cool air advected into the eastern North Pacific and the West Coast by the anomalous northerly wind on the east side of the high pressure anomaly. Frontal systems

Figure 1
COMPOSITE SLP ANOMALIES FOR COOL/WET AND WARM/WET WINTER MONTHS
(NOVEMBER TO MARCH), 1899-1986



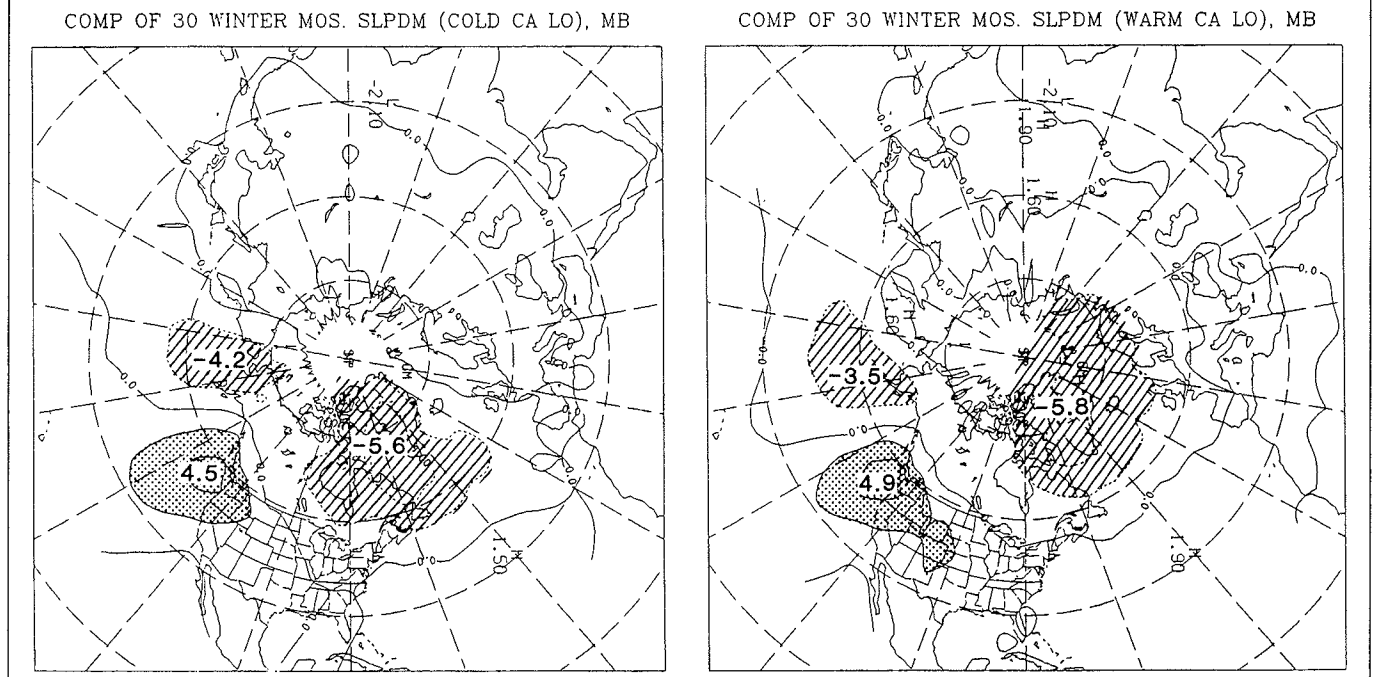
associated with this pattern often originate in the Gulf of Alaska. The broad negative anomaly in the warm/wet case is symptomatic of southerly displaced westerly winds and accompanying storm tracks across the eastern half of the basin, which would inject a relatively warm, moist air mass into California along with the storms.

Inspection of individual storms from these classes, discussed below, confirms that it is the storms themselves, not simply the intervening between-storm periods, that exhibit these anomaly patterns. Examination of winter circulation for a similar breakdown of temperature and precipitation at other regions in Oregon, Washington, Arizona, and Colorado reveals similar contrasts between cool/wet and warm/wet months, suggesting that this is a convenient way of discriminating between major types of precipitation-causing circulations in the West.

Does the cool vs. warm classification provide insight into anomalously dry spells along the West Coast? Again using composite SLP according to the California divisional precipitation and temperature classification, we can compare the anomalous circulation for the cool/dry and wet/dry categories (Figure 2).

The difference for these two patterns is quite modest, indicating the problem that a forecaster might have in trying to discriminate between these types of events. Figure 2 shows that both cool/dry and warm/dry are dominated by a high pressure anomaly to the northwest and a negative anomaly teleconnection farther west, near the Aleutian Islands. The major difference between the two patterns is that the positive anomaly for the cool/dry case is displaced farther offshore and to the north than that for the warm/dry case, which extends farther onshore, over Wyoming and Colorado. This northwest displacement in the cool/dry case presumably encourages the southward penetration of cold air from the Gulf of Alaska and the interior of North America into California. On the other hand, the broader ridge of high pressure for the warm/dry case suggests that the cold interior air is pushed

Figure 2
COMPOSITE SLP ANOMALIES FOR COOL/DRY AND WARM/DRY WINTER MONTHS
(NOVEMBER TO MARCH), 1899-1986



farther east, often east of the Rockies, and allows California to remain warm. While the contrast in the California dry patterns is subtle, this general difference is confirmed by stronger differences in the cool/dry vs. the warm/dry analogous SLP composites for Oregon coastal precipitation.

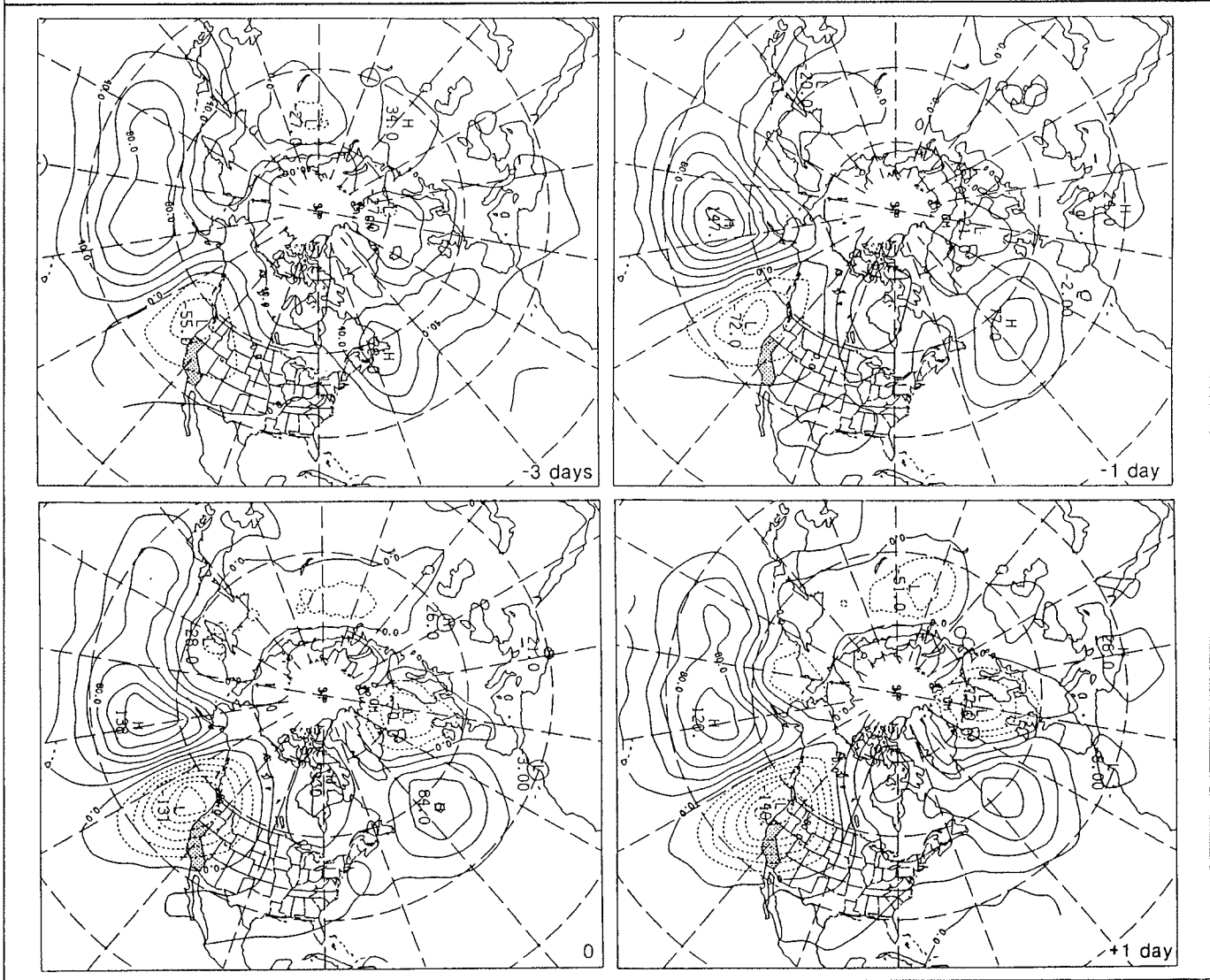
Returning to the wet monthly circulation patterns, our view is refined by examining the circulation associated with individual storms in these months. Figure 3 shows 700 mb height anomalies composited over about 20 heavy precipitation episodes for each of the cool/wet and warm/wet months. This figure actually shows the evolution of the storm circulation from about 3 days before through 1 day after the heavy precipitation period (time for each composite map is 0Z, Universal time, so the maps lead California time by about 8 hours).

Storms for these composites were selected by inspecting precipitation and temperature from the NOAA daily weather map series in several of the cool/wet and warm/wet months from the monthly divisional classification. The daily 700 mb height anomaly maps reinforce the patterns suggested above from the monthly SLP composites. If anything, the patterns are stronger, indicating these storms are fairly strongly imprinted in the monthly averages and that the cool/wet and warm/wet cases are indeed formed from distinct circulation types.

As before, for the cool/wet pattern, there is high pressure anomaly south of the Aleutians and the low pressure in the Gulf of Alaska. Interestingly, there is little evidence that the pattern propagates, although the negative anomaly center shifts eastward from offshore to nearly on the coastline between day 0 and day +1. Also there appear to be downstream teleconnections, with a strong positive anomaly southeast of Greenland and a strong negative anomaly just west of Scandinavia.

Figure 3
COMPOSITE 700 mb HEIGHT ANOMALIES FOR
COOL/WET STORMS IN NORTHERN AND CENTRAL CALIFORNIA

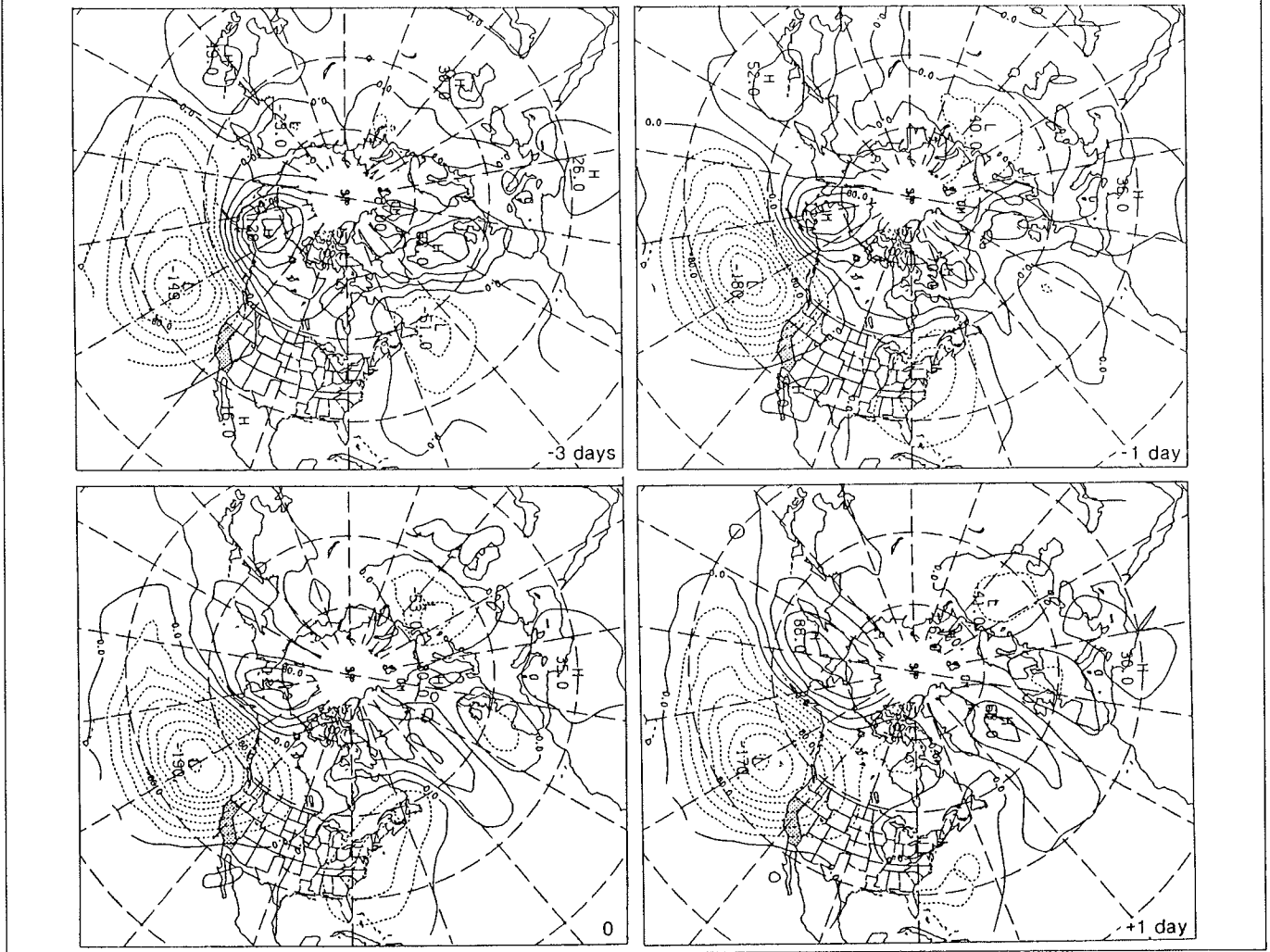
Day -3, Day -1, Day 0, and Day +1 refer to timing of 700 mb 0Z analysis relative to the target heavy rain day (Day 0) in California, as determined from the NOAA daily weather map series.



The warm/wet case (Figure 4) is dominated by a large negative anomaly that covers most of the North Pacific basin, with high pressure to the north, centered over Alaska. Again there is little evidence of propagation, but the region of strong anomalous southwesterly flow does move onshore between day -3 and day 0, and the negative anomaly center reaches its highest intensity on day 0. The message from these two patterns is very clear: the cool/wet pattern is cool because it has great southward meridional flow of cold air into the eastern Pacific, while the warm/wet pattern is dominated by strong southerly displaced zonal flow over the whole eastern North Pacific basin.

Figure 4
COMPOSITE 700 mb HEIGHT ANOMALIES FOR
WARM/WET STORMS IN NORTHERN AND CENTRAL CALIFORNIA

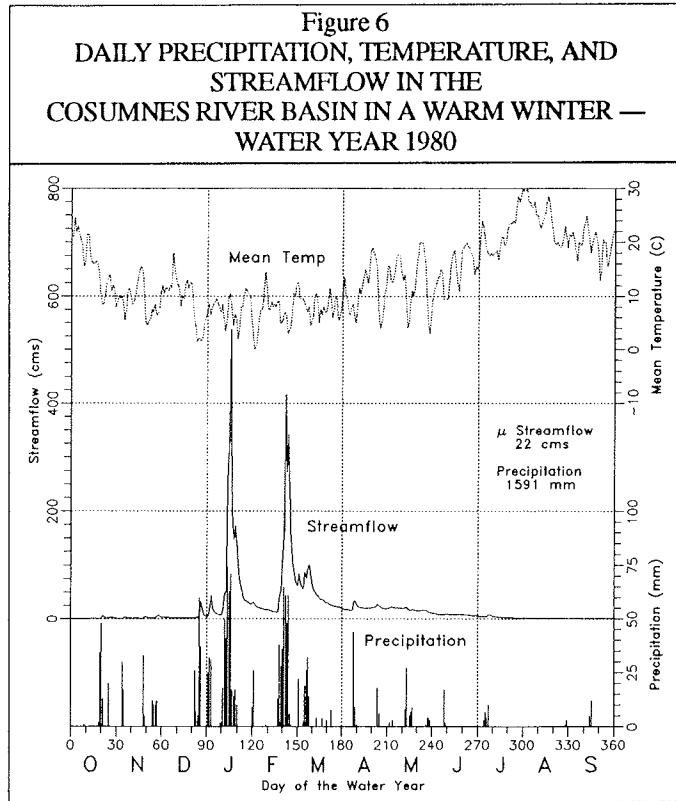
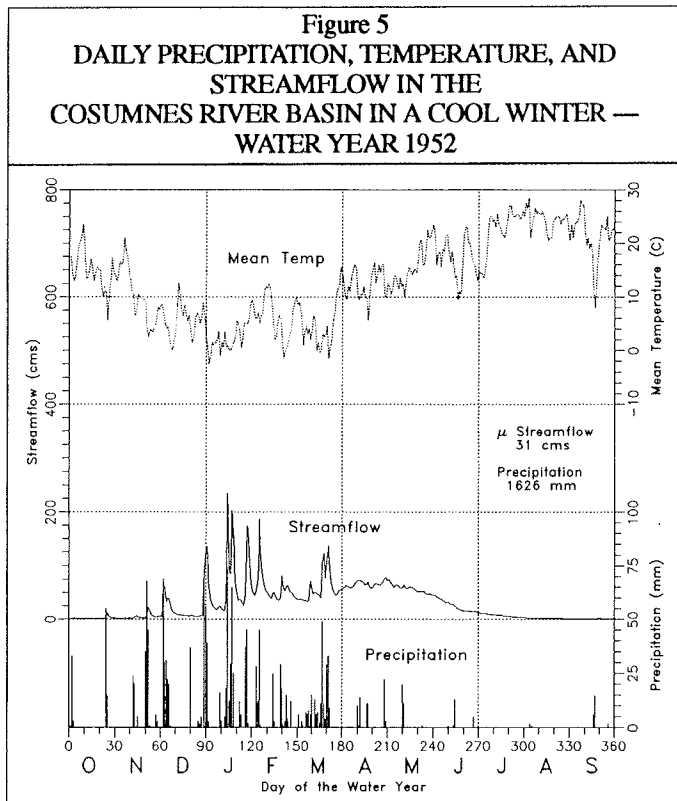
Day -3, Day -1, Day 0, and Day +1 refer to timing of 700 mb 0Z analysis relative to the target heavy rain day (Day 0) in California, as determined from the NOAA daily weather map series.



Cool vs. Warm Precipitation: Streamflow Characteristics

The second reason for studying precipitation in terms of the associated temperature is that the temperature has an impact on surface hydrology: when storms are cool they deposit more precipitation as snow than they do when they are warm. This is exemplified by two winters with heavy precipitation in the Sierra: 1952 (wet and cool, Figure 5), and 1980 (wet and warm, Figure 6).

The anomalous temperature in the Sierra during these two winters was part of broadscale conditions caused by the general orientation of the atmospheric flow, (Cayan *et al.* 1986, Namias 1979). Precipitation during these winters (Karl and Knight 1985) was also widespread, extending over much of the Southwest.) In intermediate elevation basins like Cosumnes (average elevation 1121 meters), the runoff behavior is quite sensitive to temperature anomalies. Presumably owing to the heavy snowpack in 1952 and lack of a snowpack in 1980, there is a remarkable difference in the streamflow response between



the two winters and their subsequent months. Water year 1952 had only modest streamflow during the winter storms, but extensive flow during April and May after the precipitation season ended and temperatures warmed (Figure 5). Water year 1980 had high streamflow during the two major winter storms in January and February (warm storms), but apparently had little snowpack remaining after winter, as spring streamflow was low (Figure 6).

Viewed over many winters stratified into cool and warm tercile classes (about 25 each, plotted in Figure 7), Cosumnes River exhibits an unmistakable delay of about 2 months for flow in the cool-winter year relative to the warm-winter year.

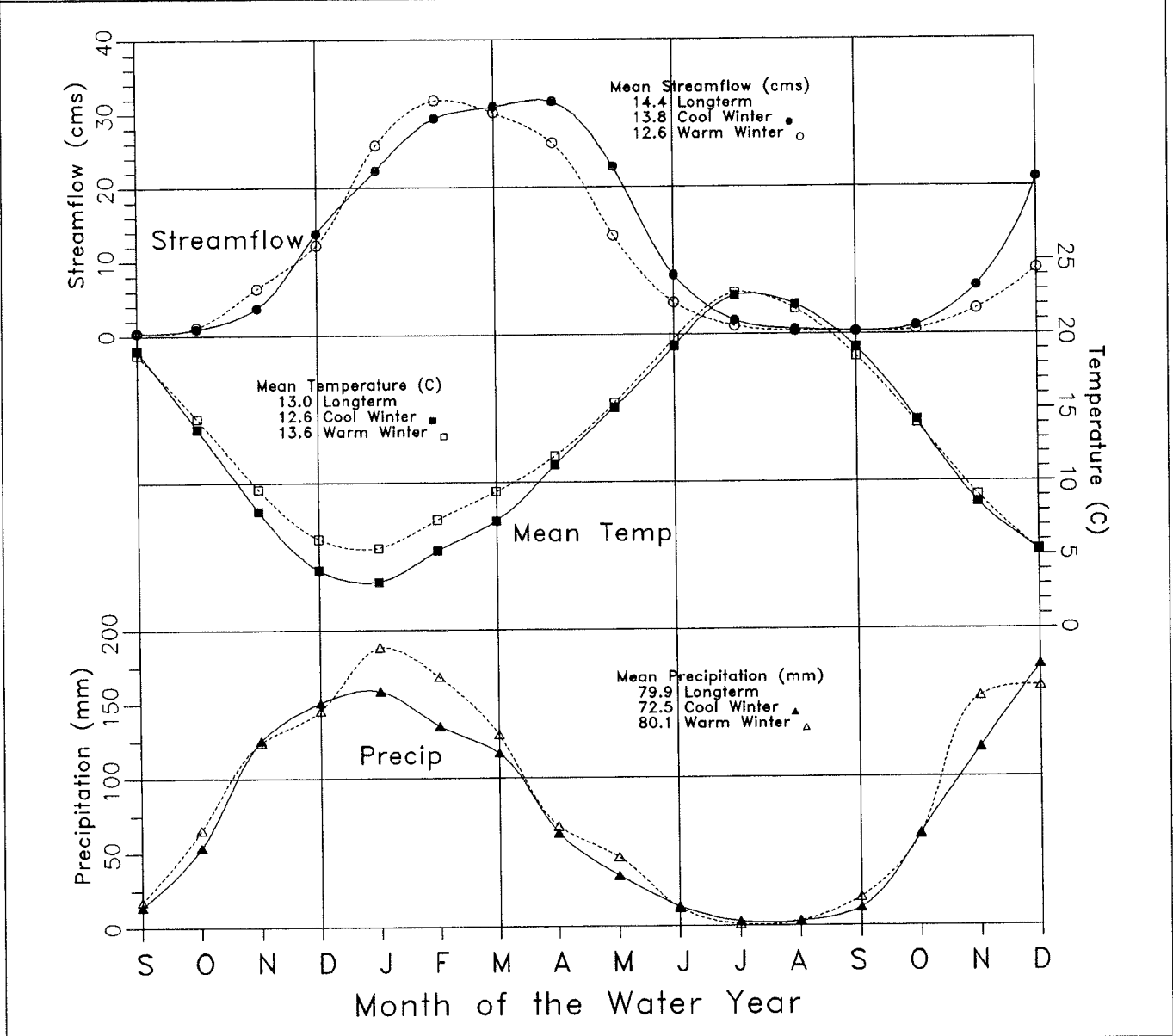
Figure 7 also suggests the intriguing possibility that the *amount* as well as the timing of the runoff is affected by precipitation. The warm year runoff was *less* than that of the cool year by about 10%, despite the fact that warm winter cases indicate about a 10% greater precipitation, especially in late winter months, as determined from NCDC divisional data in the neighborhood of this basin. This result is only suggestive because of the tentative nature of precipitation at high elevations, but inspection indicates that it is not explained by carry-over from the previous water year and that similar behavior may exist at other Sierra watersheds. Such a result would contrast with that of Karl and Reibsame (1989), who were not able to find marked temperature effects on streamflow over a broad network of streams across the conterminous United States.

Another interesting facet is that higher elevation watersheds are not as sensitive to winter temperature anomalies but may be more sensitive to those in spring. For the warm winter of 1980, there is not a large immediate streamflow response to the heavy winter precipitation at Merced River (a higher Sierra basin), apparently because precipitation there is deposited as snow. On the other hand, the spring of 1952 was relatively warm (see Figure 5) and the spring of 1980 was cool (see Figure 6), so the Merced River spring runoff

peaked *earlier* in 1952 than in 1980. This emphasizes that the snowpack “knows about” the actual temperature — not simply the temperature anomaly.

Deciphering the effects of temperature on the timing and amount of runoff from individual storms is important. The aggregates of a few (or several) storms determine the character of the entire runoff season, and several years may affect the overall hydrological balance of a watershed. Long-term trends toward earlier fractional runoff and the storage capability of the snowpack in the Sierra Nevada have been noted and are under investigation (Roos 1987 and 1989, Riddle *et al.* 1990).

Figure 7
COMPOSITE TEMPERATURE, PRECIPITATION, AND STREAMFLOW FOR YEARS WHEN WINTER MONTHS WERE IN THEIR WARMEST AND COOLEST TERCILE
 Streamflow is for Cosumnes River. Precipitation and temperature are National Climatic Data Center divisional averages.
 Dotted Line = Warmest Solid Line = Coolest



Acknowledgments

This work was supported by the U.S. Geological Survey via an Intergovernmental Personnel Agreement; by the University of California Water Resources Center, Project UCAL-W-720; and by the National Oceanic and Atmospheric Administration Climate Program Office through the Experimental Climate Forecast Center. Thanks to Dave Peterson for much support, to the sponsors of the PACLIM workshop, and to Julio Betancourt and colleagues who worked hard to organize PACLIM this year.

References

- Cayan, D.R., and J.O. Roads. 1984. "Local Relationships between United States West Coast Precipitation and Monthly Mean Circulation Parameters". *Monthly Weather Review*, 112:1276-1282.
- Cayan, D.R., C.F. Ropelewski and T. R. Karl. 1986. *An Atlas of United States Monthly and Seasonal Temperature Anomalies, December 1930-November 1984*. NOAA National Climate Program Office, Rockville.
- Cayan, D.R., and D.H. Peterson. 1989. "The Influence of North Pacific Atmospheric Circulation on Streamflow in the West". *Geophysical Monograph* 55. Available from American Geophysical Union, Washington, DC.
- Englehart, P.J. and A.V. Douglas. 1985. "A Statistical Analysis of Precipitation Frequency in the Conterminous United States, Including Comparisons with Precipitation Totals". *J. Clim. and Appl. Meteorol.*, 24:350-362.
- Enzel, Y., D.R. Cayan, R.Y. Anderson, and S.G. Wells. 1989. "Atmospheric Circulation During Holocene Lake Stands in the Mojave Desert: Evidence of Regional Climate Change". *Nature*, 341:44-48.
- Karl, T.R., and R.W. Knight. 1985. *Atlas of Monthly and Seasonal Precipitation Departures from Normal (1895-1985) for the Contiguous United States, Winter*. National Climatic Data Center, Historical Climatology Series.
- Karl, T.R., and W.E. Riebsame. 1989. *The Impact of Decadal Changes in Mean Precipitation and Temperature on Runoff*. Unpublished. National Climatic Data Center. Asheville, NC.
- Klein, W.H., and H.J. Bloom. 1987. Specification of Monthly Precipitation Over the United States from the Surrounding 700mb Height Field. *Mon. Wea. Rev.*, 115:2118-2132.
- Namias, J. 1979. "Northern Hemisphere Seasonal 700 mb Height and Anomaly Charts, 1947-1978, and Associated North Pacific Sea Surface Temperature Anomalies" in *CALCOFI Atlas No. 27*. Ed. A. Fleminger. Marine Life Res. Prog., Scripps Inst. of Oceanogr., La Jolla, CA.
- Riddle, L., D.R. Cayan, and E. Aguado. 1990. "The Influence of Seasonal Precipitation and Temperature Variations on Runoff in California and Southwest Oregon". *Proceedings of the 7th Pacific Climate Workshop (PACLIM)* Pacific Grove, CA, 1989.
- Roos, M. 1987. "Possible Changes in California Snowmelt Runoff Patterns". *Proceedings of the 4th Pacific Climate Workshop (PACLIM)*, Pacific Grove, CA, March 22-26, 1987.

- Trenberth, K.E., and D.A. Paolino. 1980. "The Northern Hemisphere Sea-Level Pressure Data Set: Trends, Errors, and Discontinuities". *Mon. Wea. Rev.*, 108:855-872.
- Wagner, A.J., and T.N. Maisel. 1988. "Northern Hemisphere 700-mb Teleconnections Based on Half-Monthly Mean Anomaly Data Stratified by Season and by Sign". *Proceedings of the Twelfth Annual Climate Diagnostics Workshop, Salt Lake City, UT, Oct. 12-16, 1987*. U.S. Dept. of Commerce. NTIS No. PB88-191747. pp. 228-237.
- Weare, B.C., and M.A. Hoeschele. 1983. "Specification of Monthly Precipitation in the Western United States from Monthly Mean Circulation". *J. Climate Appl. Meteor.*, 22:1000-1007.
- Weaver, R.C. 1962. *Meteorology of Hydrologically Critical Storms in California*. Hydrometeorological Report 37, U.S. Department of Commerce, Weather Bureau, Washington, DC.

Air Temperature Trends in California

James D. Goodridge

“Greenhouse heating” of the atmosphere due to trace gases seems apparent to those who model with averages but not to those who examine individual temperature records. Temperature trends are on the minds of all those concerned with the environmental influence of the increasing human population. The big problem remains — where and how do we take the Earth’s temperature?

Landsberg (1981) reported on Luke Howard’s study of urban/rural temperature differences for London in 1807 to 1816, which were clearly attributed to urban heat island effects associated with coal burning and severe atmospheric pollution. Landsberg’s book, *The Urban Climate*, is a landmark example of the hundreds of reports on urban heat islands throughout the world.

Jones *et al.* (1982) reported on Northern Hemisphere temperature averages based on the World Weather Record dataset, described by Quayle (1989) and compiled by Jenny (1975), in which California was represented by seven stations. In 1986, Jones *et al.* expanded the World Weather Record to include stations in the western United States compiled by Bradley *et al.* (1982). More recently, Hanson and Lebedeff (1988) incorporated the compilation and corrections of the U.S. Historical Climatological Network by Quinlan *et al.* (1987). The network has 33 California records for the 1910 to 1989 period.

In California, there are 112 temperature records for 1910 to 1989; all of them are used here to examine trends in annual temperature. These records are part of the National Weather Services network, and are published by the National Climatic Data Center in the monthly *Climatological Data*. Not all of the California temperature records were problem-free. Missing monthly values were estimated from nearby stations in a few cases, and some annual values were estimated as well. The intent was to develop a data series that resembled the observed data, with no corrections for station moves or changes in time of observation.

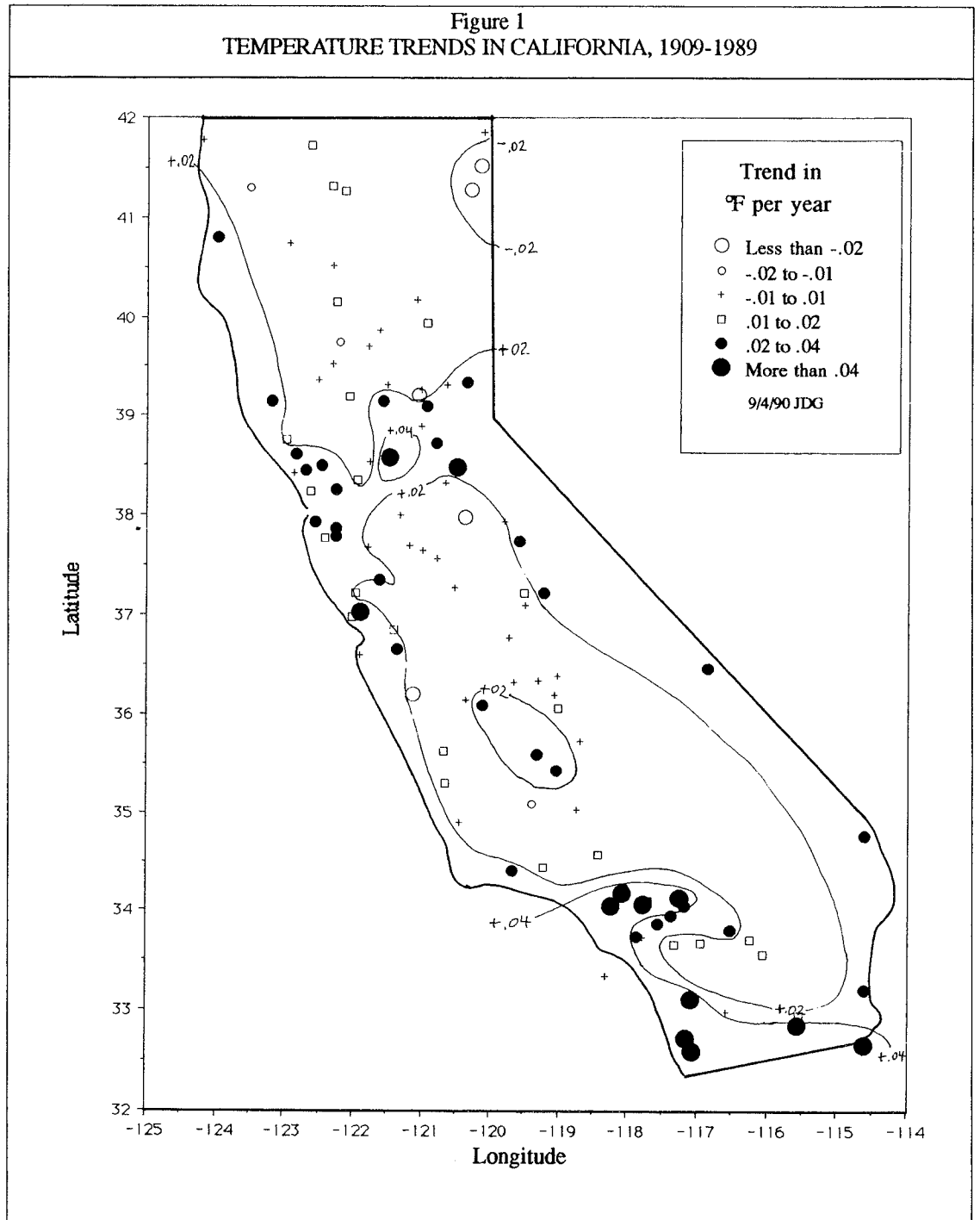
California temperature records are averaged in various ways here to provide an overview of the effects of averaging temperature data. Temperature trends of individual stations are plotted on Figure 1. Areas of upward temperature trends correspond with areas containing California’s major population centers.

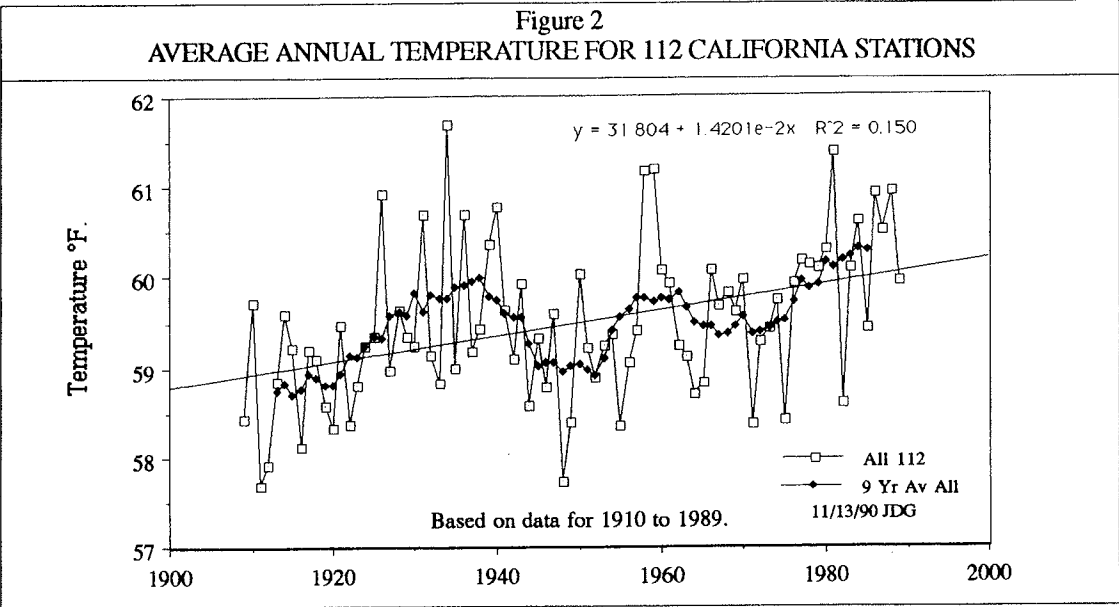
The average temperature of all 112 California records, plotted on Figure 2, has an 80-year trend of +0.014°F per year. The highest average temperature was in 1934, and lowest mean annual temperature was in 1948.

The 112 temperature records were also averaged by county population. Three size categories were selected based on the 1989 population:

Category	Population Range	Temperature Trend
Small Counties	4,000 to 99,000	+0.005°F
Mid-size Counties	109,000 to 635,000	+0.011°F
Large Counties	664 to 8,710	+0.026°F

Temperature trends were calculated for the seven climatic divisions from *Climatological Data*, for the seven stations included in the World Weather Data, and for the 33 stations from the National Historic Climate Network. The 80-year average temperature trends for California are:





Data Set	Number of Stations	°F per Year
All Stations	112	0.014
Small Counties	28	0.005
Mid-size Counties	50	0.011
Large Counties	34	0.026
North Coast 1	14	0.018
Sacramento Valley 2	26	0.006
Northeastern Interior 3	3	-0.004
Central Coast 4	14	0.015
San Joaquin Valley 5	24	0.007
South Coast 6	21	0.027
Southeastern Desert 7	10	0.026
National Historic Climatic Network	33	0.014
World Weather Records	7	0.032

The World Weather Records dataset has a strong urban bias in the California portion, as shown by the $+0.032^{\circ}\text{F}$ per year trend. This is larger than the trend for the large counties. The National Historic Climatic Network was an attempt to correct deficiencies in the World dataset by eliminating urban bias. The National Network has a 1910 to 1989 trend of $+0.014$, the same as the average of all 112 records.

Most California temperature records show a heating trend for 1910 to 1989, partly due to the choice of starting and ending dates of the study period. This study is based on an 80-year period since the method of calculating mean daily temperature (as the average of daily maximum and minimum) was uniform for all stations in the United States. Until about 1906, daily means for some stations were calculated as the mean of several daily fixed time observations. Starting this study with a base period before 1910 would further reduce the number of stations available for comparison. Only three stations in California have temperature records extending back to 1850: San Diego, San Francisco, and Sacramento. The first reported temperature record for California was at Fort Ross, with data from 1837 to 1840 (Chernykh 1841).

The main reason for the heating trend in California temperature records is urban heat island or thermal pollution associated with a large population where temperature is measured. The population of California has increased by a factor of 12 — from 2.4 million to 29 million people during the 80 years of this study.

Not all regions of California have shared this growth. For example, the Glenn County population has grown from 7,000 to 24,000, and the 80-year temperature trend is -0.002 . In Modoc County, the population has grown from 6,200 to 9,500, and the temperature trend has averaged -0.010 for three of its communities: Alturas, Fort Bidwell, and Cedarville.

Of the 112 California temperature stations, 20 show a cooling trend. Declining temperature trends are not in urban centers, but in small towns and rural areas. Figure 1 shows the annual temperature trend plotted for each station. Regions with 0.02°F increases are generally the urban centers of San Francisco/Sacramento and San Diego/Los Angeles. However, urban centers are not the only regions with increasing temperature trends. Air temperature in coastal California was highly correlated with sea surface temperature. In these areas, the trend of increasing air temperature corresponds to a period of declining cold water upwelling near the shore of the eastern North Pacific Ocean, starting about 1975.

Beginning in 1947, data on sea surface temperature in the North Pacific Ocean are plentiful. Sea surface temperature studies from offshore 5° grid points reported here cover 43 years, 1947 to 1989. These grid points are in the eastern North Pacific Ocean, north of latitude 30°N and east of longitude 160°W . Sea water temperature data for ocean grid points, supplied by Cayan (1990), are plotted on Figure 3, along with trends at adjacent near-shore stations. The shore and near-shore stations have a notable heating trend, contrasting sharply with the trend of -0.0145°F at the 48 mid-ocean 5° grid points plotted on Figure 4. The SST reflects part of a roughly 20-year cyclic variation, as shown on Figures 5 and 6. This cyclic variation in SST was described by Newell (1989), who attributes it to the solar magnetic cycle.

The trend in upwelling at three ocean stations off the West Coast is shown on Figure 7 (from Bakun 1986). Bakun's upwelling index, like the SST data of Figures 5 and 6, is represented here as a 9-year running average. A decline in cold water upwelling near the shore starts about 1975, and the SST trend responded by not declining in the 1980s as would be expected from a well defined 20-year cyclic pattern.

Average annual air temperature at California stations was correlated with average annual sea surface temperature at one ocean grid point centered at latitude 35°N and longitude 125°W . The correlation (R^2) is highest (0.5) at coastal stations and is near zero at the interior desert stations, as shown on Figure 8.

When the National Climate Program Act was passed 10 years ago, it was hoped that the number of temperature measuring stations for California would increase, but the reality is that the number continues to decline (Figure 9). The federal response to the temperature measurement problem has been to eliminate stations — some with as much as 100 years of record — and spend millions on “greenhouse” studies.

Figure 3
TRENDS IN SEA SURFACE TEMPERATURE AND NEAR-SHORE TEMPERATURE

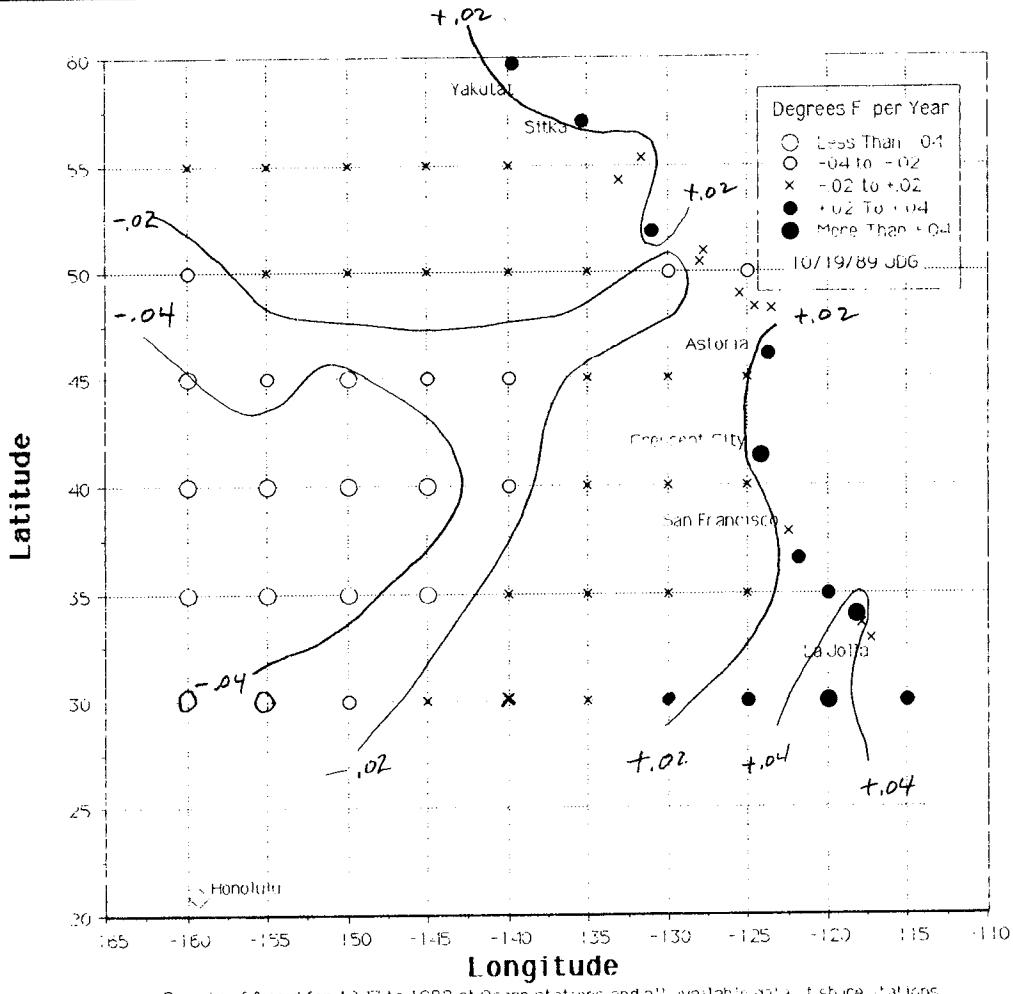


Figure 4
TREND IN SEA SURFACE TEMPERATURE, EASTERN NORTH PACIFIC OCEAN

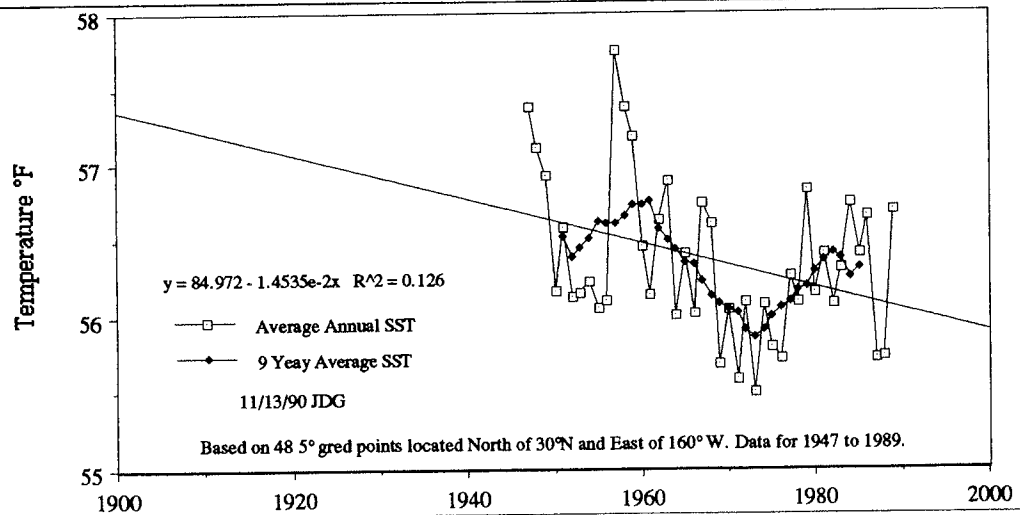


Figure 5
SEA SURFACE TEMPERATURE AT OFFSHORE STATIONS
 9-Year Running Average

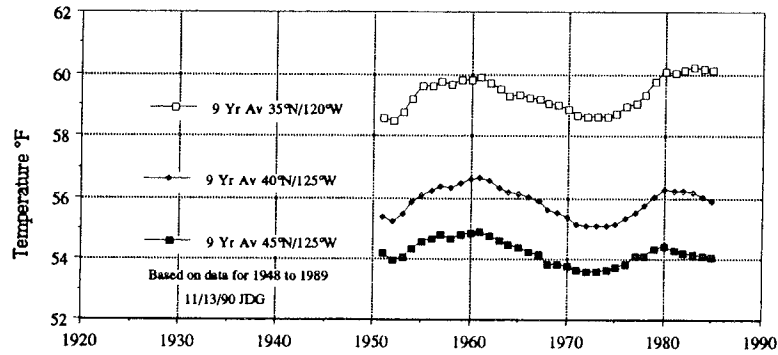


Figure 6
SEA SURFACE TEMPERATURE AT NEAR-SHORE STATIONS
 9-Year Running Average

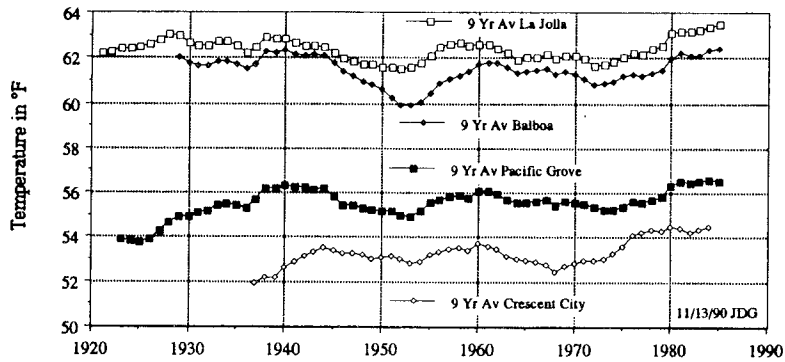


Figure 7
BAKUN'S UPWELLING INDEX
 9-Year Running Average

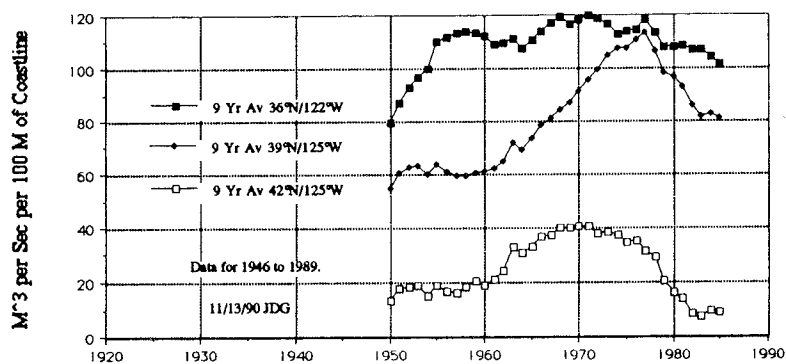


Figure 8
CORRELATION BETWEEN AIR TEMPERATURE AND SEA SURFACE TEMPERATURE

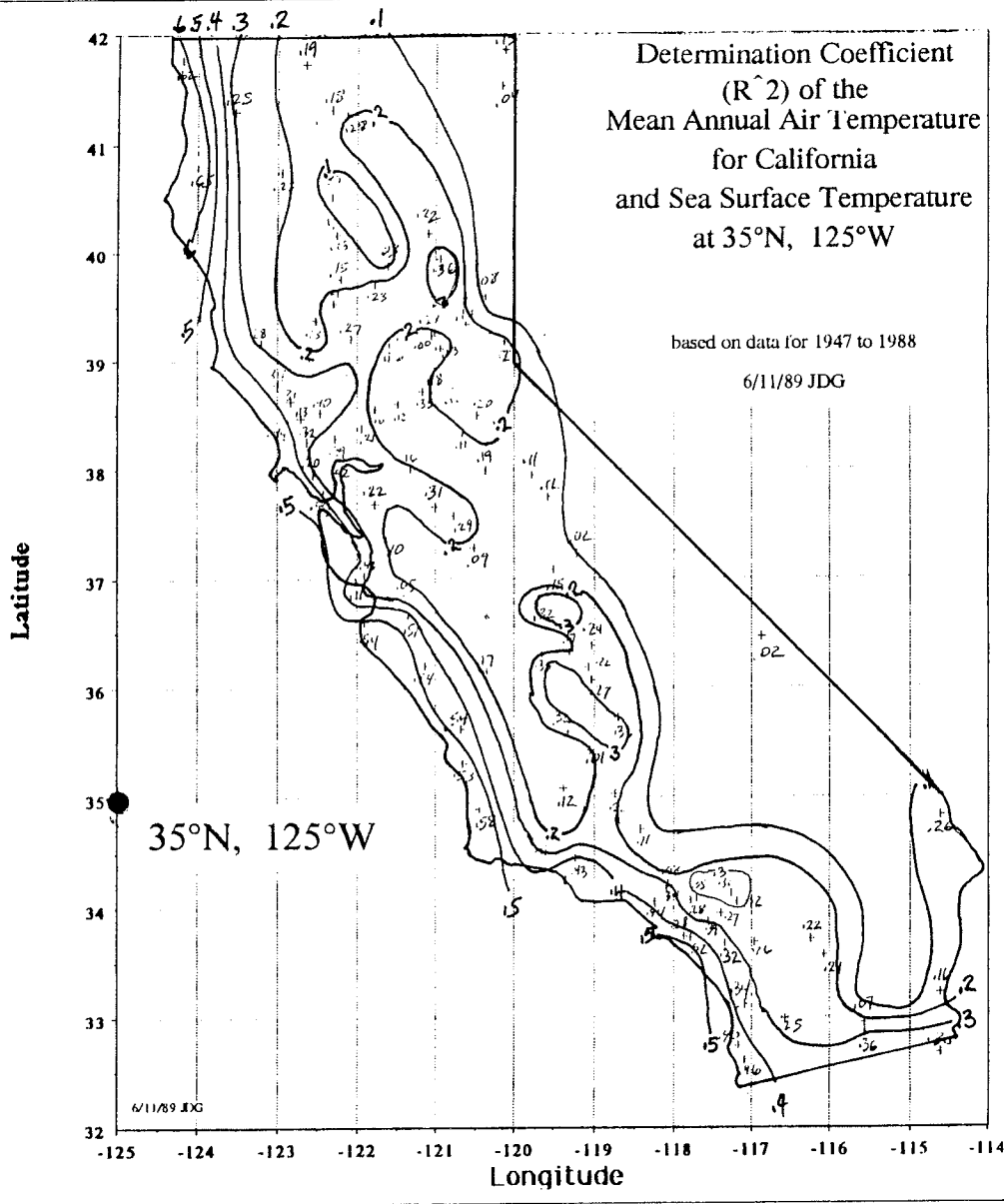
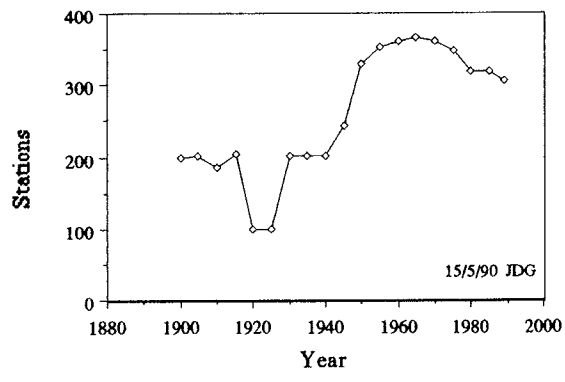


Figure 9
NUMBER OF TEMPERATURE STATIONS IN CALIFORNIA



No of temperature records published in Climatological Data.

Forces acting on air temperature trends, such as the influence of sea surface temperature and urban waste heat, are masked by averaging all records together. Thermometers exposed over blacktop runways or roads may not be compatible with data collected over sodded ground. The traditional "cotton region shelter" has louvers that protect thermometers from the sun, but nothing protects them from long-wave radiation from hot pavement. With shelters over grass, the long-wave radiation may not have been a problem.

We need more answers about the spectral distribution of radiation from the urban environment and how our instrument shelters and thermometers respond to it. It is too early to attribute heating trends to a "greenhouse effect".

Bibliography

- Bakun, A. 1973. *Coastal Upwelling Indices, West Coast of North America 1946-71*, NOAA Technical Report NMFS SSRF-671. Seattle, WA. Updated in J.E. Mason and A. Bakun. 1986. *Upwelling Index Update, U.S. West Coast, 33N-48N Latitude*, NOAA-TM-NMFS-SWFC-67. Monterey, CA.
- Bradley, R.S., R.G. Barry, and G. Kiladis. 1982. *Climatic Fluctuations of the Western United States During the Period of Instrumental Records*. Contribution 25, University of Amherst.
- Cayan, D. 1990. "Monthly Sea Surface Temperature for 1947 to 1989 for a 5 Degree Grid on the North Pacific Ocean". Private communication. Climate Research Division, Scripps Institution of Oceanography, University of California, La Jolla.
- Chernykh, E.L. 1840. "On the Agriculture of Upper California". *The Journal of Rural Economy and Sheep Raising*. No. 9, University Press. Moscow.
- Hanson, J., and S. Lebedeff. 1988. "Global Surface Air Temperatures: Update 1987". *American Geophysical Union*.
- Jones, P.D., T.M.L. Wigley, and P.M. Kelley. 1982. "Variations in Surface Air Temperatures: Part 1. Northern Hemisphere, 1881-1980". *Monthly Weather Review* 110(2).
- Jones, P.D., S.C.B. Raper, R.S. Bradley, D.F. Diaz, P.M. Kelley, and T.M.L. Wigley. 1986. "Northern Hemisphere Surface Temperature Variations: 1851-1984". *J. Climate Appl. Meteor.* 25:2.
- Landsberg, H.E. 1981. *The Urban Climate*. Academic Press National Climatic Data Center, Climatological Data, a monthly publication since 1897 for each state.
- Newell, N.E., R.E. Newell, J. Hsiung, and W. Zhongxiang. 1989. "Global Marine Temperature Variation and the Solar Magnetic Cycle". *Geophysical Research Letters* 16(4).
- Quayle, R.G. 1989. "The Wolbach Dataset for Climate Monitoring — Philanthropy and Climatology". *Bull. of the American Meteorological Society* 70(12).
- Quinlan, F.T., T.R. Karl, and C.N. Williams Jr. 1987. *United States Historical Climatological Network (HNC) Serial Temperature and Precipitation Data*. Carbon Dioxide Information Analysis Center, Numeric Data Collection NDP-019. Oak Ridge TN.

One Hundred Years of Rainfall Trends in California

James D. Goodridge

ABSTRACT: This paper is an examination of precipitation trends in California for 100 years based on 96 rain records. The study resulted from an attempt to develop a wetness index for the San Francisco Bay area, where declining rainfall trends indicated a lot more rainfall in the first 50 years of the study period. A regular pattern of decline was found in California coastal stations, concurrent with an increasing trend at inland stations.

This study looks at interregional correlations in total water year (October to September) rainfall, as well as historical trends in water supply from 1891 to 1990. An index of rainfall was developed by averaging 96 rain records that are continuous for 100 years. It was uncertain at the start whether apparent trends in long records were climatic events or if they were discontinuities in observational technique or gage exposure. Based on similarities in adjacent records, it was concluded that the higher rainfalls before about 1910 at stations like Eureka, Upper Mattole, Fort Ross, Pilarcitos, Mt. Hamilton, Los Gatos, Paso Robles, and Big Bear Lake were real.

One hundred years of rainfall record could hardly be observed by one person, and seldom by the same family or institution. Even the best rainfall records have discontinuities because of changing observers, gage locations, vegetation, or conditions surrounding the gage. Many earlier gages were exposed on roof tops, and others were influenced by trees growing too near. The records of this study are as reported, with no corrections or adjustments.

The records were obtained mainly from the National Climatic Data Center's publication *Climate Data*, but also from other sources, including California Department of Water Resources, San Francisco Water Department, Marin Municipal Water District, and the Sweetwater Authority. Table 1 lists the records and their locations.

Three periods of above average rainfall are apparent from this study: in the 1910s, 1940s, and 1980s. Figure 1 shows average rainfall and a 9-year running average from the 96 rain records. Average rainfall for the 100 years is 23.09 inches. The slightly declining trend shown is not thought to be significant. It is interesting that in the first 50 years, only 1890 had more than 35 inches of rainfall, whereas five of the second 50 years exceeded 35 inches — 1941, 1958, 1978, 1982, and 1983.

In some areas of California, the 100-year rainfall trends have regional characteristics that vary from the statewide average. An outstanding example is the San Francisco peninsula and generally the coastal region, where rainfall has declined in the past 100 years. Another is the San Joaquin Valley, which has a generally increasing trend. Trends in long-term rainfall at individual rain records are plotted on Figure 2.

The year of maximum rainfall was 1890, when 28 of the 96 stations reported the highest rainfalls. Average annual rainfall for 1890 was 43.11 inches. The second wettest year was

Table 1
LOCATION OF CALIFORNIA RAINFALL STATIONS WITH 100 YEARS OF DATA

Station Name	Climatic Division	Latitude dd.dd	Longitude ddd.dd	Elevation Feet	Station Name	Climatic Division	Latitude dd.dd	Longitude ddd.dd	Elevation Feet
Calistoga	No Co	38.58	-122.58	364	San Francisco	Cen Co	37.78	-122.42	52
Eureka	No Co	40.80	-124.17	43	San Jose	Cen Co	37.33	-121.90	300
Ft Ross	No Co	38.52	-123.25	116	San Luis Obispo	Cen Co	35.30	-120.67	224
Healdsburg	No Co	38.62	-122.83	101	Santa Maria	Cen Co	34.95	-120.43	300
Kentfield	No Co	37.95	-122.55	80	Upper Crystal	Cen Co	37.50	-122.32	95
Lagunitas Lake	No Co	37.95	-122.58	785	Watsonville	Cen Co	36.92	-121.75	120
Napa	No Co	38.28	-122.27	73	Santa Cruz	Cen Co	36.98	-122.02	28
San Rafael	No Co	38.00	-122.52	120	Antioch	S J Val	38.02	-121.75	494
Santa Rosa	No Co	38.45	-122.70	167	Bakersfield	S J Val	35.43	-119.50	331
Ukiah	No Co	39.15	-123.20	623	Fresno	S J Val	36.77	-119.72	47
Upper Mattole	No Co	40.25	-124.18	255	Galt	S J Val	38.25	-121.30	284
Weaverville	No Co	40.73	-122.92	2050	Ione	S J Val	38.35	-120.93	38
Auburn	Sac V	38.92	-121.08	1292	Lodi	S J Val	38.12	-121.28	125
Bowman Dam	Sac V	39.45	-120.65	5365	Los Banos	S J Val	36.05	-120.85	172
Capay 4W	Sac V	38.70	-122.12	300	Mendota	S J Val	36.78	-120.33	150
Chico	Sac V	39.70	-121.82	185	Merced	S J Val	37.28	-120.52	91
Colfax	Sac V	39.10	-120.95	2418	Modesto	S J Val	37.65	-121.00	108
Colusa	Sac V	39.20	-122.02	60	Newman	S J Val	37.35	-121.08	155
Davis	Sac V	38.53	-121.77	60	Oakdale	S J Val	37.77	-120.85	393
Dunsmuir	Sac V	41.22	-122.27	2420	Porterville	S J Val	36.07	-119.02	344
Folsom	Sac V	38.70	-121.15	350	Rector	S J Val	36.30	-119.23	1745
Grass Valley	Sac V	39.22	-121.07	2693	Sonora	S J Val	37.98	-120.38	12
Gridley	Sac V	39.37	-121.70	97	Stockton	S J Val	38.00	-121.32	3975
Marysville	Sac V	39.15	-121.58	60	Tehachapi	S J Val	35.13	-118.45	293
Mt Shasta City	Sac V	41.32	-122.32	3544	Tulare	S J Val	36.32	-119.33	115
Nevada City	Sac V	39.25	-121.00	2520	Turlock	S J Val	37.48	-120.85	325
Orland	Sac V	39.75	-122.20	254	Visalia	S J Val	36.33	-119.30	134
Placerville	Sac V	38.60	-120.80	1890	Anahein	So Co	33.83	-117.87	6750
Red Bluff	Sac V	40.15	-122.25	341	Big Bear Lake	So Co	34.25	-116.92	4650
Redding	Sac V	40.58	-122.40	577	Cuyamaca	So Co	32.98	-116.58	375
Sacramento	Sac V	38.58	-121.48	25	El Toro Multon	So Co	33.60	-117.70	822
Vacaville	Sac V	38.37	-121.95	104	Glendora	So Co	34.13	-117.85	417
Williams	Sac V	39.15	-122.15	90	Los Angeles	So Co	34.05	-118.23	53
Willows	Sac V	39.53	-122.20	140	Oxnard	So Co	34.20	-119.18	864
Woodland	Sac V	38.68	-121.80	69	Pasadena	So Co	34.15	-118.12	20
Berkeley	Cen Co	37.87	-122.25	299	Port Hueneme	So Co	34.15	-119.21	1335
Chabot Reservoir	Cen Co	37.73	-122.12	245	Redlands	So Co	34.05	-117.18	840
Gilroy	Cen Co	37.02	-121.57	205	Riverside FS3	So Co	33.95	-117.38	1050
Hollister	Cen Co	36.85	-121.40	284	San Bernardino	So Co	34.12	-117.28	13
King City	Cen Co	36.20	-121.13	320	San Diego	So Co	32.73	-117.18	1560
Livermore	Cen Co	37.68	-121.77	490	San Jacinto	So Co	33.78	-116.95	100
Los Gatos	Cen Co	37.22	-121.98	428	Santa Barbara	So Co	34.42	-119.70	310
Mt Hamilton	Cen Co	37.33	-121.65	4206	Sweet Water	So Co	32.69	-117.01	118
Niles 1 SW	Cen Co	37.58	-121.97	100	Tustin Irwin	So Co	33.73	-117.78	45
Paso Robles	Cen Co	35.63	-120.68	700	Ventura	So Co	34.28	-119.30	-21
Pilarcitos	Cen Co	37.55	-122.42	625	Indio	Desert	33.73	-116.27	914
Salinas	Cen Co	36.67	-121.60	80	Needles	Desert	34.77	-114.62	194
San Andreas	Cen Co	37.35	-122.40	377	Yuma	Desert	32.67	-114.60	

Figure 1
AVERAGE ANNUAL RAINFALL FOR CALIFORNIA

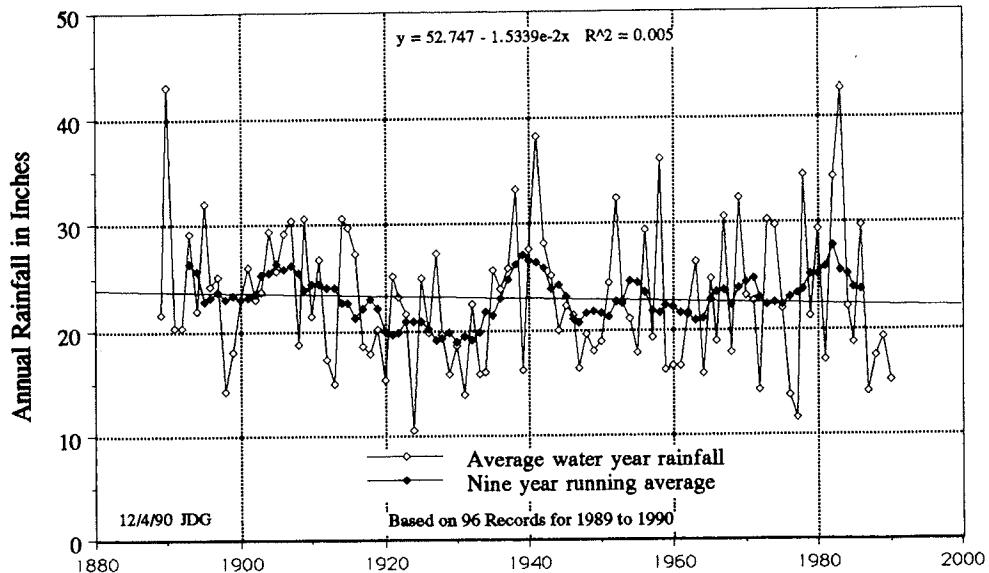
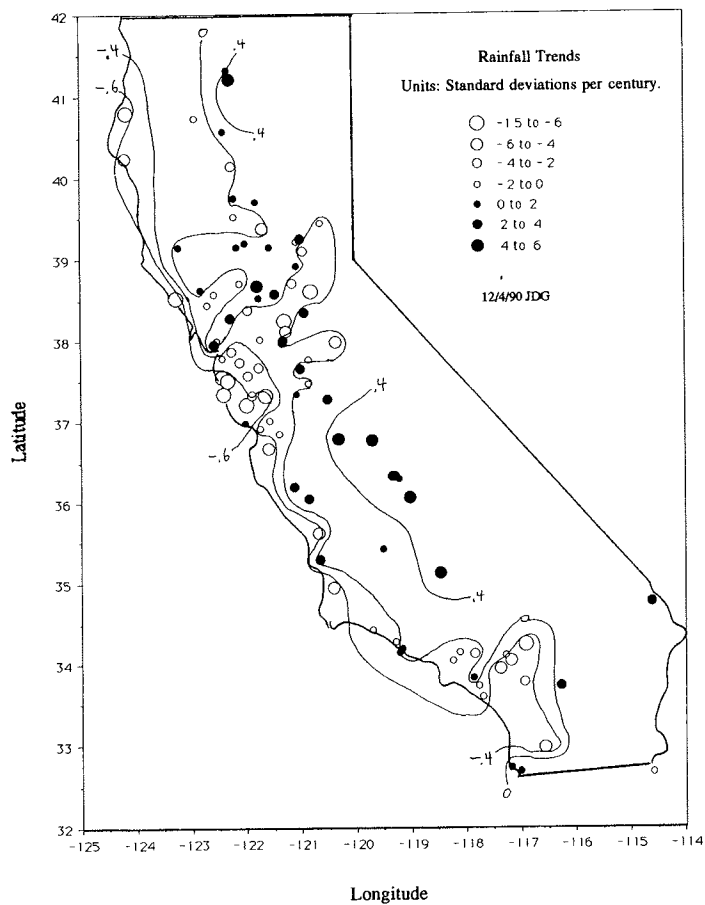


Figure 2
100-YEAR RAINFALL TREND

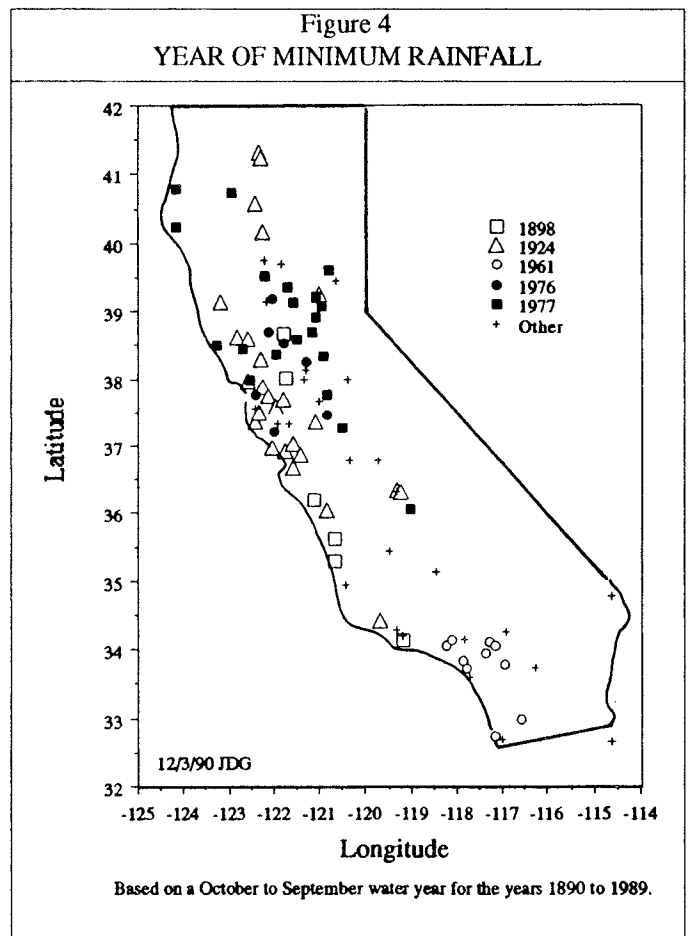
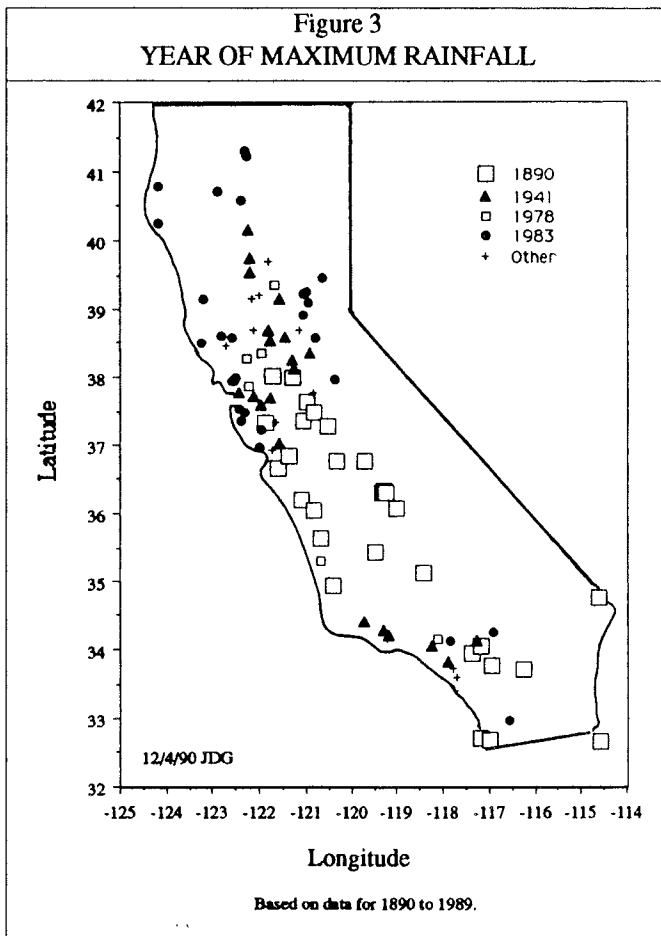


1983, when 27 stations reported record amounts and the state average was 42.75 inches. The other notably wet year was 1941, when the average was 38.28 inches, and 20 of the 96 stations reported the wettest year, as shown on Figure 3.

The driest year was 1924, when the state average rainfall was only 10.50 inches. More stations in the San Francisco Bay region reported 1924 as the driest year than in any other region. The second driest year was 1977, when the average was 11.57 inches. The 1977 drought was worst in Central and Northern California, as shown in Figure 4.

Regional rainfall correlations were studied, with data organized by the climatic divisions used in *Climatological Data*. The inter-regional correlations are listed below. Actual values are the square of the correlation coefficient.

	North Coast	Sacramento Valley	Central Coast	San Joaquin	South Coast	Desert
North Coast	1.000					
Sacramento Valley	0.908	1.000				
Central Coast	0.796	0.885	1.000			
San Joaquin Valley	0.647	0.794	0.869	1.000		
South Coast	0.247	0.366	0.524	0.603	1.000	
Desert	0.004	0.014	0.032	0.055	0.231	1.000
Number of Stations	12	23	20	20	18	3

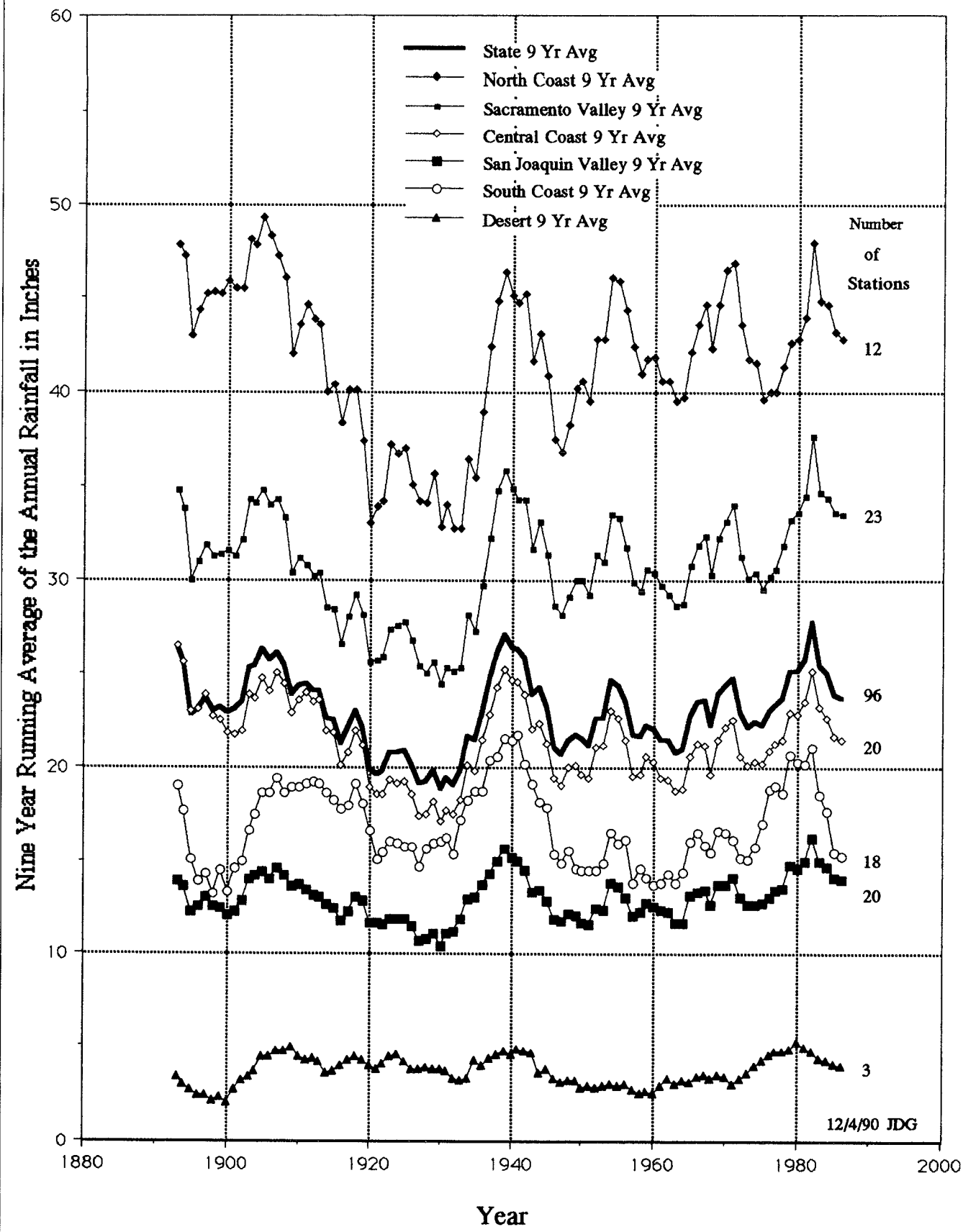


Regional rainfall indexes are shown on Figure 5. These curves represent 9-year running averages of all rain gages in each region. The relatively high values from about 1905, 1940, and 1983 are quite noticeable in each of the six regions. The index of all rainfall records of this study included in Figure 5 contains decade averages of rain for the 100 years. Water year total rainfall is available from the author on 3.5-inch Macintosh diskettes, in Excel format.

A half-dozen stations reported 6 consecutive years with below average rainfall beginning in 1984. Some of the most drought-stricken areas are Gilroy, Salinas, Fort Ross, Big Bear Lake, Redlands, Riverside, and San Jacinto.

The current drought (1987 to 1990), which follows a sequence of wet years (1978 to 1983) seems quite severe, but compared with the dry spell from about 1917 to 1934, it is minor. A 1980 report, *Annual Precipitation For California Since 1600 Reconstructed from Western American Tree Rings*, by Harold Fritts and Geoffrey Gordon of the Laboratory of Tree Ring Research in Tucson, indicates there was a prolonged dry spell in California from about 1755 to 1820.

Figure 5
 REGIONAL RAINFALL TRENDS IN CALIFORNIA, 1889 TO 1989



12/4/90 JDG

1976 Step in the Pacific Climate: Forty Environmental Changes Between 1968-1975 and 1977-1984

Curtis C. Ebbesmeyer, Daniel R. Cayan, Douglas R. McLain,
Frederic H. Nichols, David H. Peterson, and Kelly T. Redmond

Abstract: Examination of 40 time series of multidisciplinary environmental variables from the Pacific Ocean and the Americas, collected in 1968 to 1984, demonstrated the remarkable consistency of a major climate-related, step-like change in 1976. To combine the 40 variables (*e.g.*, air and water temperatures, Southern Oscillation, chlorophyll, geese, salmon, crabs, glaciers, atmospheric dust, coral, CO₂, winds, ice cover, Bering Strait transport) into a single time series, standard variants of individual annual values (subtracting the mean and dividing by a standard deviation) were averaged. Analysis of the resulting time series showed that the single step in 1976, separating the 1968-1975 period from the 1977-1984 period, accounted for 89% of variance within the composite time series. Apparently, one of the Earth's large ecosystems occasionally undergoes large abrupt shifts.

Introduction

The numerous time series of environmental variables are becoming increasingly valuable as concerns arise from human influence on the Earth's ecosystem, particularly as the variables may be critical to comprehensive models describing the Earth's dynamics. Forecasts of global climate change often predict smoothly varying temporal fluctuations; however, some variables have shown fairly abrupt changes over time (McLain 1983, Trenberth 1990). We thought that by combining a large number of environmental variables, the temporal variability could be clarified, thereby providing guidance to modelers.

Through our interest in the temporal structure of environmental variables and our participation in a 7-year series of climate meetings (Peterson 1989), we became aware of the broad diversity of Pacific Ocean environmental variables for a variety of disciplines for which long data sets are available.

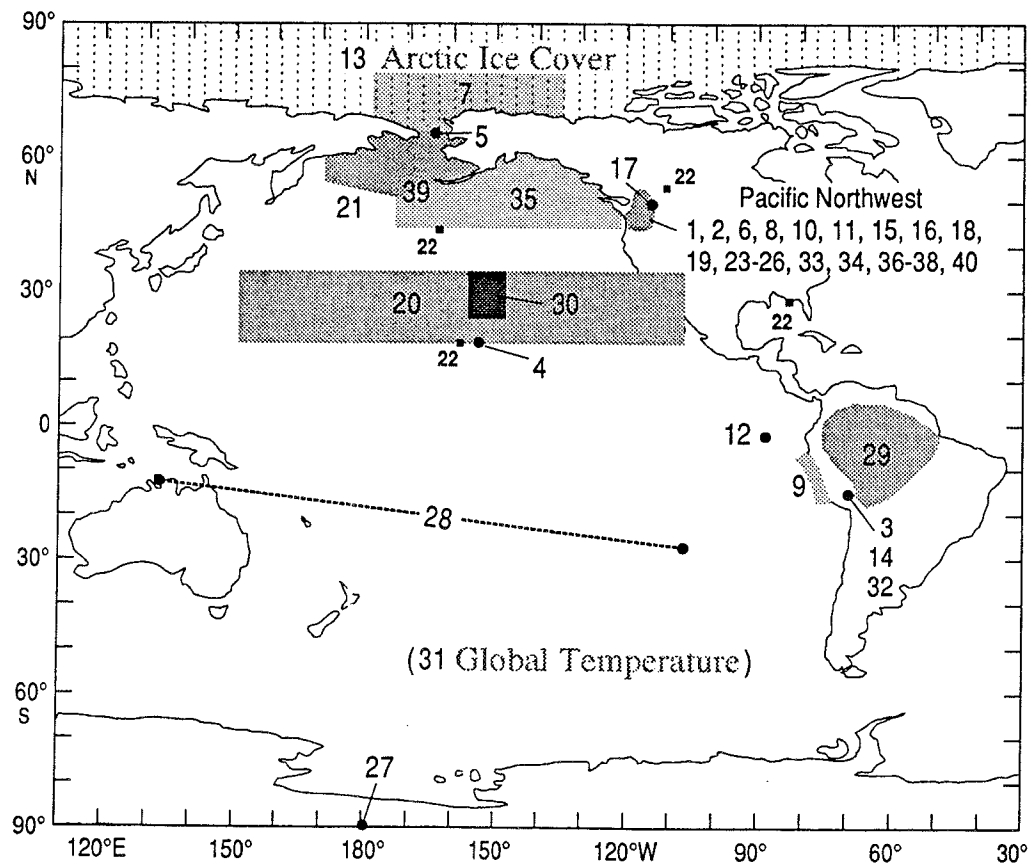
The variables for which we found appropriate data sets (covering the same time span and bracketing the environmental change in 1976) included an array of atmospheric and oceanic characteristics from the broader Pacific basin and from a more localized Northeast Pacific region including Puget Sound (Figure 1; Table 1). If, as we suspected from initial inspections, many variables underwent a sharp change in a single year, plans for dealing with future environmental change would have to include rapid, perhaps unexpected shifts.

Approach

A number of previous studies were structured using three elements of an experiment — subject, stimulus, response (Aitchison and Brown 1969, Benjamin and Cornell 1970, Montroll and Badger 1974). We adopted a similar approach.

Figure 1
LOCATIONS OF THE 40 ENVIRONMENTAL VARIABLES

Circled numbers indicate the rank (lowest to highest) of the step's magnitude for each variable (*d*):
average standard deviate of 1977-1984 minus that for 1968-1976 (see Table 1)



Subject

The data sets we examined fall in two categories:

- Those obtained in several comparatively small regions of the Pacific ecosystem because of practical concern about urban effects.
- Those collected at the Pacific basin scale with reference to the natural variability of the climate.

Consequently, we were able to examine the response of the overall Pacific Ocean, as well as that of one small portion, the Pacific Northwest including Puget Sound. By these selections, variability was characterized over a range of spatial scales, from variability in a single estuary (Puget Sound) to variability over the entire Pacific Ocean and some adjacent areas.

Stimulus

A number of Pacific Ocean environmental variables changed abruptly during 1976 (McLain 1983, Trenberth 1990). In the middle latitudes of the North Pacific, notable large-scale changes were observed in the atmospheric circulation (*e.g.*, a preponderance

Table 1
40 ENVIRONMENTAL VARIABLES RANKED ACCORDING TO THE DIFFERENCE ACROSS THE
STEP BETWEEN AVERAGES COMPUTED FOR 1968-1975 AND FOR 1977-1984

Ranked smallest to largest.
In the Step Magnitude column, asterisks (*) denote variables from the Pacific Northwest and
plus signs (+) denote variables for which signs were reversed (k=1).

Rank	Step Magnitude (d)	Environmental Variable	Notes
1	0.18*	Salinity, Puget Sound, 150-m	Annual average salinity at 150-m depth in Puget Sound's main basin (47.7-47.9°N; 122.4-122.5°W). Ebbesmeyer <i>et al.</i> (1989).
2	0.19*	Conductivity, Snake River	Annual average specific conductivity of the Snake River at King Hill (43°0.17'N; 115°12.08'W). US Geological Survey, Water Res. Div.
3	0.24+	Ice accumulation, Quelccaya ice core	Thompson and Mosley-Thompson (1989).
4	0.36	Atmospheric CO ₂ anomaly, Hawaii	Annual anomaly in concentration of atmospheric CO ₂ at Mauna Loa Observatory, HI. Keeling <i>et al.</i> (1989).
5	0.40+	Transport, Bering Strait	Annual mean volume transport through Bering Strait. Coachman <i>et al.</i> (1988).
6	0.43*	Goose nests, Columbia River	Number of Great Basin Canada goose (<i>Branta canadensis mofitti</i>) nests found annually on islands of the Hanford Reach, Columbia River. L.E. Eberhardt (pers. comm.) and Hanson <i>et al.</i> (1971).
7	0.46+	Sea ice extent, Beaufort and Chukchi seas	Area covered by ice in the Beaufort and Chukchi seas. Manak and Mysak (1987).
8	0.57*+	Water density, Puget Sound	Annual average sigma-t units computed from temperature and salinity at 150-m depth in Puget Sound's main basin. Ebbesmeyer <i>et al.</i> (1989).
9	0.61	Wind stress, Peru	April-September wind stress off Peru. Bakun (1990).
10	0.65*+	Peak water storage, Columbia River basin	Annual maximum total water storage in the basin above The Dalles, OR. Tangborn (1990).
11	0.73*+	Discharge, Fraser River, British Columbia	Annual average (January-December) discharge at Hope, BC (49°22.83'N; 121°27.08'W). Environment Canada (1989).
12	0.74+	Coral, Cd/Ca ratio, Galapagos Islands	Cd/Ca ratio in coral in the Galapagos Islands. Baumgartner, <i>et al.</i> (1989).
13	0.83+	Sea ice extent, Arctic total	Manak and Mysak (1987).
14	0.83	Oxygen isotope, Quelccaya ice cap, Peru	δ ¹⁸ O annual value from Quelccaya summit ice core (13.93°S; 70.83°W). Thompson and Mosley-Thompson (1989).
15	0.97*	Solar radiation, Puget Sound	May-July average at the University of Washington and Lake Washington. Unpublished data, M. Albright (pers. comm.), U. of Wash., Seattle.
16	0.98*+	Upwelling index, winter	Upwelling index for winter at 42°N off Washington. Norton <i>et al.</i> (1985).
17	1.01	Mass balance, Peyto glacier, Canada	Annual mass balance for Peyto glacier (51.67°N; 116.55°W). Walters and Meier (1989).
18	1.03*+	Snow depth, Mount Rainier, Washington	Snow depth on March 15 at Paradise Ranger station (46.78°N; 121.73°W). Unpublished data, National Weather Service.
19	1.06*+	Wind speed, 500 mb, Medford, Oregon	Annual mean wind speed at 500 mb, Medford, OR (42.38°N; 122.88°W). Unpublished data, Archives of Oregon Office of State Climatologist.
20	1.08	Wind speed, winter westerlies, 20-35°N; 110°W 150°E	West-to-east geostrophic wind component at 700 mb averaged during winter over area bounded by 20-30°N by 150°E-110°W.
21	1.15+	Sea ice extent, Bering Sea	Manak and Mysak (1987).

Table 1 (continued)
 40 ENVIRONMENTAL VARIABLES RANKED ACCORDING TO THE DIFFERENCE ACROSS THE
 STEP BETWEEN AVERAGES COMPUTED FOR 1968-1975 AND FOR 1977-1984

Ranked smallest to largest.
 In the Step Magnitude column, asterisks (*) denote variables from the Pacific Northwest and
 plus signs (+) denote variables for which signs were reversed (k=1).

Rank	Step Magnitude (d)	Environmental Variable	Notes
22	1.17	Pacific North American Index	December-February average (Wallace and Gutzler 1981) computed as the linear combination of normalized 500 mb height anomalies (z^*) at four locations: $PNA = \frac{1}{4}[z^*(20^\circ N, 160^\circ W) - z^*(45^\circ N, 165^\circ W) + z^*(55^\circ N, 115^\circ W) - z^*(30^\circ N, 85^\circ W)]$.
23	1.31*+	Precipitation, Cedar Lake, Washington	Annual (January-December) total at $47.42^\circ N$; $121.73^\circ W$. Climatological data for Washington, NOAA.
24	1.36*	Salinity, Puget Sound, surface	Average of monthly salinity values (May-July) near the sea surface in Puget Sound's main basin (47.7 - $47.9^\circ N$; 122.4 - $122.5^\circ W$). Unpublished data, University of Washington and Municipality of Metropolitan Seattle.
25	1.36*+	Discharge, Skagit River, Washington	Annual average discharge (January-December) at Concrete, WA; Monthly reports of Dept. of Interior, US Geological Survey.
26	1.49*+	Oxygen saturation, Puget Sound, surface	Percentage of average monthly dissolved oxygen values (May-July) near the sea surface in Puget Sound's main basin (47.7 - $47.9^\circ N$; 122.4 - $122.5^\circ W$). Unpublished data, University of Washington and Municipality of Metropolitan Seattle.
27	1.42	Atmospheric CO ₂ anomaly, South Pole	Annual anomaly in concentration of atmospheric CO ₂ at the South Pole. Keeling <i>et al.</i> (1989).
28	1.43+	Southern Oscillation Index	Standardized atmospheric pressure difference (annual average) at sea level between Darwin, Australia, and Easter Island. Climate Analysis Center, National Weather Service, NOAA, Washington, DC.
29	1.50+	Discharge, Amazon River, Manacapuru	Richey <i>et al.</i> (1989).
30	1.65	Integrated chlorophyll <i>a</i> , central North Pacific Ocean	Venrick <i>et al.</i> (1987).
31	1.70	Global mean annual air temperature	Jones <i>et al.</i> (1986).
32	1.76	Particle concentration, Quelccaya ice cap, Peru	Concentration greater than 0.63μ from Quelccaya summit ice core ($13.93^\circ S$; $70.83^\circ W$). Thompson and Mosley-Thompson (1989).
33	1.95*	Wind frequency, southerly, Tacoma, Washington	Average frequency of southerly wind (102 - $258^\circ T$) for May-July at Tacoma, WA ($47.27^\circ N$; $122.52^\circ W$). Unpublished data, Puget Sound Air Pollution Control Agency.
34	2.08*	Crab, Dungeness, Puget Sound	Commercial Dungeness crab (<i>Cancer magister</i>) production. Bumgartner <i>et al.</i> (1989).
35	2.05	Water temperature, sea surface, northeastern Pacific	Sea surface temperature over the northeast Pacific Ocean averaged from $175^\circ W$ eastward and $45^\circ N$ northward to the coast. Royer (198*).
36	2.34*	Salmon migratory route, Vancouver Islands, Canada	Fraction of Fraser River sockeye salmon (<i>Oncorhynchus nerka</i>) returning around the northern end of Vancouver Island. Hamilton (1987).
37	2.47*+	Secchi disk depth, Puget Sound	Deepest depth observed of a 0.3-m diameter white (Secchi) disk beneath the water surface (May-July average). Unpublished data, Municipality of Metropolitan Seattle.
38	2.77*	Mollusk abundance, Puget Sound, 200 m depth	Abundance of <i>Macoma carlottensis</i> at 200-m depth at station 2 ($47^\circ 42.0' N$; $122^\circ 27.2' W$) in Puget Sound's main basin off West Point. Nichols (1988).
39	2.81	Salmon catch, Alaska	Alaska salmon catch. NOAA (1988).
40	4.39*	Water temperature, Puget Sound, 150-m	Annual average at 150-m depth in Puget Sound's main basin. Ebbesmeyer <i>et al.</i> (1989).

of deepened Aleutian lows in winter) and in the distribution of sea surface temperature (*e.g.*, cooler in the west and central sectors and warmer in the east along the coast of North America).

In the tropics, there was a shift toward more frequent El Niño conditions, evident in the reduced gradient of atmospheric pressure from east to west across the Pacific basin, as well as in a tendency for warmer sea surface temperature in the central-to-eastern Pacific. Associated changes in physical and biological variables indicate several regions and disciplines followed this large-scale shift.

Therefore, we examined all the data sets for equivalent periods before and after this 1976 change (hereafter called the “step”). The 1976 step change was taken as the stimulus.

Response

To characterize the response, differences were computed between the mean of the variables before and after the step.

Methods

Data were available in the literature for a wide range of variables, but only up to 1984. Therefore, to equally weight the years before and after the step, we examined the eight years before the step (1968-1975) and the eight years after the step (1977-1984), yielding a total interval of 17 years including the year of the step (1976). By averaging over two 8-year blocks of time, we were able to estimate changes between two intervals that were approximately decadal.

To describe the Pacific environmental system, about equal numbers of variables were selected from each of the regional- and oceanic-scale data sets, yielding a total of 40 variables. To reduce bias, we tried to select variables with broad coverage of geographic and environmental disciplines and to include no more than a few of the same kind of variable. Both the dimensions and signs of the variables were eliminated.

To remove dimensions, we computed a standard deviate for each value in a time series by subtracting the mean of the time series and dividing by a standard deviation. Realizing a step was contained in the observations, we normalized with parameters not biased by the size of the step in a given time series. To do this, we subtracted the mean of the entire 17-year time series from each annual value, then divided the annual values prior to the step with the standard deviation of the first eight annual values (1968-1975) and divided those after the step with the standard deviation of the last eight annual values (1977-1984). As we found that the standard deviations were not correlated with step size and were almost identical for the first and the last eight years, bias toward the decades before or after the step was reduced.

Regarding elimination of variable signs, our sample of 40 variables is about equally divided; 22 increased and 18 decreased over the step. However, because we were most interested in magnitude of change, we reversed the signs of the 17 annual values of those variables that decreased so that prior to the step, the average value of each variable lies below the 17-year average and afterward, the average value lies above the 17-year average.

This operation enabled us to combine the 40 time series, thereby illustrating the step's average magnitude.

The computations may be expressed mathematically as follows. Given that x_i is the estimate of environmental variable x in the i^{th} year, the x_i is normalized as $v_i = (x_i - x_m) / \sigma$, where $x_m(1968-1984)$, ($\sigma 1968-1975$) if $i=1968-1975$, $s(1977-1984)$ if $i=1977-1984$, the subscript m denotes the mean of the associated variable, and σ the standard deviation computed over the years in parentheses, inclusively. The signs of v_i are rectified as $v_{ri} = (-1)^k v_i$, where $k=1$ if $v_m(1968-1975) > v_m(1977-1984)$, and $k=2$ if $v_m(1968-1975) < v_m(1977-1984)$. Then the magnitude of the step (d) may be expressed as the difference $d = |v_m(1968-1975) - v_m(1977-1984)|$.

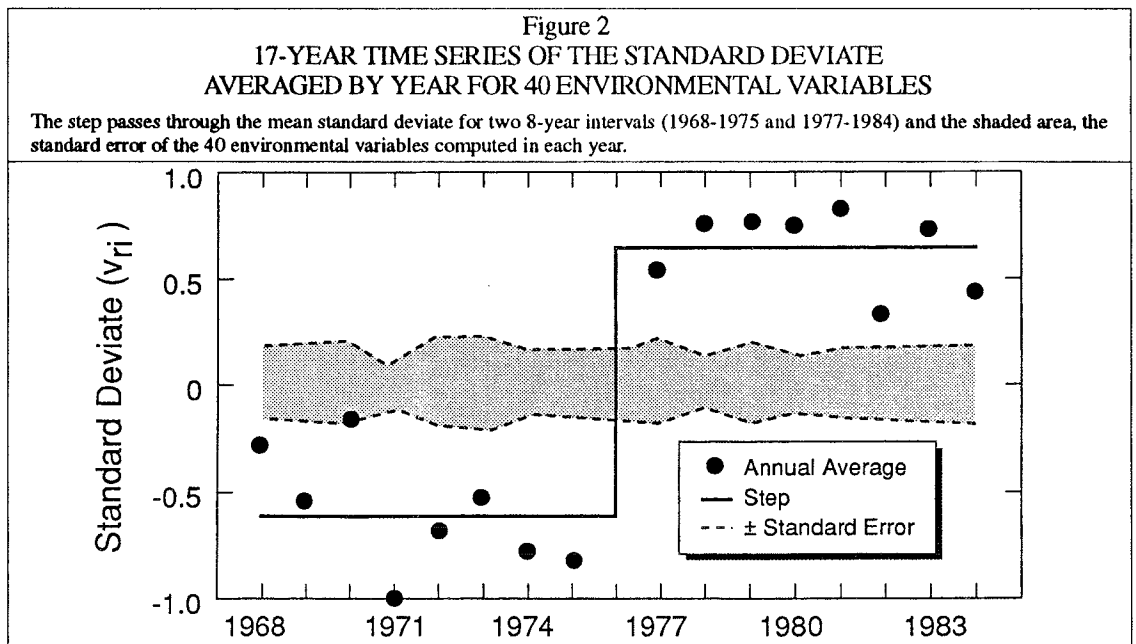
Results

Our methods described the temporal structure of the environmental time series and the step's magnitude, as follows.

Temporal Structure of Composite Time Series

The time series of the 40 variables were superimposed by calculating for each year the mean and standard deviation of the standard deviates (v_{ri}). Standard errors of the annual mean values were computed as $\pm s / \sqrt{n}$, where s the standard deviation and n is the sample size (equaling 38 variables in the average year; a few values were missing in some years). Before the step, the deviates were an average of 3.6 times below the standard error; after the step, the deviates were an average of 3.9 times above the standard error. Therefore, the deviates before and after the step were large.

Dimensions were eliminated using standard deviations computed from data before and after the step. Therefore, the step may have been influenced by temporal fluctuation of the standard deviation of the environmental variables. Since the sample size was nearly constant from year to year, the standard errors, shown in Figure 2, are indicative of the



variation of environmental variables within a given year. The lack of an apparent trend suggests that within-year variability was not a contributing factor to the step.

Further calculations were made to ascertain whether a “step” is an appropriate description of the temporal structure of the composite time series. Three kinds of variation were considered: uniform change (a line with a slope), near-step (rapid, but not instantaneous, change computed as a 3-year moving average), and the step (instantaneous change as described above). These descriptions accounted for the following percentages of the variance:

Uniform change — 59%;

Near-step — 90%; and

Step — 89% ($v_{ri}=-0.609$, 1968-1975; $v_{ri}=+0.634$, 1977-1984).

Since observations with step explained most of the variance of the composite time series, we deemed it an appropriate description.

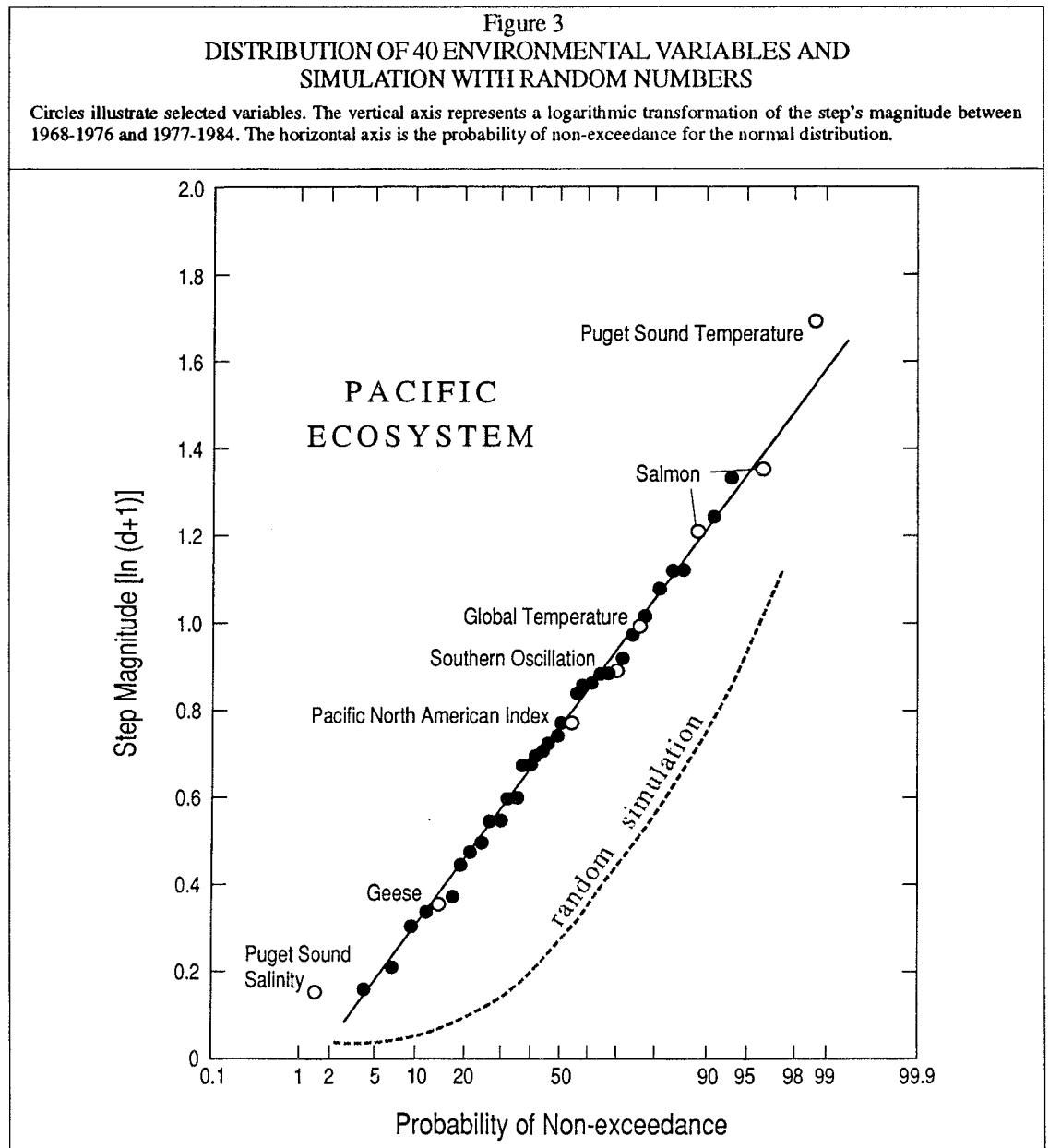
Variability of Step Magnitude

To explore the magnitude of the step, estimates of magnitude were ranked. From previous studies of natural variability, we thought logarithms of the differences across the step might be distributed with about normal probability, an hypothesis that would be supported if the logarithms occurred as a straight line on normal probability paper. The difference across the step for each environmental variable was expressed as $\ln(d+1)$, where 1 has been added to avoid negative logarithms. The values of $\ln(d+1)$ were ranked from smallest to largest and the rank (j) converted to cumulative probability (p), using the convention $p=(j-0.5)/40$ (Mann *et al.* 1974). In the graph of $\ln(d+1)$ versus p (Figure 3), the abscissa corresponds to the non-exceedance probability for a normal distribution.

To explore the ranking of the step magnitudes, three inquiries were made.

- Variables drawn from the Pacific Northwest and Pacific Ocean areas were combined, then inspected to determine whether variables from both areas occur at intervals throughout the ranking for the combined data sets (Table 1 and Figure 3). If data from the two areas were different, values for one of the areas might be expected to cluster in a portion of the overall ranking. Also, the clustering might be evident in abrupt changes in the slope of the probability distribution. Since neither clustering (Table 1) nor obvious changes of slope (Figure 3) is present, we infer that responses from the two areas are similar.
- Quantitative tests, following the method of Aitchison and Brown (1969) for log-normal distributions, showed that means and variances of the Pacific Northwest and Pacific Ocean variables were not different at the 95% limit. The foregoing analyses suggest that distributions at the two spatial scales are not substantially different.
- The distribution for the combined data was compared with a distribution constructed using random numbers (Figure 3) by simulating the time series of the variables with trials of 17 numbers drawn at random from a table of random numbers (Table 26.11, Abramowitz and Stegun 1965).

As described above, standard deviates were computed for each random number series as if it were an environmental variable. The average step magnitude for the random numbers (0.50 deviates) differed from the mean of the environmental variables (1.29 deviates) by 6-9 times the standard errors of the samples (0.10 for random numbers; 0.13 for environmental variables). The magnitudes of the step for the environmental variables appear to be substantially larger than the simulations with random numbers.



Discussion

We are in agreement with the statement of McGowan (1989):

We have very little in the way of conceptual models that provide testable predictions of the behavior of complex pelagic systems, especially how they may or may not respond to climate forcing.

Our analysis of a 17-year time series of many variables characterizing the Pacific ecosystem suggests that, after a number of years of minor interannual variability, the ecosystem may undergo a substantial shift followed by a return to secondary variability. In this sample, variables shifted in 1976 by an amount averaging 4-7 times interannual variability during the preceding and succeeding eight years.

In our sample a number of environmental variables do not show substantial change. For example, 16 of the variables had steps less than the mean-plus-one standard deviation for the random numbers (one deviate). Nevertheless, they are part of the continuum of changes associated with the overall step. Consequently, they deserve as much attention as the variables that changed substantially.

In a study of the variable at the lowest percentile (salinity in deep water in Puget Sound at the first percentile, Table 1), salinity changed by only a small amount, because influences at the oceanic scale tended to cancel those at the regional scale (Ebbesmeyer *et al.* 1989). Specifically, as the Aleutian low pressure center shifts toward the west, storm tracks shift to the south and more frequently intersect drainage basins in the Pacific Northwest. The increased runoff to Puget Sound tends to lower the deep salinity. However, as the storm tracks shift, so do the advective oceanic processes that influence the oceanic source of water for Puget Sound. While Puget Sound salinity tends to decrease as streamflow increases, the oceanic source becomes saltier, with the net result that, when averaged over a decade, the deep salinity tends to not change by significant amounts.

The foregoing example suggested to us that variables at lower percentiles are controlled by linkages that have the net effect of canceling one another, whereas linkages for the variables at higher percentiles tend to amplify one another. When viewed this way, the linkages that tend to cancel become as informative as those that greatly amplify.

Although we have focused on the Pacific Northwest, where variables range between ranks of 1 and 40, environmental variables in our sample also cluster around other regions of the Pacific ecosystem. For example, variables near Hawaii range between ranks of 4 and 30, and in northern South America they between 3 and 32. These three areas illustrate that even if an area is small compared with the overall Pacific Ocean, variability of the response remains nearly as large as that for the entire environmental system.

Conclusions

As many environmental variables describing the Pacific Ocean environmental system changed abruptly in 1976, a single step between constant values during the periods 1968-1975 and 1977-1984 accounted for 89% of the variance of a composite time series derived from annual values of 40 multidisciplinary environmental variables. Regional and

large-scale environmental variables changed by similar degrees within the overall probability distribution.

Available time series covering decades are unevenly distributed among the disciplines. Therefore, to adequately describe the Pacific system and its statistics and dynamics, many more time series of biological/chemical/physical variables spanning decades must be obtained.

Acknowledgments

We thank the sponsors and participants of the Pacific Climate (PACCLIM) workshops for their encouragement and suggestions. We also thank the following colleagues for sharing unpublished data: Mark Albright and Jack Rensel (University of Washington), Wendell Tangborn (Hymet, Inc.), and Paul R. Olson (City of Seattle). We are also grateful to Dora P. Henry for editing and Jeanne Delio-Stevens for preparing the figures.

References

- Abramowitz, M., and I.A. Stegun. 1965. *Handbook of Mathematical Functions with Formulas, Graphs, and Mathematical Tables*. National Bureau of Standards, Applied Mathematics Series 55.
- Aitchison, J., and J.A.C. Brown. 1969. *The Lognormal Distribution*. Cambridge University Press.
- Bakun, A. 1990. "Global Climate Change and Intensification of Coastal Ocean Upwelling", *Science*, 247:198-201.
- Baumgartner, T.R., J. Michaelsen, L.G. Thompson, G.T. Shen, A. Soutar, R.E. Casey. 1989. "The Recording of Interannual Climatic Change by High-Resolution Natural Systems: Tree Rings, Coral Bands, Glacial Ice Layers, and Marine Varves" in *Aspects of Climate Variability in the Pacific and the Western Americas*. Ed. D.H. Peterson. American Geophysical Union. Geophysical Monograph 55:1-14.
- Benjamin, J.R., and C.A. Cornell. 1970. *Probability, Statistics, and Decision for Civil Engineers*. McGraw-Hill.
- Bumgartner, R.H. 1989. "Puget Sound Crab and Shrimp Management" in *Status and Management of Puget Sound's Biological Resources*. Ed. J.W. Armstrong and A.E. Copping. Proceedings from the Forum on Puget Sound's Biological Resources — Status and Management, September 11-12, 1989. p. 32-47.
- Coachman, L.K. and K. Aagaard. 1988. "Transports Through Bering Strait: Annual and Interannual Variability". *J. Geophys. Res.*, 93(C12):15535-15539.
- Ebbesmeyer, C.C., C.A. Coomes, G.A. Cannon, and D.E. Bretschneider. 1989. "Linkage of Ocean and Fjord Dynamics at Decadal Period" in *Aspects of Climate Variability in the Pacific and the Western Americas*. Ed. D.H. Peterson. American Geophysical Union. Geophysical Monograph 55:399-417.
- Environment Canada. 1989. *Historical Streamflow Summary, British Columbia*. Inland Waters Directorate, Water Resources Branch, Water Survey of Canada. Ottawa.

- Fitzner, R.E. and W.H. Rickard. 1983. "Canada Goose Nesting Performance Along the Hanford Reach of the Columbia River, 1971-1981". *Northwest Science*, 57(4):267-272.
- Hamilton, K. 1987. "Interannual Environmental Variation and North American Fisheries". *Bulletin American Meteorological Society*, p. 1541-1548.
- Hanson, W.C. and L.L. Eberhardt. 1983. "A Columbia River Canada Goose Population 1959-1970". *Wildlife Monograph* No. 27, The Wildlife Society.
- Jones, P.D., T.M.L. Wigley, and P.B. Wright. 1986. "Global Temperature Variations Between 1861 and 1984". *Nature*, 322:430-434.
- Keeling, C.D., R.B. Bacastow, A.F. Carter, S.C. Piper, T.P. Whorf, M. Heimann, W.G. Mook, and H. Roeofzen. 1989. "A Three-Dimensional Model of Atmospheric CO₂ Transport Based on Observed Winds: 1. Analysis of Observational Data" in *Aspects of Climate Variability in the Pacific and the Western Americas*. Ed. D. H. Peterson. American Geophysical Union, Geophysical Monograph 55:165-236.
- Manak, D.K., and L.A. Mysak. 1987. *Climatic Atlas of Arctic Sea Ice Extent and Anomalies, 1953-1984*. Climate Research Group Report 87-8.
- Mann, N.R., R.E. Schafer, and N.D. Singpurwalla. 1974. *Methods for Statistical Analysis of Reliability and Life Data*. John Wiley and Sons.
- McGowan, J.A. 1989. "Pelagic Ecology and Pacific Climate". in *Aspects of Climate Variability in the Pacific and the Western Americas*. Ed. D.H. Peterson. American Geophysical Union, Geophysical Monograph 55:141-150.
- McLain, D.R. 1983. "Coastal Ocean Warming in the Northeast Pacific, 1976-83". in *The Influence of Ocean Conditions on the Production of Salmonids in the North Pacific*. Ed. W.G. Pearcy, Oregon State University, Sea Grant College Program, ORESU-W-83-001, pp. 61-86.
- Montroll, E.W., and W.W. Badger. 1974. *Introduction to Quantitative Aspects of Social Phenomena*, Gordon and Breach Science Publishers.
- Nichols, F.H. 1988. "Long-Term Changes in a Deep Puget Sound Benthic Community: Local or Basinwide?" in *Proceedings First Annual Meeting on Puget Sound Research*, Vol. 1, pp. 65-71.
- National Oceanic and Atmospheric Administration. 1988. "The Role of Sea Ice in Controlling Arctic Ecosystems" in *Ocean System Studies NOAA/OAR Research Strategy I, The Ocean System — Prediction and Resources*.
- Norton, J., D. McLain, R. Brainard, and D. Husby. 1985. "The 1982-83 El Niño Event Off Baja and Alta California and Its Ocean Climate Context" in *El Niño North: Niño Effects in the Eastern Subarctic Pacific Ocean*. Ed. W.S. Wooster and D.L. Fluharty. Washington Sea Grant Program, WSG-W0 85-3. p. 44-72.
- Peterson, D.H. Ed. 1989. *Aspects of Climate Variability in the Pacific and the Western Americas*. American Geophysical Union, Geophysical Monograph 55.
- Richey, J.E., C. Nobre, and C. Deser. 1989. "Amazon River Discharge and Climate Variability: 1903 to 1985". *Science*, 246:101-102.

- Royer, T.C. 1989. "Upper Ocean Temperature Variability in the Northeast Pacific Ocean: Is It an Indicator of Global Warming?" *J. Geophys. Res.*, 94(C12):18175-18183.
- Tangborn, W. 1990. "A Basin Water Storage Model for Forecasting Columbia River Runoff". Presented at Northern Hydrology Symposium, Saskatoon, Saskatchewan.
- Thompson, L.G., and E. Mosley-Thompson. 1989. "One-Half Millennia of Tropical Climate Variability as Recorded in the Stratigraphy of the Quelccaya Ice Cap, Peru". in *Aspects of Climate Variability in the Pacific and the Western Americas*, Ed. D.H. Peterson. American Geophysical Union, Geophysical Monograph 55:15-31.
- Trenberth, K.E. 1990. "Recent Observed Interdecadal Climate Changes". American Met. Soc. Special Session on Climate Variations and Joint Session on Hydrology and Climate Variations, Anaheim, CA, February 4-9.
- Venrick, E.L., J.A. McGowan, D.R. Cayan, and T.L. Hayward. 1987. "Climate and Chlorophyll *a*: Long-Term Trends in the Central North Pacific Ocean". *Science*, 238:70-72.
- Wallace, J.M., and D.S. Gutzler. 1981. "Teleconnections in the Geopotential Height Field During the Northern Hemisphere Winter". *Monthly Weather Review*, 109(4):784-812.
- Walters, R.A., and M.F. Meier. 1989. "Variability of Glacier Mass Balances in Western North America" in *Aspects of Climate Variability in the Pacific and the Western Americas*. Ed. D.H. Peterson. American Geophysical Union, Geophysical Monograph 55:365-374.

Climate Forcing of Pacific Herring Recruitment and Growth in Southern British Columbia

Daniel M. Ware

ABSTRACT: Over the last 50 years, much of the variability in ocean climate and herring recruitment has occurred at two dominant periods centered around 5 and 16 years. Herring growth has also exhibited a dominant 5- and 18-year periodicity. A recent analysis of a number of relevant time series suggests that interannual variations in oceanic conditions off the west coast of Vancouver Island affect survival of herring and their principal predator, Pacific hake, which also exhibits a marked 16-year oscillation in abundance. Thus the dynamics of the herring stock are modulated by a combination of climate and predator forcing. Much of the interannual variation in herring growth is centered around the 5-year (moderate ENSO period) and 16-year (strong ENSO period) ocean climate oscillations and the 16-year recruitment oscillation.

Introduction

The climate of the eastern Pacific Ocean oscillates at several frequencies. In the high frequency range, moderate to strong ENSO events occur about every 5-6 years (Quinn *et al.* 1978). In the mid-frequency range (decadal scale) strong ENSO events have occurred about every 12-14 years. Longer oscillations surely exist, but they have not been resolved because the relevant instrument time series are so short. However, analyses of proxy records, like Douglas' (1980) tree-ring growth data off Baja California and fish-scale deposition rates off Santa Barbara (Smith and Moser 1988), reveal longer period oscillations in ocean climate on the order of 40-65 years.

Pacific hake is currently the dominant pelagic fish species off the west coast of North America. They spawn off the Californias in winter (primarily in January). The older fish in the population migrate northward in spring as far as the west coast of Vancouver Island, where about 300-400 thousand tonnes typically arrive in mid-June. The hake's annual migration pattern defines the northern boundary of the Coastal Upwelling Domain, which extends from Baja California (25° N) to the northern tip of Vancouver Island (51° N) (Ware and McFarlane 1989). Hake are the principal predator of Pacific herring, and herring recruitment is negatively correlated with hake biomass (Ware and McFarlane 1986). Recruitment variability in hake responds to changes in oceanic conditions off Southern California during the spawning season, but the biological mechanism is not clear.

Pacific sardines also migrated to the west coast of Vancouver Island in summer to feed. Sardines were the target of a major summer fishery in this area for two decades (1925-1945) before the stock collapsed. The demise of the sardine coincided with the longest and sharpest decrease in upwelling (indexed by salinity) and temperature off British Columbia over the length of these records.

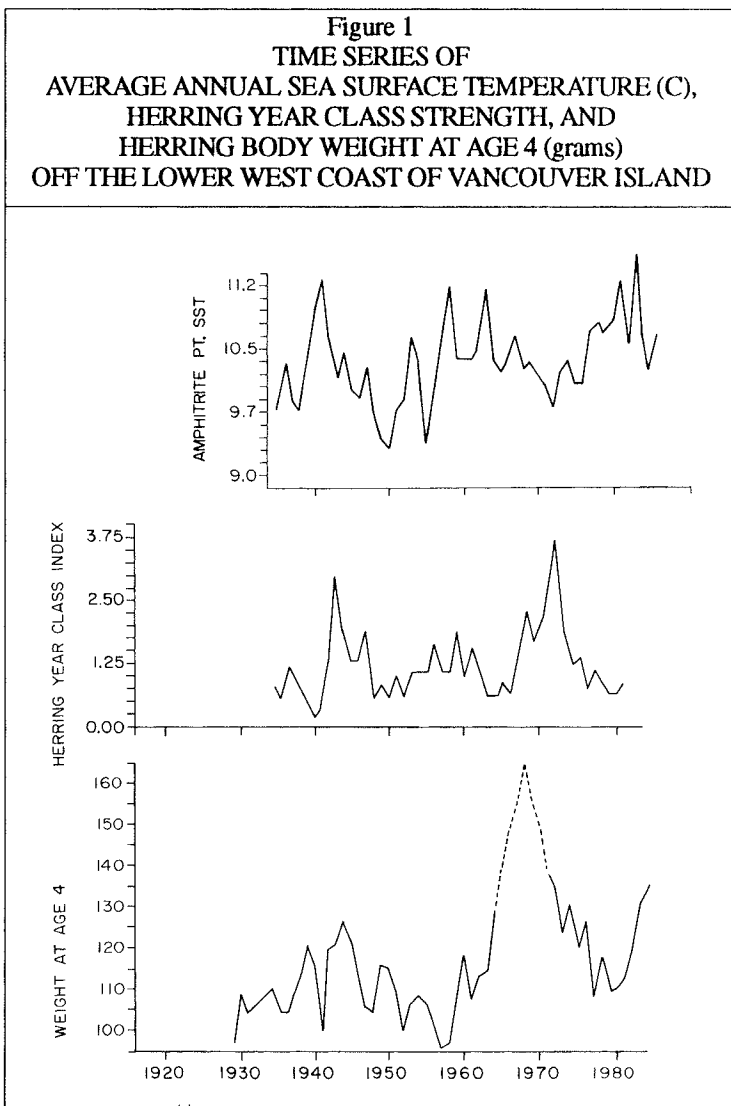
The purpose of this note is to briefly review the pattern of variability in ocean climate in the northern part of the Coastal Upwelling Domain and what is known about the effect of

ocean climate, predators, and planktonic food supply on Pacific herring recruitment and growth during this century.

Data and Results

The annual sea surface temperature (*SST*) time series off the lower west coast of Vancouver Island (Amphitrite Point lighthouse, $\sim 49^\circ$ N) comes from data compiled by the Institute of Ocean Sciences, Pat Bay, British Columbia. The herring year-class strength and weight-at-age-4 time series come from Ware (in press). Note that herring weights were not measured from 1966-1971, so the record was interpolated during this period. The dominant periodicities in these time series were determined by first taking differences to detend the data, and then calculating the auto-correlation function (*ACF*) of the time series at successive lags.

The annual, average *SST* record shows a significant time-dependent increase from 1935-1986 (Figure 1; $p=0.04$). However, there have been some notable deviations from this trend. There were three anomalously warm periods — 1939-1942, 1958-1963, and 1977-84 — each of which was punctuated by a strong ENSO event (1940/41, 1957/58, and 1982/83). There was also an anomalously cool period between 1943 and 1952.



While the *SST* has been rising, there has been a significant decrease in both the average annual salinity ($p<0.001$) and salinity during the upwelling season (May-September) off the west coast of Vancouver Island. The *SST* *ACF* showed a dominant periodicity at 5 and 17 years, while the annual salinity *ACF* peaked at 6 and 15 years.

Herring year-class strength is a relative measure of abundance in the year of birth and is defined by abundance of the year class when it first recruits to the fishery at age 3. Herring year-class strength (or recruitment) has undergone three major oscillations over the length of the record (47 years), but is stationary in the sense that there has been no significant time-dependent trend. During the period in question, year-class strength has varied by a factor of 17. The dominant periodicity in the recruitment time series in this century has occurred at average periods of 4 and 16 years. A regression analysis indicated that herring year-class strength was negatively correlated with the summer biomass of hake and the average annual *SST* herring encounter in the La Perouse bank area during their first year of life (Ware in press). Herring year-class strength was also positively correlated with the body weight at age 4.

The average weight of a herring at age 4 varied from 96 grams in 1957 to about 165 grams in 1968. The latter value is an interpolated estimate based on trends in the data before and after 1968 (Figure 1). The size-at-age record shows a minor oscillation of 5 years superimposed over a major oscillation of 25 years. The size-at-age record was broken into two segments for analysis: 1929-1961 and 1962-1984. During the first period, size-at-age (a measure of growth) was positively correlated with summer salinity and with the sardine catch. In the second period, size-at-age was negatively correlated with annual SST and with herring recruitment (*i.e.*, size-at-age-4 tends to be smaller in large year classes and larger in small year classes).

Discussion

Linkages between the time series briefly outlined here and discussed in more detail elsewhere (Ware in press) suggest that variations in ocean climate moderate herring recruitment by alternating both predator and food abundances. With respect to predators, recent field data confirm that hake are the single most important herring predator. Hake year-class strength tends to be better than average in warm years in the nursery area off California, so when these fish eventually migrate to Canadian waters to feed at about 6 years, they have a strong, negative impact on herring survival. With respect to the food supply, zooplankton biomass is negatively correlated with water temperature (Reid *et al.* 1958), so the resulting climate-forced oscillation in zooplankton may affect survival of herring directly, by changing their physiological fitness, or indirectly, by changing the abundance of alternative prey of predators that forage on both zooplankton and young-of-the-year herring.

The historical time series indicate that herring growth has responded to changes in year-class size and presumably in the food supply. My interpretation of the correlation structure of the data (Ware in press) is that higher summer salinities (and lower temperatures caused by increased upwelling along the coast) tend to support more diatoms and zooplankton. This increase in food supply:

- » *Resulted in high herring growth rates (hence the positive correlation between summer salinity and herring size-at-age),*
- » *Led to an increase in herring year-class strength, and*
- » *Attracted a greater abundance of sardine to the region, which produced higher catches.*

During the period when sardines were available off British Columbia, herring year-class strength was positively correlated with the sardine catch. This suggests that oceanic conditions responsible for attracting a high abundance of sardines also tended to produce larger year classes of herring. The supply of plankton, specifically diatoms and copepods, may be the common factor linking herring growth, year-class strength and sardine abundance.

The picture that emerges from analysis of the historical ocean climate and fisheries time series off British Columbia is that abundance of the dominant migratory predator, hake, in

the Coastal Upwelling Domain is being forced (at least in part) by the dominant 5- and 16-year oscillations in ocean climate. Consequently, both hake and ocean climate are responsible for forcing a 16-year oscillation in herring recruitment.

With respect to herring growth, much of the interannual variation is centered around the 5- and 16-year ocean climate oscillations and the 16-year recruitment oscillation. Presumably, herring weight-at-age has been rising in the late 1970s in response to the fall in year-class strength, which, in turn, is associated with a high hake biomass and anomalously high temperatures. The efficacy of this model in explaining recent changes in herring stock growth and recruitment along the lower west coast of Vancouver Island is being tested by a multidisciplinary research project around La Perouse bank (Thomson and Ware 1990)

References

- Douglas, A.V. 1980. *Geophysical Estimates of Sea-Surface Temperature Off Western North America Since 1671*. Calif. Coop. Oceanic Fisheries Investigations Report, 21:102-112.
- Quinn, W.H., D.O. Zopf, K.S. Short, and R.T.W. Kuo Yang. 1978. *Historical Trends and Statistics of the Southern Oscillation, El Niño, and Indoneisan Droughts*. Fishery Bulletin, 76:663-678.
- Reid, J.L., G.I. Roden, and J.G. Wyllie. 1958. *Studies of the California Current System*. Calif. Coop Oceanic Fisheries Investigations Progress Report 1956-58.
- Smith, P.E., and G. Moser. 1988. *CALCOFI Time Series: An Overview of Fishes*. Calif. Coop Oceanic Fisheries Investigations Report, 29:66-77.
- Thomson, R.E., and D.M. Ware. 1990. *La Perouse Project: Fifth Annual Progress Report 1989*.
- Ware, D.M. In press. "Climate, Predators, and Prey: Behaviour of a Linked Oscillating System". in *Long-Term Variability of Pelagic Fish Populations and Their Environment*. Ed. T. Kawasaki. Permagon Press.
- Ware, D.M., and G.A. McFarlane. 1989. *Fisheries Production Domains in the Northeast Pacific Ocean*. Canada Special Publication Fisheries and Aquatic Sciences, 108:359-379.
- _____. 1986. *Relative Impact of Pacific Hake, Sablefish and Pacific Cod on West Coast of Vancouver Island Herring Stocks*. Int. North Pacific Fisheries Commission Report, 47:67-77.

Upwelling, Offshore Transport, and the Availability of Rockfish in Central California

David G. Ainley, William J. Sydeman, and Richard H. Parrish

ABSTRACT: We used the diet of a seabird, the common murre (*Uria aalge*), nesting on Southeast Farallon Island and feeding in the Gulf of the Farallones, California, as an index to abundance of juvenile rockfish, then related fish abundance to indices of turbulence and upwelling over an 18-year period, 1973-1990. Strong, persistent upwelling or downwelling led to reduced availability of fish in the study area, in contrast to great abundance when upwelling was mild or pulsed. Turbulence also related to rockfish availability in a parabolic fashion, yet had an insignificant relationship with fish abundance when upwelling was simultaneously considered in regression analyses. Sea surface temperature, as an index to El Niño/Southern Oscillation (ENSO), did not relate to rockfish availability. Intensity of upwelling is increasing in eastern boundary currents, and models predict the increase will continue as a response to global warming (Bakun 1990). On the basis of our study, one effect might be that fishes thought strong enough to resist Ekman transport could be transported out of normal areas of recruitment.

Introduction

Bakun (1990) showed that intensity of upwelling in eastern boundary currents has increased over recent decades and predicted the increase would continue due to warming of land masses adjacent to these currents — a potential result of global warming. This, in turn, would increase the atmospheric pressure differential that drives upwelling-favorable winds. Bakun noted that effects of increased upwelling on marine biota could be complex. On the one hand, upwelling leads to nutrient replenishment and enhanced phytoplankton growth, supporting a more robust food web. On the other hand, the concomitant increase in wind-generated turbulence could impair nutrient and carbon transfer in higher trophic levels.

Peterman and Bradford (1987) and Cury and Roy (1989) demonstrated a curvilinear relationship between recruitment of pelagic fish larvae and wind-generated turbulence. At low velocities, winds and upwelling increased, as did recruitment. However, as wind intensity increased further, recruitment decreased. These authors concluded the pattern was due initially to the enhancement and then, at greater wind speeds, the destruction of strata in which phytoplankton were optimally available to larvae. When turbulence destroyed the feeding strata, larvae incurred higher mortality due to starvation. These authors had little evidence to evaluate whether offshore movement of larvae and eggs, a consequence of Ekman transport, could also explain or contribute significantly to the lower recruitment into coastal populations. They thought turbulence was the dominant factor, because organisms in upwelling regions avoid spawning during times of intense Ekman transport.

In addition to bearing young when Ekman transport is low, another way fish in eastern boundary currents avoid offshore transport of propagules is to bear their young alive and release them at a life stage more vigorous than eggs or larvae, *i.e.*, as juveniles fully capable of strong swimming (Parrish *et al.* 1981).

We tested one species of live-bearing rockfish (*Sebastes* spp.) to determine whether its regional presence or absence was the function of turbulence or upwelling intensity (*i.e.*, offshore transport). We used a seabird with a foraging radius of about 60 km as our "fish-sampling tool". We related fish occurrence to measures of turbulence, upwelling, and sea surface temperature (SST) over an 18-year period. The latter variable is a measure of El Niño/Southern Oscillation (ENSO), which could indirectly affect availability of fish in the region. Our results show potential repercussions of the long-term increase in intensity of upwelling in eastern boundary currents.

Methods

We determined diet composition of the common murre (*Uria aalge*), at Southeast Farallon Island, 42 km offshore from central California (Figure 1) each summer for 18 years, 1973-1990. These birds carry fish in their beaks, in full view, to provision their offspring. From a blind overlooking a group of about 100 pairs of breeding murres, we conducted standardized watches of birds returning from the sea with fish (Ainley and Boekelheide 1990). The proportion of the diet contributed by juvenile rockfish was used as an index to rockfish availability in the foraging range of the murres, a radius of about 60 km.

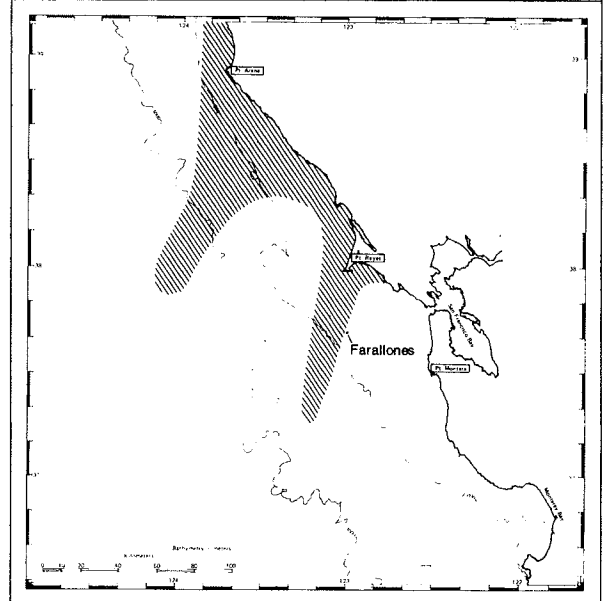
Preferred prey of the murres was juvenile rockfish, especially those closest to the island (Ainley and Boekelheide 1990). When rockfish were not available, the murres fed inshore on other species of fish. We collected data on availability of rockfish each year during June and July, the months when murres fed their young at the Farallon breeding sites.

Each June during 1983-1990, the National Marine Fisheries Service (NMFS) determined abundance and distribution of juvenile rockfish near the Farallon Islands using a more classical research method, a grid of trawl stations (Tiburon Lab 1989 [unpublished]). The proportion of juvenile rockfish in the murre diet as a measure of annual variability in presence of fish correlated with the NMFS trawl data ($r=1.0$, Spearman rank correlation) during six years (1983-1988) of overlapping study. Therefore, we believe the bird diet is a valid index to availability of juvenile rockfish in the Gulf of the Farallones.

We related the proportion of rockfish in the murre diet to indices¹ of turbulence (wind speed) and upwelling ($m^3/s-1/100$ m-1 of coastline) as well as to SST, an index of ENSO

Figure 1
GULF OF THE FARALLONES STUDY AREA
SHOWING UPWELLING PLUMES OF A
SIZE AND SHAPE TYPICAL OF
EARLY SPRING IN CENTRAL CALIFORNIA

Shape of the plume is drawn according to
Figure 4.2.2-27 in SAI 1985.



1 Provided by the National Oceanic and Atmospheric Administration, Pacific Fisheries Environmental Group, Monterey, California.

conditions, that we measured daily at Southeast Farallon. We correlated percent rockfish to oceanographic values averaged for individual and combined monthly periods preceding the June/July chick-feeding period of the murre. We used simple and multiple regression analyses to investigate relationships among these variables. We tested for curvilinear relationships by modeling the quadratic of upwelling, turbulence, and sea surface temperature. We tested for independent effects of these oceanographic variables by including them simultaneously in regression analyses.

Results

Simple regression analyses of rockfish prevalence in the murre diet against turbulence, upwelling index, and SST indicated a significant correlation with the averaged January plus February upwelling index ($UJ+F$) (Table 1, $p=0.0008$).

Table 1
RESULTS OF REGRESSION ANALYSES OF
UPWELLING, TURBULENCE, AND SEA-SURFACE TEMPERATURE ON
ROCKFISH AVAILABILITY IN THE GULF OF THE FARALLONES,
1973-1990

F and r^2 values are presented.

Months	Upwelling		Turbulence ^c		SST							
	Linear ^a F	r^2	Quadratic ^b F	r^2	Linear ^d F	r^2	Quadratic ^e F	r^2	Linear F	r^2	Quadratic F	r^2
October	1.34	0.07	1.12	0.13	0.02	0.00	1.12	0.14	0.04	0.00	0.13	0.02
November	0.01	0.00	1.55	0.17	0.00	0.00	0.89	0.11	0.07	0.00	0.11	0.01
December	0.25	0.02	0.25	0.03	0.84	0.05	2.93	0.30	0.28	0.02	0.24	0.03
January	4.17	0.21	3.59	0.32	2.63	0.15	1.81	0.21	0.13	0.01	0.16	0.02
February	2.56	0.14	2.23	0.23	1.94	0.11	1.01	0.13	0.49	0.03	1.58	0.17
March	0.69	0.04	1.23	0.14	0.99	0.06	0.77	0.10	3.08	0.16	3.63	0.33
April	0.32	0.02	0.87	0.10	0.19	0.01	0.19	0.03	1.35	0.08	1.79	0.19
May	0.03	0.00	0.30	0.04	0.02	0.00	0.02	0.00	0.00	0.00	0.02	0.00
Nov-Dec	0.04	0.00	0.76	0.09	0.70	0.04	1.26	0.15	0.18	0.01	0.09	0.01
Dec-Jan	3.98	0.19	5.90 ^f	0.44	3.02	0.17	2.46	0.26	0.04	0.00	0.03	0.00
Jan-Feb	4.57 ^f	0.221	1.78 ^g	0.61	3.42	0.19	4.22 ^f	0.38	0.29	0.02	0.48	0.06
Jan-Mar	3.01	0.16	3.18	0.30	3.04	0.17	7.76 ^g	0.53	0.93	0.05	2.23	0.23

a df = 1,16.
b df = 2,15.
c Does not include 1990 data
d df = 1,15.
e df = 2,14.
f $p < 0.05$.
g $p < 0.01$.

Of the variation in rockfish availability, 61% could be attributed to a quadratic relationship with upwelling intensity. Figure 2 is a graphical representation of the quadratic relationship of upwelling and rockfish availability, where the proportion of rockfish in the murre diet = $75.52 - 0.451 (UJ+F) - 0.0104 (UJ+F^2)$. This equation indicates that mild upwelling or downwelling during January and February led to high rockfish availability, but as intensity of downwelling or upwelling increased during these months, rockfish availability decreased. No relationship was evident later in the spring, when upwelling reaches maximum intensity (Breaker *et al.* 1983).

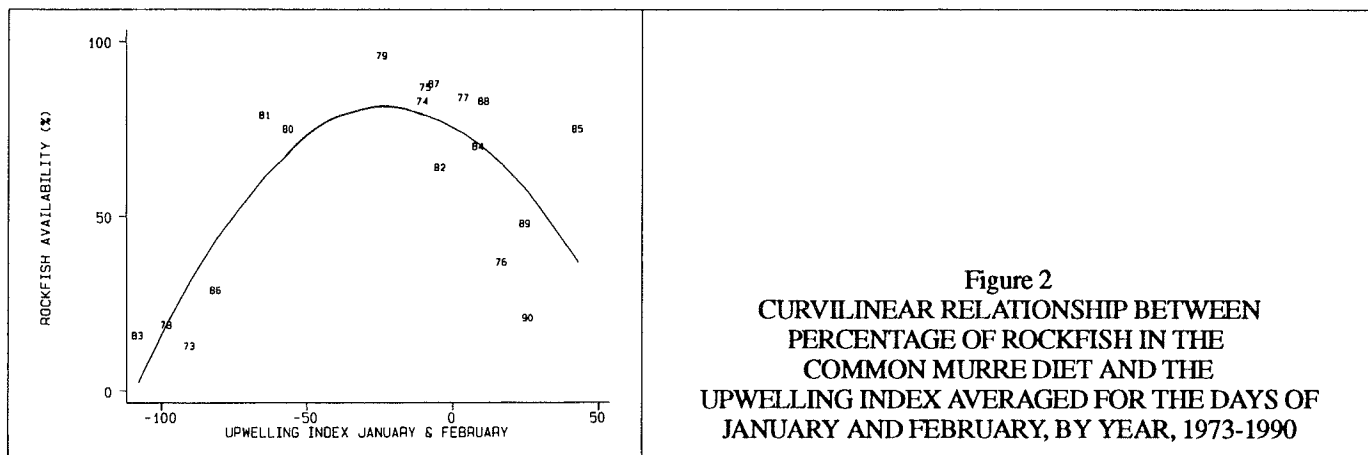


Figure 2
 CURVILINEAR RELATIONSHIP BETWEEN
 PERCENTAGE OF ROCKFISH IN THE
 COMMON MURRE DIET AND THE
 UPWELLING INDEX AVERAGED FOR THE DAYS OF
 JANUARY AND FEBRUARY, BY YEAR, 1973-1990

Rockfish availability was also highly correlated with the quadratic of turbulence ($p=0.0054$). Of the variation in rockfish availability, 53% could be attributed to a quadratic relationship with turbulence. SST did not correlate with rockfish abundance.

Multiple regression analyses indicated that the quadratic relationship between turbulence and rockfish availability was insignificant when upwelling was considered simultaneously ($F=2.37$, $df=2,12$, $p=0.1353$). Conversely, the quadratic of upwelling was still correlated with fish abundance ($F=6.81$, $df=2,12$, $p=0.0106$). SST also was insignificant in the presence of upwelling. Thus, the best regression model includes only the upwelling index as a predictive independent variable. This is not surprising, because the upwelling index combines measurements of wind speed, wind direction, and the Coriolis constant and is, therefore, a more complex environmental factor than turbulence, which is calculated on the basis of wind speed alone.

Conclusions

The rockfish most eaten by murrets at Southeast Farallon is the shortbelly rockfish (*S. jordani*) — on the order of 70% of the summer diet (Ainley and Boekelheide 1990). This species bears its young during January and February (Wyllie Echeverria 1987), just prior to the transition from winter conditions to the upwelling period (Breaker *et al.* 1983). Murrets begin to feed on these and other prey of the same size as soon as the prey appear (Ainley unpublished data). By the time juvenile fish have grown from about 1 cm to 4 cm, they are of a suitable size for transport to chicks at breeding sites.

In most years, January and February have upwelling and downwelling pulses as series of low pressure systems move into California from the Gulf of Alaska. Low pressure systems offshore produce onshore and downwelling-favorable winds. When storm fronts pass eastward, they are usually replaced by high pressure systems that bring the northwesterly and upwelling-favorable winds. Intense and persistent onshore or offshore winds seem to transport juvenile fish outside the foraging range of murrets at the Farallones.

Figure 1 depicts an upwelling plume characteristic of this coast during the early upwelling period (March/April; see also Figure 3 in Parrish *et al.* 1981). Later (June), when upwelling events are intense and continuous, plumes in this area are much broader and extend much farther offshore (SAI 1985). Along this coast, murrets tend to feed at the periphery of upwelling plumes, there being no prey in the recently upwelled water (Briggs *et al.* 1987).

Apparently, large plumes can completely displace juvenile shortbellies from the foraging range of Farallon-based murre (Ainley unpublished data).

An increase in upwelling intensity and persistence, which Bakun (1990) proposed as a possible result of global warming, has the potential to increase primary production in coastal waters of eastern boundary currents, as well as to decrease survival of eggs and larvae of spawning pelagic fishes (Bakun 1990, Cury and Roy 1989). Our analysis shows potential for an additional effect — increased transport of young fish away from traditional areas for recruitment. We base our conclusion — that offshore transport explains the pattern in presence or absence of fish — on the reasoning of Cury and Roy (1989):

Fish (in this case, rockfish) would bear their young within the central upwelling area of the California Current just before the seasonal onset of intense upwelling, because by appearing as well-developed juveniles beyond the passive (planktonic) egg and larval stage, they should be able to cope with turbulence, which is also brought by the intense, upwelling winds and which is the nemesis of smaller developmental stages of the fish.

Through natural selection, the release of juveniles during this period has evolved because upwelling events then are intermittent. Events of mild or short, intense upwelling lead to an enhanced food web. Resulting upwelling plumes displace the juveniles slightly offshore, but the young fish are able to return because between the upwelling events, slack or onshore winds propel or allow them to return shoreward. If upwelling continues to increase in intensity and persistence in eastern boundary current systems, this might lead to:

- Change in distribution of adult fish (which reside near the bottom, having settled there in their first year),
- Change in breeding phenology (if the fish had to bear young earlier and earlier to avoid upwelling), or
- Decrease in fish abundance (if they could not advance phenology for other reasons).

Any of these changes would dramatically alter the natural history patterns of higher trophic level predators, which reproduce when their prey are most abundant.

Acknowledgments

Our work on the Farallon National Wildlife Refuge was made possible through a contractual agreement and the logistic support of the U.S. Fish and Wildlife Service and the generosity of members of and donors to Point Reyes Bird Observatory (this is PRBO contribution 486). To collect SST, we participated in a shore-station program managed by Scripps Institution of Oceanography. We benefited from discussions of rockfish biology with W. Lenarz and coworkers at the Tiburon Lab of the National Marine Fisheries Service. Farallon biologists J. Lewis, S. Morrel, R. Boekelheide, T. Penniman, J. Penniman, H. Carter, P. Pyle, and S. Emslie helped determine rockfish availability. S. Emslie reviewed an earlier version of this report.

References

- Ainley, D.G., and R.J. Boekelheide. 1990. *Seabirds of the Farallon Island: Ecology, Structure and Dynamics of an Upwelling-System Community*. Stanford University Press. Palo Alto, CA.
- Bakun, A. 1990. "Global Climate Change and Intensification of Coastal Ocean Upwelling". *Science* 247:198-201.
- Breaker, L.C., P.A.W. Lewis, and E.J. Orlov. 1983. Analysis of a 12-year Record of Sea-Surface Temperatures off Pt. Sur, California. Naval Postgraduate School, Monterey, CA. NPS55-83-018.
- Briggs, K.T., D.G. Ainley, L.B. Spear, P.B. Adams, and S.E. Smith. 1988. "Distribution and Diet of Cassin's Auklet and Common Murre in Relation to Central California Upwellings". *Acta XIX Congressus Internationalis Ornithologici*. National Museum of Natural History, Ottawa. 982-990.
- Cury, P, and C. Roy. 1989. "Optimal Environmental Window and Pelagic Fish Recruitment Success in Upwelling Areas". *Canadian Journal of Fisheries and Aquatic Science*, 46:670-680.
- Parrish, R.H., C.S. Nelson, and A. Bakun. 1981. "Transport Mechanisms and Reproductive Success of Fishes in the California Current". *Biological Oceanography* 1:175-203.
- Peterman, R.M, and M.J. Bradford. 1987. "Wind Speed and Mortality Rate of Marine Fish, the Northern Anchovy (*Engraulis mordax*)". *Science* 235:354-356.
- SAI. 1987. *California Seabird Ecology Study*. Vol. II, "Satellite Data Analysis". Minerals Mangement Service, OCS Study MMS 87-0056. Washington, DC.
- Tiburon Laboratory. 1990. *Progress in Rockfish Recruitment Studies*. National Marine Fisheries Service, Southwest Fisheries Center, Administrative Report T-90-02. La Jolla, CA.
- Wyllie Echeverria, T. 1987. "Thirty-Four Species of California Rockfishes: Maturity and Seasonality of Reproduction". *Fishery Bulletin* 85:229-250.

The Role of Direct Observation in Predicting Climatic Change

Roger Y. Anderson

Introduction

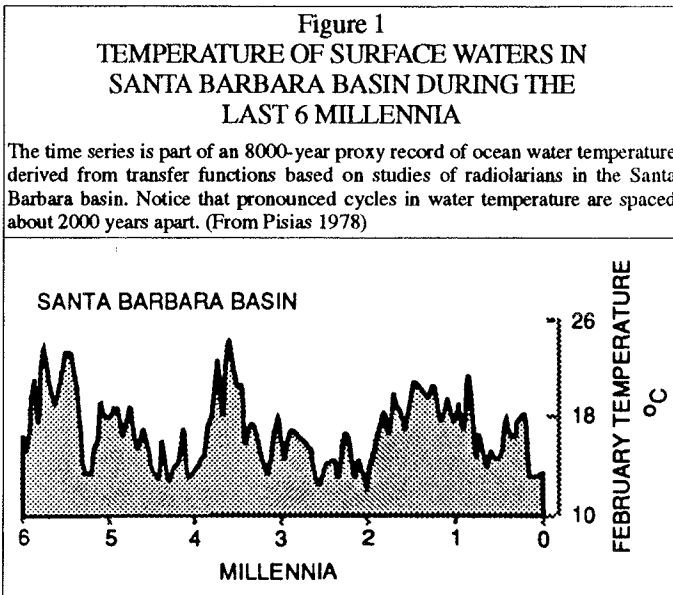
The National Oceanic and Atmospheric Administration Center for Ocean Analysis and Prediction (COAP) in Monterey, California, has assembled information to suggest how NOAA's facilities for observing the ocean and atmosphere might be applied to studies of paleoclimate. This effort resulted, indirectly, in several projects that combine direct observations of the ocean/atmosphere system with studies of past climate of the Pacific region. This article considers concepts that link the two kinds of investigations. It defines the thesis that direct observation of systems that generate paleoclimatic information is the nexus upon which understanding of climatic variability begins and upon which prediction of climate and global change depends.

A "predictive understanding" of climate change and its effects is the primary goal of climate and global change programs (CES 1989). However, both instrumental and proxy climate records reveal such a complex pattern of climatic variability that predictions, in the usual sense of predicting climatic events, would appear to be ruled out, at least within a time frame relevant to the human enterprise. Predictions in the context of global change are to be made by physical models that estimate the effect on regional climates of changes in the ocean-atmosphere system resulting from anthropogenic forcing (*e.g.*, CO₂, ozone, *etc.*). Regional climatic variability, in this same context, is important mainly for estimating the confidence level of a model prediction for a given region (CES 1989).

A climate prediction at an estimated level of confidence, however, is not a simple concept. It is widely recognized, for example, that the brief period (about 100 years) of instrumental observation is not sufficient for estimating confidence levels for the next 100 years, or even for the next few decades.

Pisias' (1978) proxy record for sea-surface temperature from the Santa Barbara basin, derived from changes in distribution of planktonic radiolarians (Figure 1), reveals three strong millennial cycles in ocean temperature over the past 6000 years. A model prediction with a confidence level based only on the previous century, made from most points in the time series, would be overtaken within a few decades by natural variability related to the strong millennial cycle. Figure 1 and the strength of the millennial cycle illustrated imply that confidence levels must be based on much longer records of variability.

This example also suggests another principle to be considered before predictions based on physical models can be applied in a practical sense. Predicting climatic change is not the goal, *per se*. Rather, it is the effect a predicted change will have on other systems that motivates efforts to predict climatic change (CES, 1989).



In this regard, climatic proxies such as a tree-ring growth layers or radiolarian abundance are, in themselves, a means for estimating effects of climatic change on the environment. For example, radiolarians in the Santa Barbara basin are, in addition to recording climatic variability, a means for estimating effects of human-induced climate change on the marine system. If changes in the winter sea surface temperature in the Santa Barbara basin can be predicted by means of a coupled ocean/atmosphere model, it follows that changes in marine plankton and effects on fisheries, *etc.*, might be predicted also.

Climate proxies have a dual function. They provide a vital record of climatic variability, and they measure the response of environmentally important systems to climatic forcing. If climate predictions are to be applied, studies of environmental response systems by means of climatic proxies are as vital to the goal prediction as are efforts toward climate modeling. Most importantly, the response systems must be calibrated quantitatively against the climatic variables (*e.g.*, temperature, precipitation, winds) that are used for output of climate models, because a response prediction for a given region without such a linkage would be largely subjective and would have limited application.

Linkage: The Key to Climate Prediction

Climatic proxies do not measure climatic variables such as temperature, precipitation, and winds directly; they must be calibrated against other observations. Three methods are generally used to convert proxies to climatic indices or variables:

- **Physical/Chemical Associations.** This method measures a physical/chemical property that is related to a climatic parameter (*e.g.*, temperature). This method is mainly applied to isotopic analyses of geologic (biologic) materials.
- **Climate-Gradient Associations.** This method is based on distribution and abundance of biologic species in a modern climatic gradient. Species abundance is measured at different localities, then compared with climatic parameters (*e.g.*, temperature) from nearby sites. Statistical procedures are

used to develop response functions that express species abundance as temperature, precipitation, *etc.*

- Time-Series Associations. This method directly and concurrently observes changes in climate-related proxies (*e.g.*, species abundance) and in climate parameters (*e.g.*, temperature) at the same site. Measurements are made at regular intervals over an extended period. A statistical association between a climate parameter and a proxy can be expressed as a climatic variable.

The second method, calibration of proxies by means of a climate gradient, has had the widest application and is most applicable to time-slice investigations and model-testing. This procedure uses instrumental climatic data along with regional surveys of biologic species abundance to statistically estimate response functions. Biologic data are compared with instrumental climatic data; therefore, the method does not depend on future observations.

The third method employs direct observation and comparison of time series of both climatic proxies and climatic variables over an extended period. This method has had limited application, and the few studies done have generally used climatic records that happened to be available from nearby instrumental recording stations.

The climate-gradient method and the time-series methods both rely on completeness and continuity of recent climatic data. Each has advantages and disadvantages. For example, the climate-gradient approach is not strongly site-dependent and assumes that the regional climatic gradient has a stronger influence on distribution of organisms than does the local environment. The climate-gradient method has been used successfully to calibrate shifting patterns of vegetation following the last glacial maximum. This application, however, lacks the temporal resolution to characterize decadal to centennial variability.

Unlike the regional climate-gradient method, the time-series or direct observation method takes advantage of differences among sites and employs a wide range of potential climatic proxies in addition to organisms, including sediment composition, texture, geochemistry, *etc.* Because the method is site-specific and site-dependent, regional climatic gradients are not a factor, and measured parameters must be calibrated against coincident changes in climatic variables over some unspecified interval.

Length of the Observation Period

An apparent disadvantage of the time-series method is the potentially long interval that may be needed to characterize the relationship between proxies and climatic variables. Few calibration studies of this type have been done. However, these examples illustrate the method and provide a rough estimate of the interval of observation that may be needed for calibration.

A Small Lake in the Mojave Desert

Lake sediments deposited 400 years ago, during the "Little Ice Age", recently were found in a dry playa in the Mojave Desert, one of the most arid regions of the world (Enzel *et al.*

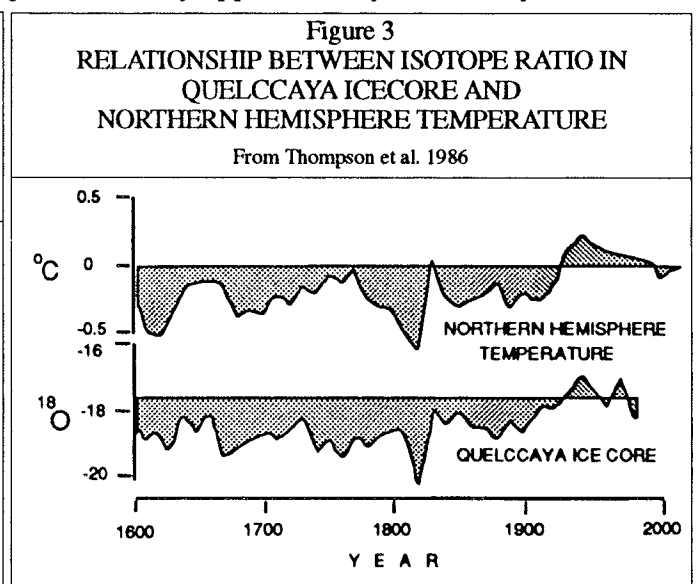
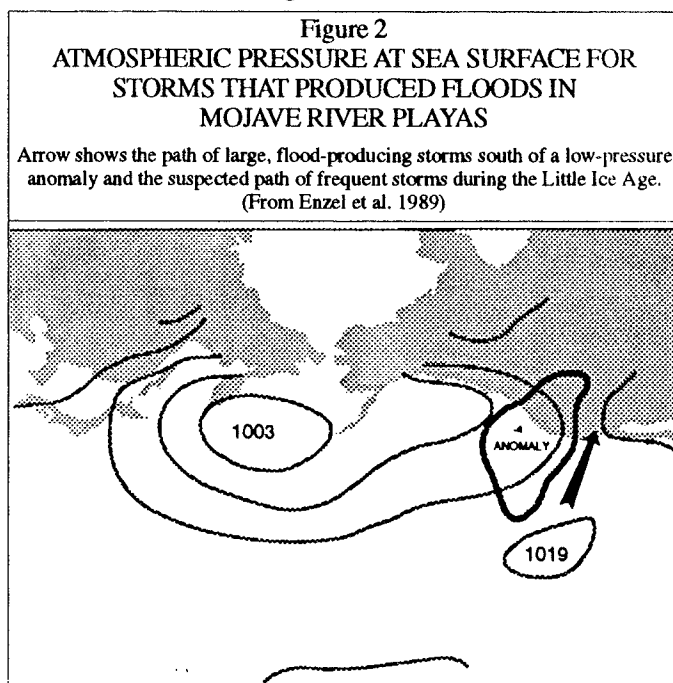
1989). The U.S. Geological Survey and the State of California have monitored hydrology of the Mojave drainage basin and have maintained records of river discharge and playa flooding since about 1900. Analysis of these records showed that river discharge from exceptionally large storms was capable of creating a temporary lake in the playa and that such storms occurred only during a particular pattern of circulation (atmospheric pressure) in the North Pacific. Enzel *et al.* (1989) were able to link synoptic climatic data from the North Pacific with the record of river discharge and floods in the Mojave drainage and identify the pattern of atmospheric pressure over the Pacific most likely to have produced a lake in the terminal playa during the Little Ice Age (Figure 2).

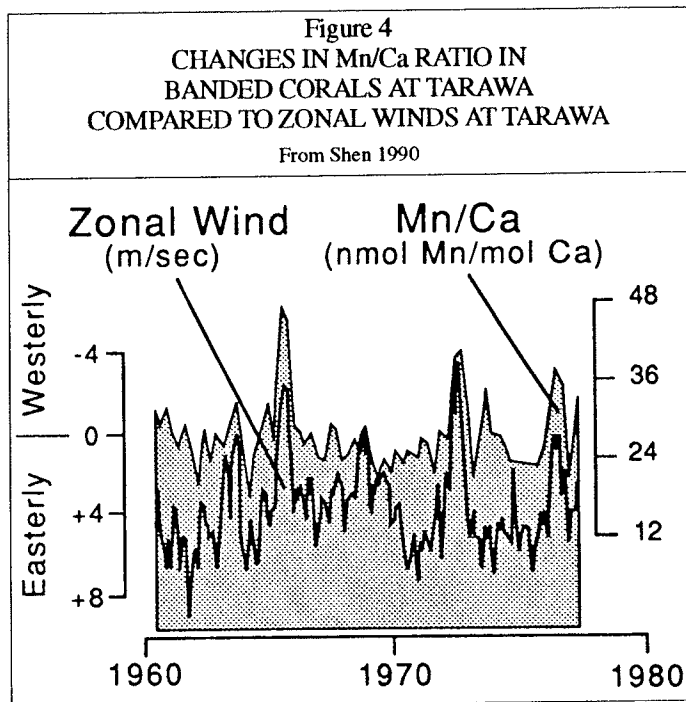
This illustrates how geologic and stratigraphic information, if accompanied by climatic and streamflow data, can be used to interpret and calibrate effects of climatic change. A reconstruction was possible because a hydrologic monitoring program had been maintained for the Mojave drainage. In this case, about 90 years of observation established the pattern of discharge and lake flooding and provided the linkage to changes in Pacific climate.

Ice Cores and Corals

Calibration by means of time-series observations is also illustrated by studies of ice cores in South America. A comparison, over the last 400 years, between time-series for oxygen isotope ratios in the Quelccaya ice core in South America and northern hemisphere temperature reveals a long-term association (Figure 3). The isotopic ratios in the ice core are a reasonable facsimile of temperature changes in the northern hemisphere, and the association appears to be partly resolved in decadal variability. In the ice-core example, for sites that are widely separated geographically, more than a hundred years of observation appear to be needed to quantify associations for interdecadal variability.

Another example shows an association between strong westerly wind anomalies that signal the onset of El Niño and Mn/Ca ratios in annually banded corals in the equatorial Pacific (Figure 4). The trace-metal ratio reproduces, only approximately, the nearby zonal wind

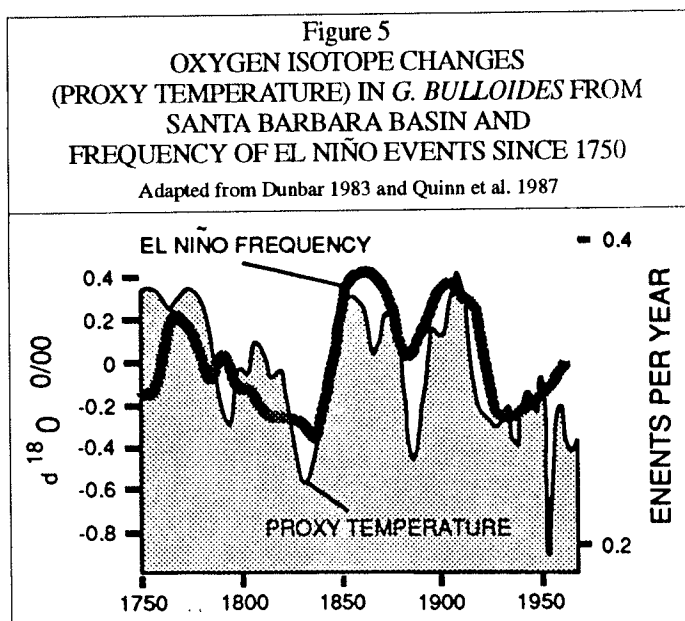




record at the island of Tarawa but exceptionally strong wind events are reflected in the Mn/Ca ratio (Shen, 1990). This example, and other parameters measured quarterly in corals suggests that the time-interval for calibrating interannual climatic variability using corals is at least several decades.

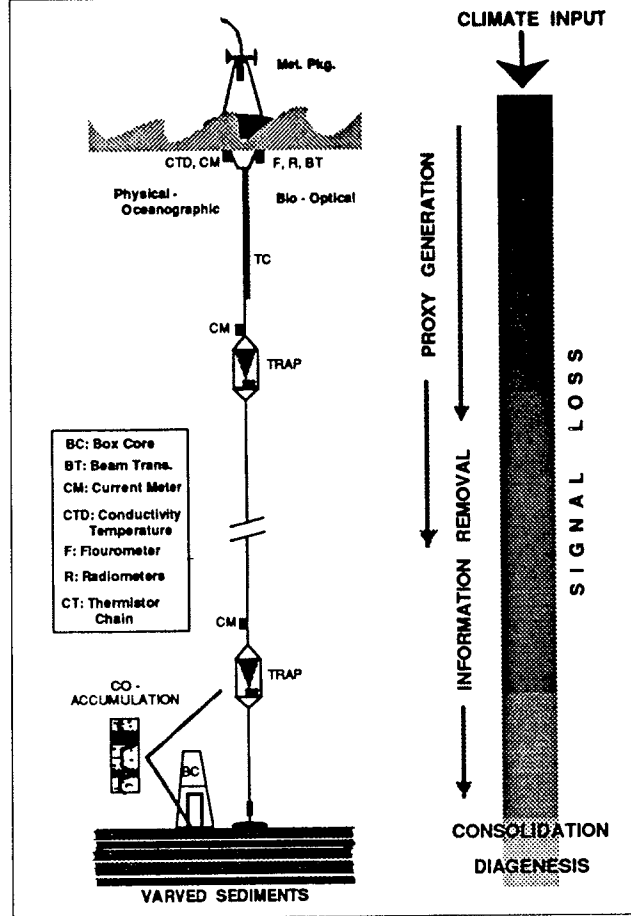
Evaluating and Extending Observations

Many decades seem to be needed to calibrate climatic proxies by the method of direct observation. However, it may be possible to reduce the period of observation through careful and comprehensive studies of the response of proxies during the annual climatic cycle. Seasonal forcing during the annual cycle is responsible for the life strategies, changes in sediment flux, and biogeochemical responses that generate climatic proxies. Responses during the annual cycle seem at least partly responsible for recording the longer and stronger cycles preserved in the sediment and stratigraphic record (Anderson 1986, Anderson *et al.* 1990). Because of the dominance of the annual cycle in processes that produce climatic proxies, it may be possible to calibrate a response to seasonal forcing and long-term changes in climate by observing relatively few annual cycles.



The Santa Barbara basin is a favorable setting for a pilot study to determine the feasibility of calibrating a wide range of potentially important climatic proxies in the marine environment. This is illustrated by the oxygen isotope record in *G. bulloides* from the Santa Barbara basin since 1750, as reconstructed by Dunbar (1983). The reconstruction (Figure 5) defines 4-5 prominent cycles in isotopic ratio believed to be associated with sea surface temperature. Superimposed on these ~50-year cycles is a plot showing changes in the frequency of El Niño events for the same interval.

Figure 6
 MOORING AND INSTRUMENT ARRAY
 TO BE USED FOR CALIBRATING
 CLIMATIC PROXIES IN MARINE SEDIMENTS



Relationship to Pacific Climate Studies

The Pacific region, including adjacent parts of continents, is especially favorable for obtaining past records of climatic variability and for calibrating climatic proxies. These records include ice cores, tree rings, widely distributed corals, and marine and lacustrine varved and laminated sediments. Many marine sites have high accumulation rates, and some are in settings that have a tendency toward anoxia that limits bioturbation and favors preservation of original structures and temporal relationships. Even if varved sediments are not preserved, such sediments may have a temporal resolution in the range of decades to centuries. Some partly ventilated basins with accumulation rates of about 10 cm/1000 years, as the Sulu Sea, have preserved millennial scale variability (Linsley 1989).

In addition to having records of long-term climatic variability, Pacific sites lie climatically upstream to important agricultural and populated regions. The effects of ENSO phenomena reach far beyond the tropical Pacific, and ENSO contributes to the patterns of interannual to millennial climatic variability that will be important in predicting the effects of regional climatic change within the human time frame.

Several paleoclimatic studies that will employ instrumental devices to observe and calibrate formation of climatic proxies have recently been initiated in the Pacific region with the aid of NOAA and other funding. For example, investigations of coral heads in the Galapagos and in the Gulf of California by R.B. Dunbar and G.M. Wellington, Rice University, will be supplemented by instrumental studies of physical oceanographic and meteorologic conditions coincident with coral growth. Elsewhere, L. Thompson, Byrd Polar Research Center, will install a meteorological and snow-monitoring system in the Cordillera Blanca, Peru, to link observations of air masses and snow accumulation to the climate record preserved in ice cores.

Comprehensive observations of the generation of marine climate proxies remain to be implemented. However, preliminary experiments using instrumented and fixed moorings similar to the mooring employed by Dickey (1988) in the Sargasso Sea and to the mooring illustrated in Figure 6 are being carried out in Monterey Bay by C. Pilska and others at the Monterey Bay Aquarium Research Institute (MBARI). In addition, three moorings that collect sediment in time-series traps and also measure physical oceanographic properties have been deployed off the Oregon coast by Piasias and other investigators at Oregon State College of Oceanography. Isolated sediment traps without other instruments are deployed in Santa Barbara basin, Guaymas basin, and Saanich Inlet.

Many lakes lie climatically downstream from the Pacific basin and are potentially favorable sites for calibrating climatic proxies found in lacustrine environments (Anderson *et al.* 1985). Methods of direct observation of the marine environment also are applicable to lacustrine systems. Although little progress toward calibrating lacustrine climatic proxies can be reported, the U.S. Geological Survey is contemplating related research in lakes in Minnesota and in Washington State.

Summary: Prospects for Observational Studies and Climate Prediction

Predicting global climate change and its regional effects is a specific objective. Given this definitive mission, the kinds of paleoclimatic records needed and the paleoclimatic research that needs to be done are also bounded and specific. Do the needed records exist? If so, will the necessary research be initiated to determine if these records can enable predictions to be obtained from climate models? One can assume future research will be focused on materials with annual to near-annual resolution, including tree rings, ice cores, corals, and laminated lacustrine and marine sediments. The regional distribution of tree-ring records, ice cores, and corals is reasonably well known; paleoclimatic investigations using these materials are underway; and climatic calibration studies for ice cores and corals are just now beginning. Comprehensive investigations of laminated marine and lacustrine sediments, on the other hand, are still in an early stage of development.

When physical climate models are developed to a stage where they are accurate on a regional scale, predictions of regional effects will require confidence estimates based on long records of regional climatic variability. Tree rings, corals, and ice cores, by themselves, will not provide records that are long enough or that have a regional distribution adequate for estimating regional variability and its effects. The long paleoclimatic records that are needed will have to come from lacustrine and marine sediments with annual to near-annual stratigraphic resolution. It is not yet known if such records are of sufficient quality or if their numbers are sufficient regionally to provide a basis for predicting effects

of regional climatic change. In any case, a major effort to investigate recent marine and lacustrine sediments, sustained at a high priority for many decades and focused on the generation of climatic proxies, is indicated if the goal is to obtain a predictive understanding of global change.

References

- Anderson, R.Y. 1986. "The Varve Microcosm: Propagator of Cyclic Bedding". *Paleoceanography* 1(4):373-382.
- Anderson, R.Y., W.E. Dean, J.P. Bradbury, and D. Love. 1985. *Meromictic Lakes and Varved Lake Sediments in North America*. U.S. Geological Survey Bulletin 1607.
- Anderson, R.Y., B.K. Linsley, and J.V. Gardner. 1990. "Expression of Seasonal and ENSO Forcing in Climatic Variability at Lower Than ENSO Frequencies: Evidence from Pleistocene Marine Varves Off California" in *Paleoclimates: The Record from Lakes, Ocean, and Land*. Ed. L.V. Benson and P.A. Myers. Palaeo. Palaeo. Palaeo. pp. 287-300.
- Committee on Earth Sciences. 1989. *Our Changing Planet: A U. S. Strategy for Global Change Research*. Washington, DCP.
- Dickey, T.D., 1988. "Recent Advances and Future Directions in Multi-Disciplinary *in situ* Oceanographic Measurement Systems" in *Toward a Theory on Biological-Physical Interactions in the World Ocean*. Ed. B.J. Rothschild. Kluwer Acad. Publ., pp. 555-598.
- Dunbar, R.B., 1983. "Stable Isotope Record of Upwelling and Climate from the Santa Barbara Basin, California" in *Coastal Upwelling*. Ed. J. Theide and E. Suess. Plenum Press. pp. 217-245.
- Enfield, D.B., 1988. "Is El Niño Becoming More Common?" *Oceanography* 1(2):23-27.
- Enzel, Y., D.R. Cayan, R.Y. Anderson, and S.G. Wells. 1989. "Atmospheric Circulation During Holocene Lake Stands in the Mojave Desert: Evidence of Regional Climatic Change". *Nature* 34: 44-47.
- Linsley, B.K. 1989. "Carbonate Sedimentation in the Sulu Sea Linked to the Onset of Northern Hemisphere Glaciation". *EOS* 70(43):1135.
- Pisias, N.G. 1978. "Paleoceanography of the Santa Barbara Basin During the Last 8000 Years". *Quaternary Research* 10:366-384.
- Quinn, W.H., V.T. Neal, and S.E. Antuñez de Mayolo. 1987. "El Niño Occurrences Over the Past Four and a Half Centuries". *Jour. Geophys. Research* 92(C13):14449-14461.
- Shen, G.T. 1990. "ENSO Indicators in Reef Corals of the Equatorial Pacific" in *Workshop on Paleoclimatic Aspects of El Niño/Southern Oscillation*. Ed. H.F. Diaz and V. Markgraf. Boulder, CO. NOAA-IN-STAAR.
- Thompson, L.G., E. Mosley-Thompson, W. Dansgaard, and P.M. Grootes. 1986. "The Little Ice Age as Recorded in the Stratigraphy of the Tropical Quelccaya Ice Cap". *Science* 234:361-364.

Initial Global Perspective of Climate for the Last Thousand Years: The Ice Core Record

Lonnie G. Thompson

Introduction

The patterns and sources of interannual, decadal, and centennial climatic variability are poorly known and constitute a significant gap in our understanding of the climate system. Comparing climate model results with systematic regional, continental, hemispheric, and global scale compilations of high-resolution paleoclimatic data increases our understanding of the system's dynamics and contributes to development of more realistic climate models.

The Earth's ice sheets and ice caps are recognized as the "best of a limited number" of libraries from which past climatic and environmental conditions may be extrapolated. Much climatic activity of significance to humanity may not be expressed strongly (or may not reach) the polar ice caps. However, ice core records can also be recovered from a select few high-altitude, low- and mid-latitude *polar-type* ice caps.

The high accumulation on these ice caps makes it possible to recover records of high temporal resolution for the last thousand years that serve valuable proxy indicators. For example, dust plays a direct role in the Earth's radiation balance and may be an important climatic determinant. Changes in atmospheric dust content (soluble and insoluble) can be reconstructed and the potential role in climatic variability assessed. These dust records also provide information about drought and volcanic activity. Net accumulation history can be extracted from annual layer thicknesses, and $\delta^{18}O$ serves as a proxy for temperature. Atmospheric gases trapped in air bubbles offer a unique record of the changes in concentrations of radiatively active gases such as carbon dioxide, methane, and nitrous oxide.

Nonpolar ice core records are particularly useful archives of pollen, diatoms, and plant fragments. These organic materials make it possible to apply AMS ^{14}C dating to establish independent dates for these ice cores.

Radiometric dating is especially important for records on millennial time scales. Thus, the variety of chemical and physical data extracted from ice caps and ice sheets provide a multifaceted record of both the climatic and environmental history of the Earth. These proxy records allow assessment of the relative importance of such components as volcanic activity, greenhouse, and atmospheric dust concentrations, as well as solar variability. Understanding the climate system with the goal of future prediction must begin with a global synthesis of its history over a period for which the most reliable, diverse, and complete sets of data exist. Longer records covering glacial/interglacial transitions, while

lacking in temporal resolution, do provide the perspective in which variations of the last thousand years must be viewed. The last thousand years is especially important because:

- It is the period most relevant to present and future human activities and upon which climatic and environmental variability due to human activities will be superimposed.
- It is a time of extremes within the Holocene warm period, including the Little Ice Age from about AD 1450 to 1900.
- It is the period of maximum data coverage.
- Multi-proxy reconstructions are possible.
- Annual (or seasonal) resolution is possible.
- Leads, lags, and rates of change within the climate system can be studied directly.
- Causes of changes in climate remain undetermined.
- Potential forcing functions can be identified and tested.

The Global Perspective

The assimilation of multifaceted ice core data sets from polar and nonpolar regions makes it possible to determine both temporal and geographical variability of any or all the individual ice core parameters, *i.e.*, dust, chemistry, gases, isotopes, *etc.* $\delta^{18}\text{O}$ records reflect, in varying degrees (see Dansgaard *et al.* 1973 and Bradley 1985):

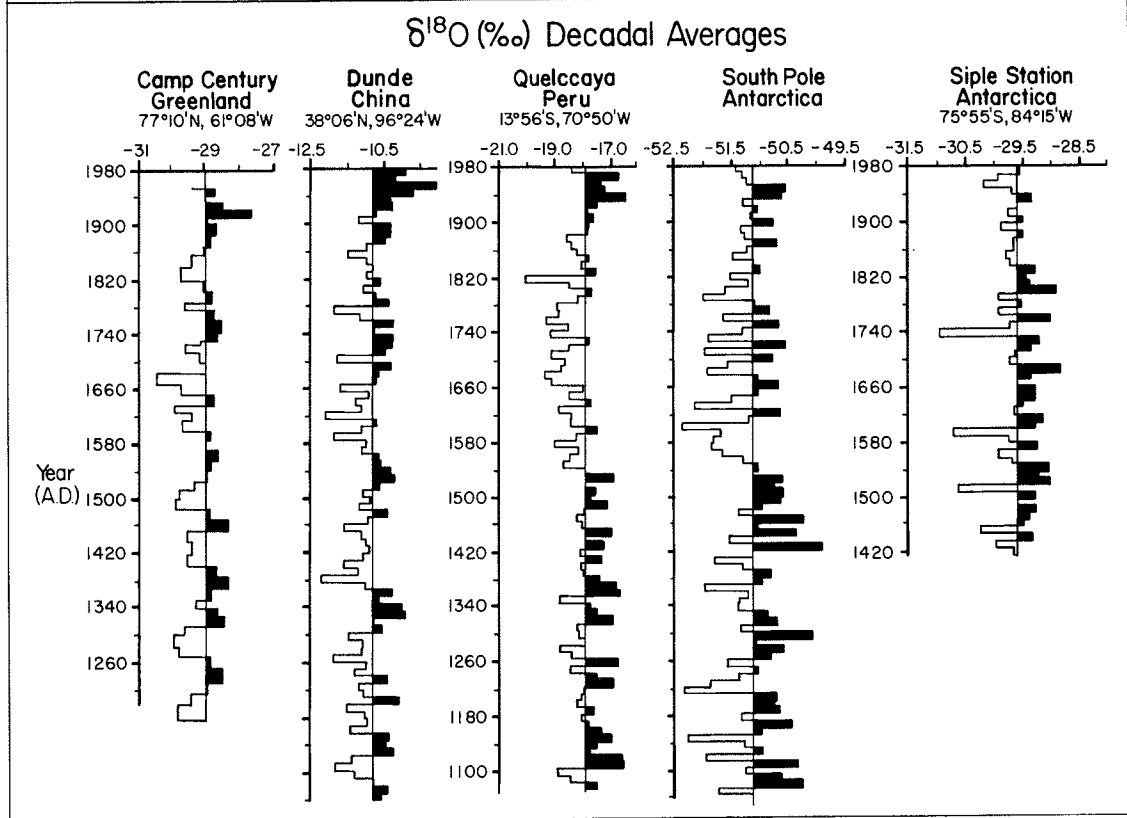
- Air temperature at which condensation occurs.
- Atmospheric processes during transport between oceanic source of water vapor and the site of deposition.
- Local conditions under which the isotope signal is modified during firnification.
- Surface elevation of the depositional site.
- Latitude of the site.

Although the correlation of atmospheric temperatures with $\delta^{18}\text{O}$ and its spatial representatives is still under discussion, the method is widely used as a proxy for climate and particularly for temperature (Dansgaard *et al.* 1973, Jouzel *et al.* 1983, Thompson *et al.* 1986, Peel *et al.* 1988).

Figure 1 provides a preliminary global perspective of the decadal and centennial variations from AD 1100 to 1980. The five sites, from north to south, are: Camp Century, Greenland (Johnsen *et al.* 1970); Dunde Ice Cap, China; Quelccaya Ice Cap, Peru (Thompson *et al.* 1986); South Pole and Siple Station, Antarctica (Mosley-Thompson *et al.* 1990).

Figure 1
DECADAL AVERAGES OF $\delta^{18}\text{O}$ RECORDS IN A NORTH-SOUTH GLOBAL TRANSECT
FROM CAMP CENTURY, GREENLAND, TO SOUTH POLE STATION, ANTARCTICA

Shaded areas represent isotopically less negative (warmer) periods, and unshaded areas represent isotopically more negative (cooler) periods relative to the mean of the individual records.



The records reveal wide diversity in detail, similar to that which would be found if only five widely dispersed meteorological stations were used to reconstruct global temperatures. However, several features stand out. For example:

- Variability of $\delta^{18}\text{O}$ was similar in the two northern hemisphere sites with a rather pronounced ~180-year oscillation in the decadal oxygen isotopic record from China.
- In the southern hemisphere, there is strong similarity between $\delta^{18}\text{O}$ from the tropical Quelccaya Ice Cap, Peru, and South Pole Station, Antarctica.
- The Little Ice Age stands out as a period of more negative isotopic values from about AD 1530 to 1900, while before and afterward, both locations were generally isotopically less negative.
- Of these five records, Siple Station is unique because during the Little Ice Age, less negative $\delta^{18}\text{O}$ isotopes and, hence, presumably warmer conditions prevailed.
- All sites show isotopically less negative conditions during the 20th century, except Siple Station, which is (in general) isotopically more negative for the last 100 years.

Interestingly, for the last 30 years, isotopic evidence (Peel *et al.* 1988, Mosley-Thompson *et al.* 1990) indicates a general trend toward less negative values, or warmer conditions. This warming trend is consistent with near-surface atmospheric temperature measurements in the Antarctic Peninsula from 1960 to 1980.

A striking feature of the $\delta^{18}\text{O}$ records in Figure 1 is the extreme warmth in central China during the last 60 years. The warmest decades were the 1940s, 1950s, and 1980s. Using the $\delta^{18}\text{O}$ record as a proxy for temperature, the last 60 years constitutes one of the warmest periods in the entire record, equaling levels of the Holocene maximum from 6000 to 8000 YBP (Thompson *et al.* 1989, Thompson *et al.* 1990).

Model results (Hansen *et al.* 1988) suggest the central part of the Asian continent may be one of the first places to exhibit an unambiguous signal of the expected greenhouse warming. Certainly the Dunde ice core $\delta^{18}\text{O}$ record suggests the recent warming on the Tibetan Plateau has been substantial. Radiosonde data from southern India (Flohn and Kapala 1989) show that, in fact, the average tropospheric temperature has increased nearly 1°C since 1965. More robust temperature/isotope transfer functions must be developed for the Tibetan Plateau and, indeed, for all regions where isotopic records from ice cores are used as proxy indicators of temperature.

Summary

Climatic and environmental records from low, middle, and high latitude ice cores greatly increase our knowledge of the course of past events. This historical perspective is essential to predict climatic oscillations, dominated as they may be by increasing greenhouse gas concentrations. Forcing factors, internal and external, that have operated in the past will continue to influence the course of events (Grove 1988).

Cores from the Dunde Ice Cap, China, may provide the first ice core record of the Holocene and late Pleistocene climate from the subtropics. The $\delta^{18}\text{O}$ record suggests that the last 60 years on the Tibetan Plateau has been one of the warmest periods in the record. Events like the Little Ice Age seem to be global in scale and, thus, should result from large-scale climatic forcing that influences the entire Earth system.

Manifestation of the Little Ice Age in any given record is quite variable. It is more distinct in higher elevation sites, such as Dunde, Quelccaya, and South Pole, than in the lower elevation sites of Camp Century and Siple Station. This may indicate the importance of climatic change as a function of elevation.

In addition, more subtle changes in climate like the Little Ice Age may be recorded more clearly farther from the mitigating influence of the oceans. The high temporal resolution available from ice cores illustrates that the transition from climatic norms may be abrupt on shorter time scales (*e.g.*, the Little Ice Age) as well as on glacial/interglacial time scales.

Tropical and subtropical ice core records provide the potential to establish long histories of El Niño/Southern Oscillation events and monsoon variability. Information about variations in their magnitude and frequency through time may provide information on the causes of these global events.

References

- Bradley, R.S. 1985. *Quaternary Paleoclimatology*. Allen and Unwin, Boston.
- Dansgaard, W., S.J. Johnsen, H.B. Clausen, and N. Gundestrup. 1973. "Stable Isotope Glaciology. *Meddelelser om Grønland*", 197:1-53.
- Flohn, H., and H. Kapala. 1989. "Changes of Tropical Sea-Air Interaction Processes Over a 30-Year Period". *Nature*, 338:244-246.
- Grove, J.M. 1988. *The Little Ice Age*. Methuen, London.
- Hansen, J., I. Fung, A. Lacis, D. Rind, S. Lebedeff, R. Ruedy, and G. Russell. 1988. "Global Climate Changes as Forecast by Goddard Institute for Space Studies Three-Dimensional Model". *Journal of Geophysical Research*, 93(D8):9341-9364.
- Johnsen, S.J., W. Dansgaard, H.B. Clausen, C.C. Langway Jr. 1970. "Climatic Oscillations 1200-2000 AD". *Nature*, 322:430-434.
- Jouzel, J., L. Merlivat, J.R. Petit, and C. Lorius. 1983. "Climatic Information Over the Last Century Deduced from a Detailed Isotopic Record in the South Pole Snow". *Journal of Geophysical Research*, 88(C4):2693-2703.
- Mosley-Thompson, E., L.G. Thompson, P.M. Grootes, and N. Gundestrup. 1990. "Little Ice Age (Neoglacial) Paleoenvironmental Conditions at Siple Station, Antarctica". *Annals of Glaciology*, 14:199-204.
- Peel, D.A., R. Mulvaney, and B.M. Davison. 1988. "Stable Isotope/Air-Temperature Relationships in Ice Cores from Dolleman Island and the Palmer Land Plateau, Antarctic Peninsula". *Annals of Glaciology*, 10:130-136.
- Thompson, L.G., E. Mosley-Thompson, W. Dansgaard, and P.M. Grootes. 1986. "The Little Ice Age as Recorded in the Stratigraphy of the Tropical Quelccaya Ice Cap". *Science*, 234:361-364.
- Thompson, L.G., E. Mosley-Thompson, M. Davis, J. Bolzan, J. Dai, T. Yao, N. Gundestrup, X. Wu, L. Klein, and Z. Xie. 1989. "Holocene/Late Pleistocene Climatic Ice Core Records from Qinghai-Tibetan Plateau Ice Cores". *Science*. 246:474-477.
- Thompson, L.G., E. Mosley-Thompson, M.E. Davis, J.F. Bolzan, J. Dai, L. Klein, N. Gundestrup, T. Yao, X. Wu, and Z. Xie. 1990. "Glacial Stage Ice Core Records from the Subtropical Dunde Ice Cap, China". *Annals of Glaciology*, 14:299-297.

Snow Accumulation Time Series and Their Climatic Interpretation

Gerald Holdsworth

ABSTRACT: Several snow accumulation time series derived from ice cores and extending over 3 to 5 centuries are examined for spatial and temporal climatic information. Where possible, integrity of the series was checked against instrumental data. It is evident that net snow accumulation at core sites is maintained roughly proportional to total precipitation there. A significant observation is the widespread depression of net snow accumulation during the latter part of the "Little Ice Age". This initially suggests sea surface temperatures were significantly depressed during the same period. However, prior to this, the available core records indicate generally higher than average precipitation rates. This also implies that influences such as shifted storm tracks or a dustier atmosphere may have been involved. Without additional spatial data coverage, these observations should properly be studied using a coupled (global) ocean/atmosphere GCM.

Introduction

Analyses of the stable isotopes of both *H* and *O*, the trace chemistry, and the particulate content (as well as some other constituents) of ice core melt water, can yield a wealth of information about atmospheric processes. Extraction of a net accumulation time series from an ice core depends on successful identification of annual layers in the core or, if annual resolution is lost, on identification of absolute time markers (such as volcanic events and with due attention to time lag effects). Between these horizons, net accumulation must be averaged. This is facilitated if an approximate numerical model can be fitted to the empirical time-depth curve. Certain corrections must then be applied to the raw data to convert to the original surface value (Thompson *et al.* 1985, Holdsworth *et al.* 1989). These site-specific corrections tend to become less reliable with depth in the core.

If the net accumulation time series, in water equivalent, is about proportional to total precipitation on a long-term average basis, then an essentially direct measure of relative site precipitation has been achieved. This stands in contrast to the method of inferring paleotemperatures from the stable isotopes of water, which results in production of indirect "proxy" data. However, these data are not consistently reliable as a paleotemperature indicator at all sites, or even at a particular site, over the time scales dealt with here (*e.g.*, see Holdsworth 1990).

With expansion of ice core drilling beyond the Arctic and Antarctic, paleoclimatic time series from lower latitudes have recently become available (*e.g.*, Thompson *et al.* 1986, Thompson *et al.* 1988, Holdsworth *et al.* 1989). It now appears relevant to compare some of these time series to see if any coherence or phase relationships exist between them and whether these may have any significance to global climate change studies covering the period before the instrumental era.

Several ice core net accumulation time series extending back 3 to 5 centuries appear to share similar gross features and, thus, may be reliable sources of paleoclimatic data. In particular, a common feature of these series is the depression of snow accumulation during

the last half of the classical "Little Ice Age". Unlike tree core sites, the uneven distribution of glaciers and, hence, ice core sites does not allow systematic data coverage. Consequently, for a complete hemispheric study, the snow accumulation time series must be augmented by other paleo (precipitation) data, such as may be provided by cores from certain suitably located trees.

Snow Accumulation Time Series

The time series for Mt. Logan (Yukon Territory, Canada) is presented in Holdsworth (1990). Several techniques were used to define annual layers. A form of verification of the last century of record against instrumental precipitation data was achieved on the reasonable assumption that teleconnections found between the snow accumulation series and precipitation in several distant regions of the northern hemisphere are real and have a physical basis (which is not discussed here). In addition, spectral analysis indicates the presence in the series of at least two cycles with a possible physical linkage (Holdsworth *et al.* 1989).

The time series for Dye 3, southern Greenland is from Reeh *et al.* (1978). This is only one of several series available. The others are from central Greenland, and they appear to be out of phase with the southern Greenland series, on both the short-term and the long-term, between about AD 1600 and about AD 1900. They are all from sites 3000 m in altitude. The isotopic "stratigraphy" here is a highly reliable way of defining annual layers. As in the case of the Mt. Logan core, this method is augmented by volcanic event time checks.

The time series for the Dunde Ice Cap, China, is from L.G. Thompson (personal communication 1990). This is another high altitude site (5300 m). The visible stratigraphy in this core is well defined and leads to the identification of annual layers.

The time series from the Quelccaya Ice Cap (5650 m) in Peru, is from Thompson *et al.* (1985, 1986). Again, the visible stratigraphy combined with derived core quantities (δ , particulates) enables a fairly accurate identification of annual layers (Thompson *et al.* 1985). Some verification of the upper part of the series is accomplished using instrumental or other data (Thompson *et al.* 1979).

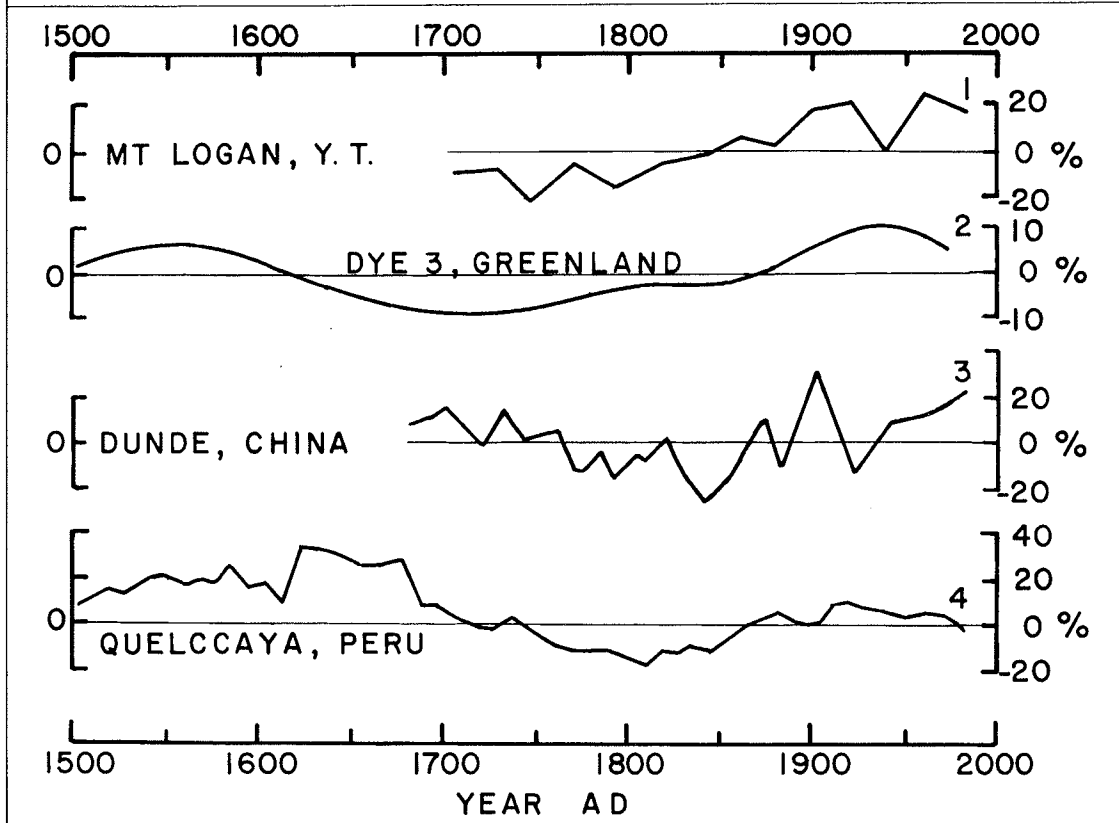
Figure 1 shows plots of the time series described above. Because the original annual data used to derive the time series presented here have been processed quite differently, for present purposes only long-term trends over 50 to 100 years should be compared. It must also be emphasized that the data are selective. First, this is due to the nature of the distribution of ice core sites. In addition, there has been selective use of existing Greenland data. The other (central) Greenland data (Reeh *et al.* 1978) show both in- and out-of-phase relationships with the Dye 3 data. This is discussed by those authors in terms of shifted storm tracks possibly related to the effects of changing sea ice cover. It is possible that the southern Greenland site may be reflecting more nearly the general hemispheric trends in precipitation.

Figure 1
ICE CORE -DERIVED NET ACCUMULATION TIME SERIES EXPRESSED AS A PERCENTAGE DEVIATION FROM THE LONG-TERM MEAN

Curves apply to the following sites (with data source):

- (1) Mt. Logan, Yukon Territory, Canada (Holdsworth 1990), 20-year running means.
- (2) Dye 3 site, southern Greenland (Reeh *et al.* 1978). This is part of a series (beginning AD 1250) that has been smoothed by a low-pass filter with a cut-off period of 120 years.
- (3) Dunde Ice Cap, China (L.G. Thompson, personal communication), 20-year running means.
- (4) Quelccaya Ice Cap, Peru (Thompson *et al.* 1985), redrawn from a curve of 10-year averages truncated at AD 1500.

Because of the mixed nature of processing the original annual data, only long-term (century) trends could be compared for purposes of this paper.



Discussion

The selected time series are principally from the northern hemisphere. The one southern hemisphere series is from a tropical site that seems to be connected with northern hemispheric climate dynamics (Thompson *et al.* 1984). Despite differences in data processing, all series show generally depressed snow accumulation from about 1700 until about 1880, which approximately coincides with the last half of the Little Ice Age". The two series that extend to 1500 (the full series begin before this date) both show elevated snow accumulation rates starting about 1500 and ending before 1700, although there is an obvious phase shift (South America lags Greenland). Because there are only two series, these comparisons may seem tenuous, but it is known (Bradley *et al.* 1987) that long-term precipitation trends are not necessary in phase in low and high latitude bands. If temperatures were generally depressed throughout the Little Ice Age, as they are believed to be (*e.g.*, Hammer *et al.* 1981), this represents an interesting climatological problem for which no satisfactory explanation seems to have been offered. Internal factors to be considered are, for example, the effects of switches from zonal to meridional flow (which would affect

storm tracks) and changes in atmospheric turbidity (which would affect temperature and precipitation rates). For example, Thompson *et al.* (1986) show elevated levels of large particles for the first half of the Peruvian Little Ice Age compared with the last half. External factors may also be involved. Grove (1988) has discussed both internal and external factors in terms of the Little Ice Age as a whole, but a clear-cut cause seems to be lacking. In absence of a greater spatial coverage of Little Ice Age time series, the problem would be better studied using a (global) coupled ocean/atmosphere GCM in which external forcing may be incorporated.

References

- Bradley, R.S., H.F. Diaz, J.K. Eischeid, P.D. Jones, P.M. Kelly, and C.M. Goodess. 1987. "Precipitation Fluctuations Over Northern Hemisphere Land Areas Since the Mid-19th Century". *Science* 237:171-175.
- Grove, J.M. 1988. *The Little Ice Age*. Methuen. London and New York.
- Hammer, C.U., H.B. Clausen, and W. Dansgaard. 1981. "Past Volcanism and Climate Revealed by Greenland Ice Cores". *Journal of Volcanology and Geothermal Research* 11:3-10.
- Holdsworth, G. 1990. "Changes in Mid-Troposphere Snow Accumulation on Mt. Logan, Yukon, Over the Last Three Centuries" in *Proceedings of the Sixth Annual Pacific Climate (PACCLIM) Workshop*. Ed. J.L. Betancourt and A.M. MacKay. Interagency Ecological Studies Program for the Sacramento-San Joaquin Estuary Technical Report 23:145-147.
- Holdsworth, G., H.R. Krouse, M. Nosal, M.J. Spencer, and P.A. Mayewski. 1989. "Analysis of a 290-Year Net Accumulation Time Series from Mt. Logan, Yukon". *IAHS Publ.* 183:71-79.
- Reeh, N., H.B. Clausen, W. Dansgaard, N. Gundestrup, C.U. Hammer, and S.J. Johnsen. 1978. "Secular Trends of Accumulation Rates at Three Greenland Stations". *Journal of Glaciology* 20:27-30.
- Thompson, L.G., S. Hastenrath, and B. Morales-Arno. 1979. "Climatic Ice Core Records from the Tropical Quelccaya Ice Cap". *Science* 203:1240-1243.
- Thompson L.G., E. Mosley-Thompson, J.F. Bolzan, and B.R. Koci. 1985. "A 1500-Year Record of Tropical Precipitation in Ice Cores from the Quelccaya Ice Cap, Peru". *Science* 229:971-973.
- Thompson, L.G., E. Mosley-Thompson, and B. Morales-Arno. 1984. "El Niño-Southern Oscillation Events Recorded in the Stratigraphy of the Tropical Quelccaya Ice Cap, Peru". *Science* 226:50-53.
- Thompson, L.G., E. Mosley-Thompson, W. Dansgaard, and P.M. Grootes. 1986. "The Little Ice Age As Recorded in the Stratigraphy of the Tropical Quelccaya Ice Cap". *Science* 234:361-364.
- Thompson, L.G., Xiaoling Wu, E. Mosley-Thompson, and Zichu Xie. 1988. "Climatic Records from the Dunde Ice Cap, China". *Annals of Glaciology* 10:178-182.

Coastal Climate Reflected in $^{13}\text{C}/^{12}\text{C}$ Ratio of Organic Carbon in Varved Sediment from Santa Barbara Basin

Arndt Schimmelmann and Mia J. Tegner

ABSTRACT: A 1844-1987 time-series of carbon stable isotope ratios from dated sedimentary total organic carbon from the center of the Santa Barbara basin is compared with historical climate and oceanographic records. Carbon derived from ^{13}C -depleted phytoplankton and ^{13}C -enriched kelp appear responsible for a large part of the isotopic variance in sedimentary total organic carbon. El Niño/Southern Oscillation events are recorded by the isotopic response of marine organic carbon in sediments.

Introduction

This study uses the laminated sediment record from the Santa Barbara basin (Schimmelmann *et al.* 1990 and references therein) and the climate history of Southern California (AD 1844-1987) to calibrate the isotopic response of sedimentary total organic carbon (TOC) to oceanographic change, especially to El Niño/Southern Oscillation (ENSO) events.

The stable isotope ratio $^{13}\text{C}/^{12}\text{C}$ (expressed as $\delta^{13}\text{C}$ value) of marine organic carbon is determined by the contributing sources (reviewed by Sackett 1989). $\delta^{13}\text{C}$ -values tend to decrease in order from macroalgae (kelp) to phytoplankton to terrigenous organic matter. The dominant source of organic carbon in the Santa Barbara basin is phytoplankton (Eppley and Holm-Hansen 1986), but phytoplankton productivity during an ENSO event is greatly diminished (Chelton *et al.* 1982; Lange *et al.* 1987 and 1990).

Until their destruction in the early 1980s, the giant kelp (*Macrocystis* spp.) forests from Point Conception to Santa Barbara were some of the largest in Southern California (Tegner and Dayton 1987). Strong ENSO and severe storm events have been linked to extensive destruction of kelp forests (Seymour *et al.* 1989), causing a short-term introduction of large amounts of ^{13}C -enriched kelp carbon into the coastal ecosystem. The isotopic composition of marine organic carbon is also influenced by isotope effects based on temperature, $p[\text{CO}_2]$, light and nutrient availability, and species composition of the biota (Rau *et al.* 1989; Sackett 1989). The sedimentary TOC isotope record integrates all carbon sources, including non-marine sources.

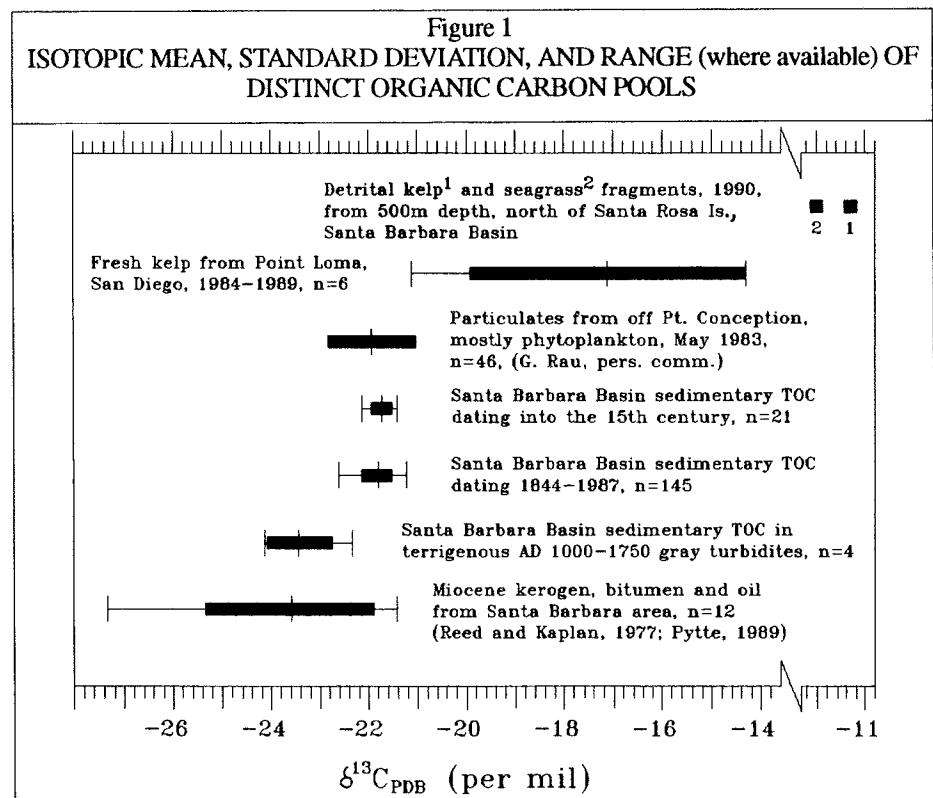
Results of this study suggest terrigenous organic carbon transported by rivers into the Santa Barbara basin is of limited significance for the isotopic composition of sedimentary TOC in the deep center of the basin. The discharge of ^{13}C -depleted sewage into Santa Barbara basin is negligible (Schaefer 1989).

Methods

Retrieval of sediment cores from 590 meters near the center of the Santa Barbara basin, subsampling, and dating procedures are described elsewhere (Schimmelmann *et al.* 1990). $\delta^{13}\text{C}$ values from sedimentary TOC, living giant kelp (*Macrocystis pyrifera*) from the Point Loma kelp forest near San Diego, and detrital kelp and seagrass (retrieved at 500-meter depth north of Santa Rosa Island in the Santa Barbara basin) were determined using the method of Nissenbaum and Serban (1987). Isotopic results are expressed in the usual $\delta^{13}\text{C}_{\text{PDB}}$ notation in per mil, with a precision of ± 0.1 per mil.

Results and Discussion

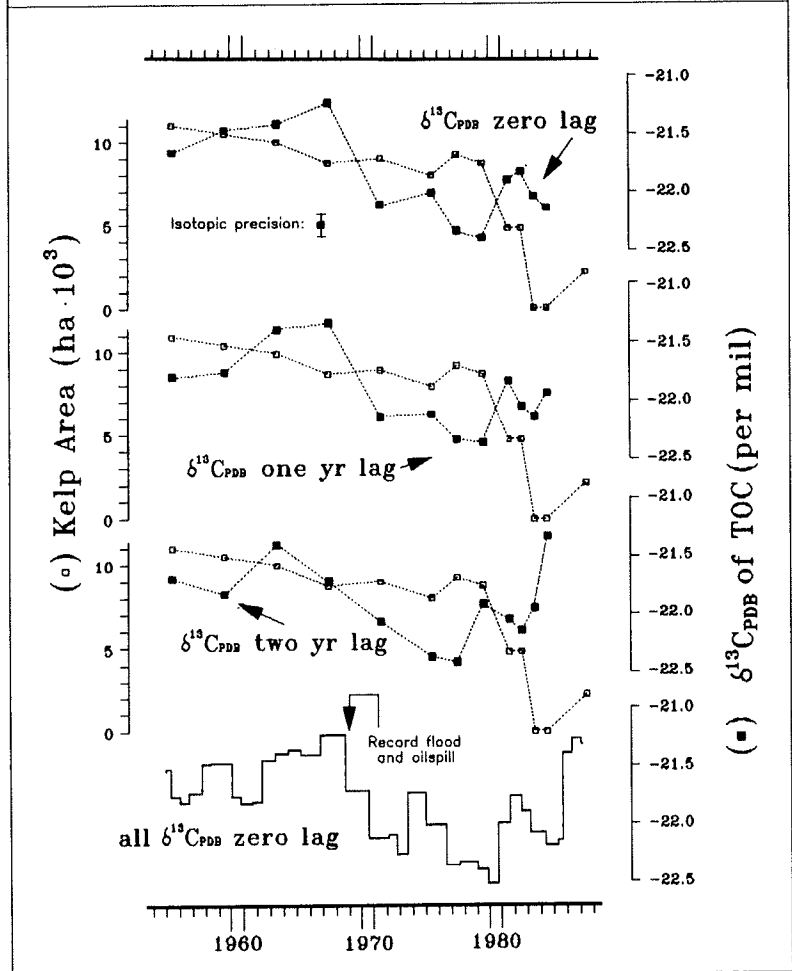
We are confident the observed isotopic differences among carbon sources shown in Figure 1 are systematic and large enough to produce signals that may be interpreted paleoclimatically, in spite of diagenetic *postmortem* isotopic changes (for example, Fenton and Ritz 1988). The stable isotope ratios of kelp samples from Point Loma are comparable with a reported mean of $\delta^{13}\text{C} = -17.7$; $\sigma = 2.3$ per mil ($n=162$) for kelp from Aleutian waters (Duggins *et al.* 1989). Therefore, kelp from the shelf neighboring the Santa Barbara basin should fall in the same range.



Our isotopic results from the youngest sediment layers (Figure 2) may not be comparable with older sediment layers, because near-surface varves are richer in living biomass and nonrefractory organic matter (Reimers *et al.* 1990, Schimmelmann unpublished data).

Figure 2
COMPARISON BETWEEN CHANGES IN THE
KELP CANOPY AREA AND THE
RESPECTIVE TRENDS OF $\delta^{13}\text{C}$ OF
SEDIMENTARY TOTAL ORGANIC CARGON

The lowermost $\delta^{13}\text{C}$ time-series displays continuous, irregularly spaced data. All other $\delta^{13}\text{C}$ data (solid squares) represent hypothetical annual intervals matching the years of kelp observation. The same kelp record is compared with $\delta^{13}\text{C}$ records lagging zero, 1, and 2 years behind to account for the time needed for transportation of kelp carbon until incorporation into sedimentary TOC.

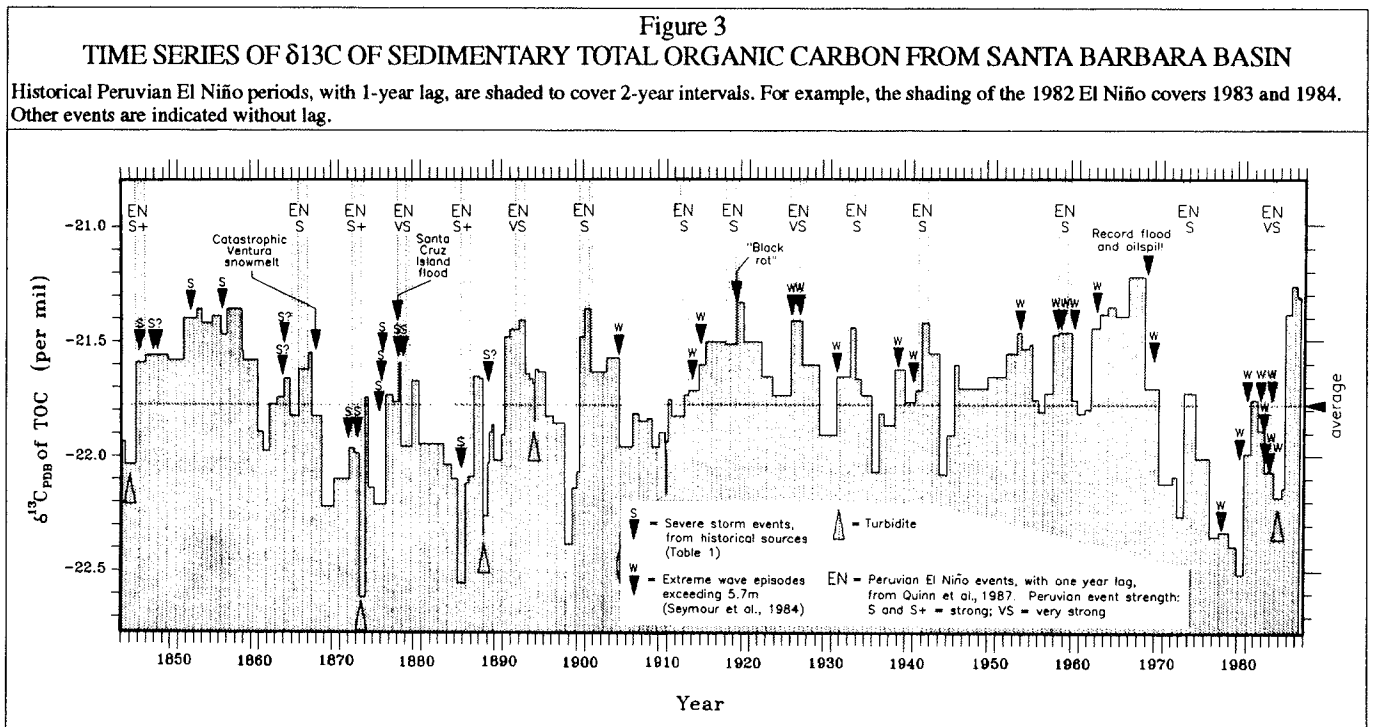


Isotopic Response of Marine Carbon to Climatic Change

Changes in the kelp canopy area of kelp beds from Santa Barbara to Point Conception were reported for distinct years between 1955 and 1979 by Harger (1983). In addition, estimates for 1981, 1983, 1984, and 1987 from a kelp harvesting company, Kelco (D. Glantz, personal communication; estimated by a different method), were adjusted by us with respect to 1975, for which both sources had estimates. Figure 2 compares the consecutive changes in kelp canopy area with the respective trends of $\delta^{13}\text{C}$ of sedimentary TOC.

The same kelp record is also compared with $\delta^{13}\text{C}$ records lagging 1 and 2 years to estimate the time needed for transportation of kelp carbon to the center of the Santa Barbara basin. Seven of eight observations from 1955 to 1981 show a negative correlation of trends between kelp area and the isotopic record with lags of zero and 1 year. A 2-tailed binomial test (Conover 1971) indicates the negative correlation is significant for lags of zero and 1

year ($p=0.035$) but not for a lag of 2 years ($p=0.64$), where only half of the trends correlate. No significant correlation is observed for 1981-1987, in part because storms and El Niño summers had reduced the standing kelp biomass to a record low (Figure 3) (Tegner and Dayton 1987, Seymour *et al.* 1989).



Our statistics suggest kelp carbon is an important factor in the isotopic mass-balance of the Santa Barbara basin ecosystem. However, the lack of proportionality between observed changes in kelp abundance and isotopic shift, especially from 1967 to 1971 (Figure 2, zero and 1-year lag), discourages simplistic isotopic mass-balance calculations and indicates the need to consider additional environmental effects.

Isotopic Influence of Non-Marine Carbon Sources

An oceanographically-interpretable, marine-derived signal in the isotopic total organic carbon record can only be expected for times when the marine carbon contribution is large enough to dominate non-marine sources. To evaluate the isotopic influence of river-transported, ^{13}C -depleted organic matter, we compared our 1844-1987 $\delta^{13}\text{C}$ -time series with statistics of severe historical floods listed by the U.S. Army Corps of Engineers (1975) as “damaging floods ... known to have occurred in the Santa Barbara area in 1862, 1875, 1877, 1883, 1907, 1909, 1911, 1914, 1918, 1938, 1941, 1943, 1952, 1967 and 1969”. Less than one-third of these severe floods coincide with or are immediately followed by a severe drop of $\delta^{13}\text{C}$ values of TOC in Figure 3 (adapting a 0.3 per mil threshold), even if a 1-year lag is assumed.

A comparison among the 1874-1987 rainfall, the 1930-1985 discharge of the Ventura and Santa Clara rivers, and our $\delta^{13}\text{C}$ -time series yields a similar result (not shown here). We concluded that only extreme floods and rapid sequences of floods have a significant impact on isotopic composition of TOC in the center of the Santa Barbara basin.

Unprecedented isotopic fluctuations of TOC deposited in Santa Barbara basin in the 1970s deserve special attention as they relate to a few unusual environmental events (Figure 3). A sequence of major oil spills in 1969 introduced large amounts of ^{13}C -depleted fossil carbon into the basin's ecosystem (Kolpack *et al.* 1971). A record flood in early 1969 caused a massive influx of terrigenous ^{13}C -depleted biomass into the basin (Drake *et al.* 1971). Independently from the 1969 events, the productivity of Santa Barbara basin declined significantly from 1968 through 1977 (Lange *et al.* 1990).

Comparison of the 1844-1987 $\delta^{13}\text{C}$ Time Series with Historical Records

Figure 3 compares the isotopic TOC time-series with historical climatic records (U.S. Geodetic and Coast Survey 1872, U.S. Coast and Geodetic Survey 1889, Ellison 1937, Mason 1961, Brewer 1966, Ruhge 1987, Seymour *et al.* 1984). Strong and very strong Peruvian El Niño years (Quinn *et al.* 1987) are indicated with a time lag of 1 year to account for progression into the northern hemisphere. Of the 15 listed ENSO events, 12 coincide with or immediately precede $\delta^{13}\text{C}$ maxima. Most storm and wave events follow the same pattern, but a rapid succession of kelp-destructing events can yield only one initial $\delta^{13}\text{C}$ spike in sedimentary TOC because kelp forests would need time for recovery.

While the correlation between tropical ENSO events and changes in the California Current is very strong, the relationship occasionally breaks down (Chelton *et al.* 1982). It is noteworthy that the Peruvian El Niño events in 1932 and 1972 are represented by $\delta^{13}\text{C}$ -peaks in Figure 3, although we have little or no physical/ oceanographic evidence of ENSO influence during 1933/34 and 1973/74 in the California borderland.

The finding of a $\delta^{13}\text{C}$ maximum in our time series represents insufficient evidence to document an ENSO event. In any case, and especially for pre-1525 sediments, one could identify prospective sediment layers as ENSO event deposits using their distinctive microfossil assemblages (Lange *et al.* 1987 and 1990) and paleoclimatically relevant biomarkers (McCaffrey *et al.* 1990). Our carbon isotopic approach is thus useful for rapid screening of large numbers of sediment samples. Prospective ENSO layers could then be scrutinized by more specialized methods.

Conclusion

In agreement with historical weather records and direct kelp observations, we present evidence from the 19th and 20th centuries that the combined marine-derived organic carbon from phytoplankton and kelp responded isotopically to oceanographic changes. The laminated sediment record of the Santa Barbara basin extends several thousand years into the past. This offers an opportunity to reconstruct the frequency of prehistoric ENSO events as they are recorded in sedimentary organic matter.

Acknowledgments

This work was supported by National Science Foundation grants ATM87-23024 to W.H. Berger and OCE87-00989 to P.K. Dayton and M.J. Tegner.

References

- Brandt, R.P. 1923. "Potash from Kelp: Early Development and Growth of the Giant Kelp, *Macrocystis pyrifera*". *U.S. Department of Agriculture Bulletin* 1191:1-40.
- Brewer, W.H. 1966. *Up and Down California in 1860-1864*. University of California Press. Berkeley.
- Chelton, D.B., P.A. Bernal, and J.A. McGowan. 1982. "Large-Scale Interannual Physical and Biological Interactions in the California Current". *Journal of Marine Research* 40:1095-1125.
- Conover, W.J. 1971. *Practical Nonparametric Statistics*. Wiley. New York. pp.96-97.
- Drake, D.E., P. Fleischer, and R.L. Kolpack. 1971. "Transport and Deposition of Flood Sediment, Santa Barbara Channel, California". in *Survey of the Santa Barbara Channel Oil Spill 1969-1970*. Ed. R.L. Kolpack. Allan Hancock Foundation. University of Southern California, Los Angeles. 2:95-113.
- Duggins, D.O., C.A. Simenstad, and J.A. Estes. 1989. "Magnification of Secondary Production by Kelp Detritus in Coastal Marine Ecosystems". *Science* 245:170-173.
- Ellison, W.H. (Editor). 1937. *The Life and Adventures of George Nidever (1802-1883)*. University of California Press, Berkeley.
- Eppley, R.W., and O. Holm-Hansen. 1986. "Primary Production in the Southern California Bight". in *Lecture Notes on Coastal and Estuarine Studies*. Ed. W. Eppley. Plankton Dynamics of the Southern California Bight. Springer, Berlin. 15:176-215.
- Fenton, G.E., and D.A. Ritz. 1988. "Changes in Carbon and Hydrogen Stable Isotope Ratios of Macroalgae and Seagrass During Decomposition". *Estuarine, Coastal and Shelf Science* 26:429-436.
- Harger, B. 1983. "An Historical Overview of Kelp in Southern California". in *The Effects of Waste Disposal on Kelp Communities*. Ed. W. Bascom. Institute of Marine Resources. University of California, La Jolla. pp.70-83.
- Kolpack, R.L., J.S. Mattson, H.B. Mark Jr., and T.C. Yu. 1971. "Hydrocarbon Content of Santa Barbara Channel Sediments". in *Survey of the Santa Barbara Channel Oil Spill 1969-1970*. Ed. R.L. Kolpack. Allan Hancock Foundation. University of Southern California, Los Angeles. 2:276-295.
- Lange, C.B., W.H. Berger, S.K. Burke, R.E. Casey, A. Schimmelmann, A. Soutar, and A.L. Weinheimer. 1987. "El Niño in Santa Barbara Basin: Diatom, Radiolarian and Foraminiferan Responses to the 1983 El Niño Event". *Marine Geology* 78:153-160.
- Lange, C.B., S.K. Burke, and W.H. Berger. 1990. "Biological Production Off Southern California Is Linked to Climatic Change". *Climatic Change* 16:319-329.
- Mason, J.D. (Editor). 1961. *Reproduction of Thompson and West's History of Santa Barbara & Ventura Counties*. Howell-North, Berkeley, CA.
- McCaffrey, M.A., J.W. Farrington, and D.J. Repeta. 1990. "The Organic Geochemistry of Peru Margin Surface Sediments: I. A Comparison of the C₃₇ Alkenone and Historical El Niño Records". *Geochimica et Cosmochimica Acta* 54:1671-1682.

- Nissenbaum, A., and A. Serban. 1987. "Enzymatic (?) Activity Associated with Humic Substances in Deep Sediments from the Cariaco Trench and Walvis Ridge". *Geochimica et Cosmochimica Acta* 51:373-378.
- Pytte, M.H. 1989. "Comparison of Monterey Formation Kerogens from the Salinas Basin and Santa Barbara Area, California". *Organic Geochemistry* 14:233-245.
- Quinn, W.H., V.T. Neal, and S.E. Antuñez de Mayolo. 1987. "El Niño Occurrences Over the Past Four and a Half Centuries". *Journal of Geophysical Research* 92(C13):14,449-14,461.
- Rau, G.H., T. Takahashi, and D.J. Des Marais. 1989. "Latitudinal Variations in Plankton $\delta^{13}\text{C}$: Implications for CO_2 and Productivity in Past Oceans". *Nature* 341:516-518.
- Reed, W.E., and I.R. Kaplan. 1977. "The Chemistry of Marine Petroleum Seeps". *Journal of Geochemical Exploration* 7:255-293.
- Reimers, C.E., C.B. Lange, M. Tabak, and J.M. Bernhard. 1990. "Seasonal Spillover and Varve Formation in the Santa Barbara Basin, California". *Limnology and Oceanography* (in press).
- Ruhge, J.M. 1987. *Gunpowder and Canvas*. Quantum Imaging Associates. Goleta, CA.
- Sackett, W.M. 1989. "Stable Carbon Isotope Studies on Organic Matter in the Marine Environment". in *Handbook of Environmental Isotope Geochemistry*. Eds. P. Fritz and C.H. Fontes. Elsevier, Amsterdam. 3:139-169.
- Schaefer, H. 1989. "Improving Southern California's Coastal Waters". *Journal of the Water Pollution Control Federation* 61:1395-1401.
- Schimmelmann, A., C.B. Lange, and W.H. Berger. 1990. "Climatically Controlled Marker Layers in Santa Barbara Basin Sediments, and Fine-Scale Core-to-Core Correlation". *Limnology and Oceanography* 35:165-173.
- Seymour, R.J., R.R. Stange, D.R. Cayan, and R.A. Nathan. 1984. "Influence of El Niños on California's Wave Climate". in *Proceedings of the Nineteenth Coastal Engineering Conference*. Ed. B.L. Edge. American Society of Civil Engineers, New York. pp.577-592.
- Seymour, R.J., M.J. Tegner, P.K. Dayton, and P.E. Parnell. 1989. "Storm Wave Induced Mortality of Giant Kelp, *Macrocystis pyrifera*, in Southern California". *Estuarine, Coastal and Shelf Science* 28:277-292.
- Soutar, A., and P.A. Crill. 1977. "Sedimentation and Climatic Patterns in the Santa Barbara Basin During the 19th and 20th Centuries". *Geological Society of America Bulletin* 88:1161-1172.
- Tegner, M.J., and P.K. Dayton. 1987. "El Niño Effects on Southern California Kelp Forest Communities". *Advances in Ecological Research* 17:243-279.
- U.S. Army Corps of Engineers. 1975. *Flood Plain Information*. Santa Barbara Stream Group, Los Angeles District, Los Angeles.
- U.S. Coast and Geodetic Survey, Pacific Coast. 1889. *Coast Pilot of California, Oregon, and Washington*. Washington.
- U.S. Geodetic and Coast Survey. 1872, 1875. *Annual Reports*. Washington.

Eastern Tropical Pacific Corals Monitor Low Latitude Climate of the Past 400 Years

Robert B. Dunbar, Gerard M. Wellington,
Mitchell W. Colgan, and Peter W. Glynn

ABSTRACT: We have measured coral growth band thickness and skeletal stable isotopic composition through a 371-year transect (AD 1583-1954) from a massive specimen of *Pavona clavus* from the Galápagos Islands. The Galápagos are well situated for recording variations in the relative influence of the Peru Current, Panama Current, and Equatorial Undercurrent. Annual growth rates since 1583 have varied from 5 to 22 mm yr⁻¹, with an average of 13 mm yr⁻¹. Variance in thickness of the annual growth bands is concentrated at periods of 23, 11, 5.5, and 3.3 years. These periods are similar to those of the sunspot cycle (11 years), double sunspot (Hale) cycle, and their harmonics. The maximum range in annual average $\delta^{18}\text{O}$ is about 1.2‰, equivalent to 5°C if seawater isotopic composition at this site has remained constant. Most short-term and decadal variations from the long-term mean correspond to temperature changes on the order of 1 to 2°C. Warmer than average intervals include the years 1650-1670, 1700-1800, and 1870-1895; cooler conditions prevailed during 1600-1650, 1800-1825, and 1910-1950. There is considerable variance in the $\delta^{18}\text{O}$ record within the ENSO frequency band, as well as at longer periods of 30 and 50 years. Longer (and very short) period variability is reduced in the latter part of the record (1826-1954), where the dominant variance occurs at a period of 22 years. We observe a general cooling trend during 1860-1954, corresponding to the end of the Little Ice Age, an interval characterized by general warming at many mid-latitude sites. Variance at sunspot cycle frequencies in growth rate, stable isotopic, and trace element composition implies a direct or indirect link between the solar cycle and climate modulation in the eastern Pacific.

Introduction

Climatic perturbations during the late Holocene have occurred on time scales of centuries (e.g., Little Ice Age, circa AD 1500-1900) to years (El Niño/Southern Oscillation). The Little Ice Age was marked by several periods of glacial advance and generally cooler temperatures in Europe and North America (Lamb 1969, Bryson 1974; see Grove 1988 for review). Oscillations of the Little Ice Age type have apparently occurred throughout the Holocene (Denton and Karlin 1973), and such events are probably superimposed on the major glacial/interglacial cycles of the Pleistocene. A thorough understanding of the cause and effect of these “natural” century- to millennia-scale climate fluctuations is needed before anthropogenic climate modification can be accurately assessed or predicted.

The majority of climate reconstructions that extend through the Little Ice Age have been derived from continental recording systems such as tree rings, varved lake sediments, and glacial ice cores (e.g., Fritts 1966, Jacoby and D'Arrigo 1989, Lough and Fritts 1990, Anderson *et al.* 1984, Thompson *et al.* 1986, Jousel *et al.* 1983, and many others). There have been few studies of the Little Ice Age using tracers from marine environments; however, these show that ocean surface conditions at a number of locations were altered during the 1700s through late 1800s (Dunbar 1983, Juillet *et al.* 1983, Druffel 1982, Glynn *et al.* 1983, Leventer and Dunbar 1982), almost certainly with concomitant changes in the CO₂ flux between the ocean and atmosphere (Druffel 1985, Patzold 1986). The link between the Little Ice Age and atmospheric CO₂ levels can be assessed only if we can

obtain a reliable reconstruction of changes in ocean temperature and circulation across a range of latitudes.

Carbonate sedimentary systems at low latitudes offer unique opportunities for paleoclimate studies. Because of their rapid accretion rates and sensitivity to surface water conditions, shallow water carbonates are well suited for high frequency climate reconstructions. Here we describe the use of a massive reef coral from the Galápagos archipelago for such studies.

Massive corals exhibit large seasonal variations in skeletal extension and calcification rates and produce annual couplets of high and low density bands (Buddemeier *et al.* 1974). Annual growth bands are clearly revealed via x-radiography, and accurate chronologies can be defined that are similar in utility to those developed using tree rings. During coral growth, the stable oxygen isotopic ratio of the accreting carbonate varies as a function of seawater temperature and isotopic composition (see Swart 1983 for review). Although corals accrete aragonite several parts per mil depleted in ^{13}C and ^{18}O relative to equilibrium values (Weber and Woodhead 1972), calibration studies have shown that in high growth rate portions of a coral skeleton, the ^{18}O disequilibrium offset is constant (McConnaughey 1986, 1989). In areas where seawater $\delta^{18}\text{O}$ variations are small or well known, water temperatures inferred by isotopic analysis are accurate to within 0.5 to 1.5°C (Dunbar and Wellington 1981, Weil *et al.* 1981, Patzold 1984, McConnaughey 1989). In areas where seawater temperature variations are small, $\delta^{18}\text{O}$ time series in corals have been used to infer variability in seawater isotopic composition caused by ENSO-related rainfall anomalies (Cole and Fairbanks 1990).

Most previous collections of long-lived massive reef corals have been restricted to the western sides of the oceans (*e.g.*, Caribbean, Great Barrier Reef, Indonesian archipelago) (Patzold 1986, Druffel 1982, Druffel and Linnick 1978, Isdale 1984, Wefer 1983, Macintyre and Smith 1974). Although seasonal variability is resolvable in these areas, the seawater temperature range is generally small. We have examined the growth band and stable isotopic stratigraphy of a large coral colony from the Galápagos Islands in the eastern tropical Pacific, where seasonal and interannual variations in temperature are much larger.

Galápagos Islands and Urvina Bay

The Galápagos Islands sit astride the equator, about 1,000 kilometers west of mainland Ecuador (Figure 1). There are two distinct seasons: a wet-warm season from January to May and a dry-cool season the rest of the year. During the cool season, the Peru Oceanic Current and Peru Coastal Current carry relatively cool (20-24°C, subtropical, saline (35 parts per mil) waters in a northwesterly direction to join with the South Equatorial Current (Figure 2). The seasonality of these currents is governed by the intensity of the southeast tradewinds, which generally are strongest in August and September and weakest in February and March, corresponding respectively to the dry-cool and wet-warm seasons in Galápagos. The Equatorial Undercurrent (Cromwell Current) flows beneath and counter (west to east) to the westward-flowing South Equatorial Current. This current is presently confined between 2°N and 3°S latitude and has an average thickness of 200 meters. Its core is generally found at depths >100 meters, but it tends to shoal as it approaches the Galápagos. As this current approaches the island pedestals of Fernandina and Isabela, it is

UR-86 grew in a location surrounded on three sides by basalt ridges. A small area of this ridge system, in the northern part, was emergent during low tide. To the northwest was a deep, low-relief basalt field. This configuration provided good circulation and exchange with oceanic waters seaward of the reef. The sand channel adjacent to UR-86 is composed of coarse sand and pebble-sized bioclastic debris. The absence of fine sand and silt in the area surrounding the colony suggests water circulation was vigorous.

Methods

About 180 kilograms of skeletal material from the UR-86-1 transect was shipped to Rice University and reassembled. X-ray slabs 6-mm thick were cut perpendicular to density bands using a high speed band saw. The slabs were then cleaned with deionized water and x-rayed (35 KV, 3 ma, 95 seconds) with a Phillips Radiflour medical x-ray unit, using Kodak X-OMAT-G x-ray film. X-ray positive prints were used for developing a chronology based on annual dense bands (Figure 4). Band thickness was determined by measuring the distance between the base of each high density band using the x-ray positives. Individual band thickness was generally uniform across each section. In cases where band thickness varied, the most rapidly growing portion was measured.

Sub-annual samples for stable isotopic analysis were collected by drilling with a Dremel tool and diamond-tipped dental drill bit at about 1-mm intervals. Samples for annual trace element and isotopic analysis were prepared by Glen Shen (Lamont-Doherty Geological Observatory) by cutting small blocks from the x-ray slabs using the x-ray negatives as a guide for locating the base of each high density band. These blocks were ultrasonically cleaned in deionized water and treated with 0.15 N HNO₃ (3 minutes), a 50/50 mixture of 30% H₂O₂ and 0.2N NaOH (20 minutes), and 0.15 N HNO₃ (an additional 3 minutes) to remove contaminating metals from surfaces. Cleaned blocks were gently crushed, then washed again with distilled water. The 280-700 μ m fraction was split into aliquots for stable isotopic analysis and trace metal determination (Shen *et al.* 1991). From each annual and subannual sample, 1 to 3 mg of aragonite powder was prepared for isotopic analysis at Rice University by vacuum roasting for 1 hour at 275°C. Samples were dissolved in 100% H₃PO₄ at 50°C; the resulting CO₂ gas was analyzed with a VG Micromass 602 double-collecting mass spectrometer upgraded with SIRA series electronics. NBS-20 was analyzed two or three times daily to provide standardization. Of 351 annual samples for UR-86-1, 222 years were analyzed in duplicate and 51 years were analyzed in triplicate. Average standard deviation for replicate samples is 0.067 parts per mil for $\delta^{18}\text{O}$ and 0.085 parts per mil for $\delta^{13}\text{C}$. Spectral analysis was accomplished using the FORTRAN program "Power", written in 1966 by the Health Sciences Computing Facility, UCLA, and revised in 1981 by B. Molfino and J. Morley (Lamont-Doherty Geological Observatory).

Coral Growth Chronology

A positive x-radiograph collage of UR-86-1 shows well developed annual density banding (Figure 4). Age at the top of the section is set at AD 1954, the year of uplift and death of the coral colony. Based on counts of the annual light/dark couplets, the growth record spans 371 years. Growth bands are relatively thick (1 to 2 cm) and may be clearly resolved below the top 70 cm of the sequence. Growth bands are thinner and considerably less distinct in the uppermost part of the record; we assign an age estimate error of about

Figure 4
POSITIVE X-RAY PRINTS OF UR-86-1, A 5.5-METER-LONG SECTION FROM A COLONY OF
PAVONA CLAVUS FROM THE URVINA BAY UPLIFT, GALÁPAGOS ISLANDS

Annual bands are an average of 13 mm thick. Steel pins were placed on the x-ray slabs every 5 cm for scale. These show up as short black lines sub-parallel to annual banding. Estimated year of growth is given every 10 years, from AD 1583 to 1954. Open arrows show correlation horizons between sections. Open stars show hiatuses or growth discontinuities. Thick black lines normal to annual bands show transects selected for detailed sub-annual studies.



± 5 years to this portion. Several growth discontinuities or hiatuses are evident in the band stratigraphy, most notably at AD 1673, 1720, 1747, 1752, 1886, and 1888. The absence of extensive bioerosion at these horizons leads us to believe they represent relatively brief periods (<1 year). Based on band-counting alone, we have estimated an age error of ± 10 years at the base of the section (AD 1583). Our age assignments have been preliminarily confirmed by ^{230}Th mass spectrometric analyses performed by Bruno Hamelin (Lamont-Doherty Geological Observatory) based on the technique of Edwards *et al.* (1987) and reported by Shen *et al.* (1991). Four ^{230}Th mass spectrometric analyses on coral samples from the 1664-1666 and 1652-1654 levels yield ages that differ by an average of 10 to 14 years from the band-counted ages. Better age control for these and other late Holocene corals may become available as the ^{230}Th mass spectrometric technique is optimized for very young samples.

The x-ray collage shows considerable interannual variation in growth band thickness and density. Unusually dense bands with irregular boundaries are often associated with growth discontinuities or hiatuses (*e.g.*, AD 1673 and 1747) and may indicate environmental conditions unfavorable to coral growth. In their reconstruction of El Niño occurrences during the past 450 years based on historical records, Quinn *et al.* (1987) report strong to very strong ENSO events at AD 1671, 1720, 1747, 1761, 1884, and 1891. These dates either correspond precisely to or are within several years of the dates assigned to the six hiatuses in UR-86-1. Given the impact of the 1982-83 ENSO on coral growth in the eastern Pacific (see review by Glynn 1990), we might expect the interruption of coral growth to be a common feature of strong El Niños. We note, however, that Quinn *et al.* (1987) describe many strong to very strong El Niños that apparently have not perturbed the growth of this colony (*e.g.*, very strong events at AD 1728, 1791, 1877, and 1925). We also note that even small uncertainties in growth band age assignment make it difficult to attribute individual features of the band record to specific ENSO events. While many growth discontinuities and anomalous density bands within this band record very likely reflect ENSO-related environmental perturbations, the band record alone is not a reliable indicator of either ENSO occurrence or strength. Character of the growth bands is discussed more completely in Dunbar *et al.* (1991).

Band Thickness

A 371-year record of growth band thickness is shown in Figure 5. Coral growth rates since 1583 have ranged from 5 to 22 mm yr⁻¹, with an average of 13 mm yr⁻¹. Growth rates are highest during the mid- to late 1800s and lowest from 1900-1954. Superimposed on these long-term changes in growth rate is a higher frequency rhythmicity, clearly evident in both the raw and filtered data. Spectral analysis of the unfiltered data reveals a concentration of variance at periods of about 23, 11, 5.5, and 3.3 years (Figure 6). Periods of 23, 11, and 5.5 years are equivalent to periods of the double sunspot (Hale) cycle, sunspot cycle, and half sunspot cycle. Our growth band data suggest a strong solar link that directly or indirectly influences coral growth rate. Coral growth is sensitive to changes in water temperature, light intensity (cloud cover), and food supply; the dominant factor in this case is not yet clear.

Variance at periods of about 20 and 11 years is also evident in skeletal manganese concentrations in this coral (Shen *et al.* 1991). On a seasonal time-scale, skeletal Mn/Ca

Figure 5
 TIME SERIES OF ANNUAL GROWTH BAND THICKNESS FROM UR-86-1 AND
 THE SAME DATA (lower graph) WITH 7-POINT MOVING AVERAGE FILTER

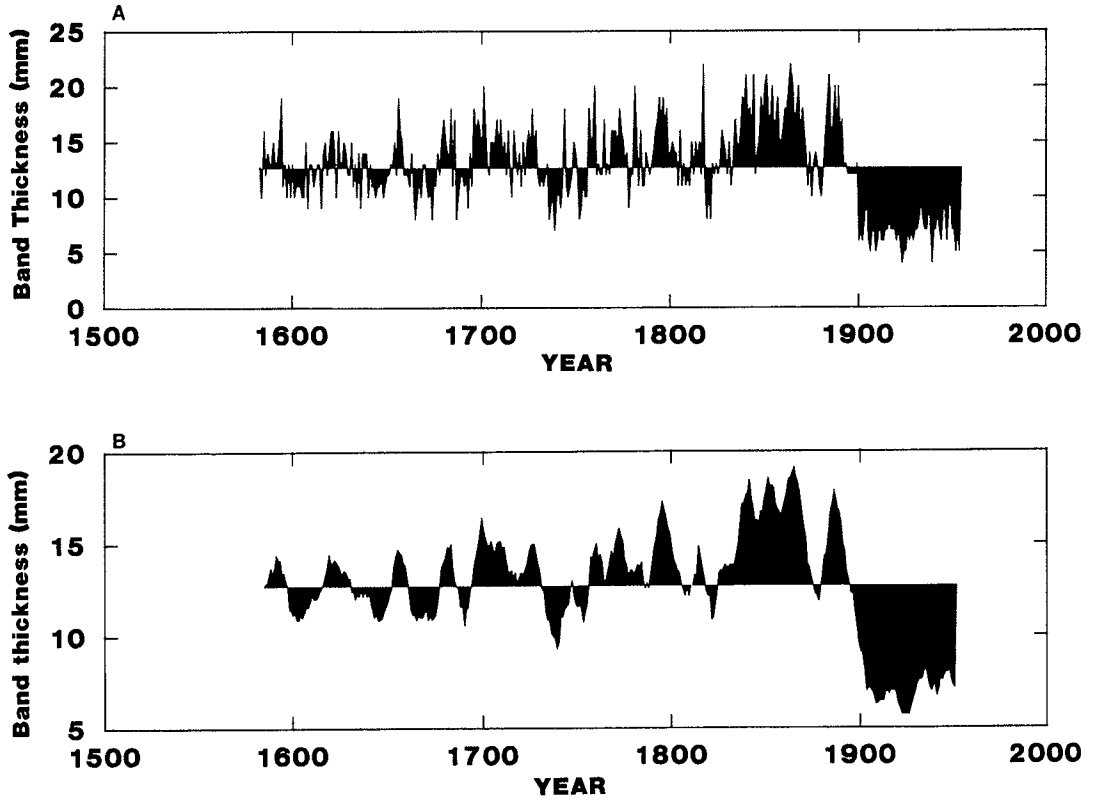
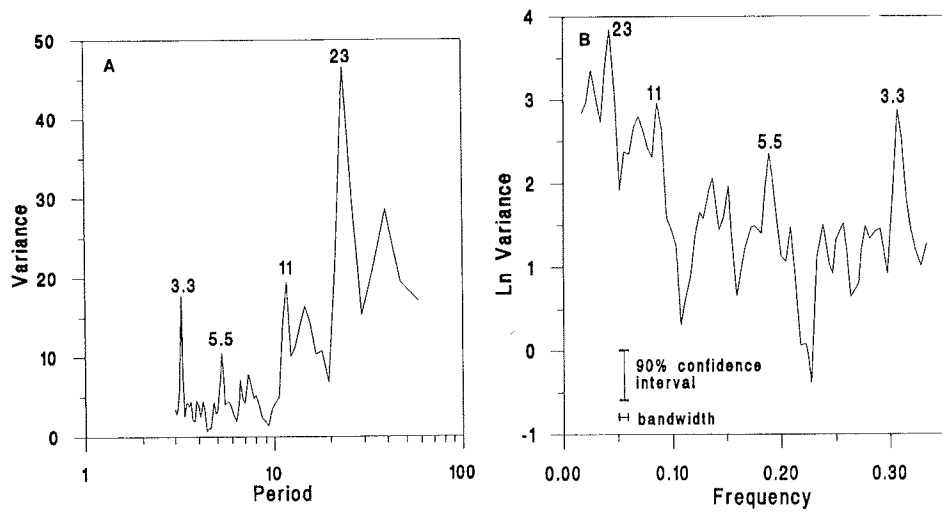


Figure 6
 POWER SPECTRAL ANALYSIS RESULTS FOR ANNUAL BAND THICKNESS DATA
 EXPRESSED AS VARIANCE VERSUS PERIOD IN YEARS (left graph) AND
 THE SAME RESULTS EXPRESSED AS Ln VARIANCE VERSUS FREQUENCY



No prewhitening, linear detrend, 117 lags.

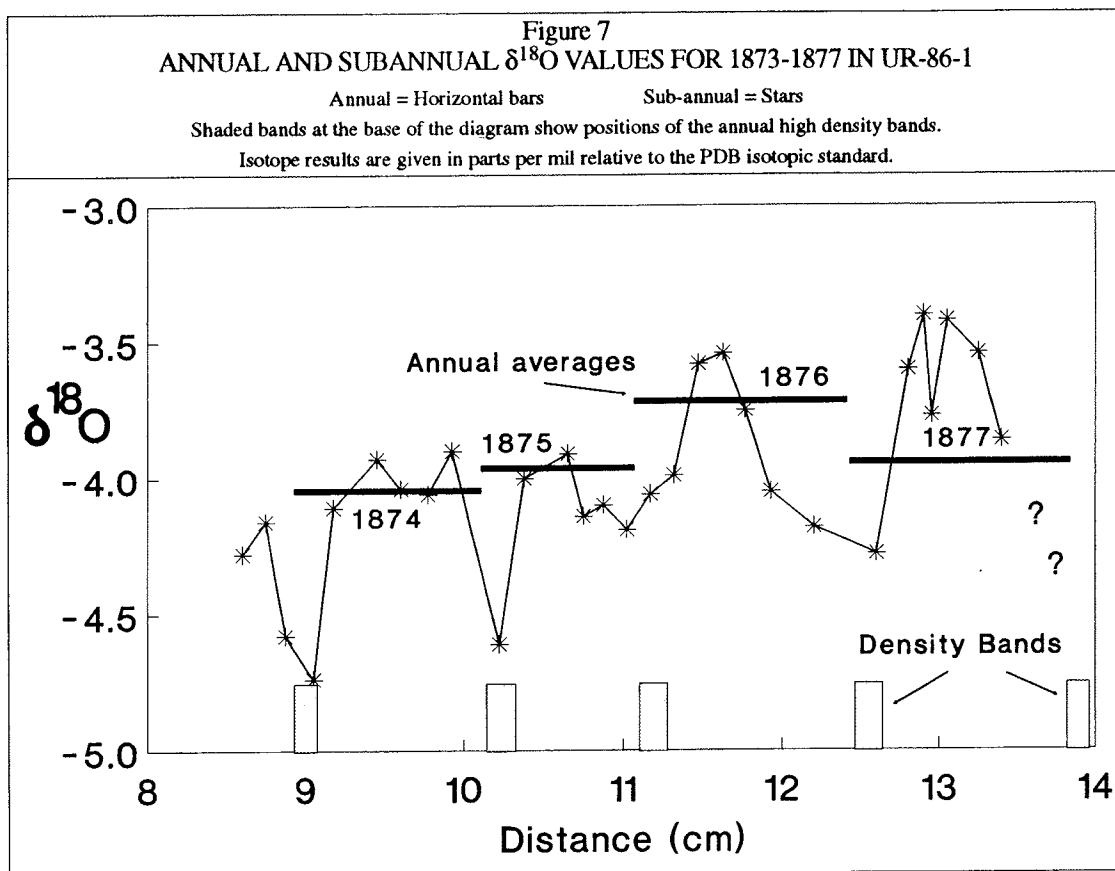
ratios vary in response to seasonal upwelling. The precise cause of the longer term variability is not known; besides upwelling, release of Mn from sediments, aeolian flux, volcanic events, and smaller scale tectonic activity can all influence the Mn/Ca ratio of coralline aragonite. Collectively, the cyclical nature of growth rate and Mn/Ca variations over a period of >350 years argues for an external environmental cause and may provide strong evidence for a high frequency solar/climate relationship.

Oxygen Isotopes

We measured $^{18}\text{O}/^{16}\text{O}$ and $^{13}\text{C}/^{12}\text{C}$ ratios of annual samples over the interval 1604-1954. Sub-annual isotopic variability (8-14 samples yr^{-1}) was examined along several 3- to 5-year transects to characterize a "normal" annual cycle and to test the efficiency of the annual sampling scheme for detecting ENSO-scale events. Figure 7 is a comparison of isotopic results from annual averages and sub-annual samples. The average seasonal range in $\delta^{18}\text{O}$ is about 0.8 parts per mil, equivalent to a temperature range of 3 to 4°C if variations in seawater $\delta^{18}\text{O}$ are negligible. A similar seasonal range of 0.8 to 0.9 parts per mil was observed along a transect extending from 1965 to 1984 in a specimen of *Pavona clavus* collected live from the submerged portion of the Urvina Bay reef (Dunbar *et al.* 1991). There are no instrumental seawater temperature records from Urvina Bay, but temperature variations implied by these isotopic ranges are roughly consistent with the average annual range in monthly mean sea surface temperature of 4.5°C (1965-1976) measured at the Charles Darwin Research Station on Santa Cruz Island (Glynn and Wellington 1983).

The lowest $\delta^{18}\text{O}$ values are within or immediately below the annual high density bands, consistent with field observations that high density bands form during the warm months of January through May (Glynn and Wellington 1983). The $^{18}\text{O}/^{16}\text{O}$ ratios of the annual samples are most representative of the ^{18}O -enriched portion of the sub-annual transect; however, the general interannual isotopic trend recorded by the sub-annual samples is faithfully registered by the annual samples as well. For example, both sub-annual and annual samples show enrichment in ^{18}O in aragonite accreted during AD 1876.

Conversion of isotopic results to absolute paleotemperatures is complicated by uncertainties about variations in $\delta^{18}\text{O}$ of sea water. We note, however, that seasonal and interannual salinity variations in the Galápagos region are smaller (<3 parts per mil) than in the Gulf of Panama (up to 10 parts per mil) and that the magnitude of surface salinity variability in the eastern equatorial Pacific decreases from east to west (Wyrski *et al.* 1966, Glynn and Wellington 1983, EastroPac Atlas). McConnaughey (1986, 1989) discusses the seawater isotopic data and points out that while low temperature waters in the area probably have relatively constant $\delta^{18}\text{O}$ values, warm water masses may be enriched (South Pacific gyre source) or depleted (Gulf of Panama source) in ^{18}O . The net influence of ENSO in the region is most likely a decrease in seawater $\delta^{18}\text{O}$, in part because of increased dilution by ^{18}O -depleted precipitation. The effect of seawater isotopic composition on coralline $\delta^{18}\text{O}$ values would be additive with temperature during El Niños; for example, both would produce a low ^{18}O anomaly. Based on the collective evidence, we estimate that the "normal" seawater $\delta^{18}\text{O}$ range along the west coast of Isabela Island is less than 0.3 parts per mil, equivalent to a temperature variation of about 1°C. Accurate seasonal (and ENSO event) measurements of seawater salinity, temperature, and $\delta^{18}\text{O}$ at the study site are required to fully utilize information from the stable isotopic records.



Annual average $\delta^{18}\text{O}$ values from AD 1604 through 1954 are shown in Figure 8. The maximum range in $\delta^{18}\text{O}$ is about 1.2 parts per mil, equivalent to 5°C . Most deviations from the mean correspond to temperature changes on the order of 1 to 2°C . “Cool” and “warm” intervals lasting one to several decades are evident in the annual data as well as the filtered data. Warm periods include 1650-1670, 1700-1800, and 1870-1895; cooler conditions prevailed during 1600-1650, 1800-1825, and 1910-1950. There is considerable variance in the $\delta^{18}\text{O}$ record within the ENSO frequency band, as well as at longer periods of 30 and 50 years (Figure 9). The longer (and very short) period variability is reduced in the latter part of the record (1826-1954) where the dominant variance occurs at a period of about 22 years (Figure 10).

The extent to which individual ENSO events are recorded in the stable isotopic stratigraphy is not yet known. In many eastern tropical Pacific areas, major ENSO events may be sufficiently stressful that coral growth ceases (Glynn 1990). If the environmental recording system turns off during very strong events, coral-based isotopic and trace element records from these areas may contain information biased towards “anti-ENSO” or weak ENSO periods. If the stable isotope variations shown in Figure 7 are driven primarily by ENSO related changes in seawater temperature and isotopic composition, we make the following tentative observations. ENSO-scale events at this location occurred more frequently during the Little Ice Age and were superimposed on longer period climate cycles of 30 and 50 years which may have modulated the strength of ENSO phenomena. Variance at “normal” ENSO periods (e.g. years) is reduced during the last 100 years of the record; however the variance at a period of 22 years, equivalent to the Hale cycle period, may imply a link between the solar cycle and climate modulation in the eastern Pacific, as has been previously suggested by Anderson (1990).

Figure 8
 TIME SERIES OF ANNUAL $\delta^{18}\text{O}$ FOR UR-86-1 AND
 THE SAME DATA (lower graph) WITH 7-POINT MOVING AVERAGE FILTER

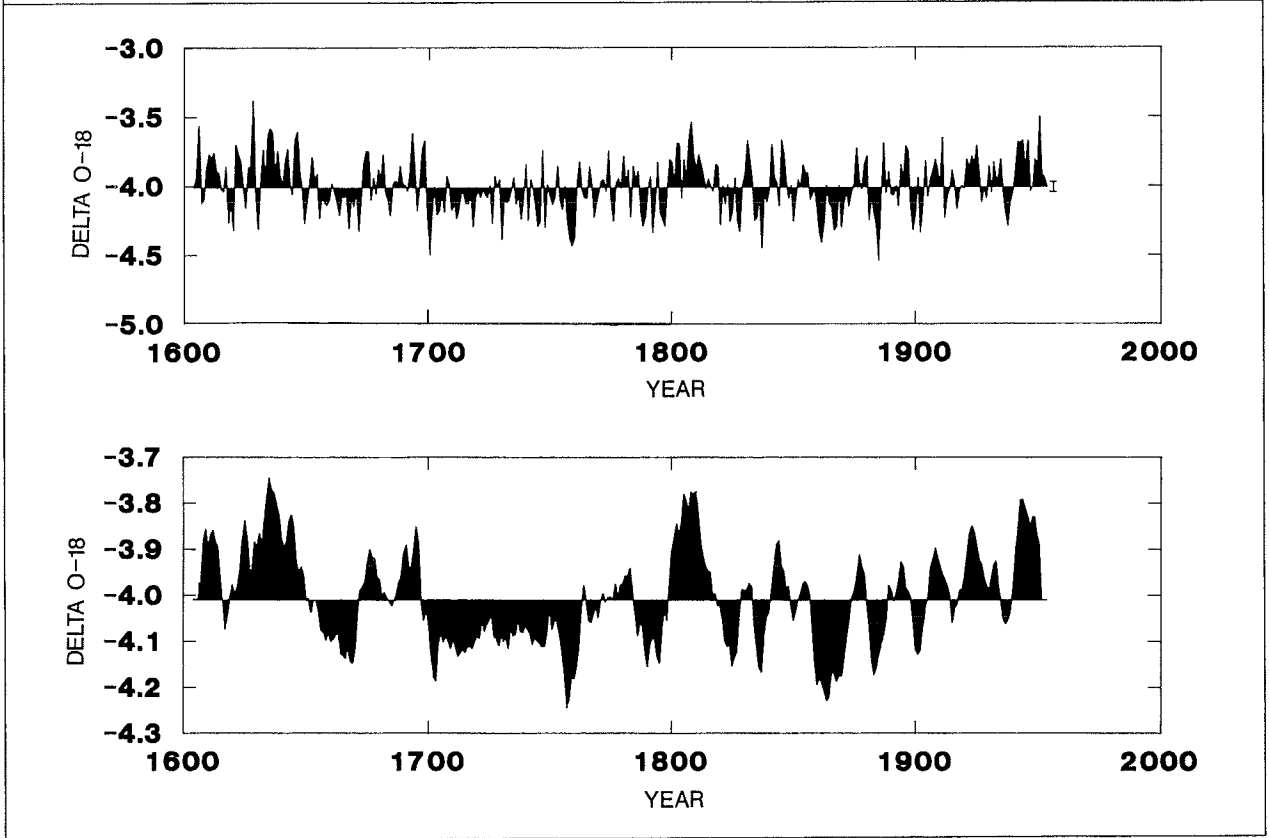


Figure 9
 POWER SPECTRAL ANALYSIS RESULTS FOR
 ANNUAL $\delta^{18}\text{O}$ DATA, 1604-1954.

No prewhitening, linear detrend, 117 lags.
 Expressed as Variance versus Period, in years.

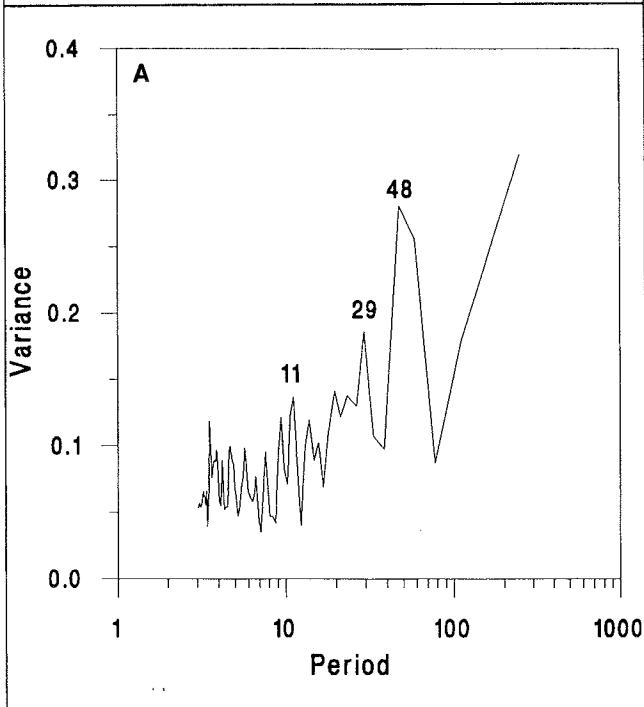
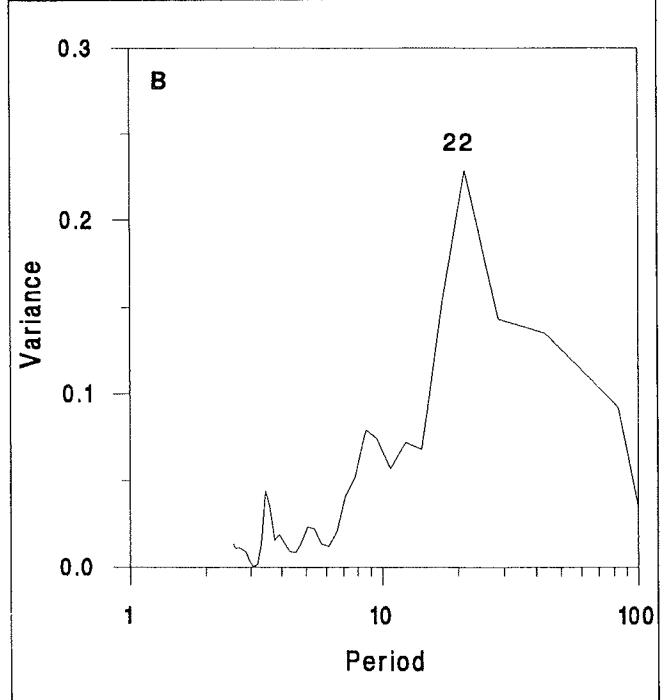


Figure 10
 POWER SPECTRAL ANALYSIS RESULTS FOR
 ANNUAL $\delta^{18}\text{O}$ DATA, 1826-1954.

No prewhitening, linear detrend, 43 lags.
 Expressed as Variance versus Period, in years.



Another intriguing aspect of the data is that the period from about 1860-1954, corresponding to the end of the Little Ice Age, is characterized by a general cooling trend, rather than warming. At this location, cooling may result from increased influence of the Equatorial Undercurrent, greater trade wind induced upwelling, and/or spin-up of the South Pacific gyre. Discrimination among these possibilities awaits the acquisition of additional long-term records and accurate calibration of isotopic and chemical indices at specific coral collection sites.

Conclusions

Results of this and other recent studies (Cole and Fairbanks 1990, Shen *et al.* 1991, Druffel *et al.* 1990, McConnaughey 1989, Lea 1989) show the potential utility of coral skeletons for high resolution paleoclimate studies and underscore the need for a multi-tracer (stable isotopes, trace element, *etc.*), multi-site approach for developing coral-based climate reconstructions. Accurate calibration of the contemporary record (which may be site-specific) is a prerequisite for validating retrospective studies.

- Growth rates of a specimen of *Pavona clavus* from the Galápagos range from 5 to 22 mm yr⁻¹ between 1583 and 1954. Variance at periods of 23, 11, and 5.5 years over the entire 371-year record suggests a link between the solar cycle and an undetermined factor controlling coral growth rate.
- Between 1604 and 1954, annual average $\delta^{18}\text{O}$ values vary over a range of 1.2 parts per mil, equivalent to a temperature range of 5°C if seawater isotopic composition has remained constant. Decadal scale variability is generally expressed as shifts of 0.3 to 0.5 parts per mil (1 to 2°C) from the long-term mean. We have identified warm intervals at 1650-1670, 1700-1800, and 1870-1895 and cool periods at 1600-1650, 1800-1825, and 1910-1950.
- Variance in $\delta^{18}\text{O}$ during first 250 years is concentrated in the ENSO band and at longer periods of about 30 and 50 years. In the latter part of the record, the dominant variance occurs at a period of 22 years, again suggesting a solar cycle link.
- We see a general trend to higher $^{18}\text{O}/^{16}\text{O}$ ratios (cooler conditions) during 1860-1954, corresponding to the end of the Little Ice Age, when many northern hemisphere climate records show general warming. At this location, isotopic fluctuations likely represent the varying influence of the Equatorial Undercurrent (cooler), Peru Current (moderate), and Panama Current (warm).
- The extent to which ENSO effects can be resolved from the isotopic and growth band record at site is not yet known. Resolution awaits calibration studies.

Acknowledgments

We thank Dave Mucciarone, Bill Jones, and Gwen Goodman for assistance with the stable isotope analyses. Edith Pestana assisted with coral x-raying and curation. Glen Shen graciously supplied splits of his specially cleaned trace element samples for stable isotope analysis. We thank Bruno Hamelin (LDGO) for providing mass spectrometric dates for UR-86-1. Dave Hollander (ETH, Zürich) assisted Mitch Colgan during collection of UR-86-1. Support for this research has come at various times from NSF (OCE-8415615 and OCE-8716726 to PWG, EAR-8516528 to RBD) and most recently from NOAA (D-AC-827 to RBD and GMW).

References

- Anderson, R.Y. 1990. "Solar-Cycle Modulations of ENSO: A Possible Source of Climatic Change" in *Proceedings of the 6th Annual Pacific Climate (PACLIM) Workshop*. Ed. J.L. Betancourt and A.M. MacKay, California Department of Water Resources, Technical Report 23, pp. 77-81.
- Anderson, R.Y., W.E. Dean, J.P. Bradbury, and D. Love. 1984. *Meromictic, Varved, and Laminated Lakes in North America*. U.S. Geological Survey Bulletin 1167, pp. 1-15.
- Bryson, R.A. 1974. "A Perspective on Climatic Change". *Science* 184:753-760.
- Buddemeier, R.W., J.E. Maragos, and D.W. Knutson. 1974. "Radiographic Studies of Reef Coral Exoskeletons: Rates and Patterns of Coral Growth". *Jour. Exp. Mar. Biol. Ecol.* 14:179-200.
- Cole, J.E., and R.G. Fairbanks. 1990. "The Southern Oscillation Recorded in the $\delta^{18}\text{O}$ of Corals from Tarawa Atoll". *Paleoceanography* 5:669-683.
- Colgan, M.W., and D.L. Malmquist. 1987. "The Urvina Bay Uplift: A Dry Trek through a Galápagos Coral Reef". *Oceanus* 30:61-68.
- Couffer, J.C. 1956. "The Disappearance of Urvina Bay". *Natural History* 65:378-383.
- Denton, G.H., and W. Karlin. 1973. "Holocene Climatic Variations: Their Pattern and Possible Cause". *Quaternary Research* 3:155-203.
- Druffel, E.M. 1985. "Detection of El Niño and Decade Time Scale Variations of Sea Surface Temperature from Banded Coral Records: Implications for the Carbon Dioxide Cycle" in *The Carbon Cycle and Atmospheric CO₂: Natural Variations Archean to Present*. Ed. E.T. Sundquist and W.S. Broecker. American Geophysical Union Geophysical Monograph 32:111-122.
- _____. 1982. "Banded Corals: Changes in Oceanic Carbon-14 During the Little Ice Age". *Science* 218:13-19.
- Druffel, E.M., R.B. Dunbar, G.M. Wellington, and S.A. Minnis. 1990. "Reef-Building Corals and Identification of ENSO Warming Episodes". in *Global Ecological Consequences of the 1982-83 El Niño/Southern Oscillation*. Ed. P.W. Glynn. Elsevier Press, Holland. (In press.)
- Druffel, E.M., and T.W. Linnick. 1978. "Radiocarbon in Annual Coral Rings of Florida". *Geophysical Research Letters* 5:913-916.

- Dunbar, R.B. 1983. "Stable Isotope Record of Upwelling and Climate from Santa Barbara Basin, California". in *Coastal Upwelling: Its Sediment Record*. Ed. J. Thiede and E. Suess. Plenum Press, New York. pp.217-46.
- Dunbar, R.B., and G.M. Wellington. 1981. "Stable Isotopes in a Branching Coral Monitor Seasonal Temperature Variation". *Nature* 293:453-455.
- Dunbar, R.B., G.M. Wellington, M.W. Colgan, and P.W. Glynn. 1991. "A 371-Year Climate Record from a Massive Reef Coral in Urvina Bay, Galapagos" for submission to *Paleoceanography*.
- Edwards, R.L., J.H. Chen, T.L. Ku, and G.L. Wasserburg. 1987. "Precise Timing of the Last Interglacial Period from Mass Spectrometric Determination of Thorium-230 in Corals". *Science* 236:1547-1553.
- Fritts, H.C. 1966. "Growth Rings of Trees: Their Correlation with Climate". *Science* 154:973-979.
- Glynn, P.W. 1990. "Coral Mortality and Disturbances to Coral Reefs in the Tropical Eastern Pacific" in *Global Ecological Consequences of the 1982-83 El Niño/Southern Oscillation*. Ed. P.W. Glynn. Elsevier Press, Holland (in press).
- Glynn, P.W., E.M. Druffel, and R.B. Dunbar. 1983. "A Dead Central American Coral Reef Tract: Possible Link with the Little Ice Age". *Jour. Mar. Res.* 41:605-637.
- Glynn, P.W., and G.M. Wellington. 1983. *Corals and Coral Reefs of the Galapagos Islands*. University of California Press, Berkeley.
- Grove, J.M. 1988. *The Little Ice Age*. Methuen, NY.
- Isdale, P. 1984. "Fluorescent Bands in Massive Coral Record Centuries of Coastal Rainfall". *Nature* 310:578-579.
- Jacoby, G.C., and R. D'Arrigo. 1989. "Reconstructed Northern Hemisphere Annual Temperature Since 1671 Based on High-Latitude Tree-Ring Data from North America". *Climatic Change* 14:39-59.
- Jouzel, J., L. Merlivat, J.R. Petit, and C. Lorius. 1983. "Climatic Information Over the Last Century Deduced from a Detailed Isotopic Record in the South Pole Snow". *Jour. Geophys. Res.* 88:2693- 2703.
- Julliet, A., and L.D. Labeyrie. 1983. "Oxygen Isotope Composition of Diatom Silica and Silicoflagellate Assemblages Changes in the Gulf of California: A 700-Year Upwelling Study" in *Coastal Upwelling: Its Sediment Record of Ancient Coastal Upwelling*. Ed. J. Thiede and E. Suess. Plenum Press, NY. pp. 217-246.
- Lamb, H.H. 1969. "Climatic Fluctuations" in *World Survey of Climatology, 2: General Climatology*. Ed. Flohn. Elsevier, NY. pp. 173-249.
- Lea, D.W., E.A. Boyle, and G.T. Shen. 1989. "Coralline Barium Records Temporal Variability in Equatorial Pacific Upwelling". *Nature* 340:373-376.
- Leventer, A., and R.B. Dunbar. 1988. "Recent Diatom Record of McMurdo Sound, Antarctica: Implications for History of Sea Ice Extent". *Paleoceanography* 3:259-274.
- Lough, J.M., and H.C. Fritts. 1990. "Historical Aspects of El Niño/Southern Oscillation — Information from Tree Rings" in *Global Ecological Consequences of the 1982-83 El Niño/Southern Oscillation*. Ed. P.W. Glynn. Elsevier Press, Holland (in press).

- Macintyre, I.G., and S.V. Smith. 1974. "X-Radiographic Studies of Skeletal Development in Corals with Radiometric Growth Rates". *Proc. 2nd Intl. Coral Reef Symposium*, Brisbane, Australia. 2:277-287.
- McConnaughey, T.A. 1989. "¹³C and ¹⁸O Isotopic Disequilibrium in Biological Carbonates". *I: Patterns, Geochimica et Cosmochimica*. 53:151-162.
- _____. 1986. *Oxygen and Carbon Isotope Disequilibria in Galapagos Corals: Isotopic Thermometry and Calcification Physiology*. Ph.D. Dissertation, University of Washington.
- Patzold, J. 1986. "Temperature and CO₂ Changes in Tropical Surface Waters of the Phillipines During the Past 120 Years: Record in the Stable Isotopes of Hermatypic Corals". *Berichte, Geologisches/Palaontologisches Institut der Universitat Kiel, B.R. Deutschland*, 12:1-82.
- _____. 1984. "Growth Rhythms Recorded in Stable Isotopes and Density Bands in the Reef Coral *Porites lobata* (Cebu, Phillipines)". *Coral Reefs* 3:78-90.
- Quinn, W.H., V.T. Neal, and S.E. Antuñez de Mayolo. 1987. "El Niño Occurrences Over the Past Four and a Half Centuries". *J. Geophys. Res.* 92:449-461.
- Robinson, G.R. 1987. "Negative Effects of the 1982-83 El Niño on Galápagos Marine Life". *Oceanus* 30:42-47.
- Shen, G.T., R.B. Dunbar, G.M. Wellington, M.W. Colgan, and P.W. Glynn. 1991. "Paleochemistry of Manganese in Corals from the Galapagos Islands". *Coral Reefs* (in press).
- Swart, P.K. 1983. "Carbon and Oxygen Isotope Fractionation in Scleractinian Corals: A Review". *Earth Sciences Reviews* 19:51-80.
- Thompson, L.G., E. Mosley-Thompson, W. Dansgaard, and P.M. Grootes. 1986. "The Little Ice Age as Recorded in the Stratigraphy of the Tropical Quelccaya Ice Cap". *Science* 234:361-364.
- Weber, J.N., P. Dienes, P.H. Weber, and P.A. Baker. 1976. "Depth-Related Changes in the ¹³C/¹²C Ratio of Skeletal Carbonate Deposited by the Caribbean Reef-Frame Building Coral *Montastrea annularis*: Further Implications for a Model of Stable Isotope Fractionation by Scleractinian Corals". *Geochimica et Cosmochimica Acta* 40:31-39.
- Weber, J.N., and P.J. Woodhead. 1972. "Temperature Dependence of Oxygen-18 Concentration in Reef Coral Carbonates". *Jour. Geophys. Res.* 77:463- 473.
- Wefer, G. 1983. "Die Verteilung Stabiler Sauerstoff — Und Kohlenstoff-Istope in Kalkschalen Mariner Organismen — Grundlage Einer Isotopischen Palaokologie". *Habilitationsschrift*. Universitat Kiel, B.R. Deutschland.
- Weil, S.M., R.W. Buddemeier, S.V. Smith, and P.M. Kroopnick. 1981. "The Stable Isotopic Composition of Coral Skeletons: Control by Environmental Variables". *Geochimica et Cosmochimica Acta* 45:1147-1153.
- Wellington, G.M., R.B. Dunbar, and D. Mucciarone. 1991. "Stable Isotope Signature of ENSO in Eastern Tropical Pacific Reef Corals". for submission to *Coral Reefs*.
- Wyrtki, K. 1966. "Oceanography of the Eastern Equatorial Pacific Ocean". *Oceanography and Marine Biology*. Annual Review. 4:33-68.

Inter-Regional Correlation in Tree-Growth Variations in the Western United States, 1513-1964, at ENSO, Sunspot, and Longer Frequency Bands

David M. Meko

Abstract: Cross-spectral analysis of regional tree-ring data suggests the spatial pattern of correlation between moisture variations in the Sierra Nevada of central California and in other parts of the western United States is frequency dependent. Short wavelengths (2.8 to 10.7 years), perhaps associated with El Niño/Southern Oscillation, are strongly coherent both to the north (Oregon) and to the south (Southern California). Longer wavelengths (45 to 75 years) are strongly coherent only to the north. Frequency bands corresponding to annual sunspot series were associated with relatively weak patterns of spatial correlation.

Introduction

Indices of ring-widths from drought-sensitive trees provide proxy climatic series several centuries long over much of the mountainous western United States (Stockton *et al.* 1985). These data are particularly useful for their unique information on climate variations on decadal-and-longer time scales. One type of question that can be addressed with tree-ring data is whether growth variations (and inferred moisture variations) in major runoff-producing areas have marched in step with major swings of known geophysical or astronomical time series. Such linkage would have important implications for water resources planning.

In this paper, tree-growth variations in the Sierra Nevada mountains of central California are compared with variations in other regions of the western United States using cross-spectral analysis. The significance of inter-regional correlation in growth is tested at four specific frequency bands associated with the following phenomena: El Niño/Southern Oscillation (ENSO), annual sunspot series, double sunspot series, and "long-wave" features.

Tree-Ring Data

Forty-one chronologies of ring-width indices, all covering the period 1700-1964, were grouped into five regions (Figure 1). The central California Sierras, region 2, is the focus of this paper. Other regions are referred to as Oregon (1), Southern California (3), Wyoming (4), and Colorado (5). A subset of 26 of these chronologies (Table 1) provided time coverage for AD 1513-1964, the period of analysis for this study. A preliminary correlation analysis showed the 1513-1964 subset was representative of growth variations of the full set for 1700-1964 in each of the five regions. The first eigenvector of growth, 1513-1964, in each region was used to weight the chronologies into regional growth series. To facilitate interregional comparison, regional growth series were then standardized to zero mean and unit variance.

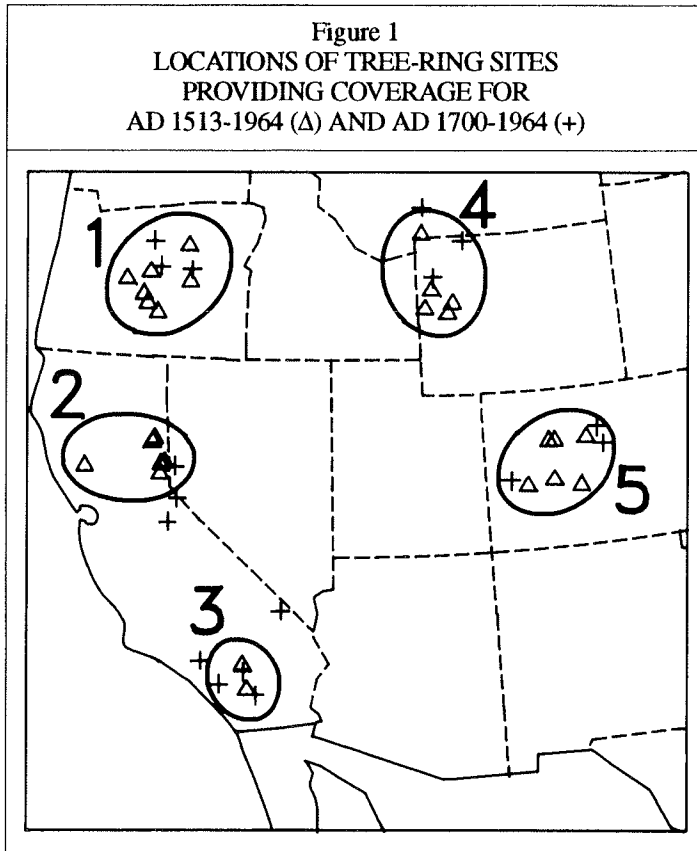


Table 1
IDENTIFICATION NUMBER, STATE,
REGION, AND SPECIES CODE FOR
EACH TREE-RING CHRONOLOGY
USED IN THE STUDY

Identifi- cation	State	Region	Species
SPR661	OR	1	Western Juniper
CAL661	OR	1	Western Juniper
COM661	OR	1	Western Juniper
FRE661	OR	1	Western Juniper
HOR661	OR	1	Western Juniper
LIT661	OR	1	Western Juniper
LOS641	OR	1	Ponderosa Pine
394649	CA	2	Jeffrey Pine
LEM571	CA	2	Jeffrey Pine
ANT571	CA	2	Jeffrey Pine
ANT641	CA	2	Ponderosa Pine
DON571	CA	2	Jeffrey Pine
SJM641	CA	2	Ponderosa Pine
005520	CA	3	Big-Cone Spruce
006649	CA	3	Ponderosa Pine
GRDDF9	MT	4	Mixed
282540	WY	4	Mix ed
283590	WY	4	Limber Pine
051549	WY	4	Douglass Fir
552590	WY	4	Limber Pine
112549	CO	5	Douglass Fir
118629	CO	5	Undetermined Pine sp.
121549	CO	5	Douglass Fir
115549	CO	5	Douglass Fir
116549	CO	5	Douglass Fir
113629	CO	5	Pinyon Pine

Methods

Spectral and cross-spectral analysis of regional growth series followed methodology described in Bloomfield (1976). The purpose of the spectral analysis was to display the distribution of variance as a function of frequency, rather than to test for periodicity. Each regional series was prepared for spectral analysis by subtracting its mean, tapering 5% of the data on each end with a raised-cosine filter, and padding with zeros to length 512 years. The periodogram was computed using a fast Fourier transform algorithm, then smoothed successively by 5-weight and 7-weight Daniell filters to produce the estimated spectrum. Approximate 95% confidence limits for spectral estimates were calculated based on the assumption of a chi-squared distribution (page 196 in Bloomfield 1976). A null continuum was computed by smoothing the periodogram successively with two very broad (length 33 and 77) Daniell filters.

Cross-spectral estimates were also based on periodogram smoothing, although in this case by rectangular rather than Daniell filters, and series were not padded or tapered beforehand. Therefore, sample length was 452 years, with Fourier frequencies at $0/452$, $1/452$, $2/452$, ... and $0.5 \text{ cycle yr}^{-1}$.

Lengths of periodogram filters were chosen to bracket the desired range of wavelengths for each key frequency. The exact endpoints of these ranges are necessarily dependent on the discrete frequencies at which periodogram estimates are available for the given sample size (452 years). Filter lengths and characteristics are listed in Table 2.

Filter	Number of Weights	Central		Period Range (yrs)
		Period (yrs)	Frequency (yr ⁻¹)	
1	5	56.5	0.0177	45 - 75
2	9	22.6	0.0442	18.8 - 28.3
3	17	11.0	0.0907	9.2 - 13.7
4	119	4.4	0.2235	2.8 - 10.8

The percentage of tree-ring variance for region 2 in each of the four key frequency bands was computed by summing the appropriate range of raw-periodogram ordinates and dividing by the total variance.

The significance test on which this paper focuses is based on the estimated squared-coherence from cross-spectral analysis. Let $s_{X,Y}(\omega)^2$ be the sample squared-coherence and $r_{X,Y}(\omega)$ be the theoretical coherence. If $r_{X,Y}(\omega)=0$, the probability of a sample squared-coherence being less than a given level $\sigma(p)^2$ is p , where:

$$\sigma(p)^2 = 1 - (1-p) g^2 / (1-g^2)$$

If the time series has not been tapered or padded, the quantity g^2 in the above equation is simply equal to the sum of the squares of the weights of the function used to smooth the periodogram. For example, for the 5-weight rectangular filter, each weight is 0.2, the sum of squares of weights equals 0.2, and the 95% and 99.9999% confidence limits for squared-coherence are:

$$\sigma(0.999999)^2 = 1 - (1 - 0.999999) 0.2 / (1 - 0.2) = 0.53$$

$$\sigma(0.999999)^2 = 1 - (1 - 0.999999) 0.2 / (1 - 0.2) = 0.97$$

Results

The tree-ring time series for region 2 shows considerable large-amplitude swings from the mean, especially in the last 100 years: prominent troughs in growth are located at about 1870 and 1940, and peaks in the early 1900s and near 1960 (Figure 2). The corresponding spectrum is predominantly low frequency, with a maximum near a wavelength of 64 years (Figure 3). Frequencies near the single and double sunspot cycles have spectral peaks, but the 95% confidence band around these still includes the null continuum.

Spectra of growth for the other four regions are similarly dominated by variance at low frequencies (Figure 4). In regions 1, 4, and 5 the highest peak is also the lowest-frequency peak. This peak is at the same wavelength (64 years) for the Oregon and central California series, but shortens to 51.2 years for Wyoming and lengthens to 102 years for Colorado.

Figure 2
INDEX OF REGIONAL TREE GROWTH VARIATIONS FOR REGION 2
STANDARDIZED TO ZERO MEAN AND UNIT STANDARD DEVIATION

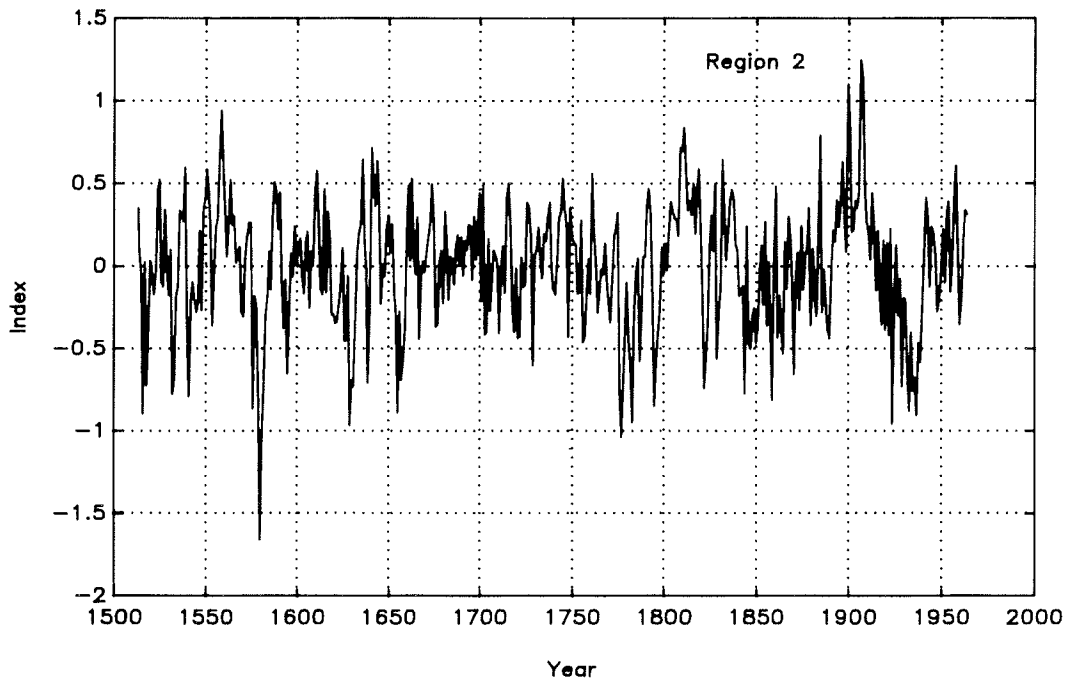


Figure 3
ESTIMATED SPECTRUM OF TREE-RING INDEX FOR REGION 2

Also shown are 95% confidence bands around the spectral estimates, a smooth underlying null continuum, and the raw periodogram ordinates (+). The window used to smooth the raw periodogram to estimate the spectrum is inset.

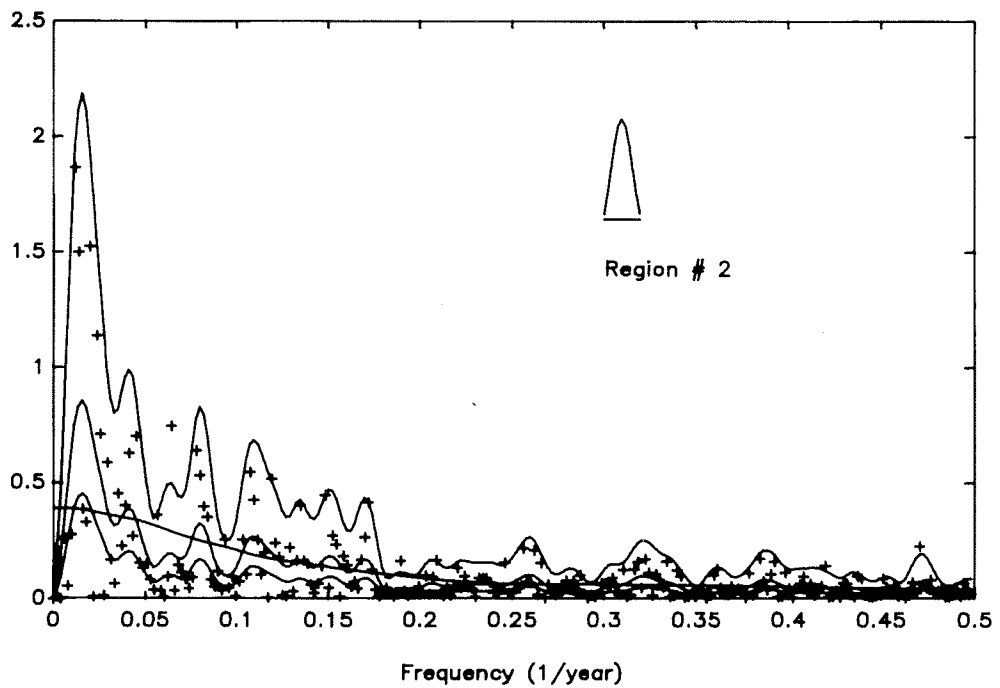
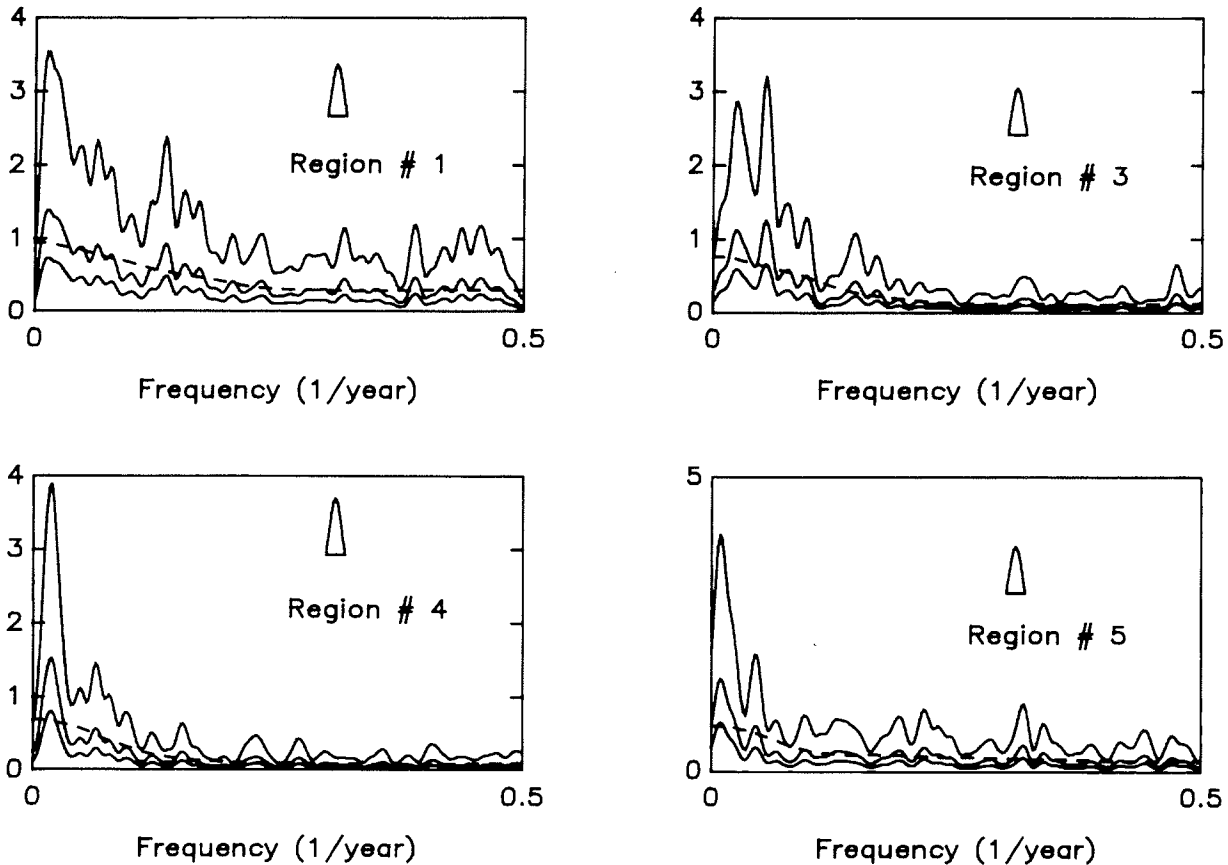


Figure 4
ESTIMATED SPECTRA, 95% CONFIDENCE BANDS, AND NULL CONTINUUM FOR
REGIONAL GROWTH SERIES, REGIONS 1,3,4,5

The periodogram smoothing window is inset on each figure. Series for region 5 is plotted with slightly compressed y-scale relative to other series.



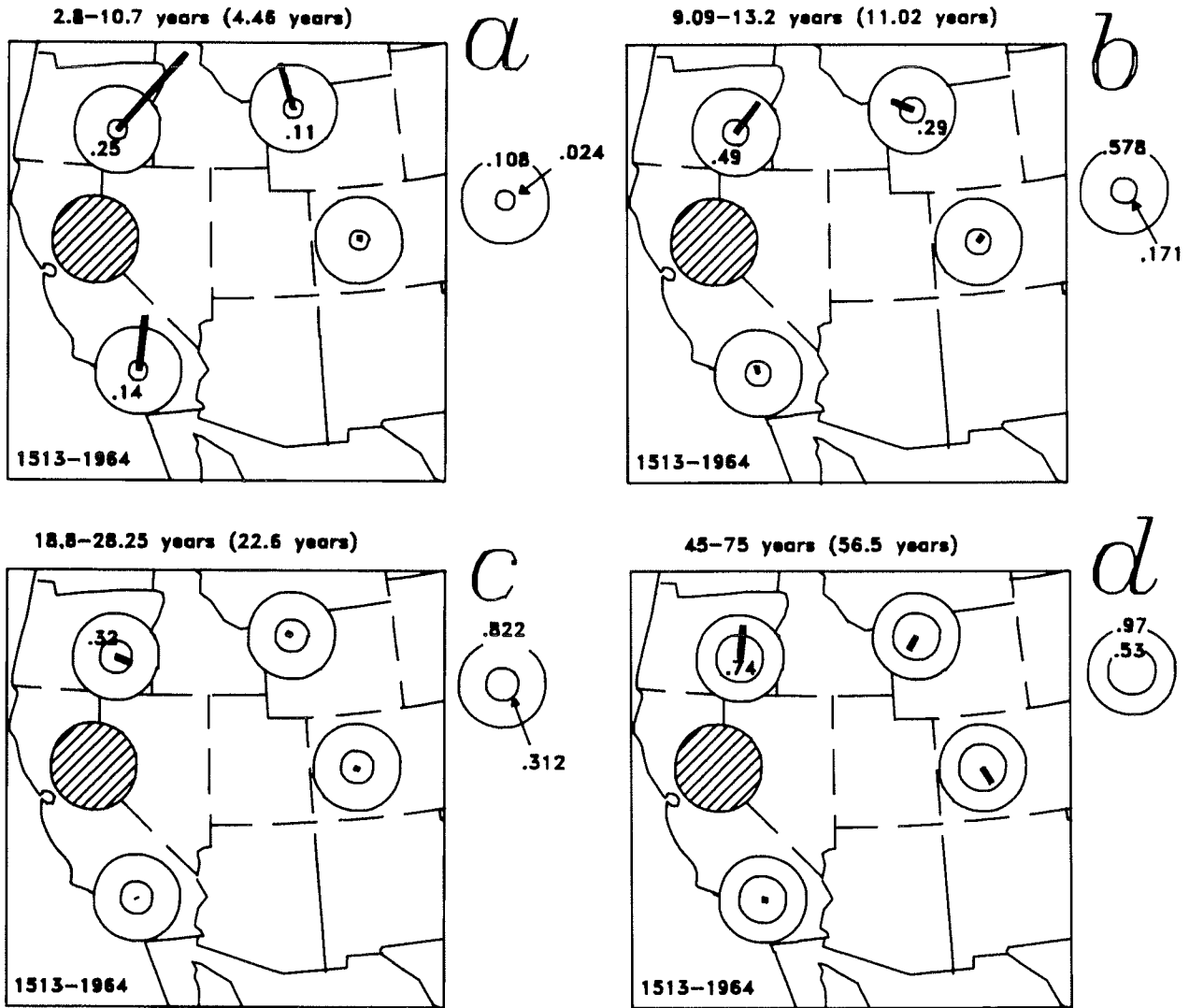
The southern California (region 3) spectrum differs markedly from the others in that the main variance component is shifted from very low to intermediate frequencies. Here the two dominant peaks are at 18.3 years and 39.4 years.

The method used to display the cross-spectral results was to plot estimated squared-coherence as bars on a series of maps (Figure 5). A separate map is shown for each key frequency-range. Length of a bar is proportional to the squared-coherence of a region's growth series with the series from central California. Angle of the bar from the vertical is proportional to the phase: straight up indicates growth variations are perfectly in phase; straight down indicates opposite (180 degrees out of) phase. Significance of the squared-coherence is found by comparing the length of the bar to radii of circles drawn at the 95% and 99.9999% confidence limits. For example, for the ENSO band (Figure 5a), the squared-coherence of region 1 with region 2 is highly significant and essentially in phase: the sample squared-coherence of 0.25 is expected less than 1 in a million times by chance (0.0001% confidence limit of 0.108).

The ENSO band represents 39% of the variance of the central California series. Growth variations in this band are strongly coherent and in phase with the Oregon, Wyoming, and southern California series (Figure 5a). Correlation drops below 95% significance with Colorado and Arizona.

Figure 5
 MAPS SUMMARIZING RESULTS OF CROSS-SPECTRAL ANALYSIS OF
 EACH REGIONAL GROWTH SERIES WITH THE SERIES FOR REGION 2

Shown are the estimated squared-coherence (bars), its 95% and 99.9999% confidence limits (circles), and the phase (angle from the vertical). A key to the magnitude of the specified confidence limits is shown in the circles to the right of each map. Squared-coherence values are listed on the maps when they exceed the 95% confidence limit.



The single-sunspot band represents 13% of the variance for central California. Significance of squared-coherence estimates is lower than for the ENSO band, though still exceeding 95% for Oregon and Wyoming (Figure 5b). The most striking difference from the plot for the ENSO band is that correlation drops below significance with southern California.

The double-sunspot band represents 9% of the variance for central California. This is the least spatially coherent of the four patterns (Figure 5c). The squared-coherence is barely significant at the 95% level with the Oregon series, and not significant with any other region. Even for the Oregon relationship, the series appear to be about one-quarter cycle, or 5 years, out of phase.

The 45-75 year band represents 12% of the variance for central California, about the same amount as the single-sunspot band. A strong in-phase relationship is shown with Oregon at this band (Figure 5d). In contrast to the ENSO frequency band, the correlation with southern California is essentially zero. The pattern of bars suggests the possibility of an opposite-phase relationship with the Wyoming and Colorado series at this band. One possible explanation, though highly speculative given the low significance levels of squared-coherence, is that long waves at this time-scale are preferably anchored such that the northeastern and northwestern regions were affected by opposing moisture regimes. Previous studies have shown a similarly large, spatially coherent, spectral feature at near 60 years in tree-ring data from the western fringe of the northern U.S. Great Plains (Meko 1982, Stockton and Meko 1983).

Conclusions

The results suggest a frequency dependence not only in the strength but also in the sign of correlation between moisture variations in the Sierra Nevada mountains of central California and in other regions. While variations in the ENSO frequency band (2.8-10.7 years) are strongly coherent and in-phase both to the north and south, variations at low frequencies (45-75 years) show in-phase coherence only to the north. Moreover, there is a hint of an opposite-phase relationship with moisture variations at low frequencies in the Colorado Rockies. No evidence was found of unusually distinct patterns of spatial correlation at either the single- or double-sunspot cycles. To some extent, this is negative evidence for a solar-climate signal, at least for the central California Sierras. A different picture could, of course, come from similar analyses keyed on other regions — for example, regions to the east not under such a strong winter-dominant precipitation regime as region 2.

Acknowledgment

This work was supported by the National Science Foundation, grant ATM-88-14675.

References

- Bloomfield, P. 1976. *Fourier Analysis of Time Series: An Introduction*. John Wiley & Sons.
- Meko, D.M. 1982. "Drought History in the Western Great Plains from Tree Rings". *Proceedings of the International Symposium on Hydrometeorology*. American Water Resources Association.
- Stockton, C.W., W.R. Boggess, and D.W. Meko. 1985. "Climate and Tree Rings". in *Paleoclimate Analysis and Modeling*. Ed. A.D. Hecht. John Wiley & Sons.
- Stockton, C.W., and D.M. Meko. 1983. "Drought Recurrence in the Great Plains as Reconstructed from Long-Term Tree-Ring Records". *J. of Climate and Applied Climatology* 22(1):17-29.

Geochemical Evidence for Enhanced Upwelling and Organic Productivity During the Late Quaternary on the Continental Margin of Northern California

Walter E. Dean, James V. Gardner, and Roger Y. Anderson

ABSTRACT: The present upper water mass of the northeastern Pacific Ocean off California has a well developed oxygen-minimum zone between 600 and 1000 meters wherein concentrations of dissolved oxygen are less than 0.5 ml/L. Even at such low concentrations, benthic burrowing organisms are abundant enough to destroy millimeter-scale laminations by thoroughly bioturbating the surface and near-surface sediments. These organisms also consume large quantities of organic carbon produced by large seasonal stocks of plankton in the overlying surface water that are supported by high concentrations of nutrients in the California Current upwelling system. The result is that concentrations of biogenic silica in surface sediments are highest in the oxygen-minimum zone, reflecting the high diatom production in the overlying water, but concentrations of residual organic carbon are lower in sediments in the oxygen-minimum zone than in sediments above and below it.

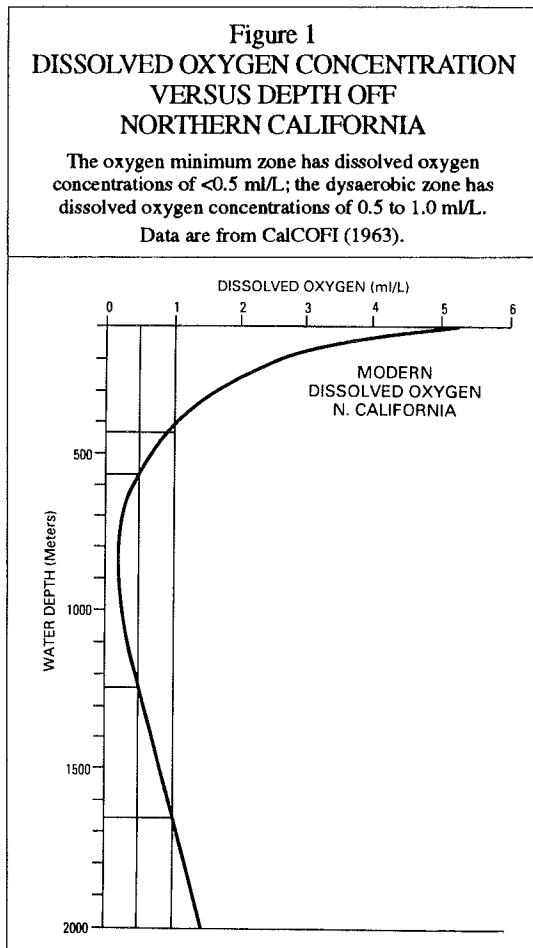
Laminated sediments are preserved in upper Pleistocene sections of cores collected on the continental slope at water depths within the present oxygen-minimum zone from at least as far north as the Klamath River and as far south as Point Sur. Comparison of sediment components in the laminae with those delivered to sediment traps as pelagic marine "snow" show the dark/light lamination couplets are indeed annual (varves). These upper Pleistocene varved sediments contain more abundant lipid-rich "sapropelic" (Type II) organic matter than the bioturbated and oxidized Holocene sediments. The stable carbon-isotopic composition of the organic matter does not change with time, indicating the greater abundance of Type II organic matter in the varved sediments is not due to a change in source but, rather, represents a greater degree of preservation of organic matter. The organic-carbon-rich varved sediments also contain higher concentrations of sulfide-sulfur, indicating a higher rate of sulfate reduction due to the presence of more "reactive" organic matter. Concentrations of several redox-sensitive trace elements, especially Cr, Cu, Ni, V, and Zn, also are enriched in the varved sediments. The presence of carbon-, sulfur-, and metal-rich sediments, as well as lack of bioturbation, all support the theory that the oxygen-minimum zone in the northeastern Pacific Ocean was more intense — in fact, anoxic — during the late Pleistocene in response to greater coastal upwelling and higher organic productivity.

Introduction

Marine environments that are effectively anoxic (*i.e.*, contain <0.1 ml/L dissolved oxygen) and that have preserved laminations occur in silled basins with bathymetric barriers and restricted circulation. Examples are:

- Guaymas basin in the Gulf of California (Calvert 1964 and 1966, Schrader *et al.* 1980, Schrader and Baumgartner 1983).
- Santa Barbara basin on the Southern California borderland (Hulsemann and Emery 1961, Soutar and Crill 1977, Pisias 1978, Thornton 1984).
- Bahia de Soledad along the Pacific coast of Baja California (Soutar *et al.* 1981).
- Saanich Inlet (Gross *et al.* 1963, Gucluer and Gross 1964).

More rarely, open continental slopes in areas of strong coastal upwelling, such as off Peru (deVries and Schrader 1981, Reimers and Suess 1983), Namibia, southwest Africa (Calvert and Price 1983), and California (Mullins *et al.* 1985, Thompson *et al.* 1985, Gardner and Hemphill-Haley 1986, Anderson *et al.* 1987 and 1989), have a strongly developed oxygen-minimum zone (OMZ, <0.5 ml/L dissolved oxygen) and preserve laminated sediments during times when the minimum was essentially zero (<0.1 ml/L dissolved oxygen).



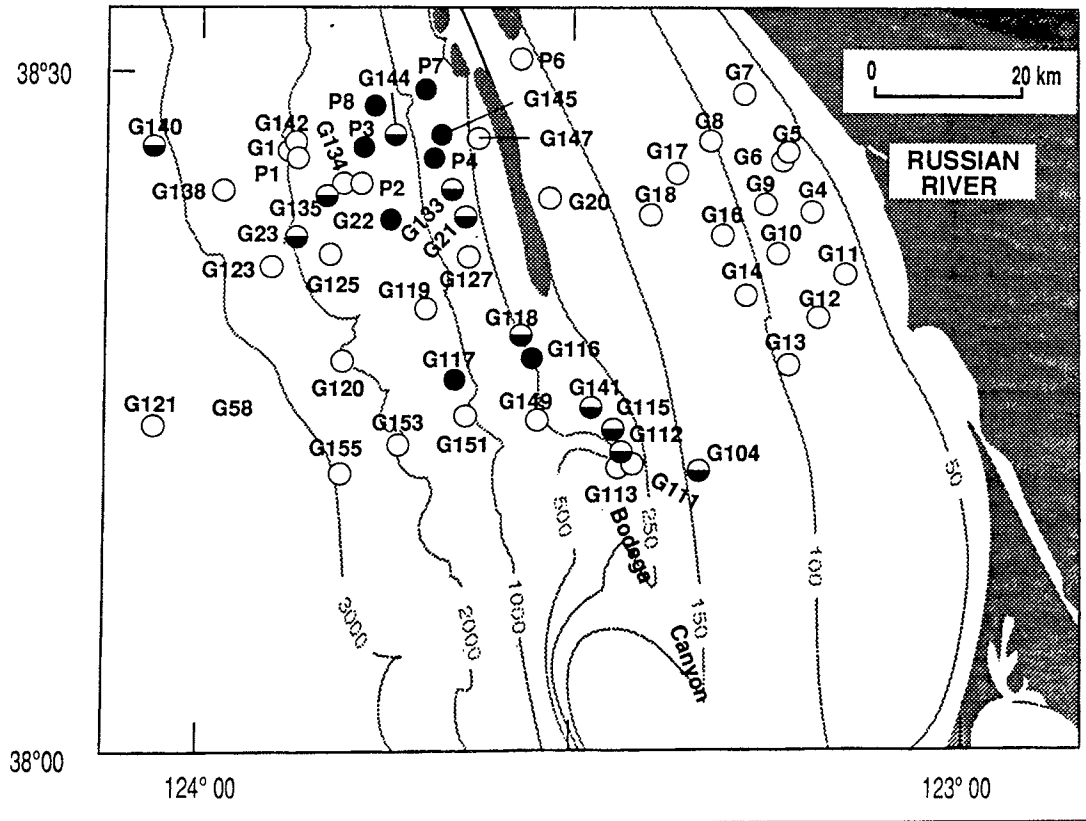
The continental margin off Northern California is characterized by high organic productivity in response to nutrients supplied by strong seasonal coastal upwelling, which, in turn, is driven by the southward-flowing California Current (Huyer 1983). Because of this high productivity, the present surface water mass off Northern California has an OMZ between 600 and 1200 meters, with concentrations as low as 0.2 ml/L at 800 meters (CalCOFI 1963) (Figure 1). The dysaerobic zone (0.5-1.0 ml/L dissolved oxygen) extends from about 400 to 1600 meters. These low concentrations of dissolved oxygen, even in the core of the OMZ, are sufficient to support a burrowing benthic fauna.

During 1980 and 1981 the U.S. Geological Survey conducted several cruises off the coast of Northern California to characterize sediments on the continental shelf, slope, and basin above, within, and below the OMZ. Gravity, piston, and box cores were collected as part of this investigation (Figure 2). Sediments recovered in most cores were bioturbated, greenish-gray diatom-bearing clays or silty clays, but cores collected on the upper slope between 500 and 1500 meters contained laminated sediment below a 5- to 80-cm-thick surface layer of bioturbated sediment (Gardner and Hemphill-Haley 1986, Anderson *et al.* 1987 and 1989). Sediments below the laminated/bioturbated contact are not continuously laminated but, rather, consist of interbeds of laminated and bioturbated sediment that alternate on a scale of centimeters to decimeters. The youngest dated laminations occur in core G117 (Gardner and Hamphill-Haley 1986). Since 1986, more work and dating have been done on this core, and it now appears the contact between the laminated and bioturbated sections of the core is an erosional unconformity that truncates the laminated sequence.

Three radiocarbon dates have been obtained from Core G117: one conventional ¹⁴C date from above the unconformity and one conventional and one accelerator mass spectrometer (AMS) ¹⁴C date from below the unconformity. The two conventional ¹⁴C dates are from 8-cm-long samples of bulk sediment, and the AMS ¹⁴C date is from a small sample of bulk sediment. Assuming a zero age for the top of the core, the calculated sedimentation rate for the bioturbated sediment above the unconformity is 0.8 cm/ky. The two ¹⁴C dates below the unconformity give a sedimentation rate of 0.7 cm/ky. Interpolating to the unconformity from both sides suggests the unconformity separates sediment that is about 19 ky old from sediment about 14.5 ky old.

Figure 2
LOCATIONS OF GRAVITY (G) AND PISTON (P) CORES ON THE CONTINENTAL MARGIN
OFF THE
RUSSIAN RIVER, NORTHERN CALIFORNIA, USED IN THIS STUDY

Cores indicated by a solid circle contain some distinctly laminated sediments; cores indicated by a half-solid circle contain mostly bioturbated sediments but with some zones containing faint, indistinct, or discontinuous laminations; cores indicated by an open circle contain only bioturbated sediments. Bathymetric contours are in meters.



This exercise also suggests conditions that allowed preservation of varves at this site were active at 19 ka. In addition, the OMZ index for core G117, based on the style and type of trace bioturbation (Anderson *et al.* 1989), suggests conditions at 19 ka were strongly anoxic and not just dysaerobic. Consequently, sometime between about 19 and 14.5 ka, bottom conditions changed from fully anoxic to sufficiently aerobic to permit a burrowing benthic fauna.

Dark/light laminae couplets, where best developed, are about 1-mm thick and represent annual accumulations of sediment (varves) (for descriptions, see Gardner and Hemphill-Haley 1986, Anderson *et al.* 1987, 1989). Diatom assemblages in the laminae couplets can be matched to seasonal diatom data from a sediment trap of the type described by Anderson (1977) that was deployed 260 meters above the sea floor at a water depth of 2196 meters from September 16, 1980, to October 12, 1981. The summer upwelling diatom assemblage, dominated by *Skeletonema costatum*, is similar to that in the light laminae, and the winter, non-upwelling assemblage, dominated by *Thalassiosira pacifica*, is similar to that in the dark laminae (Gardner and Hemphill-Haley 1986).

Since the initial investigations in 1980 and 1981, more than two dozen cores have been identified that contain millimeter-scale laminations from as far south as Point Sur and as

far north as the Klamath River area, a distance of more than 400 km (Anderson *et al.* 1987, 1989). Of the cores with locations shown in Figure 2, eight contain some distinctly laminated sediments and twelve contain mostly bioturbated sediments but with some zones of faint, indistinct, or discontinuous laminations. The varve laminae are best developed in two gravity cores that are the focus of this report: core G117, from a water depth of 695 meters, and core G145, from a depth of 698 meters. For reference, we also present data from a piston core from below the OMZ but within the dysaerobic zone (core P3, depth 1600 m) and two deep-water cores from well below the OMZ (core G121, depth 3580 m, and core G138, depth 2530 m).

Presence of laminated sediments in the subsurface in upper-slope cores suggests that during the late Pleistocene, the OMZ was more intense, with concentrations of dissolved oxygen low enough to eliminate burrowing organisms (Gardner and Hemphill-Haley 1986). A similar conclusion was reached by deVries and Schrader (1981) for termination of the laminated facies on the Peru margin. The purpose of this report is to present results of organic and inorganic geochemical investigations of laminated and bioturbated sediments in these cores, particularly as they relate to the origin, nature, and degree of preservation of the contained organic matter.

Methods

The type of organic matter in sediment samples from the two cores that contain laminated sediments taken within the OMZ (G117 and G145) and from the two deep-water reference cores that contain bioturbated sediments taken from well below the OMZ (G138 and G121) was determined by Rock-Eval pyrolysis. The Rock-Eval method provides a rapid determination of the hydrogen and oxygen richness and degree of preservation of sedimentary organic matter (for details, see Espitalie *et al.* 1977, Tissot and Welte 1984, and Peters 1986). Concentrations of free and adsorbed hydrocarbons and CO₂ released by programmed heating of the sample in a stream of helium are measured as areas under peaks on a pyrogram. These peak areas, when calibrated and normalized to percent organic carbon (C_{Org}), yield a hydrogen index (HI) and oxygen index (OI), expressed as milligrams of hydrocarbons (HC) and CO₂, respectively, per gram of C_{Org}. The Rock-Eval II instrument used for analyses also determines the percent C_{Org}. Values of HI and OI correlate well with atomic H:C_{Org} and O:C_{Org} ratios determined in the same samples by other methods (*e.g.*, Tissot and Welte 1984).

Stable isotope ratios in organic carbon were determined by standard techniques described by Pratt and Threlkeld (1984) and Dean *et al.* (1986). Results are reported in the standard per mil δ -notation relative to the University of Chicago Pee Dee belemnite (PDB) marine-carbonate standard:

$$\delta \text{ parts per mil} = ((R_{\text{sample}}/R_{\text{PDB}}) - 1) \times 10^3$$

where R is the ratio ¹³C/¹²C.

Sediment samples for inorganic geochemical analyses were air dried and ground in a ceramic mill to pass a 100-mesh sieve. Concentrations of 10 major and minor elements (Si, Al, Fe, Mg, Ca, Na, K, Ti, P, and Mn) were measured by wavelength-dispersive X-ray fluorescence spectrometry (Baedeker 1987). Concentrations of 14 trace elements (Ba,

Co, Cr, Cu, La, Ga, Li, Ni, Pb, Sc, Sr, V, Y, and Zn) were determined by inductively coupled, argon-plasma, emission spectrometry (Baedecker 1987). Total carbon and total sulfur were determined by the LECO induction-furnace gasometric method. Carbonate carbon was determined by coulometry (Engleman *et al.* 1985). Values of C_{org} determined by difference between total carbon and carbonate carbon agree well with values of C_{org} determined with the Rock-Eval II instrument, but the Rock-Eval results will be used in our discussions.

Results and Interpretations

Rock-Eval Pyrolysis and Organic Carbon

Samples from the laminated zones in cores G117 and G145 contain more organic matter (higher concentrations of C_{org}) that is distinctly enriched in hydrogen (higher values of HI) relative to the bioturbated sediments (Figures 3 and 4). The organic matter preserved in the deep-water reference cores (G121 and G138) has characteristics in terms of amount (% C_{org}) and richness (HI) that are very similar to the organic matter in core G145. Variations in hydrogen richness of organic matter may be due to variations in degree of preservation of the organic matter or due to mixing of H-rich marine organic matter with H-poor terrestrial organic matter (Tissot and Welte, 1984). The distinct trend of increasing H-richness in surface sediments from the mouth of the Russian River to the basin (Figure 5) suggests variations in HI may be due to mixing of organic matter types from marine and terrestrial sources. Isotopic composition of the organic carbon can help to distinguish between mixing and preservation.

Stable-Carbon Isotope Composition of Organic Matter

The isotopic composition of modern marine phytoplankton and terrestrial plants and the organic matter derived from them often provide distinct signatures that can be used to determine source of organic matter in sediments. Ten samples of plankton from the North Pacific between 20° and 40° N, analyzed by Rau *et al.* (1982), had values of $\delta^{13}C$ ranging from about -19.8 to -23.4 parts per mil, and eight of the ten samples had values between -19.8 and -22 parts per mil (Figure 6). Values of -20 to -22 parts per mil are typical of marine plankton from intermediate latitudes (Deines 1980).

Values of $\delta^{13}C$ of particulate organic matter (POM) derived from marine plankton tend to be lower than those of plankton by several per mil. For example, samples of North Pacific POM reported by Rau and others (1987) have $\delta^{13}C$ values that range from about -20 to -24 parts per mil, and samples from sediment traps in the VERTEX 5 experiment 1500 km west of Monterey, California, have values ranging from about -22.5 to -24 parts per mil (Rau *et al.* 1986). The isotopic composition of terrestrial vegetation can vary widely, but values of $\delta^{13}C$ for higher terrestrial vegetation (C3 plants) generally range from -22 to -32 parts per mil, and most are in the range of -24 to -28 parts per mil. In other words, marine organic matter tends to have $\delta^{13}C$ values in the low negative 20s terrestrial organic matter tends to be in the high negative 20s. With these values in mind, let us examine the isotopic composition of organic matter in the Northern California margin cores.

Values of $\delta^{13}\text{C}$ in cores G117 and G145 are mostly in the range of -22.5 to -23.5 parts per mil (Figures 3 and 4), almost exactly in the range of POM off Monterey (Figure 6). The fact that most $\delta^{13}\text{C}$ values in cores G117 and G145 are slightly lighter (more negative) than typical North Pacific plankton and POM may be due to a minor contribution of isotopically lighter terrestrial organic matter. By this argument, the distinctly lighter values of $\delta^{13}\text{C}$ in core G138 suggest that this locality on the basin floor receives an even larger contribution of terrestrial organic matter, probably transported down Bodega Canyon (Figure 2). In contrast, the heavier values of $\delta^{13}\text{C}$ in core P3 (water depth 1600 m), upslope from G138

Figure 3
 PROFILES OF PERCENT TOTAL ORGANIC CARBON, VALUES OF $\delta^{13}\text{C}$ ORGANIC CARBON, PERCENT TOTAL SULFUR, ROCK-EVAL H-INDEX, PARTS PER MILLION Ni, AND PERCENT TOTAL Si VERSUS DEPTH IN CORE G117
 Laminated intervals are indicated next to the depth scale at the left of the profiles.

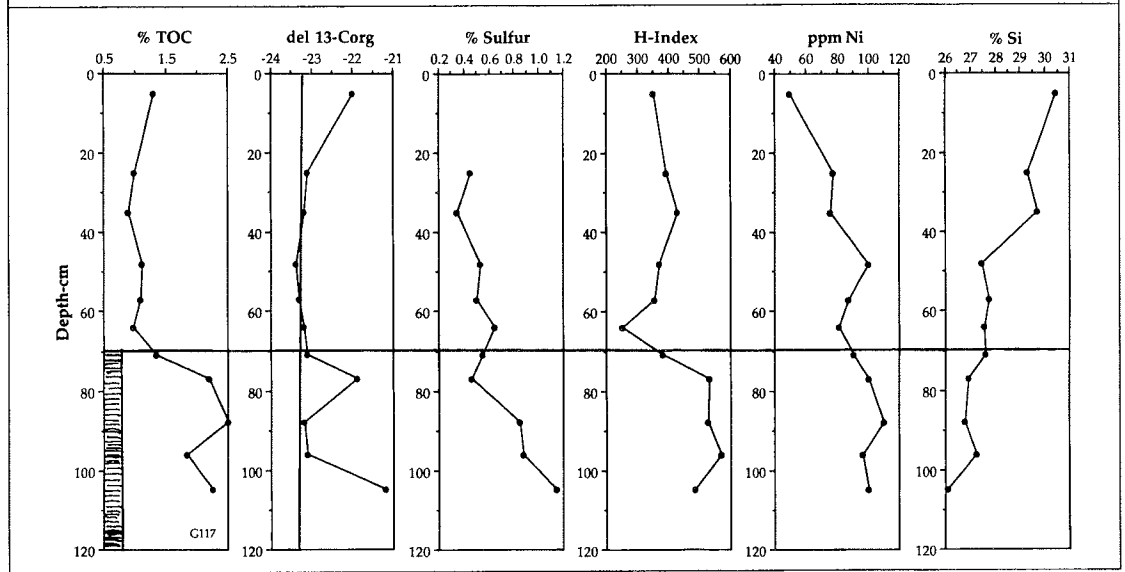


Figure 4
 PROFILES OF PERCENT TOTAL ORGANIC CARBON, VALUES OF $\delta^{13}\text{C}$ ORGANIC CARBON, PERCENT TOTAL SULFUR, ROCK-EVAL H-INDEX, PARTS PER MILLION Ni, AND PERCENT TOTAL Si VERSUS DEPTH IN CORE G145
 Laminated intervals are indicated next to the depth scale at the left of the profiles.

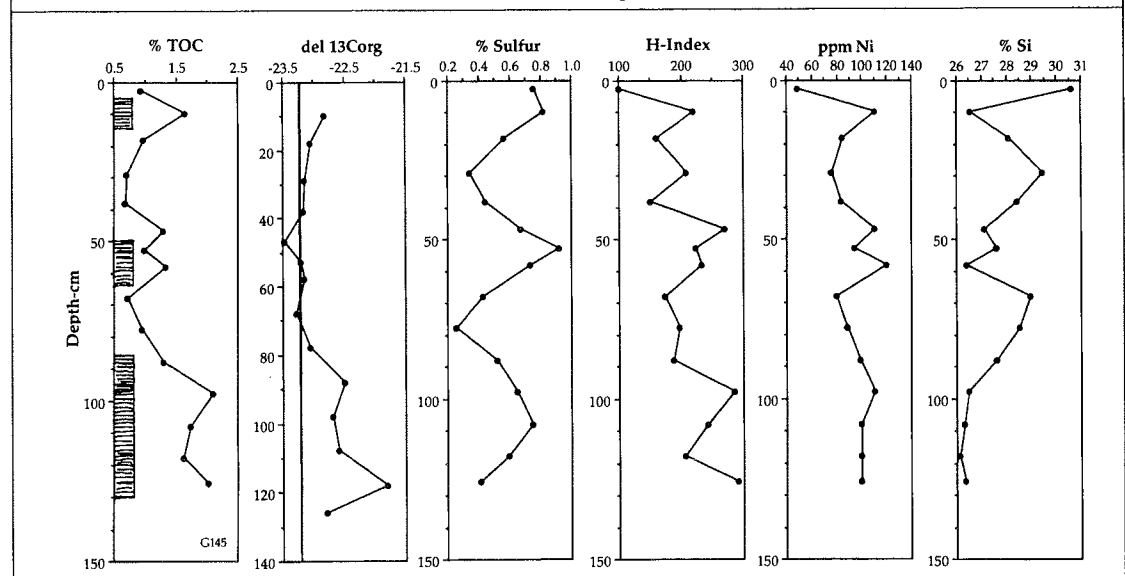


Figure 5
WATER DEPTH VERSUS
ROCK-EVAL H-INDEX IN
SURFACE SEDIMENTS (Top 5cm) ON THE
CONTINENTAL MARGIN OFF THE
RUSSIAN RIVER, NORTHERN CALIFORNIA

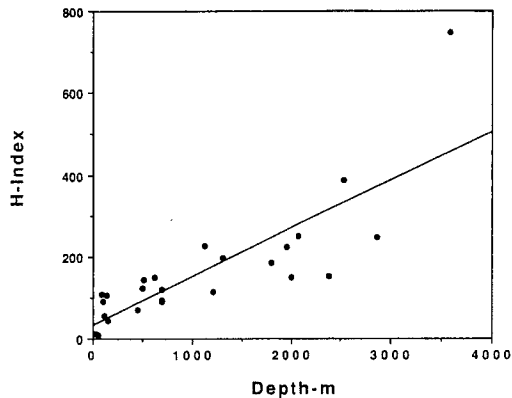
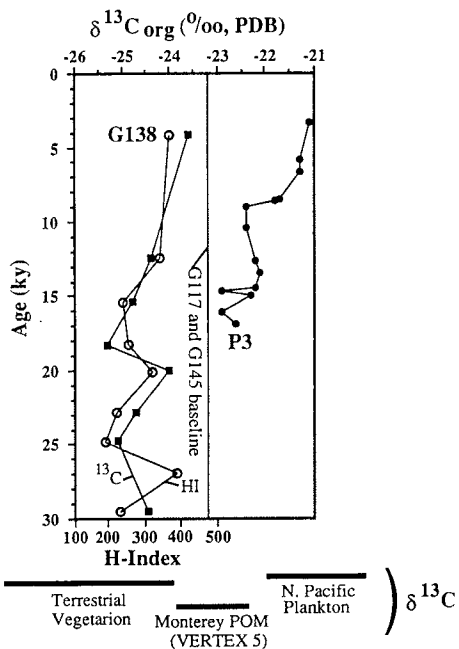


Figure 6
PROFILES OF $\delta^{13}\text{C}_{\text{org}}$ VERSUS AGE FOR
SAMPLES FROM CORES G138 AND P3 AND
H-INDEX VERSUS AGE FOR
SAMPLES FROM CORE G138
(open circles)



Data for core G138 are from Table 1.

Data for core P3 are unpublished data provided by Greg Rau.

Baseline for $\delta^{13}\text{C}_{\text{org}}$ in cores G117 and G145 are from Figures 3 and 4 respectively.

Ranges of $\delta^{13}\text{C}_{\text{org}}$ values for North Pacific plankton are from Rau et al. (1987).

Ranges of $\delta^{13}\text{C}_{\text{org}}$ values for VERTEX 5 particulate organic matter (POM) are from Rau et al. (1986).

Ranges of $\delta^{13}\text{C}_{\text{org}}$ values for terrestrial organic matter are summarized from Deines (1980).

and downslope from G145, suggest this locality receives less terrestrial organic matter. The increase in $\delta^{13}\text{C}$ since the last glacial maximum in G138 and P3 suggests the influx of terrestrial organic matter to the basin floor was even greater during eustatic sea level low stands when the shoreline was about 40 km farther west.

With regard to interpreting HI and OI values in terms of source versus preservation, it is significant that, except for the laminated intervals at the bases of cores G117 and G145, there is not a good correlation between values of $\delta^{13}\text{C}$ and HI in these two cores. If decreasing HI values were due to mixing of marine with terrestrial organic matter, we would expect to find a concomitant decrease in $\delta^{13}\text{C}$ values, which is exactly what we find for core G138 where the organic matter has become more marine in character (higher HI, less negative $\delta^{13}\text{C}$) over the last 30 ky. There is no such correlation for cores G117 and G145, and there is an average $\delta^{13}\text{C}$ of about -23 parts per mil across the complete range of HI values. Therefore, we interpret $\delta^{13}\text{C}$ results in cores G117 and G145 as representing a fairly constant baseline of dominantly marine organic matter with average $\delta^{13}\text{C}$ values of about -23.2 parts per mil and with occasional intervals or "pulses" of higher marine productivity represented by $\delta^{13}\text{C}$ values of -21 to -22.5 parts per mil.

Iron-Sulfur-Carbon Systematics

The laminated sediments also tend to have higher concentrations of sulfur than the bioturbated sediments (Figures 3 and 4). This reflects a higher rate of sulfate reduction due to the presence of more "reactive", H-rich organic matter in the laminated sediments (*e.g.*, Berner and Westrich 1985). All samples have an average S:C ratio close to 0.4, which is the average ratio for Holocene "normal marine" sediments (those deposited under an oxic water column but that contain sufficient organic matter to cause pore waters to go anoxic after deposition) (Raiswell and Berner 1986). Such a relationship indicates the sediments were not iron-limited but availability of reactive carbon ultimately limited pyrite formation in these sediments (Dean and Arthur 1989).

Trace-Element Geochemistry

Results of major-, minor-, and trace-element analyses show that several trace transition elements, especially Cr, Cu, Ni, V, and Zn, are enriched in the C_{org} -rich laminated sediments. This relationship is shown by plots of ppm Ni versus depth

in Figures 3 and 4. The greatest contrast is the difference between the concentration of Ni in the surface sediment and in the laminated intervals.

There is a tendency in the literature to attribute a causal relationship to the commonly observed correlation between metal concentration and C_{org} concentration, usually through some process of biological uptake, sorption, or "scavenging", although the fundamental physical, chemical, and biological processes involved in this scavenging are poorly understood (Honeyman *et al.* 1988). However, recent work has shown that trace-metal uptake is mainly controlled by particle concentration and surface chemistry, not by biological uptake (*e.g.*, Balistrieri *et al.* 1981, Collier and Edmond 1984, Wong and Wood 1984, Nyffeler *et al.* 1986; Honeyman *et al.* 1988).

A compilation of particle-concentration and Thorium adsorption-rate data by Honeyman *et al.* (1988) shows a linear correlation between the two variables over seven orders of magnitude of particle concentration and over a wide range of organic productivity. In other words, particles are particles, be they inorganic or organic. Data used by Honeyman *et al.* were for thorium, but the principle applies to many other metals. In highly productive areas (such as the continental margin off Northern California) many particles are of biological origin, but in terms of adsorption characteristics, they are still just particles.

This generality is modified somewhat by the types of particles and their surface chemistry, as demonstrated by Balistrieri *et al.* (1981) and Balistrieri and Murray (1982), who showed that iron and manganese oxides and, in particular, organic compounds with large, active surface areas can adsorb high concentrations of metals. In the data sets used by Honeyman *et al.* (1988), particles of silt and clay from the Amazon have a lower adsorption rate for a given particle concentration because these particles have a lower unit surface area. On the other hand, particles from the California Current (Coale and Bruland 1987) contain abundant organic compounds with large, active surface areas, and these particles have a slightly higher adsorption rate for a given particle concentration. The excellent correlation between organic productivity and Th-removal rate in the California Current system led Coale and Bruland to conclude that metal removal was by active biological uptake. However, the compilation by Honeyman *et al.* strongly suggests that flux rate of particles (marine snow) is the master variable governing metal adsorption rates.

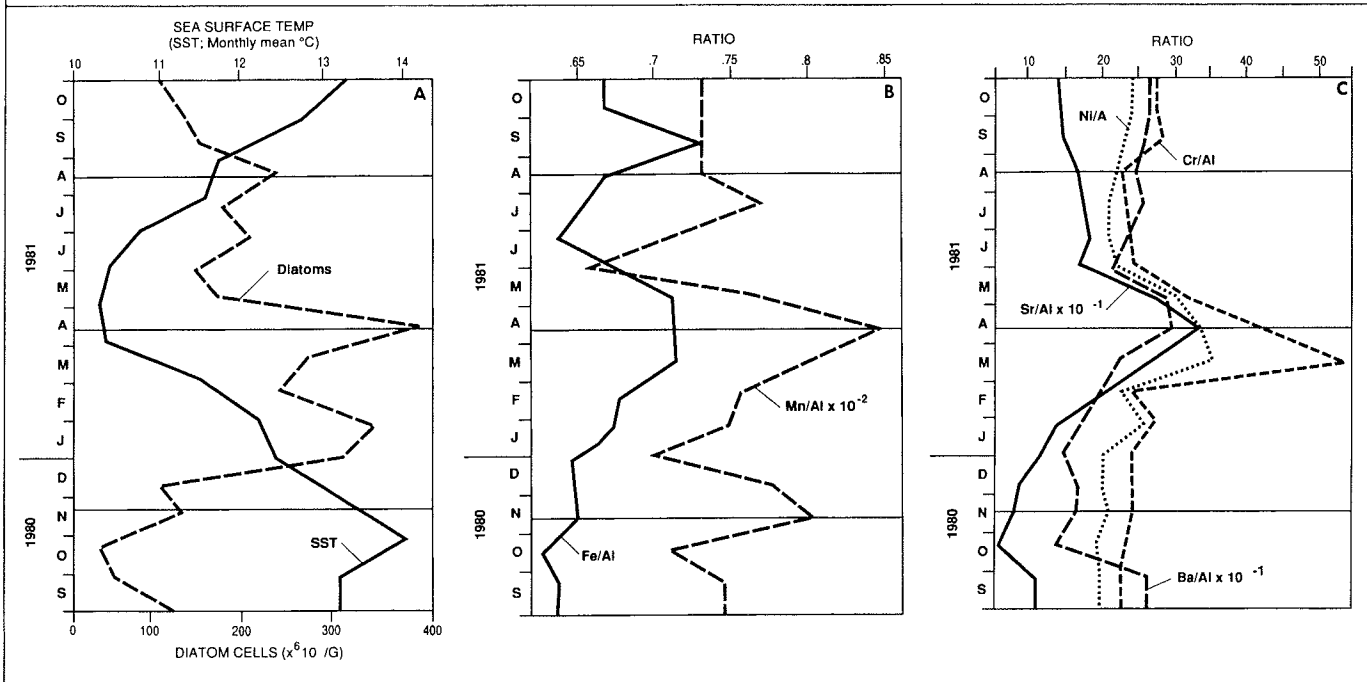
This relationship is demonstrated by our sediment-trap data, which show that highest flux rates of particles occur during spring diatom blooms (Figure 7), and this period also corresponds to highest concentrations of metals, expressed in Figure 7 as metal:Al ratios.

Biogenic Silica and Organic Carbon Production

Figures 3 and 4 show that the down-core variation in concentration of total Si in cores G117 and G145 is exactly opposite to that of C_{org} ; that is, values of total Si are lowest and concentrations of C_{org} are highest in the laminated sediments. If laminated sediments with higher concentrations of C_{org} record periods of increased upwelling and organic productivity, and if that increased productivity is due mainly to diatoms, then we would expect total Si to be highest in the laminated sediments. The modern distribution of total Si in surface sediments (top 5 cm) in the study area (Figure 8A) shows total Si concentrations are highest in sediments within the OMZ, which is what we expected because of increased diatom production in surface waters of this area. All of this reasoning assumes, of course,

Figure 7
PLOTS OF DIATOM CONCENTRATION (A) AND METAL-TO-ALUMINUM RATIOS (B AND C) VERSUS TIME
FROM SEPTEMBER 1980 TO OCTOBER 1981 FOR SAMPLES FROM A SEDIMENT TRAP ON THE CONTINENTAL
SLOPE OFF NORTHERN CALIFORNIA

Sea surface temperature also is shown on plot A.



that the higher values of total Si are due to biogenic Si above some background level of detrital, nonbiogenic Si.

To obtain an estimate of the background level of detrital Si, we assumed the lowest Si:Al ratio in each core represents the background detrital Si:Al. These background Si:Al values are 3.6 for G117 and 3.4 for G145. The average Si:Al ratio for the deep-water reference cores are 3.6 for G121 and 3.4 for G138. These ratios can then be used to compute the detrital Si fraction. We call the difference between total Si and detrital Si “excess Si”, and we assume most of this excess Si is biogenic. Results of these calculations for G117 and G145 are shown in Figure 9. The shaded area between the plots of total and detrital Si represents biogenic Si with lowest concentrations in the laminated sediments. If we apply the excess calculation to total Si in surface sediments (Figure 8A), using a “detrital” Si:Al ratio of 3.5, the resulting pattern of excess Si (Figure 8B) shows a much more restricted distribution than does total Si. Highest concentrations of excess Si (assumed to be biogenic Si) occur between 150 and 500 meters (Figure 8B) and rapidly decrease with increasing water depth (Figure 10).

We are still left with questions of why the concentration of biogenic silica decreases so rapidly with depth within a core and why it is lowest in the laminated sediments. Our answer to both questions is excess alkalinity, although we do not have pore water data to prove it. The diatoms dissolve in anoxic, alkaline pore waters, and the most alkaline pore waters would be in the laminated sediments where anaerobic decomposition of organic matter by sulfate reduction would have produced the greatest concentrations of H₂S and HCO₃⁻, thereby increasing the alkalinity. Anaerobic decomposition in the laminated sediments may have proceeded to methanogenesis, which would further increase alkalinity. This same phenomenon occurs in Black Sea sediment, where a large flux of biogenic

Figure 8
ISOPLETHS OF PERCENT TOTAL Si AND BIOGENIC Si IN SURFACE SEDIMENTS ON THE CONTINENTAL MARGIN OFF THE RUSSIAN RIVER, NORTHERN CALIFORNIA

Triangles are locations of box cores (B); closed circles are locations of gravity cores (G); open circles are locations of piston cores (P).

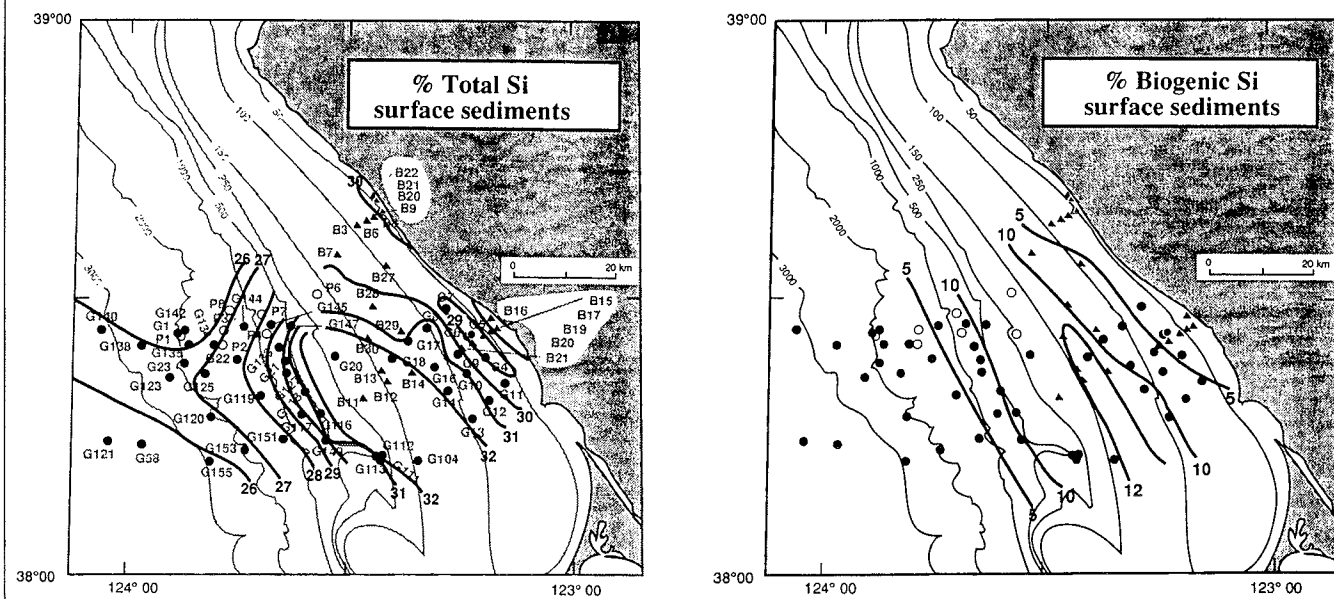


Figure 9
PERCENT TOTAL Si AND PERCENT DETRITAL Si VERSUS DEPTH FOR SAMPLES FROM CORES G117(A) AND G145 (B)

The difference between total and detrital Si (shaded areas) is excess Si and is mainly biogenic Si.

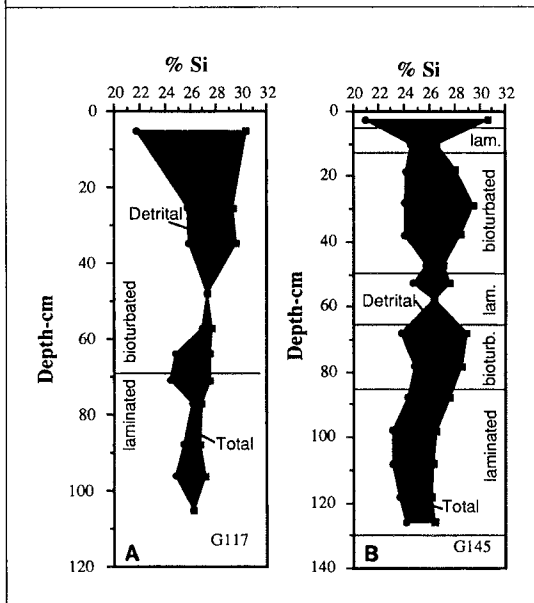
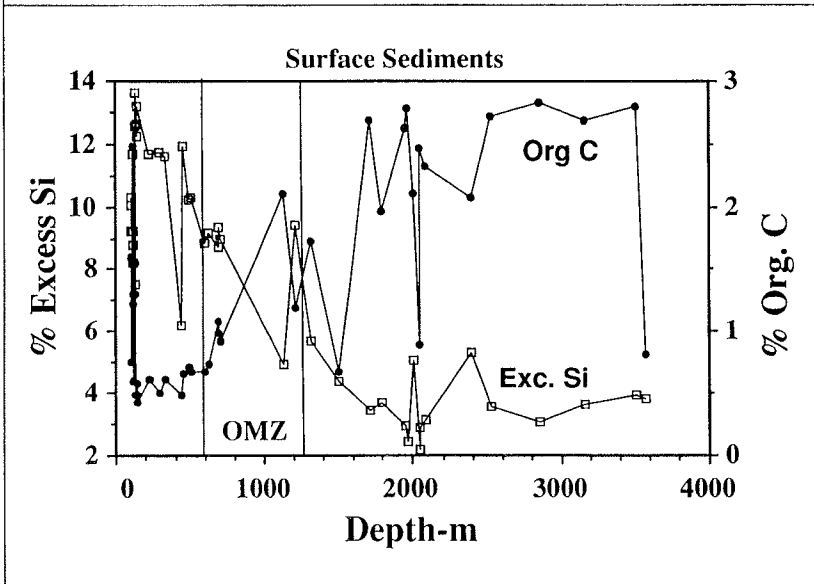


Figure 10
PERCENT EXCESS SILICA AND PERCENT ORGANIC CARBON IN SURFACE SEDIMENTS VERSUS WATER DEPTH FOR THE CONTINENTAL MARGIN OFF THE RUSSIAN RIVER, NORTHERN CALIFORNIA

Because of the extreme variation in concentration of Si and, particularly, organic carbon in shallow-water cores, data were plotted only for cores taken in water depths of >100 meters.



silica from diatoms and silicoflagellates is dissolved within the top 4-5 centimeters, the so-called “fluff” layer (PilskaIn 1990).

If excess Si in surface sediments (Figures 8B and 10), where Si dissolution has not occurred, is indeed biogenic Si and, therefore, the differences in surface distribution of excess Si shown in Figure 8B represent differences in diatom productivity in the overlying water, then a plot of excess Si versus water depth (Figure 10) can be interpreted to represent the average position of the core of highest diatom productivity. The surprising observation is that the maximum concentration of C_{org} does not correspond to the maximum concentration of excess Si. In fact, concentrations of these two parameters show opposite distribution patterns. Excess Si concentration is *greatest* between 150 and 500 meters and *decreases* offshore, whereas C_{org} concentration is *lowest* between 150 and 500 meters and *increases* offshore. This distribution suggests that less C_{org} is being preserved in sediments in the same area where it is being produced in greatest quantities in the overlying water.

A similar distribution of C_{org} content is in the data of Thompson *et al.* (1985) for sediments in a high-productivity upwelling area off Monterey Bay, although they did not discuss this distribution. One possible explanation for lowest concentration of C_{org} beneath areas of highest production is that sedimentation rate is higher under the high-productivity zone and this would tend to dilute the C_{org} content. Another possible explanation is that where C_{org} production is greatest, C_{org} consumption, both in the water column and by benthic organisms, also is greatest. This is why there is an OMZ in the first place. It may be that benthic consumption of C_{org} per unit area of sea floor is much greater under a shallow, high-productivity area than in a deeper area.

Part of the reason for higher C_{org} concentrations in deeper water may be textural; that is, the deeper sediments generally contain a higher proportion of clay that adsorbs more organic matter. On average, however, coarser sediments contain about the same range of C_{org} concentrations as clay-rich sediments. Consequently, most of the depth distribution of C_{org} concentration must be due to some other cause, whereby C_{org} is being consumed in greater quantities on the sea floor under where it is being produced in greatest quantities in the overlying water. Probably the main cause for the reduced C_{org} concentration is greater consumption by benthic organisms at the top of the OMZ. The implication is that as long as the OMZ is not anoxic, benthic organisms have plenty of food. A corollary to this implication is that if the bottom waters become anoxic and eliminate the benthic community, the excess C_{org} pool will be better preserved, reduced only by anaerobic decomposition, resulting in higher concentrations of C_{org} , which is what we observe in the laminated sediments.

The increased C_{org} consumption at the top of the OMZ may be a consequence of the *edge effect* described by Thompson *et al.* (1985) and Mullins *et al.* (1985) for the OMZ off Monterey. They found the abundance of all major invertebrate groups greatest in the upper part of the OMZ. Some invertebrates, such as echinoderms, were most abundant in sediments under the core of the OMZ (O_2 concentrations as low as 0.3 ml/L), and richness of benthic Foraminifera species also was greatest in the core of the OMZ.

Dissolved oxygen concentrations in the OMZ in the Santa Cruz basin are as low as 0.19 ml/L at 700 meters, yet the sediments support a surprisingly large epifaunal population (Edwards 1985). Mullins *et al.* (1985) point out that the edges of the OMZ, in addition to being highly productive benthic communities, also are “hot spots” of biogeochemical

activity, where nitrite produced by denitrification in the core of the OMZ is reoxidized to biologically usable nitrate (Anderson 1982). The upper part of the OMZ is, thus, a region of increased nutrient cycling and can support bacteria-based benthic communities such as bacterial mats (Williams and Reimers 1983) that provide additional sources of food for benthic invertebrates.

Organic-Carbon Burial: Anoxia versus Productivity

Pedersen and Calvert (1990) stated that the fundamental control on the accumulation of organic carbon is primary productivity and not anoxia and that there is no evidence for enhanced preservation of organic matter in sediments deposited under oxygen minima. To illustrate their point, they cite examples where the maximum **residual** C_{org} concentration **in the sediments** does not always correspond to the position of the OMZ. We suggest that sediments on the Northern California margin in general and late Pleistocene sediments in particular are striking examples of enhanced preservation of organic matter in sediments deposited under a high-productivity upwelling area with a dysaerobic to anoxic oxygen-minimum zone.

Pedersen and Calvert (1990) overlooked two important points in the argument over productivity versus anoxia in the preservation of C_{org} -rich sequences.

The first point is that under oxic or even dysaerobic bottom waters (most OMZs) consumption of organic matter by benthic organisms may severely reduce the **residual** organic matter ultimately preserved, but overall these areas of high productivity that result in oxygen minima also result in accumulation of C_{org} -rich sediments. On face value, the observed distributions of residual C_{org} and excess Si concentrations **in surface sediments** off Northern California (Figure 15 of work cited) would tend to support Pedersen and Calvert's case, because the highest concentrations of **residual** C_{org} are not in sediments deposited within the OMZ. However, if our model is correct, one would not expect to preserve increased C_{org} concentrations in sediments beneath a zone of high organic production in the surface waters. Increased consumption by larger populations of benthic invertebrates and micro-organisms, particularly at the edges of an oxic or dysaerobic OMZ, would deplete C_{org} in the surface sediments, and higher sedimentation rate would dilute the C_{org} concentration. By trying to correlate maximum contents of C_{org} with minimum concentrations of dissolved oxygen, Pedersen and Calvert missed the point that the presence of an OMZ indicates high productivity and areas of high productivity, in general, are areas of enhanced preservation of C_{org} .

The second point Pedersen and Calvert missed, or at least failed to emphasize, is the importance of laminated sediments as an indicator of anoxia. Hence, they make statements such as "anoxic environments are not, *ipso facto*, sites where organic matter is preferentially preserved" [p. 458] and "The simple presence of anoxia does not foster burial of organic-rich sediments" [p. 464]. In a high productivity, oxygen-deficient environment, such as off Northern California, if organic productivity is increased through more vigorous upwelling and nutrient supply, then the concentration of O_2 in an OMZ may drop from, say, 0.5 ml/L to 0.1 ml/L or lower. As far as any benthic fauna is concerned, this is an anoxic environment and the benthic faunas disappear. Under these conditions, laminations are preserved, consumption of C_{org} is restricted to anaerobic decomposition, and a much larger proportion of the C_{org} flux is preserved as residual C_{org} . The point is, **laminated**

sediments do indicate anoxia that produced a benthic environment very different from the oxic environment with bioturbating epi- and infaunas.

Conclusions

High concentrations (up to 3% organic carbon) of well preserved, lipid-rich (H-rich) organic matter is accumulating in diatomaceous sediments on the continental margin off Northern California to depths of at least 3500 meters. This organic matter is derived from high organic productivity in response to active seasonal (summer) upwelling driven by the southward-flowing California Current. Today, there is sufficient dissolved oxygen at all depths to support a benthic fauna, even though there is a well developed oxygen-minimum zone (as low as 0.2 ml/L dissolved oxygen) between 600 and 1200 meters water depth.

During the late Pleistocene, laminated (varved) sediments were preserved within the present OMZ, indicating that at that time the OMZ was anoxic (<0.1 ml/L dissolved oxygen) and, therefore, lacked a burrowing epi- and infauna so that benthic consumption of organic matter was restricted to anaerobic decomposition. Higher concentrations of more hydrogen-rich marine organic matter were preserved in these laminated sediments. From this observation we infer that upwelling and organic productivity in this area were greater during the late Pleistocene. Because stronger upwelling under the California Current implies greater wind stress by atmospheric circulation on the northeast Pacific Ocean, the stratigraphic record of laminated and bioturbated sediments off Northern California should contain a detailed high-resolution paleoclimatic record of changes in atmosphere/ocean circulation.

Sediment-trap data show highest concentrations of metals are associated with higher particle flux rates during spring diatom blooms. Higher overall particle flux rates due to higher organic productivity during times of laminated sediment accumulation resulted in accumulation of higher metal concentrations in the laminated sediments relative to interbedded bioturbated sediment. The laminated sediments also contain higher concentrations of sulfur, indicating a higher rate of sulfate reduction due to the presence of more "reactive" H-rich organic matter in the laminated sediments. The concentration of biogenic Si is lower in the laminated sediments than in the interbedded bioturbated sediments, indicating greater dissolution of biogenic Si in more alkaline pore fluids of the anoxic laminated sediment.

Higher concentrations of biogenic Si from diatoms, but lower concentrations of organic carbon, are preserved in surface sediments near the top of the OMZ relative to both shallower and deeper sediments. This indicates less residual C_{org} is preserved in sediments in the same area where organic matter is produced in greatest quantities in the overlying water. This difference in apparent production and preservation of organic matter probably is due to higher benthic consumption by large populations of benthic microorganisms and invertebrates at the edges of an oxic or dysaerobic OMZ. This means accumulation of C_{org} should not necessarily be expected to be greatest within the OMZ, or at least at the upper edge of the OMZ. Regardless of the locus of maximum accumulation of organic carbon relative to the OMZ, the important points are that because of upwelling and high surface water productivity, **there is an OMZ and there is preservation of high concentrations of organic matter under this zone.** Sediments containing up to 3% organic carbon in water depths up to 3500 meters are organic-carbon-rich by almost anyone's definition.

Although modern sediments on the continental margin off Northern California represent an impressive accumulation of organic matter, under an oxic to dysaerobic OMZ, the upper Pleistocene sediments are a striking example of **enhanced** preservation of organic matter in sediments deposited under an **anoxic** OMZ. These sediments show that **laminated sediments do indicate anoxia** and that anoxia produced a benthic environment very different from the oxic environment with bioturbating epi- and infauna. We conclude that anoxic environments are indeed sites where organic matter is preferentially preserved and that anoxia does indeed foster the burial of organic matter. This study shows that it is important to distinguish between processes within oxic, dysaerobic, and anoxic OMZs.

References

- Anderson, J.J. 1982. "The Nitrite-Oxygen Interface at the Top of the Oxygen Minimum Zone in the Eastern Tropical North Pacific". *Deep Sea Research* 29:1193-1201.
- Anderson, R.Y. 1977. "Short Term Sedimentation Response in Lakes in Western United States as Measured by Automated Sampling". *Limnology and Oceanography* 22:423-433.
- Anderson, R.Y., E. Hemphill-Haley, and J.V. Gardner. 1987. "Persistent Late Pleistocene-Holocene Seasonal Upwelling and Varves Off the Coast of California". *Quaternary Research* 28:307-313.
- Anderson, R.Y., J.V. Gardner, and E. Hemphill-Haley. 1989. "Variability of the Late Pleistocene-Early Holocene Oxygen-Minimum Zone Off Northern California". in *Climatic Change in the Eastern Pacific and Western Americas*. Ed. D.H. Peterson. American Geophysical Union Monograph 55:75-84
- Balistrieri, L., P.G. Brewer, and J.W. Murray. 1981. "Scavenging Residence Times of Trace Metals and Surface Chemistry of Sinking Particles in the Deep Ocean". *Deep-Sea Research* 28A:101-121.
- Balistrieri, L., and J.W. Murray. 1982. "The Surface Chemistry of MnO₂ in Major Ion Seawater". *Geochimica et Cosmochimica Acta* 46:1041-1052.
- Baedecker, P.A. (Ed.). 1987. *Methods for Geochemical Analysis*. U.S. Geological Survey Bulletin 1770.
- Berner, R.A., and J.T. Westrich. 1985. "Bioturbation and the Early Diagenesis of Carbon and Sulfur". *American Journal of Science* 285:193-206.
- CalCOFI (California Cooperative Oceanic Fisheries Investigations). 1963. *Atlas Series, State of California, Marine Research Committee*. Scripps Inst. Oceanography.
- Calvert, S.E. 1986. "Oceanographic Controls on the Accumulation of Organic Matter in Marine Sediments". in *Marine Petroleum Source Rocks*. Ed. J. Brooks and A.J. Fleet. London. Geological Society Special Publication 26:137-152.
- _____. 1966. "Origin of Diatom-Rich, Varved Sediments from the Gulf of California". *Journal of Geology* 74:546-565.
- _____. 1964. "Factors Affecting Distribution of Laminated Diatomaceous Sediments in Gulf of California". in *Marine Geology of the Gulf of California*. Ed. T.H. Van Andel and G.G. Shor. American Association of Petroleum Geologists Memoir 3:311-330.

- Coale, K.H., and K.W. Brueland. 1987. “ ^{234}Th : ^{238}U Disequilibria Within the California Current”. *Limnology and Oceanography* 32:189-200.
- Collier, R., and J. Edmond. 1984. “The Trace Element Geochemistry of Marine Biogenic Particulate Matter”. *Progress in Oceanography* 13:113-199.
- Dean, W.E., and M.A. Arthur. 1989. “Iron-Sulfur-Carbon Relationships in Organic-Carbon-Rich Sequences I: Cretaceous Western Interior Seaway”. *American Journal of Science* 289:708-743.
- Dean, W.E., M.A. Arthur, and G.E. Claypool. 1986. “ $^{13}\text{C}/^{12}\text{C}$ of Organic Carbon in Cretaceous Deep-Sea Black Shales: Influence of Source, Diagenesis, and Environmental Factors”. *Marine Geology* 70:119-157.
- Deines, P. 1980. “The Isotopic Composition of Reduced Organic Carbon”. in *Handbook of Environmental Isotope Geochemistry, Vol. 1, The Terrestrial Environment*. Ed. P. Fritz and J.-C. Fontes. Elsevier. pp. 329-406.
- deVries, T.J., and H.J. Schrader. 1981. “Variation of Upwelling/Oceanic Conditions During the Latest Pleistocene through Holocene Off the Central Peruvian Coast: A Diatom Record”. *Marine Micropaleontology* 6:157-167.
- Edwards, B.D. 1985. “Bioturbation in a Dysaerobic Bathyal Basin: California Borderland”. in *Biogenic Structures: Their Use in Interpreting Depositional Environments*. Ed. H.A. Curran. Society of Economic Paleontologists and Mineralogists Special Publication 35:309-331.
- Engleman, E.E., L.L. Jackson, D.R. Norton, and A.G. Fischer. 1985. “Determination of Carbonate Carbon in Geological Material by Coulometric Titration”. *Chemical Geology* 53:125-128.
- Espitalie, J., J.L. Laporte, M. Madec, F. Masrquis, P. Leplat, J. Paulet, and A. Boutefeu. 1977. “Methode Rapide de Caracterisation des Roches Mertes de Leur Potential Petrolier en de Leur Degre d’Evolution”. *Revue de l’Institut Francais de Petrole* 32:23-42.
- Froelich, P.N., G.P. Klinkhammer, M.L. Bender, N.A. Luedtke, G.R. Heath, D. Cullen, P. Dauphin, D. Hammond, B. Hartmann, and V. Maynard. 1979. “Early Oxidation of Organic Matter in Pelagic Sediments of the Eastern Equatorial Atlantic: Suboxic Diagenesis”. *Geochimica et Cosmochimica Acta* 43:1075-1090.
- Gardner, J.V., and E. Hemphill-Haley. 1986. “Evidence for a Stronger Oxygen-Minimum Zone Off Central California During Late Pleistocene to Early Holocene”. *Geology* 14:691-694.
- Gross, M.G., S.M. Gucluer, J.S. Creager, and W.A. Dawson. 1963. “Varved Marine Sediments in a Stagnant Fjord”. *Science* 141:918-919.
- Gucluer, S.M, and M.G. Gross. 1964. “Recent Marine Sediments in Saanich Inlet, A Stagnant Marine Basin”. *Limnology and Oceanography* 9:359-376.
- Honeyman, B.D., L.S. Balistrieri, and J.W. Murray. 1988. “Oceanic Trace Metal Scavenging: The Importance of Particle Concentration”. *Deep-Sea Research* 35:227-246.
- Hulsemann, J., and K.O. Emery. 1961. “Stratification in Recent Sediments of Santa Barbara Basin as Controlled by Organisms and Water Character”. *Journal of Geology* 69:279-290.

- Huyer, A. 1983. "Coastal Upwelling in the California Current System". *Progress in Oceanography* 12:259-284.
- Jacobs, L., and S. Emerson. 1985. "Partitioning and Transport of Metals Across the O₂/H₂S Interface in a Permanently Anoxic Basin: Framvaren Fjord, Norway". *Geochimica et Cosmochimica Acta* 49:1433-1444.
- McArthur, J.M. 1989. "Carbon Isotopes in Pore Water, Calcite, and Organic Carbon from Distal Turbidites of the Madeira Abyssal Plain". *Geochimica et Cosmochimica Acta* 53:2997-3004.
- Mullins, H.T., J.B. Thompson, K. McDougall, and T.L. Vercoutere. 1985. "Oxygen-Minimum Zone Edge Effects: Evidence from the Central California Coastal Upwelling System". *Geology* 13:491-494.
- Nyffeler, U.P., P.S. Santschi, and Y.-H. Li. 1986. "The Relevance of Scavenging Kinetics to Modeling of Sediment-Water Interactions in Natural Systems". *Limnology and Oceanography* 31:277-292.
- Pedersen, T.E., and S.E. Calvert. 1990. *Anoxia vs. Productivity: What Controls the Formation of Organic-Carbon-Rich Sediments and Sedimentary Rocks?* American Association of Petroleum Geologists Bulletin 74:454-466.
- Peters, K.E. 1986. *Guidelines for Evaluating Petroleum Source Rock Using Programmed Pyrolysis*. American Association of Petroleum Geologists Bulletin 70:318-329.
- Pilskaln, C.H. 1990. "Composition of Black Sea Basin Fluff Layer and Underlying Surface Sediments: Implications for Recent Mechanisms of Particulate Deposition and Geochemical Transformations Occurring at the Sediment/Water Interface" (abs). *Transactions of the American Geophysical Union* 71:151.
- Pisias, N.G. 1979. "Model for Paleoceanographic Reconstruction of the California Current During the Last 8000 Years". *Quaternary Research* 11:373-386.
- _____. 1978. "Paleoceanography of the Santa Barbara Basin During the Last 8000 Years". *Quaternary Research* 10:366-384.
- Pratt, L.M., and C.N. Threlkeld. 1984. "Stratigraphic Significance of ¹³C/¹²C Ratios in Mid-Cretaceous Rocks of the Western Interior, U.S.A." in *Mesozoic of Middle North America*. Ed. D.F. Stott and D.J. Glass. Canadian Society of Petroleum Geology, Memoir 9:305-312.
- Raiswell, R., and R.A. Berner. 1986. "Pyrite and Organic Matter in Phanerozoic Normal Marine Shales". *Geochimica et Cosmochimica Acta* 50:1967-1976.
- Rau, G.H., M.A. Arthur, and W.E. Dean. 1987. "¹⁵N/¹⁴N Variations in Cretaceous Atlantic Sedimentary Sequences — Implication for Historic Changes in Marine Nitrogen Biogeochemistry". *Earth and Planetary Science Letters* 82:269-279.
- Rau, G.H., D.M. Karl, D.J. Des Marais, G.A. Knauer, and J. Martin. 1986. "δ¹³C and δ¹⁵N Variations in Sedimenting POM: Results from VERTEX 5" (abs). *Transactions of the American Geophysical Union*.
- Rau, G.H., R.E. Sweeney, and I.R. Kaplan. 1982. "Plankton ¹³C:¹²C Ratio Changes with Latitude: Differences between Northern and Southern Oceans". *Deep Sea Research* 29:1035-1039.

- Reimers, C.E., and E. Suess. 1983. "Late Quaternary Fluctuations in the Cycling of Organic Matter Off Central Peru: A Proto-Kerogen Record". in *Coastal Upwelling, Its Sediment Record, Part A: Responses of the Sedimentary Regime to Present Coastal Upwelling*. Ed. E. Suess and J. Thiede. Plenum Press. pp. 497-526.
- Schrader, H.J., and T. Baumgartner. 1983. "Decadal Variation of Upwelling in the Central Gulf of California". in *Coastal Upwelling, Its Sediment Record*. Ed. J. Thiede and E. Suess. NATO Conference Series IV:247-276.
- Schrader, H.J., K. Kelts, J. Curray, *et al.* 1980. "Laminated Diatomaceous Sediments from the Guaymas Basin Slope (Central Gulf of California): 250,000-Year Climate Record". *Science* 207:1207-1209.
- Soutar, A., and P.A. Crill. 1977. *Sedimentation and Climatic Patterns in the Santa Barbara Basin During the 19th and 20th Centuries*. Geological Society of America Bulletin 88:1161-1172.
- Soutar, A., R. Johnson, and T.R. Baumgartner. 1981. "In Search of Modern Depositional Analogs to the Monterey Formation". in *The Monterey Formation and Related Rocks of California*. Ed. R.G. Garrison, K.E. Pisciotto, C.M. Isaacs, and J.C. Ingle. Society of Economic Paleontologists and Mineralogists Special Publication. pp. 123-147.
- Thompson, J.B., H.T. Mullins, C.R. Newton, and T.L. Vercoutre. 1985. "Alternative Biofacies Model for Dysaerobic Communities". *Lethaia* 18:167-179.
- Thornton, S.E. 1984. "Basin Model for Hemipelagic Sedimentation in a Tectonically Active Continental Margin: Santa Barbara Basin, California Continental Borderland". in *Fine-Grained Sediments: Deep-Water Processes and Facies*. Ed. D.A.V. Stow and D.J.W. Piper. Geological Society of London Special Publication 15:378-394.
- Tissot, B.P., and D.H. Welte. 1984. *Petroleum Formation and Occurrence*. Second Edition. Springer-Verlag.
- Wang, H.-K., and J.M. Wood. 1984. "Bioaccumulation of Nickel by Algae". *Environmental Science and Technology* 18:106-109.
- Williams, L.A., and C. Reimers. 1983. "Role of Bacterial Mats in Oxygen-Deficient Marine Basins and Coastal Upwelling Regimes: Preliminary Report". *Geology* 11:267-269.

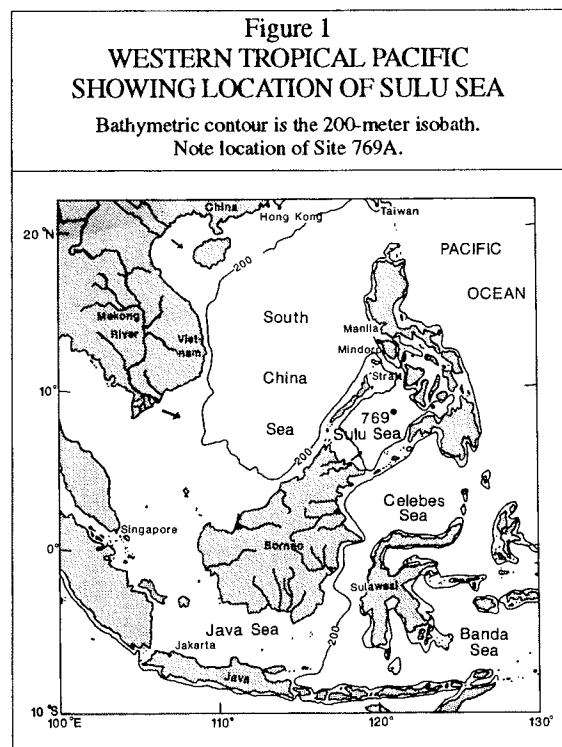
The Younger Dryas and Millennial-Scale Oceanographic Variability in the Sulu Sea, Tropical Western Pacific

Braddock K. Linsley

ABSTRACT: A high resolution, AMS ^{14}C -dated sediment record from the Sulu Sea clearly indicates the Younger Dryas climatic event affected the western equatorial Pacific (Linsley and Thunell 1990). Presence of the Younger Dryas in the tropical western Pacific indicates this climatic event is not restricted to the North Atlantic nor to high latitudes, but is global in extent. In addition, the planktonic $\delta^{18}\text{O}$ record and bulk CaCO_3 records both reveal millennial-scale variability. Spectral analysis of the $\delta^{18}\text{O}$ record shows increased variance at 2.5 Ka. The CaCO_3 accumulation rate record also shows increased variance at 2.5 Ka and at 3.5 Ka, with the 2.5 Ka cycle dominant after about 13 Ka. Similar ~2.5 Ka millennial climatic cycles have been recorded in late Pleistocene $\delta^{18}\text{O}$ records from the Indian Ocean, Quaternary continental and alpine glaciers, Holocene tree rings, and in Permian varved evaporite deposits, suggesting that about 2.5 Ka is an inherent climatic rhythm. The Younger Dryas occurs within these millennial cycles, suggesting its occurrence in the Indonesian tropics may be an expression of a 2.5-Ka millennial-scale climate cycle. In this context, the Younger Dryas is not unique, but apparent in numerous paleoclimatic records due to the rapid climatic change during the last deglaciation.

Introduction

High-accumulation-rate deep-marine sediments as found near continental margins offer the opportunity to examine higher frequency oceanographic and climatic change than open-ocean records with lower accumulation rates. The Sulu Sea, in the humid Indonesian tropics of the western Pacific, is a deep basin (>4800 meters) surrounded by a shelf most of which is less than 100 meters deep (Figure 1).



Tropical monsoonal climatic conditions and tectonic activity in the region have created one of the highest fluxes of river-borne sediment in the world (Milliman and Meade 1983). As a result, sedimentation rates are generally high. The isolated configuration of the Sulu Sea restricts circulation in the basin, resulting in anomalously warm and dysaerobic deep waters. The low dissolved oxygen content of intermediate and deep waters combined with high sediment accumulation rates has resulted in reduced benthic mixing of sediments.

Oceanographic conditions in the Sulu Sea are strongly influenced by the monsoonal climate of the Indonesian region and by the quasi-permanent Indonesian low pressure system. In addition, the Indonesian region was climatically important during the Pleistocene because vast areas of shallow shelves were exposed during sea level low stands. Sea level changes would have strongly influenced oceanographic conditions in the Sulu Sea, where a drop of 120 meters during the last glacial maximum (Curry 1964, Milliman and Emery 1968, Fairbanks 1989) is sufficient to almost isolate the basin from surrounding seas, potentially changing surface and deep water conditions.

To elucidate high-frequency oceanographic and climate change in the Sulu Sea, the upper 3.5 meters of sediment from Ocean Drilling Program (ODP) Hole 769A was sampled at 2.5-centimeter intervals. Sedimentation rates in this portion of the record range from 11 to 16 cm/Ka. The detailed sampling (about 250-year intervals) spans the last 22 Ka. The high sedimentation rates and close sampling interval yield a record comparable in resolution to that of core V23-81, the "type-section" for the Younger Dryas in the North Atlantic (Broecker *et al.* 1988).

Detailed time series of planktonic foraminiferal $\delta^{18}\text{O}$ and species abundances record the presence of the Younger Dryas between about 11 and 10 Ka (Linsley and Thunell 1990). In addition, the *Globigerinoides ruber* $\delta^{18}\text{O}$ data and CaCO_3 accumulation data record 2.5-Ka millennial-scale oceanographic variability, with the Younger Dryas falling within these millennial cycles. This paper presents evidence for millennial-scale variability and a brief discussion of the relationship of the Younger Dryas in the Indonesian tropics to a millennial climate cycle.

The Younger Dryas Climatic Event

It has been suggested that during the transition from the last glacial climatic regime to the Holocene, a brief return to glacial-like conditions, referred to as the Younger Dryas, occurred between about 11 and 10 Ka. The Younger Dryas has primarily been identified in records from Europe (Bjorck and Moller 1987, Lundquist 1987, and Manqerud 1987) and from the North Atlantic (Ruddiman *et al.* 1977, Ruddiman and McIntyre 1981a and 1981b), although a number of recent studies have documented a Younger Dryas-like event in areas far removed from the North Atlantic (Chinzei and Oba 1986, Chinzei *et al.* 1987, and Kallel *et al.* 1988).

Recently, using radiocarbon-dated submerged coral reefs from Barbados, Fairbanks (1989) showed that the transition from the last glacial maximum to the Holocene was marked by two periods of extremely rapid sea level rise, centered at about 12 and 9.5 Ka. The Younger Dryas occurred between these two periods.

In the Sulu Sea, planktonic foraminiferal $\delta^{18}\text{O}$ and abundance data both record significant changes during Younger Dryas time (Linsley and Thunell 1990). In particular, a 0.4 parts per mil increase in the $\delta^{18}\text{O}$ value of *Globigerinoides ruber* (white variety) and the reappearance of the cool water planktonic foraminifera, *Neogloboquadrina pachyderma* dextral, occur during the Younger Dryas at this location. Their data do not show whether the Younger Dryas event in the Sulu Sea is the result of surface water temperature changes, salinity changes, or a combination of both. Changes in surface salinities could have been

accomplished through local or global processes. They conclude that a salinity change is the more plausible explanation.

Specifically, a comparison of the Sulu Sea $\delta^{18}\text{O}$ record with the estimated $\delta^{18}\text{O}$ change of mean ocean water (Fairbanks 1989) suggests the period immediately preceding the Younger Dryas was a time of lowered surface water salinities. Intensification of the monsoon climate system and increased precipitation at about 11 Ka is one mechanism that may have resulted in local salinity changes. Meltwater pulses from the Tibetan Plateau is another possible cause.

Oceanographic Setting

Surface waters of Southeast Asian Seas have high temperatures and low salinities typical of humid tropical regions. The large excess of rainfall over evaporation creates an average surface salinity of 34 parts per mil. Annual temperature variations in the region are less than 2°C, but salinity is extremely variable because of high rainfall and river runoff and the intricate geographical structure of the area (Wyrski 1961).

The Mindoro Strait, at 420 meters deep, controls the deep-water ventilation rate in the basin (see Figure 1) (Frische and Quadfasel 1990, Wyrski 1961, and Van Reil 1943). Currently, deep water below the thermocline is uniformly warm (10°C), is dysaerobic, and has the same physical properties as water entering from the China Sea. Concentration of dissolved oxygen is low throughout the deep waters (<1.2 ml/L), corresponding to only 20% saturation at the prevailing salinity and temperature.

Warm bottom waters in the Sulu Sea result in excellent biogenic carbonate preservation. The carbonate compensation depth (CCD) is currently at ~4800 meters, while the carbonate lysocline occurs near 4000 meters (Linsley *et al.* 1985, Exon *et al.* 1981, Thunell Unpublished Data). In contrast, in the South China Sea the CCD is at 4000 meters and the lysocline is at 3500 meters (Rottman 1979). The South China Sea is open to the western Pacific and is well aerated at depth by cold bottom water.

Methods

Ocean Drilling Program (ODP) Leg 124 cored Site 769 at 3643-meter water depth on a bathymetric high in the center of the Sulu Sea (see Figure 1). This site was chosen specifically to avoid turbidite sedimentation and to obtain a continuous, high-resolution Neogene record. Samples were taken at 2.5-cm intervals in the upper 3.5 meters of core collected at Hole 769A for a high resolution study of the last deglaciation. Analytical methods for the isotopic analysis of *G. ruber* (white variety, 250-400 μm size fraction) and the planktonic foraminiferal faunal analyses are discussed in Linsley and Thunell (1990). Replicate sample analysis yielded a standard deviation from the mean of ± 0.07 parts per mil for S^{18}O .

Calcium carbonate analyses were performed at 5-cm intervals. Samples were freeze-dried, and a split of each sample was analyzed for bulk CaCO_3 . Carbonate carbon was measured by titration using a Coulometer, with replicate analyses yielding a standard deviation of $\pm 0.5\%$. CaCO_3 mass accumulation rates (MAR; $\text{g/cm}^2/\text{Ka}$) were calculated following the

methods of Gardner *et al.* (1984) using the continuously measured wet-bulk density (WBD) obtained from the shipboard gamma-ray attenuation porosity evaluator (GRAPE). WBD was converted to dry-bulk density (DBD) by the following relationship: $DBD \text{ g/cm}^3 = WBD \text{ g/cm}^3 - (0.01025 \times \text{porosity})$ (van Andel *et al.* 1975). The product of the average accumulation rates and the DBD gives bulk sediment MAR ($\text{g/cm}^2/\text{Ka}$). Mass accumulation rates of bulk CaCO_3 were determined by multiplying the bulk accumulation rate by the weight percent CaCO_3 fraction in the sample.

Age Model

The chronology for the upper 350 centimeters of Hole 769A is based on three AMS ^{14}C ages. Specimens of *G. ruber* yielded corrected ages of $9,720 \pm 80$ years from 107 cm, $11,100 \pm 185$ years from 128 cm, and $18,320 \pm 155$ years from 245 cm. A correction factor of -400 years was applied to each date to account for the difference in ^{14}C between the atmosphere and surface water (Bard 1988).

Ages for individual samples were estimated assuming constant sedimentation rates between ^{14}C dates. Sample ages for the upper part of the core (above the first ^{14}C date) were derived assuming the top of the core has an age of zero. Likewise, sample ages below 245 cm (18,320 years) were extrapolated using the sedimentation rate calculated for the core interval from 128 to 245 cm. The ^{14}C ages indicate sedimentation rates in the core vary from ~ 11 cm/1000 years during the Holocene to ~ 16 cm/1000 years during the last glacial.

Analytical Results

The $\delta^{18}\text{O}$ and CaCO_3 MAR records are displayed in Figure 2. The high resolution $\delta^{18}\text{O}$ time series reveals small (~ 0.3 parts per mil) millennial oscillations during the last 25 Ka, which may be related to salinity changes (Linsley and Thunell 1990). CaCO_3 MAR shows high-frequency fluctuations from glacial stage 2 through the Holocene. At 11 Ka (the beginning of the Younger Dryas), CaCO_3 accumulation reaches high values of ~ 2.5 $\text{g/cm}^2/\text{Ka}$ and then decreases to relatively low values of ~ 1.7 $\text{g/cm}^2/\text{Ka}$ between ~ 11 and 10 Ka.

Spectral characteristics of the last 25 Ka of the *G. ruber* $\delta^{18}\text{O}$ record and bulk CaCO_3 MAR record were examined using standard time series procedures (Jenkins and Watts 1968) (Figures 3 and 4). For the $\delta^{18}\text{O}$ record, the upper 3.5 meters of Site 769A was interpolated at 250-year intervals. The CaCO_3 record was interpolated at 400-year intervals due to its 5-cm sample interval. One-third lags of the autocovariance function were used to estimate the spectra. A prewhitening filter was used to emphasize the higher frequency variability.

Spectral analysis indicates that for $\delta^{18}\text{O}$, significant variance is concentrated at a period of 2.5 Ka, with a broader, less defined increase in variance at about a 1.5 Ka period. The 2.5-Ka millennial oscillations are absent from 9.0 Ka to the present. Spectral analysis of the CaCO_3 record indicates variance is also concentrated at 2.5 Ka, as well as at 3.5 and 1.7 Ka, with the 2.5 Ka cycle dominant between about 13 Ka and 5 Ka.

Figure 2
OXYGEN ISOTOPIC PROFILE OF *G. RUBER* (above) (250-Year Sample Interval) AND CALCIUM CARBONATE MASS ACCUMULATION RATE RECORD (below) (400-Year Sample Intervals)

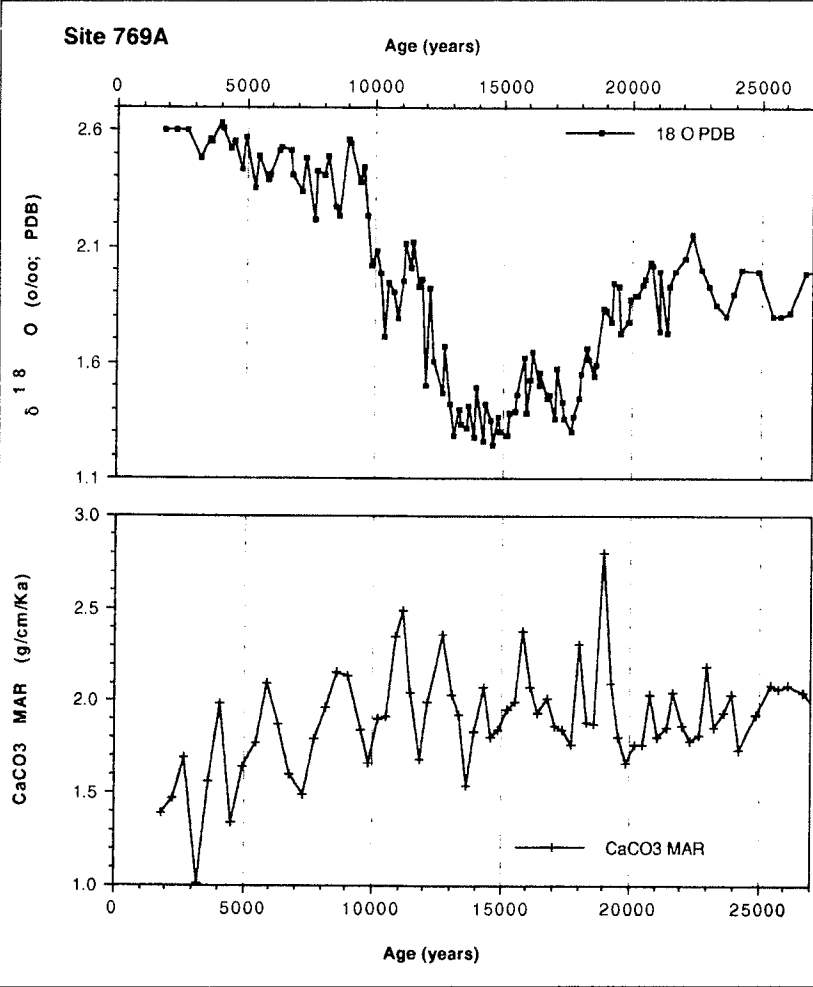


Figure 3
SPECTRAL ESTIMATES OF $\delta^{18}\text{O}$ OF THE PLANKTONIC FORAMINIFERA *G. RUBER* FROM SITE 769A (0-4 meters)

The upper 4 meters was interpolated at 250-year intervals. One-third lags of the autocovariance function were used to estimate the spectra. A prewhitening filter has been used to emphasize the higher frequency variability. Variance is concentrated at 2.5 Ka, with a broader peak at about 1.5 Ka. The bandwidth and 95% confidence interval are shown.

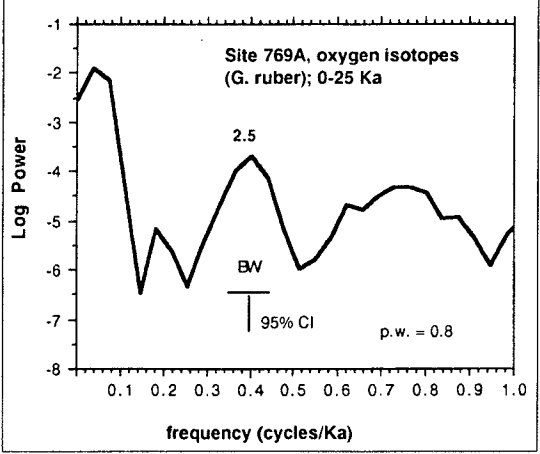
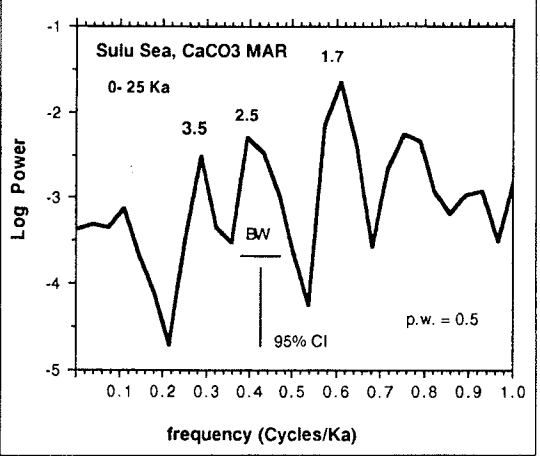


Figure 4
SPECTRAL ESTIMATES OF BULK CALCIUM CARBONATE FROM SITE 769A (0-4 meters)

Due to a 5-cm sample interval, the upper 4 meters of calcium carbonate record was interpolated at 400-year intervals. One-third lags of the autocovariance function were used to estimate the spectra. A prewhitening filter has been used to emphasize the higher frequency variability. Variance is concentrated at 1.7, 2.5, and 3.5 Ka, very similar to the spectral estimates of the $\delta^{18}\text{O}$ record from this site. The bandwidth and 95% confidence interval are shown.



Stable Isotopic and Faunal Signature

The Barbados sea level record (Fairbanks 1989) shows two meltwater events, just before (~12 Ka) and just after (~9.5 Ka) the Younger Dryas. In this context, the Younger Dryas is not unique but is distinguished because it was a brief interval between two periods of lowered surface salinities. According to Fairbanks (1989), the extremely high discharge rates during these two meltwater pulses caused rapid decreases in the $\delta^{18}\text{O}$ of surface waters.

Examination of the Hole 769A $\delta^{18}\text{O}$ record reveals that Younger Dryas time is indeed bracketed by two brief intervals of light $\delta^{18}\text{O}$ values that may be equivalent to the two meltwater pulses identified by Fairbanks (1989). Specifically, there is a 0.85 parts per mil decrease in $\delta^{18}\text{O}$ between 15 and 11.5 Ka in the Sulu Sea record (Figure 2). In comparison, the $\delta^{18}\text{O}$ change of mean ocean water was only 0.4 to 0.5 parts per mil during this period (Fairbanks 1989). If this difference was due to a local salinity change, and if the deglacial $\delta^{18}\text{O}$ /salinity relationship was similar to that for the modern North Pacific (Craig and Gordon 1965), then surface water salinities in the Sulu Sea at 11.5 Ka would have been about 1 parts per mil lower than during Younger Dryas time.

Similarly, the difference in $\delta^{18}\text{O}$ between 15 Ka and 10.5 Ka (mid-Younger Dryas time) in our Sulu Sea record is only 0.5 parts per mil (Figure 2), about equal to the $\delta^{18}\text{O}$ change of mean ocean water at this interval. This suggests $\delta^{18}\text{O}$ values in the Sulu Sea during Younger Dryas time were not anomalously *heavy*, but rather that the preceding 1,000 years was a time of anomalously *light* $\delta^{18}\text{O}$ values. This may also be the case for the other millennial-scale oscillations in the $\delta^{18}\text{O}$ record.

Numerous rivers drain into the region, potentially affecting the $\delta^{18}\text{O}$ record. In particular, the Mekong River, which has headwaters in the Tibetan Plateau, empties into the southern end of the South China Sea (Figure 1). The Mekong River has a discharge of 470 km³/year, the ninth largest river in the world (Boreland 1973). For comparison, the Mississippi River, the sixth largest in the world, has a discharge of 580 km³/year (Milliman and Meade 1983).

Calcium Carbonate Accumulation

The high-frequency CaCO₃ oscillations at Site 769A do not appear to be related to dissolution/preservation cycles. The planktonic foraminifera are remarkably well preserved throughout the 25-Ka record except for a brief interval between 0.25 and 0.40 meter, which also contains abundant volcanic ash. In addition, the pteropod and CaCO₃ MAR records do not seem related, supporting the lack of a dissolution effect on the CaCO₃ record.

During the Younger Dryas, CaCO₃ MAR exhibits a sharp decrease, slightly lagging the $\delta^{18}\text{O}$ record. However, similar decreases occurred repeatedly throughout the last 25 Ka, so this is not a unique expression of the Younger Dryas. Grain-size analysis of the terrigenous fraction in these samples shows no correspondence to the CaCO₃ oscillations, suggesting terrigenous dilution is not the cause. Trace metal data from the longer record from Site 769A, spanning the last 750 Ka, suggest glacial times had higher rates of productivity and greater accumulation rates of certain trace metals and CaCO₃ (Linsley

and von Breyman in press). This is in accord with results of Romine (1982) and Rea *et al.* (1986), who find greater equatorial wind shear during glacial times, which could have affected hydrographic dynamics of the western Pacific and Sulu Sea. A thicker warmwater lens in the western Pacific and reduced amounts of high total CO₂ Pacific Intermediate water could have affected the CO₂ content of Sulu Sea deep water. Although the cause of these CaCO₃ cycles at Hole 769A remains unclear, primary productivity changes and variable carbonate flux to the sea floor appear to be the most plausible explanation.

Possible Relationship of the Younger Dryas to Millennial Climatic Variability

Data from Hole 769A suggest that an additional hypothesis regarding the origin of the Younger Dryas should be considered. The proxy evidence of oceanographic and climatic change found at Hole 769A suggests millennial-scale oceanographic variability has influenced the Sulu Sea. At Hole 769A, the Younger Dryas occurs within this millennial cycle, which is most clearly expressed in the CaCO₃ accumulation and $\delta^{18}\text{O}$ records.

Evidence for millennial-scale climatic variability has been found in a variety of high accumulation rate geologic settings. A 2,500-year climatic cycle is depicted in a summary spectrum of climatic variability compiled by Mitchell (1976).

Evidence for a millennial cycle has also been documented in the advance and retreat of Quaternary glaciers (Denton and Karlen 1973) and in the H/D isotopic ratio and CO₂ concentration of late Pleistocene glacial ice (Oeschger *et al.* 1985). Oxygen isotopic records (Dansgaard *et al.* 1984, Benoist *et al.* 1982) and deuterium isotopic records (Yiou *et al.* 1989) from Quaternary ice cores from Antarctica and Greenland display about a 2.5 Ka period, as well as others between 2 and 15 Ka. These records reflect changes in surface air temperature.

In late Pleistocene-Holocene marine records, Pestiaux *et al.* (1987) have documented spectral density peaks at 10.2, 4.6, and 2.3 Ka in planktonic $\delta^{18}\text{O}$ records from the monsoonal region of the Indian Ocean. They suggest the climatic system is characterized by a highly nonlinear response to orbital forcing. Millennial-scale changes in upwelling and productivity in the eastern Pacific appear in time series records compiled by Pisias (1978) and Juillet-leclerc and Schrader (1987). Off the coast of Northern California, millennial-scale upwelling variability in the late Pleistocene has been recorded by alternately varved and bioturbated sediments (Linsley *et al.* 1990, Anderson *et al.* 1990). In addition, the Barbados coral sea level record of the last 17,000 years compiled by Fairbanks (1989) documents two distinct meltwater pulses centered at 12.0 and 9.5 Ka. The timing of these increases in meltwater discharge appear to fit within a millennial cycle, although there is no astronomical explanation for separate meltwater pulses.

In the Permian, the varved evaporitic Castle formation records strong salinity cycles manifested as Halite bedding thickness changes (Anderson 1982). The average period of the oscillations is about 2,500 varve years, with increased variance between 1800 and 3000 years.

Causes of these millennial-scale paleoclimatic fluctuations are not known. Pestiaux *et al.* (1987) have suggested that an approximate 2.5 Ka period is one of several harmonics of the 19- to 23-Ka precession and 41-Ka obliquity orbital cycles. The presence of these

harmonics was predicted by LeTreut and Ghil (1983) and LeTreut *et al.* (1988) using nonlinear climatic oscillator models. Millennial-scale periodicity has also been attributed to changes in solar activity (Bray 1971, Denton and Karlen 1973, Anderson 1982, and Anderson *et al.* 1989 and 1990). The solar activity hypothesis is supported by the ^{14}C record in Holocene tree rings, a proxy for solar activity. The tree-ring records contain a dominant periodicity at 2.4 Ka (Suess 1980, Damon and Linwick 1986, Stuiver and Braziunus 1989).

Whatever the cause of the ~2.5 Ka millennial climatic cycle, in the Sulu Sea the position of the Younger Dryas within millennial cycles in $\delta^{18}\text{O}$ and CaCO_3 suggests the occurrence of the Younger Dryas in the Indonesian tropics may be an expression of a millennial-scale climatic cycle. In this context, the Younger Dryas is not in itself a unique event. Lack of significant millennial $\delta^{18}\text{O}$ oscillations after about 9 Ka and the change in the period of the CaCO_3 cycles at about 13 Ka suggest changes in climatic boundary conditions during deglaciation are somehow responsible.

References

- Anderson, R.Y. 1982. "A Long Geoclimatic Record from the Permian". *J. Geophys. Res.* 87(C9):7285-7294.
- Anderson, R.Y., B.K. Linsley, and J.V. Gardner. 1990. "Expression of Seasonal and ENSO Forcing in Climatic Variability at Lower than ENSO Frequencies: Evidence from Pleistocene Marine Varves Off California". In *Paleoclimates: The record from Lakes, Ocean, and Land*. Ed. L.V. Benson and P.A. Meyers. Paleo., Paleo., Paleo. pp. 287-300.
- Bard, E. 1988. "Correction of Accelerator Mass Spectrometry ^{14}C Ages Measured in Planktonic Foraminifera: Paleoceanographic Implications". *Paleoceanography* 3(6):635-645.
- Benoist, J.P., F. Glangeaud, N. Martin, J.L. Lacoume, L. Lorius, and A. Oulahman. 1982. "Study of Climatic Series by Time-Frequency Analysis". In *Proceedings of the ICASSP82*. New York. IEEE Press. pp. 1902-1905.
- Bjorck, S., and P. Moller. 1987. "Late Weichselian Environmental History in Southeastern Sweden During the Deglaciation of the Scandinavian Ice Sheet". *Quaternary Research* 28:1-37.
- Boreland, W.M. 1973. *Pa Mong Phase II, Supplement to Main Report (Hydraulics and Sediment Studies)*. U.S. Bureau of Reclamation. 2 volumes.
- Bray, J.R. 1971. "Solar-Climate Relationships in the Post-Pleistocene". *Science* 171:1242-1243.
- Broecker, W.S., M. Andree, W. Wolfli, H. Oeschger, G. Bonani, J. Kennett, and D. Peteet. 1988. "The Chronology of the Last Deglaciation: Implication to the Cause of the Younger Dryas Event". *Paleoceanography* 3(1):1-19.
- Chinzei, K., H. Fujioka, H. Kitazatom, I. Koizumi, T. Oba, M. Oda, H. Okada, T. Sakai, and Y. Tanimura. 1987. "Postglacial Environmental Change of the Pacific Ocean Off the Coast of Central Japan". *Marine Micropaleont.* 11:273-291.

- Chinzei, K., and T. Oba. 1986. "Oxygen Isotope Studies of the Deep Sea Sediments Around Japan, Recent Progress of Natural Sciences in Japan, Vol. II". *Quaternary Research*. Science Council of Japan, pp. 35-43.
- CLIMAP. 1976. "The Surface of the Ice Age Earth". *Science* 191:1131-1137.
- Craig, H., and L. Gordon. 1965. "Isotopic Oceanography: Deuterium and Oxygen¹⁸ Variation in the Ocean and Marine Atmosphere". In *Symposium on Marine Chemistry*. Ed. D. Schink and J. Corless. Narragansett Marine Laboratory Occasional Publication 3.
- Curray, J.R. 1964. "Transgressions and Regressions". In *Papers on Marine Geology*. Ed. R.C. Miller. Shephard Commemorative Volume. Macmillan, New York. pp.175-203.
- Damon, P.E., and T.W. Linwick. 1986. "Geomagnetic-Heliomagnetic Modulations of Atmospheric Radiocarbon Production". *Radiocarbon* 28:266-278.
- Dansgaard, W., S.J. Johnsen, H.B. Clausen, D. Dahl-Jensen, N. Gundestrup, C.H. Hammer, and H. Oeschger. 1984. "North Atlantic Oscillations Revealed by Deep Greenland Ice Cores". *Geophysical Monograph* 29:288-298.
- Denton, G.H., and W. Karlen. 1973. "Holocene Climatic Variations — Their Pattern and Possible Causes". *Quaternary Research* 3:155-205.
- Exon, M.F., F.-W. Haake, M. Hartmann, F.-C. Kogler, P.J. Muller, and M.J. Whiticar. 1981. "Morphology, Water Characteristics and Sedimentation in the Silled Sulu Sea, Southeast Asia". *Marine Geology* 39:165-195.
- Fairbanks, R. 1989. "A 17,000-Year Glacio-Eustatic Sea Level Record: Influence of Glacial Melting Rates on the Younger Dryas Event and Deep Ocean Circulation". *Nature* 342:637-642.
- Frische, A., and D. Quadfasel. 1990. "Hydrography of the Sulu Sea". In *Proc. of the Ocean Drilling Program*. Initial Reports. 124 College Station, TX.
- Gardner, J.V., W.E. Dean, and C.R. Wilson. 1984. *Carbonate and Organic-Carbon Cycles and the History of Upwelling at DSDP Site 532, Walvis Ridge, South Atlantic Ocean*. Ed. W.W. Hay, J.C. Sibeut, et al. Washington, DC. U.S. Government Printing Office. Initial Reports, Deep-Sea Drilling Project. 95:905-921.
- Jenkins, G.M., and D.G. Watts. 1968. *Spectral Analysis and Its Applications*. Holden-day, San Francisco.
- Juillet-leclerc, and H. Schrader. 1987. "Variations of Upwelling Intensity Recorded in Varved Sediment from the Gulf of California During the Past 3000 Years". *Nature* 329:146-149.
- Kallel, N., L.D. Labeyrie, M. Arnold, H. Okada, W.C. Dudley, and J.-C. Duplessy. 1988. "Evidence of Cooling During the Younger Dryas in the Western North Pacific". *Oceanol. Acta* 11(4):369-375.
- LeTreut, H., and M. Ghil. 1983. "Orbital Forcing Climatic Interactions and Glaciation Cycles". *Journal of Geophysical Research* 88:5167-5190.
- LeTreut, H., J. Portes, J. Jouzel, and M.Ghil. 1988. "Isotopic Modeling of Climatic Oscillations: Implications for a Comparative Study of Marine and Ice Core Records". *Journal of Geophysical Research* 93:9365-9383.

- Linsley, B.K., R.Y. Anderson, and J.V. Gardner. 1990. "Rapid $\delta^{18}\text{O}$ and $\delta^{13}\text{C}$ Isotopic Shifts Preserved in Late Pleistocene Marine Varves on the California Margin". In *Sixth Annual Pacific Climate (PACLIM) Workshop*. Ed. J.L. Betancourt and A.M. MacKay. Asilomar, CA. California Dept. of Water Resources Technical Report 23. pp.83-86.
- Linsley, B.K., and R.C. Thunell. 1990. "The Record of Deglaciation in the Sulu Sea: Evidence for the Younger Dryas Event in the Western Tropical Pacific". In J.P. Kennett, Ed. *Paleoceanography* 5(6):1025-1039.
- Linsley, B.K., R.C. Thunell, C. Morgan, and D.F. Williams. 1985. "Oxygen Minimum Expansion in the Sulu Sea, Western Equatorial Pacific, During the Last Glacial Low Stand of Sea Level". *Marine Micropaleontology* 9:395-418.
- Linsley, B.K., and M.T. von Breyman. In Press. "Geochemical and Isotopic Record in the Sulu Sea During the Last 0.75 Ma: Evidence for Enhanced Productivity During Glacials". In *Proc. of the Ocean Drilling Program. Scientific Research. Assessment of Surface Water Variability and Paleoproductivity Changes*. Ocean Drilling Program Leg 124, Scientific Results.
- Lundquist, J. 1987. "Glaciodynamics of the Younger Dryas Marginal Zone in Scandinavia". *Geografiska Annaler* 69A:305-320.
- Mangerud, J. 1987. "The Allerod/Younger Dryas Boundry". In *Abrupt Climatic Change*. Ed. W.H. Berger and L.D. Labeyrie. Reidel, Boston. pp.163-171.
- Milliman, J.D., and K.O. Emory. 1968. "Sea Levels During the Past 35,000 Years". *Science*. 162:1121.
- Milliman, J.D., and R.H. Meade. 1983. "Worldwide Delivery of River Sediment to the Oceans". *J. Geol.* 91(1):1-21.
- Mitchell, J.M. 1976. "An Overview of Climatic Variability and Its Causal Mechanisms". *Quat Res.* 6:481-493.
- Oeschger, H., B. Stauffer, R. Finkel, and C.C. Langway Jr. 1985. "Variations in the CO_2 Concentration of Occluded Air and of Anions and Dust in Polar Ice Cores". In *The Carbon Cycle and Atmospheric CO_2 : Natural Variations Archean to Present*. Ed. E.T. Sunquist and W.S. Broecker. AGU Geophys. Monograph Series 32:132-153.
- Pestiaux, P., J.C. Duplessy, and A. Berger. 1987. "Paleoclimatic Variability at Frequencies from 10^{-4} - 10^{-3} Cycles per Year". In *Climate-History, Periodicity and Predictability*. Ed. M.R. Rampino, J.E. Sanders, W.S. Newman, and L.K. Konigsson. pp.285-299.
- Pisias, N.G. 1978. "Paleoceanography of the Santa Barbara Basin During the Last 8000 Years". *Quat. Res.* 10:366-384.
- Rea, D.K., L.W. Chambers, J.M. Chuey, T.R. Janecek, M. Leinen, and N.G. Pisias. 1986. "A 420,000-Year Record of Cyclicity in Oceanic and Atmospheric Processes from the Eastern Equatorial Pacific". *Paleoceanography* 1:577-586.
- Romine, K. 1982. "Late Quaternary History of Atmospheric and Oceanic Circulation in the Eastern Equatorial Pacific". *Marine Micropaleontology* 7:163-187.

- Rottman, M.L. 1979. "Dissolution of Planktonic Foraminifera and Pteropods in the South China Sea Sediments". *J. Foraminiferal Res.* 9(1):41-49.
- Ruddiman, W.F., and A. McIntyre. 1981a. "The North Atlantic Ocean During the Last Deglaciation". *Palaeogeogr. Palaeoclimatol. Paleocol.* 35:145-214.
- _____. 1981b. "The Mode and Mechanism of the Last Deglaciation: Oceanic Evidence". *Quat. Res.* 16:125-134.
- Ruddiman, W., C.D. Sancetta, and A. McIntyre. 1977. "Glacial/Interglacial Response Rate of Subpolar North Atlantic Waters to Climatic Change: The Record in Ocean Sediments". *Philos. Trans. R. Soc. London.* Ser. B. 280:119-142.
- Stuiver, M., and T.F. Braziunas. 1989. "Atmospheric ^{14}C and Century-Scale Solar Oscillations". *Nature* 338:405-408.
- Suess, H.E. 1980. "The Radiocarbon Record in Tree Rings of the Last 8000 Years". *Radiocarbon* 22:200-209.
- van Andel, T.H., G.R. Heath, and T.C. Moore Jr. 1975. "Cenozoic History and Paleoceanography of the Central Equatorial Pacific Ocean". *Mem. Geol. Soc. Am.* 143.
- Van Riel, P.M. 1943. *The Snellius Expedition 1929-1930, Oceanographic Results, Part V, The Bottom Water.* Introductory Remarks and Oxygen Content, 2. Brill, Leiden. pp.1-76.
- Wyrtki, K. 1961. *Scientific Results of Marine Investigations of the South China Sea and the Gulf of Thailand, Physical Oceanography of the Southeast Asian Waters.* Univ. of California, Scripps Inst. Oceanography, La Jolla, CA. p.195.

High- and Low-Latitude Climate Interactions: Evidence for Enhanced Aridity of Asian Monsoon Dust Source Areas After 2.4 MYR from ODP Leg 117 Magnetic Susceptibility Data

Peter deMenocal and Jan Bloemendal

ABSTRACT: Whole-core magnetic susceptibility can sometimes be used as a rapid and sensitive indicator of variations in the concentration of terrigenous material. We apply this approach to study the evolution of Plio-Pleistocene climatic cycles of terrigenous sedimentation at Ocean Drilling Program Site 721, on the Owen Ridge in the Arabian Sea. Aerosol and sediment studies have shown that terrigenous sedimentation on the Owen Ridge is dominated by variations in the supply of eolian dust borne by summer southwest monsoon winds. Terrigenous extraction analyses of the Site 721 sediments show that magnetic susceptibility is a conservative and sensitive tracer of the terrigenous (eolian) fraction variations at Site 721.

Spectral analysis of the susceptibility time series spanning the last 3.2 Myr show the record varies strongly at earth orbital periodicities. Prior to about 2.4 Myr, the record varies predominantly at the 23 and 19 kyr periodicities, corresponding to orbital precession; after 2.4 Myr it shows a significant increase in 41-kyr power corresponding to orbital obliquity. This shift coincides with the rapid expansion of Northern Hemisphere ice sheets at about 2.37 Myr. General circulation model experiments and paleoclimatological evidence from northeast Africa suggest the increase in 41-kyr power after 2.4 Myr may be reflecting periodic increases in monsoon dust source area aridity associated with the coeval expansion of Northern Hemisphere ice sheets, which varied predominantly at this periodicity.

Introduction

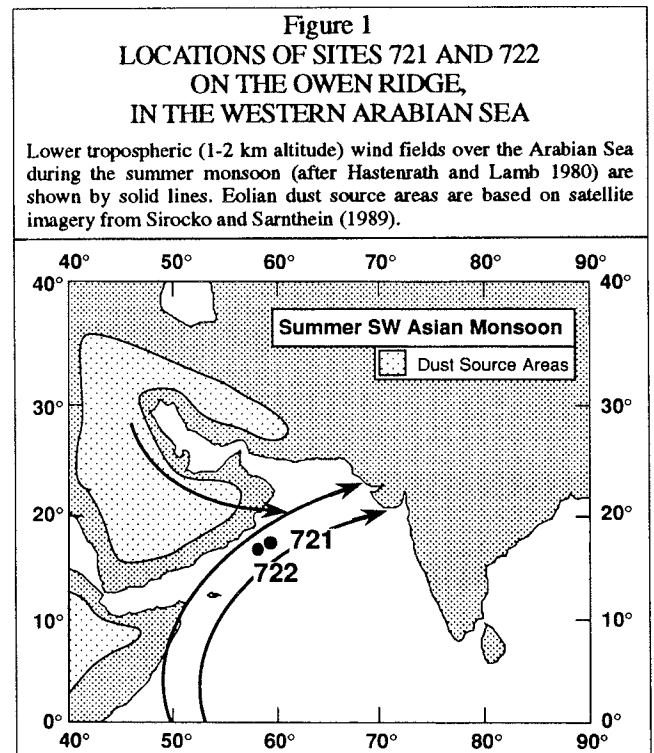
Orbital perturbations that result from gravitational interactions with the moon and with the other planets give rise to cyclical variations of 100 kyr in Earth orbital eccentricity, 41 kyr in obliquity, and 23-19 kyr in precession (Berger 1978). These variations are climatically important, because they affect seasonal distribution of solar insolation received at any given latitude. Statistical analyses of the foraminiferal $\delta^{18}\text{O}$ record from deep-sea cores, which is largely a measure of glacial ice volume (Shackleton and Opdyke 1976), show that growth and decay of ice sheets have been strongly modulated by orbital insolation variations (Imbrie *et al.* 1984).

Similarly, other major components of climate, such as sea surface temperature, Asian and African monsoon intensity, deep circulation, and atmospheric CO_2 , vary predominantly at orbital periodicities (Ruddiman and McIntyre 1984, Pokras and Mix 1985, Mix and Fairbanks 1985, Prell and Van Campo 1986, Raymo *et al.* 1989). However, measurement of conventional paleoclimatic indicators (*e.g.*, oxygen and carbon isotopes, carbonate, opal, and terrigenous fraction content) in deep-sea sediments is time consuming, so paleoclimatic indicators are needed that can be measured more rapidly.

Magnetic susceptibility is a measure of the concentration of magnetic material in a sample. It is not a remanence measurement; it is determined by the ratio of induced magnetization

to an applied field and reflects the integrated contribution of all magnetic constituents. Since the terrigenous fraction of most deep-sea sediments contains trace amounts (typically <0.01%) of strongly ferrimagnetic minerals (*e.g.*, magnetite), variations in magnetic susceptibility are usually monitoring variations in terrigenous concentration. Provided susceptibility is shown to be a conservative indicator of the terrigenous fraction, its link to paleoclimate is through climatically-controlled variations in the supply of terrigenous and biogenic components (Kent 1982, Robinson 1986, Doh *et al.* 1988, Bloemendal *et al.* 1988, Bloemendal and deMenocal 1989, deMenocal *et al.* In Press). It is this link between climate and sediment magnetism that is investigated here.

The major aim of Ocean Drilling Program Leg 117 in the Arabian Sea was to study the late Neogene evolution of the Asian monsoon. The origin and dynamics of the modern Asian monsoon are complex, but observational and theoretical studies have provided a general understanding of its larger scale features (Hastenrath 1985). Northern Hemisphere heating during summer develops an intense low pressure cell over the Tibetan Plateau, which enables regional cyclonic circulation to prevail from May to September (Hastenrath and Lamb 1979). In the northwest Arabian Sea, strong southwest winds parallel the Arabian coast, carrying eolian detritus from northeast Africa and Arabia to the Arabian Sea and bringing the monsoon rains to southern Asia (Figure 1). Intensity of the summer Asian monsoon has been tied to orographic effects of the Himalayan mountains and the Tibetan Plateau, which tend to enhance the convergence of moist convection and latent heat (Ramage 1965, Hahn and Manabe 1975).



Both general circulation model (GCM) experiments (Kutzbach 1981, Prell and Kutzbach 1987) and analyses of eolian and biogenic components in deep-sea cores (Pokras and Mix 1985, Prell and Van Campo 1986, Prell and Kutzbach 1987) have shown that seasonal insolation variations resulting from orbital precession have modulated the intensity of the Asian and African monsoons. Precession affects low-latitude summer insolation at periodicities of 23 and 19 kyr (Berger 1978); maximum summer insolation is achieved when

the summer solstice coincides with perihelion (*e.g.*, 11 Kyr BP), and paleoclimatic data have shown that the African and Asian monsoon systems were intensified at these times (Pokras and Mix 1985, Prell and Van Campo 1986, Clemens and Prell 1990).

Methods, Time-Control, and Power Spectral Analysis

Site 721 is in 2028-meter-deep water near the crest of the Owen Ridge in the Arabian Sea and rises 2000 meters above the surrounding bathymetry. Satellite imagery (Sirocko and Sarnthein 1987) and sediment core studies (Sirocko and Sarnthein 1987, Clemens and Prell 1990) show that terrigenous sedimentation in the Arabian Sea is dominantly eolian. Volume magnetic susceptibility was measured on whole core sections at 5-centimeter intervals using a pass-through sensor. Three holes were drilled at Site 721 (A, B, and C), and between-hole correlations using the susceptibility data were used to construct complete composite sequences (deMenocal *et al.* In Press) (Figure 2).

Age models were constructed using bio- and magnetostratigraphic datums. Mean sedimentation rate determined from these data is ~ 3.5 cm/kyr. Oxygen isotope data (Clemens and Prell In Prep.) were used to establish age/depth relationships for the interval 0-1 Myr. The final age model included as many datums as possible within a series of straight-line segments. The Site 721 magnetic susceptibility time series is shown in Figure 3. The time series was divided into overlapping 0.4-Myr intervals, and spectral analysis was performed on each interval using the Blackman-Tukey method (Imbrie *et al.* 1984).

The 0.4-Myr-interval power spectra results, shown in Figure 4, indicate a shift in spectral character at about 2.4 Myr. Before 2.4 Myr, the data vary predominantly at the 23 and 19 kyr precessional periodicities. The variance associated with this precession component significantly exceeds that associated with obliquity for all intervals before 2.4 Myr. After 2.4 Myr, there is a significant increase in variance at the 41-kyr periodicity and a corresponding reduction in variance at the 23-kyr and 19-kyr periodicities. The increased variance at the 41-kyr periodicity persists over the entire 0-2.4 Myr interval.

To examine coherency between the orbitally-driven insolation variations (*the forcing*) and the susceptibility variations (*the response*), the susceptibility time series were filtered using a bandpass filter centered at 22 kyr, corresponding to orbital precession. The extracted component was then correlated (*tuned*) to the calculated precession curve using an inverse correlation method (Imbrie *et al.* 1984, Martinson *et al.* 1982). The filtered susceptibility data at Site 721 exhibit the modulated character of the precessional curve (Figure 5). Coherency is 0.84 over the 3.2-1.6 Myr interval and is even higher (0.89) from 3.2-2.4 Myr. Although the tuning procedure maximizes correlation between the two signals, the coherency of the 400-kyr and 100-kyr modulation envelopes is a real component of the susceptibility data. These results show the strong orbital control of the Site 721 susceptibility record and a shift from strong precessional forcing before and strong obliquity forcing after about 2.4 Myr. This raises the questions of what aspect(s) of the relevant climate systems does the susceptibility record reflect, and what is the significance of the periodicity shift at 2.4 Myr?

Figure 2
INTER-HOLE CORRELATIONS USING THE
MAGNETIC SUSCEPTIBILITY DATA,
SITE 721

Shaded areas represent sections missing between core breaks; these were used to construct a composite sequence, a portion of which is shown to the right. The susceptibility data were also used to constrain the position of the Matuyama-Gauss Chronozone boundary (2.47 Myr; at 88.30 mbsf composite depth).

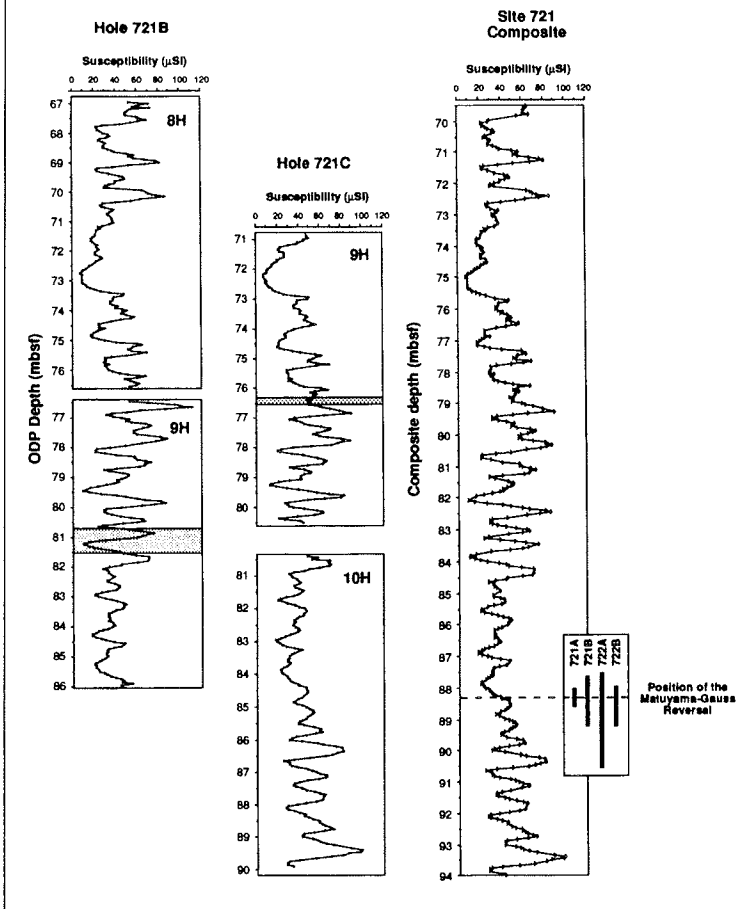


Figure 3
MAGNETIC SUSCEPTIBILITY TIME-SERIES,
SITE 721

Age control from 0-1 Myr was based on $\delta^{18}\text{O}$ stratigraphy (Clemens and Prell In Press). Age control from 3.2-1.0 Myr was based on bio- and magnetostratigraphic datums.

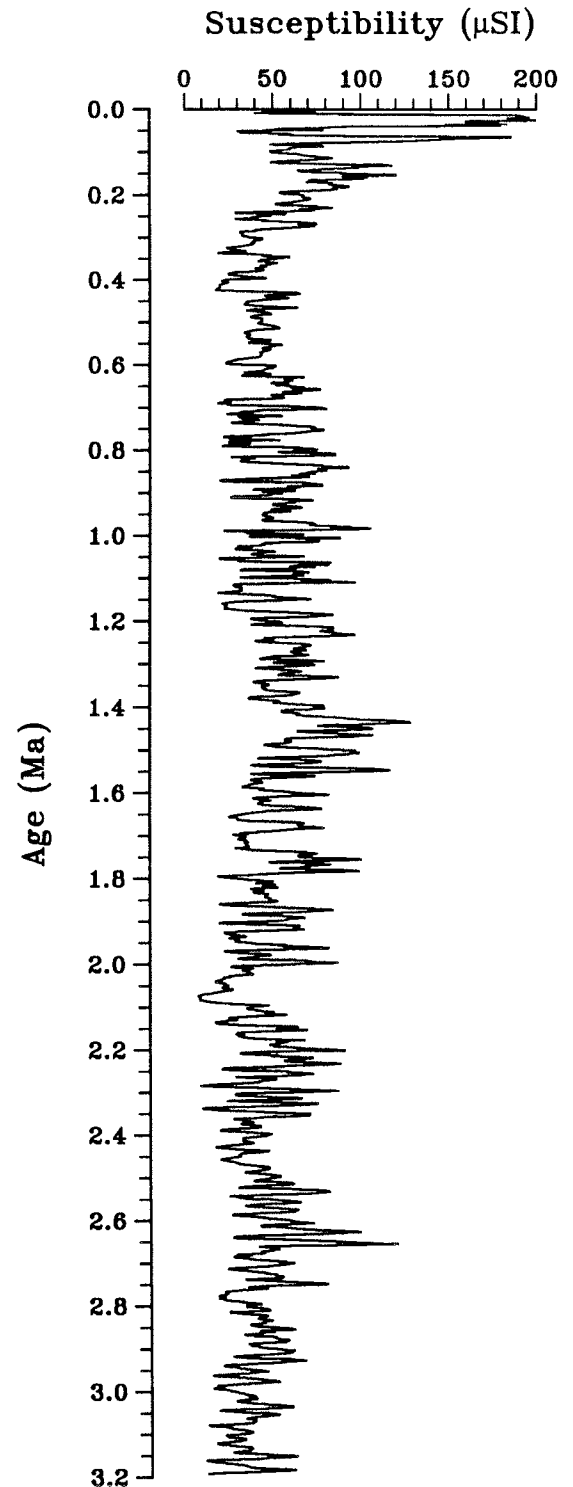


Figure 4
POWER SPECTRA CALCULATED FOR OVERLAPPING 400-KYR SEGMENTS OF THE
SUSCEPTIBILITY TIME SERIES

Data are shown as scaled variance. Note the increase in 41-kyr power after about 2.4 Myr.

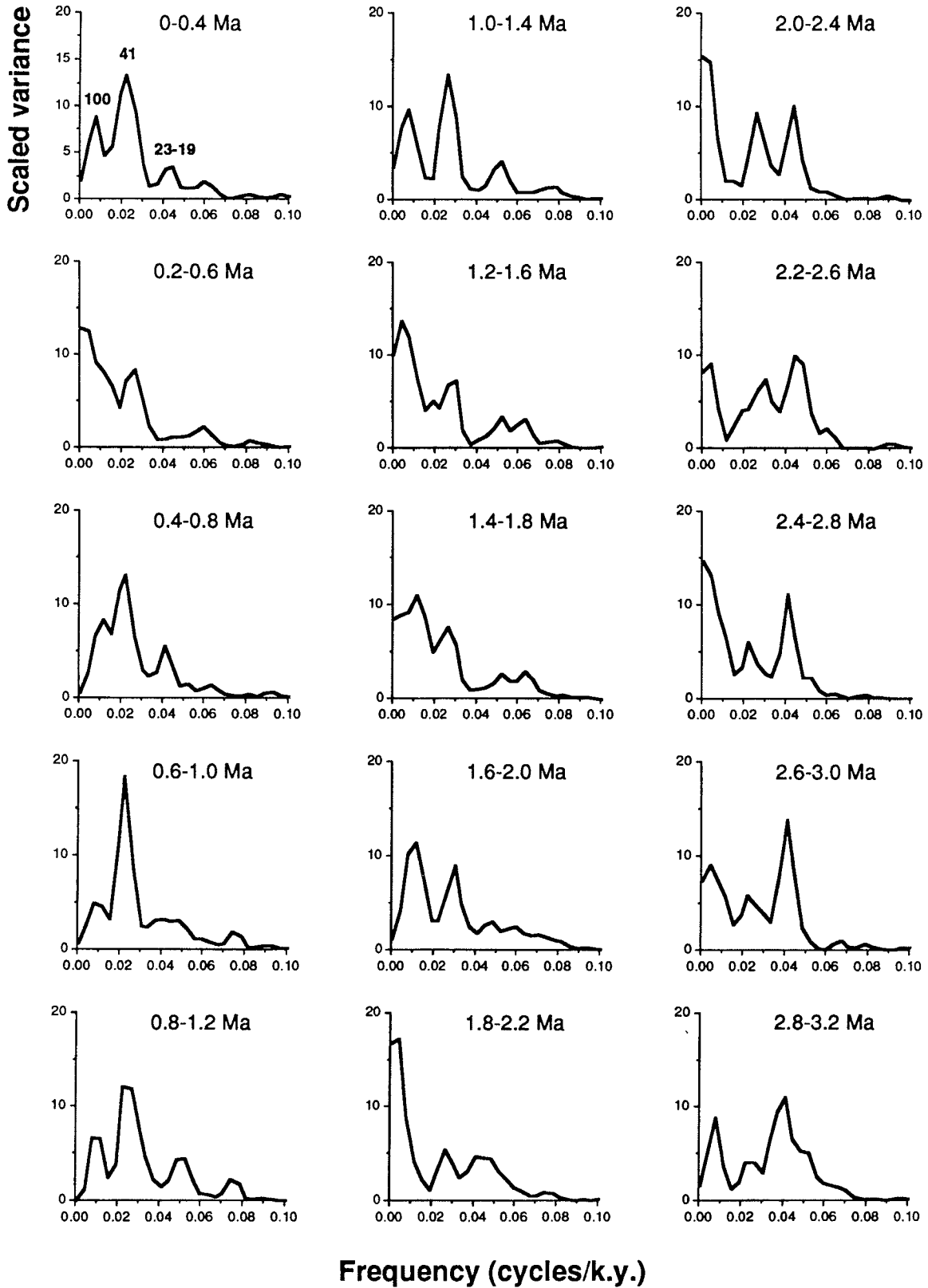
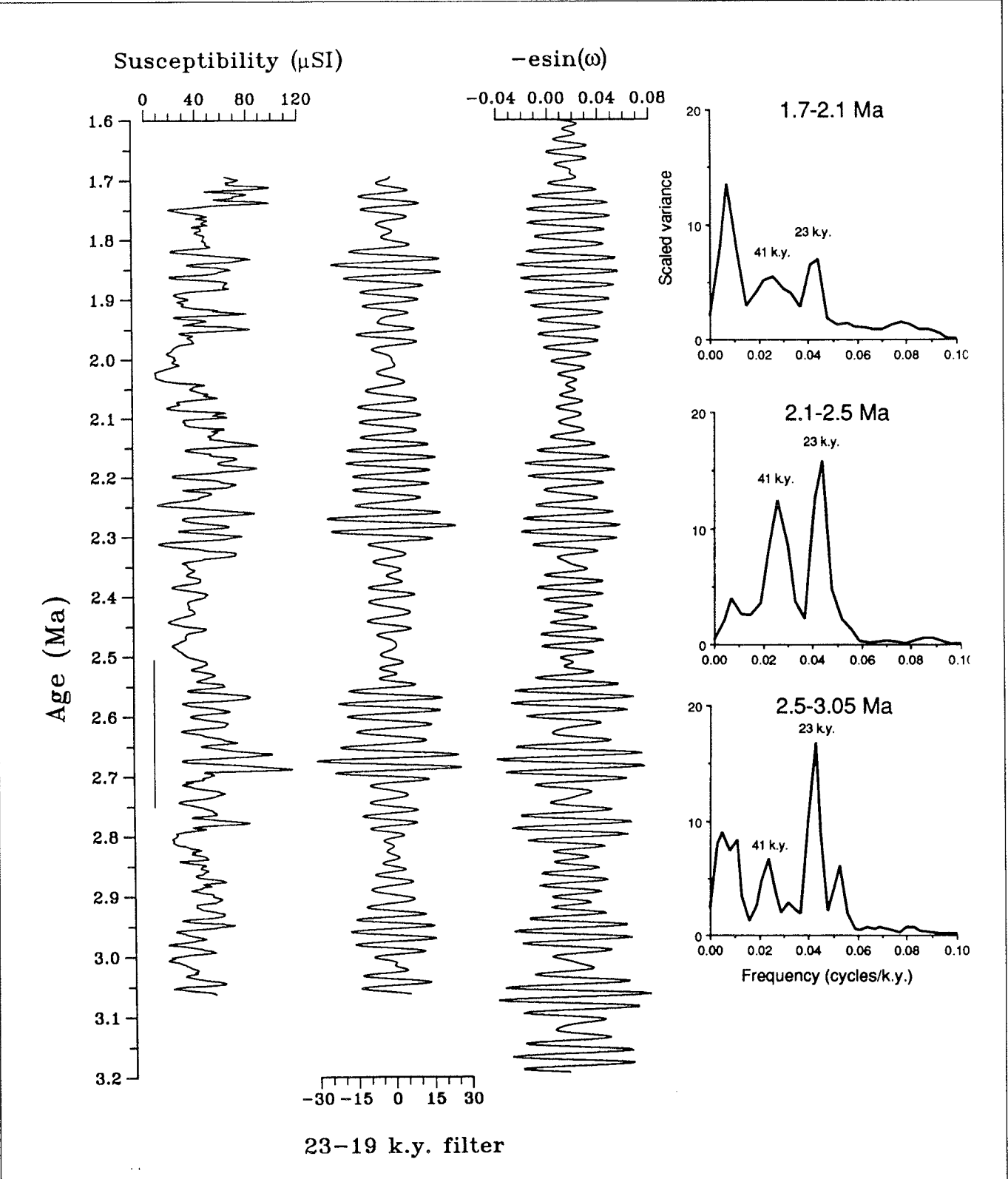


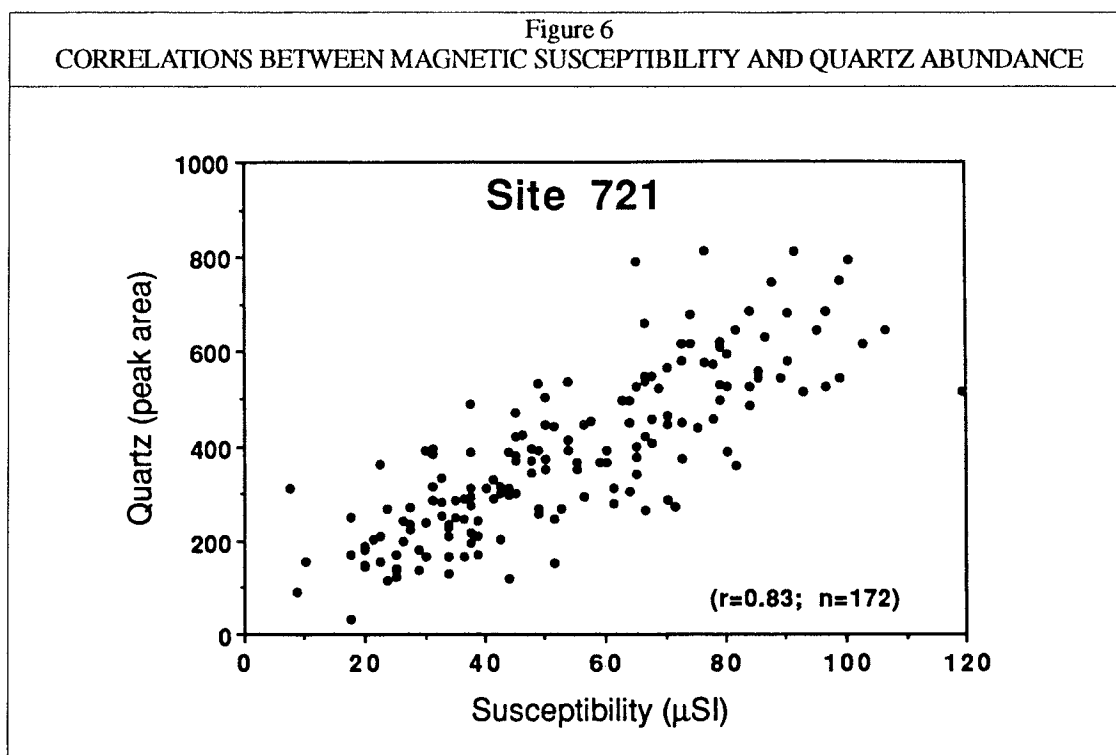
Figure 5
 CALCULATED PRECESSION ($-\sin(\omega)$), 22-KYR BANDPASS FILTER OF THE SUSCEPTIBILITY RECORD, AND
 RAW SUSCEPTIBILITY RECORD FOR THE 3.2-1.6 MYR INTERVAL, SITE 721

The filtered susceptibility data were correlated (phase-locked) to precession using a signal correlation package (Martinson et al. 1984) to demonstrate the degree of coherency between the presumed isolation forcing ($-\sin(\omega)$) and the climate response (susceptibility). Coherency is highest (0.89) between precession and the filtered susceptibility over the 3.2-2.5 Myr interval; coherency of the entire 3.2-1.6 Myr interval is 0.86. The vertical line to the left shows the interval selected for the flux calculations.



Climatic Origin of the Susceptibility Variations

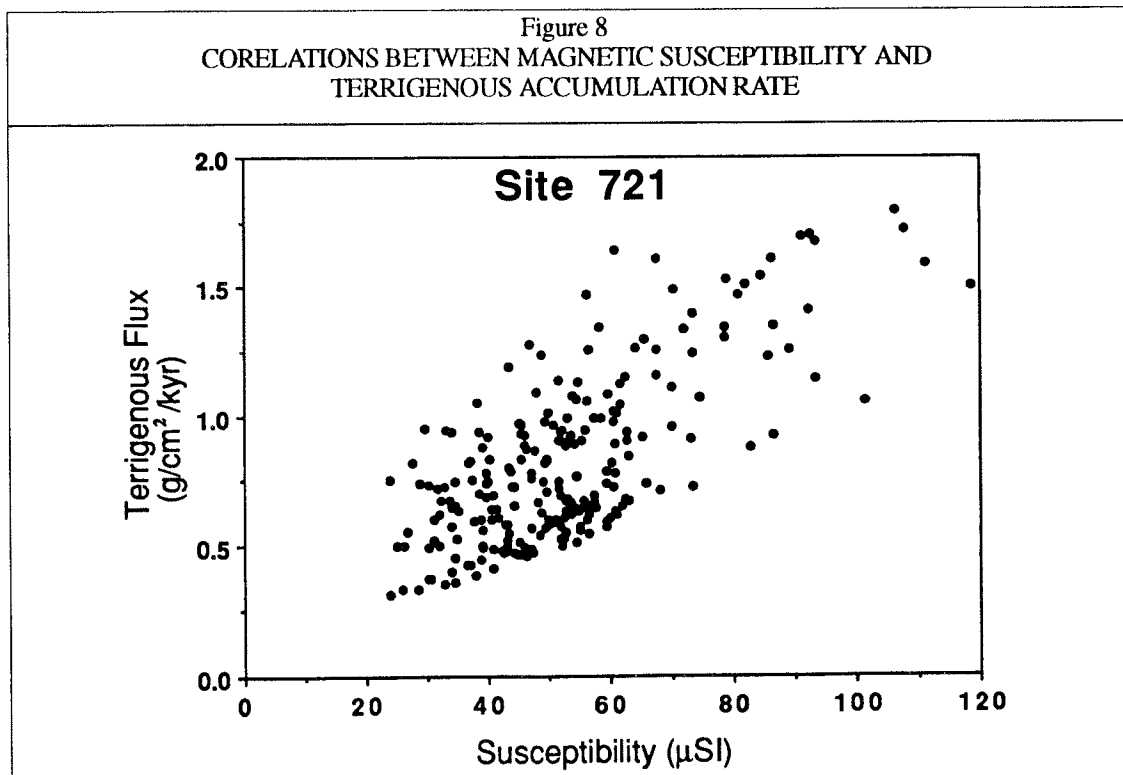
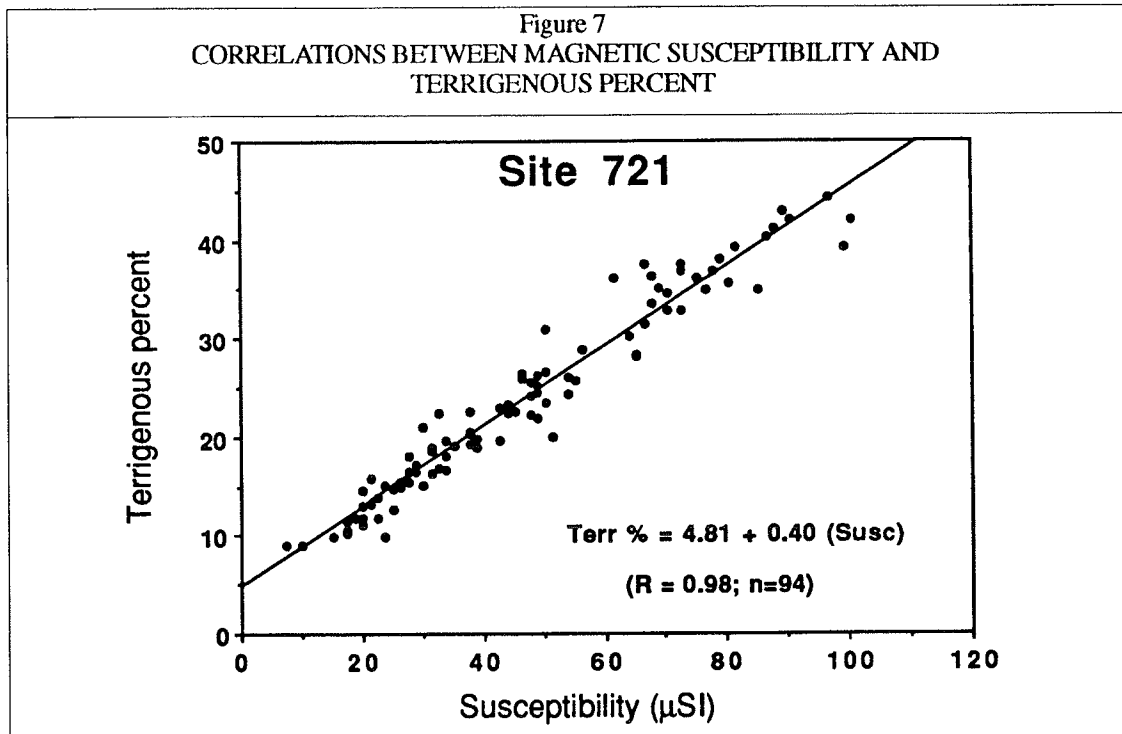
Terrigenous extraction following procedures of Clemens and Prell (1990) was conducted on 94 samples from Site 721 (deMenocal *et al.* In Press). Samples were subjected to sequential chemical extractions of biogenic carbonate, opal, and organic carbon to isolate the mineral (eolian) fraction. The strong correlation between susceptibility and terrigenous percent ($r=0.98$) shows susceptibility is an accurate proxy indicator of terrigenous content. Figure 6 shows the advantage of using susceptibility; the terrigenous extraction analyses required about 2 hours per sample, whereas magnetic susceptibility was measured in 10 seconds on whole, unsplit cores.



Results of bulk sample X-ray diffraction analyses are shown in Figure 7. The strong correlation between susceptibility and quartz ($r=0.83$) reflects the eolian origin of the terrigenous fraction variations. There is also a strong positive correlation between susceptibility and dolomite ($r=0.70$). Aerosol studies have shown that quartz (and dolomite) are dominant constituents of summer monsoon dust (Stewart *et al.* 1965, Goldberg and Griffin 1970, Kolla and Biscaye 1977, Sirocko and Sarnthein 1989, Nair *et al.* 1989).

Using the “tuned” Site 721 susceptibility record to generate detailed age/depth relationships for a short interval between 2.7 and 2.5 Myr and available dry bulk density data, we converted the terrigenous concentrations to terrigenous accumulation rates. Figure 8 shows the strong positive correlation between susceptibility and terrigenous accumulation rate. These data indicate that susceptibility variations are reflecting variations in terrigenous supply rather biogenic dilution; the correlation between susceptibility and biogenic accumulation rate was poor. A study of late Pleistocene terrigenous accumulation on the Owen Ridge by Clemens and Prell (1990) supports this conclusion.

The strong correlation between susceptibility and the concentration and accumulation rate of terrigenous sediment, and the occurrence within this fraction of minerals indicative of an eolian source, leads us to conclude that the Site 721 susceptibility record is a direct expression of variations in the eolian supply of terrigenous material by the Asian monsoon.



Origin of the 2.4-Myr Shift in Variance

The predominance of 23 and 19 kyr variance in the susceptibility records prior to 2.4 Myr suggests that terrigenous deposition from the Asian summer monsoons was largely modulated by summer insolation variations due to precession. Atmospheric GCM experiments have shown that, in the absence of other factors, monsoonal circulation is extremely responsive to precessional variations in local summer insolation and that the response is approximately linear (Prell and Kutzbach 1987). We interpret the strong precessional-band susceptibility variance prior to 2.4 Myr to reflect predominance of insolation-driven variations in summer monsoon intensity or source area aridity.

The marked increase in variance at the 41 kyr periodicity after about 2.4 Myr coincides with initiation of major Northern Hemisphere glaciation (Shackleton *et al.* 1984), and GCM results and geological evidence suggest this may reflect ice sheet effects on source areas of monsoon dust in northeast Africa and Arabia. The increase in power at 41 kyr is particularly significant, because the late Pliocene marine $\delta^{18}\text{O}$ record varies almost purely at this periodicity (Ruddiman *et al.* 1989, Raymo *et al.* 1989).

General circulation model experiments have suggested that northeastern Africa and Arabia may have experienced enhanced aridification when ice sheets were more extensive than today. Experiments with the GISS II GCM show that inclusion of LGM ice alone causes dramatic cooling (-5 to -10°C) and significant rainfall decreases (1-2 mm/day) over northeastern Africa, Arabia, and Mesopotamia during winter (Rind 1987, deMenocal and Rind In Prep.). This is apparently a direct effect of the downstream advection of cooler and drier air from the high-latitude Fennoscandian ice sheets. These results suggest that monsoon dust source areas are subject to enhanced aridification during times of increased high-latitude ice sheet cover. Late Pleistocene paleoclimate data from this region and the adjacent Arabian Sea support this relationship (Kolla and Biscaye 1977, Van Campo *et al.* 1982, Clemens and Prell 1990, Bonnefille *et al.* 1990).

Terrestrial paleoclimate data from northeastern Africa support a transition to a regionally cooler and drier climate at about 2.4 Myr. The strongest evidence for east African cooling and drying at 2.4 Ma is based on palynological data from diatomite sediments at Gadeb (Ethiopian Highlands), where a vegetation descent of at least 1-1.5 km has been shown to occur at some point between two radiometrically-dated tuff layers at 2.51 Myr and 2.35 Myr (Bonnefille 1983). The Gadeb pollen data (at 2300 msl) show an abundance of shrub, heath, and grass (largely *Ericaceae* and *Gramineae*) pollen types, which today are found only in the cooler montane climate above about 3500 msl. The temperature decrease is equivalent to about $4-6^\circ\text{C}$ (Bonnefille 1983).

This shift to regionally cooler and drier conditions at about 2.4 Myr is also supported by pollen data from lower Omo, near Lake Turkana, where there is a coeval expansion of savanna grasslands (Bonnefille 1976). Bonnefille and Letouzey (1976) have shown that fossil wood and fruits with rain forest affinities disappeared from the lower Omo region at about this time. Abell (1982) and Cerling *et al.* (1977) have presented stable isotopic evidence from Lake Turkana gastropods and pedogenic carbonate horizons that also support a trend toward reduced precipitation between two radiometrically dated tuffs at 3.2 Myr and 1.9 Myr.

Acknowledgments

We thank the members of the shipboard scientific and technical party of Leg 117 for their help in performing the whole-core susceptibility measurements and the X-ray diffraction mineralogy. We thank Rebecca Esmay and Bettina Domeser for their assistance in the terrigenous extraction and XRD laboratory work. Computing facilities were provided by the Borehole Research Group. W. Ruddiman, J. King, S. Clemens, and D. Murray provided constructive comments.

This research was supported by funding from USSAC and by National Science Foundation grant OCE-89-11206.

References

- Abell, P.I. 1982. "Paleoclimates at Lake Turkana, Kenya, from Oxygen Isotope Ratios of Gastropod Shells". *Nature* 297:321-323.
- Berger, A.L. 1978. "Long-Term Variations of Caloric Solar Insolation Resulting from Earth's Orbital Variations". *Quat. Res.* 9:139-167.
- Bloemendal, J., and P. deMenocal. 1989. "Evidence for a Shift in the Climatic Variability of the African and Asian Monsoons at 2.5 Ma: An Application of Whole-Core Magnetic Susceptibility Measurements to Paleoclimatology". *Nature* 342:897-899.
- Bloemendal, J., B. Lamb, and J. King. 1988. "Paleoenvironmental Implications of Rock-Magnetic Properties of Late Quaternary Sediment Cores from the Eastern Equatorial Atlantic". *Paleoceanography* 3:61-87.
- Bonnefille, R. 1983. "Evidence for a Cooler and Drier Climate in the Ethiopian Uplands, 2.5 Ma Ago". *Nature* 303:487-491.
- _____. 1976. "Palynological Evidence for an Important Change in the Vegetation of the Omo Basin Between 2.5 and 2.0 Ma". In *Earliest Man and Environments in the Lake Rudolf Basin*. Ed. Y. Coppens *et al.* Univ. of Chicago Press. pp.421-431
- Bonnefille, R., J.C. Roeland, and J. Guiot. 1990. "Temperature and Rainfall Estimates for the Past 40,000 Years in Equatorial Africa". *Nature* 346:347-349.
- Bonnefille, R., and R. Letouzey. 1976. "Fruits Fossiles D'Antrocaryon Dans la Vallée de l'Omo (Éthiopie)". *Adansonia* 16:65-82.
- Cerling, T.E, R.L. Hay, J.R. O'Neil. 1977. "Isotopic Evidence for Dramatic Climate Changes in East Africa During the Pleistocene". *Nature* 267:137-138.
- Clemens, S., and W. Prell. 1990. "Late Pleistocene Variability of Arabian Sea Summer-Monsoon Winds and Dust Source Aridity: An Eolian Record from the Lithogenic Component of Deep-Sea Sediments". *Paleoceanography* 5:109-146.
- deMenocal, P.B. J. Bloemendal, and J.W. King. In Press. "A Rock-Magnetic Record of Monsoonal Dust Deposition to the Arabian Sea: Evidence for a Shift in the Mode of Deposition at 2.4 Ma". In *Scientific Rep. of the ODP 117, Part B*.

- deMenocal, P. and D. Rind. In Prep. "Effects of Insolation, Ice Cover and Orography on the Winter and Summer Asian Monsoon: Results from the GISS II General Circulation Model".
To be submitted to *J. Atmos. Sci.*
- Doh, S-J., J. King, and M. Lienen. 1988. "A Rock-Magnetic Study of GPC-3 from the Central North Pacific and Its Paleooceanographic Implications". *Paleoceanography* 3(1):89-112.
- Goldberg, E.D., and J.J. Griffin. 1970. "The Sediments of the Northern Indian Ocean". *Deep-Sea Res.* 17:513-537.
- Hahn, D.G., and S. Manabe. 1975. "The Role of Mountains in the South Asian Monsoon Circulation". *J. Atmos. Sci.* 32:1515-1541.
- Hastenrath, S. 1985. *Climate and the Circulation of the Tropics*, Boston, D.Reidel Publ.
- Hastenrath, S., and P.J. Lamb, P.J. 1979. *Climate Atlas of the Indian Ocean. Surface Climate and Atmospheric Circulation*, Part I. Madison, WI, University of Wisconsin Press.
- Imbrie, J., N.J. Shackleton, N.G. Pisias, J.J. Morley, W.L. Prell, D.G. Martinson, J.D. Hays, A. McIntyre, and A.C. Mix. 1984. "The Orbital Theory of Pleistocene Climate: Support from a Revised Chronology of the Marine O-18 Record". In *Milankovitch and Climate*, Vol. 2. Ed. A.L. Berger *et al.* Hingham, MA, D. Reidel Publ. pp.269-305.
- Kent, D.V. 1982. "Apparent Correlation of Paleomagnetic Intensity and Climatic Records in Deep-Sea Sediments". *Nature* 299:538-539.
- Kolla, V. and P. Biscaye. 1977. "Distribution and Origin of Quartz in the Sediments of the Indian Ocean". *J. Sediment. Petrol.* 47:642-649.
- Kutzbach, J.E. 1981. "Monsoon Climate of the Early Holocene: Climate Experiment with the Earth's Orbital Parameters for 9,000 Years Ago". *Science* 214:59-61.
- Martinson, D.G., W. Menke, and A. Stoffa. 1984. "An Inverse Approach to Signal Correlation". *J. Geophys. Res.* 87:4807-4818.
- Mix, A.C., and R.G. Fairbanks. 1985. "North Atlantic Surface-Ocean Control of Pleistocene Deep-Ocean Circulation". *Earth and Planet. Sci. Lett.* 73:231-243.
- Nair, R.R., V. Ittekkot, S.J. Manganini, V. Ramaswamy, B. Haake, E.T. Degens, B.N. Desai, and S. Honjo. 1989. "Increased Particle Flux to the Deep Ocean Related to Monsoons". *Nature* 338:749-751.
- Pokras, E.M., and A.C. Mix. 1985. "Eolian Evidence for Spatial Variability of Late Quaternary Climates in Tropical Africa". *Quat. Res.* 24:137-149.
- Prell, W.L., and J.E. Kutzbach. 1987. "Monsoon Variability Over the Past 150,000 Years". *J. Geophys. Res.* 92:8411-8525.
- Prell, W.L., and E. Van Campo. 1986. "Coherent Response of Arabian Sea Upwelling and Pollen Transport to Late Quaternary Monsoonal Winds". *Nature* 323:526-528.
- Ramage, C.S. 1965. "The Summer Atmospheric Circulation Over the Arabian Sea". *J. Atmos. Sci.* 23:144.

- Raymo, M.E., W.F. Ruddiman, J. Backman, B. Clement, and D.G. Martinson. 1989. "Late Pliocene Variation in Northern Hemisphere Ice Sheets and North Atlantic Deep Water Circulation". *Paleoceanography* 4:413-446.
- Rind, D. 1987. "Components of the Ice Age Circulation". *J. Geophys. Res.* 92:4241-4281.
- Robinson, S.G. 1986. "The Late Pleistocene Record of North Atlantic Deep-Sea Sediments Revealed by Mineral-Magnetic Measurements". *Phys. Earth Planet. Inter.* 42:22-47.
- Ruddiman, W.F., and A. McIntyre. 1984. "Ice-Age Thermal Response and Climatic Role of the Surface Atlantic Ocean, 40°N to 63°N". *Geol. Soc. Amer. Bull.* 95:381-396.
- Ruddiman W.F., M.E. Raymo, D.G. Martinson, B. Clement, and J. Backman. 1989. "Pleistocene Evolution: Northern Hemisphere Ice Sheets and the North Atlantic Ocean". *Paleoceanography* 4:353-412.
- Shackleton, N.J., *et al.* 1984. "Oxygen Isotope Calibration of the Onset of Ice-Rafting and History of Glaciation in the North Atlantic Region". *Nature* 307:620-623.
- Shackleton, N.J., and N. Opdyke. 1976. "Oxygen Isotope and Paleomagnetic Stratigraphy of Pacific Core V28-239 Late Pliocene to Latest Pliocene". In *Investigations of Late Quaternary Paleoceanography and Paleoclimatology*. Ed. R.M. Cline and J.D. Hays. *Geol. Soc. Amer. Mem.* 145:449-464.
- Sirocko, F., and M. Sarnthein. 1989. "Wind-Borne Deposits in the Northwestern Indian Ocean: Record of Holocene Sediments versus Modern Satellite Data". In *Paleoclimatology and Paleometeorology: Modern and Past Patterns of Global Atmospheric Transport*. Ed. M. Leinen and M. Sarnthein. Kluwer Academic Publishers. pp.401-433.
- Stewart, R., O. Pilkey, and B.W. Nelson. 1965. "Sediments of the Northern Arabian Sea". *Marine Geol.* 3:411-427.
- Van Campo, E., J.C. Duplessy, and M. Rossignol-Strick. 1982. "Climatic Conditions Deduced from a 150-KY Oxygen Isotope-Pollen Record from the Arabian Sea". *Nature* 296:56-59.

Stable Isotopes in Paleosols and Origins of the Asian Monsoon

Jay Quade and Thure E. Cerling

ABSTRACT: The stable isotopic composition of buried soil carbonate and organic matter from northern Pakistan and Nepal can be used to reconstruct aspects of the paleoecology of riverine floodplain ecosystems over the past 17 Myr. Probable dry woodland dominated the floodplain biomass of large rivers ancestral to the modern Indus and Ganges up to 7.3 Myr. Between 7.3 and about 6 Myr, tropical grasses gradually displaced woodland and have dominated floodplain biomasses to the present. The paleovegetational transition beginning about 7.3 Myr likely signals the onset of the strongly seasonal precipitation pattern that typifies the monsoonal climate of the region today. One possible modern analog to the dry woodland soils of the Miocene are found under the Sal woodlands of the northern Indian subcontinent, while undisturbed modern analogs to the Plio-Pleistocene floodplain grasslands can still be found in the Chitwan area of southern Nepal.

Stable Isotopes in Paleosols

Isotopic results for both carbon and oxygen are presented in the usual δ notation as the per mil deviation of the sample CO_2 from the PDB standard, where:

$$R = {}^{13}\text{C}/{}^{12}\text{C} \text{ or } {}^{18}\text{O}/{}^{16}\text{O}, \text{ and } \delta = \left\{ \frac{R_{\text{sample}}}{R_{\text{standard}}} - 1 \right\} \times 1000$$

There are few techniques available for paleoecological reconstruction using fluvial deposits. Recently, Cerling (1984) and Cerling *et al.* (1989) demonstrated the utility of stable isotope analysis from paleosols in paleoecological reconstruction. The carbon isotopic composition of carbonates and organic matter is determined by the isotopic composition of plants at the site over the life of the soil. In low latitude settings such as the Indian subcontinent, two main metabolic pathways are followed by nearly all plants result in two non-overlapping isotopic groupings. C_4 plants include grasses favoring warm growing seasons and, therefore, nearly all grasses at low elevation in the tropics and in the monsoon belts. C_4 plants average -13 parts per mil worldwide. C_3 plants include all trees and nearly all shrubs at low latitudes, and they average around -27 parts per mil.

One consequence of this is that grasses and organic humus in soils derived from the grasses is distinctly enriched in ^{13}C in comparison to organic matter derived from trees and shrubs. Thus, the proportion of C_3 to C_4 plants (or grassland *versus* woodland) once at a site can be directly deduced from the carbon isotopic composition of paleosol organic matter. Although soil organic matter is rarely preserved in the geologic record, soil carbonate can also be used, and it is commonly preserved.

Soil carbonate displays a systematic 14 to 16 parts per mil enrichment in ^{13}C in comparison to coexisting organic matter. As plants respire and decay, they produce soil-respired CO_2 of similar isotopic composition to their own bulk isotopic composition. Carbon species in soil solution equilibrate with this reservoir before precipitation as carbonate (Quade *et al.* 1989), thus preserving the isotopic composition of the original soil biomass. The 14 to 16 parts per mil resulting difference is slightly temperature-dependent and arises

from the phase transformation from CO₂ to solid carbonate and from gas diffusive effects (Cerling 1984, Cerling *et al.* 1989). Carbonate precipitated in the presence of a pure C₃ biomass, therefore, will have a $\delta^{13}\text{C}$ (PDB) composition of around -11 to -12 parts per mil; a pure C₄ biomass will result in values of +1 to +3 parts per mil.

The $\delta^{18}\text{O}$ (PDB) composition of soil carbonate is determined by temperature and the isotopic composition of soil water. Cerling (1984) found a strong positive correlation between the $\delta^{18}\text{O}$ of soil carbonate and average annual rainfall, although in deserts a 2 to 3 parts per mil enrichment occurs in carbonate, possibly due to evaporation (Quade *et al.* 1989).

Stable Isotopic Record from the Indian Subcontinent

Siwalik Group rocks crop out in a nearly continuous belt stretching from northern Pakistan to Assam in northeastern India. The Siwaliks were deposited by the major rivers ancestral to the modern Indus and Ganges in a deep foreland trough beginning 15 to 20 Myr ago in most areas. We sampled paleosols of ten sections in northern Pakistan and in central and eastern Nepal. Sampling density in Pakistan was highest, averaging about one paleosol per 130,000 years over a 17-Myr span.

Prior to 7.3 Myr, the $\delta^{13}\text{C}$ (PDB) composition of paleosol carbonate falls between -12 and -9 parts per mil in Pakistan (Figure 1). This indicates a pure or nearly pure C₃ biomass was present as the soils were forming. After 7.3 Myr, the $\delta^{13}\text{C}$ (PDB) of soil carbonate begins to increase, reflecting entry of C₄ plants into the floodplain ecosystem. A pure or nearly pure C₄ biomass dominated the floodplain throughout the Plio-Pleistocene. This shift is also reflected in buried soil organic matter, which is common in the upper part of the record but rare before 6 Myr. Organic matter averages about -13 parts per mil in the Plio-Pleistocene (Quade *et al.* 1990) and -24 parts per mil before then, consistent with pure C₄ or nearly pure C₃ biomasses. Most important, soil carbonate is consistently 14 to 16 parts per mil enriched with respect to coexisting organic matter, arguing against diagenetic alteration of either phase.

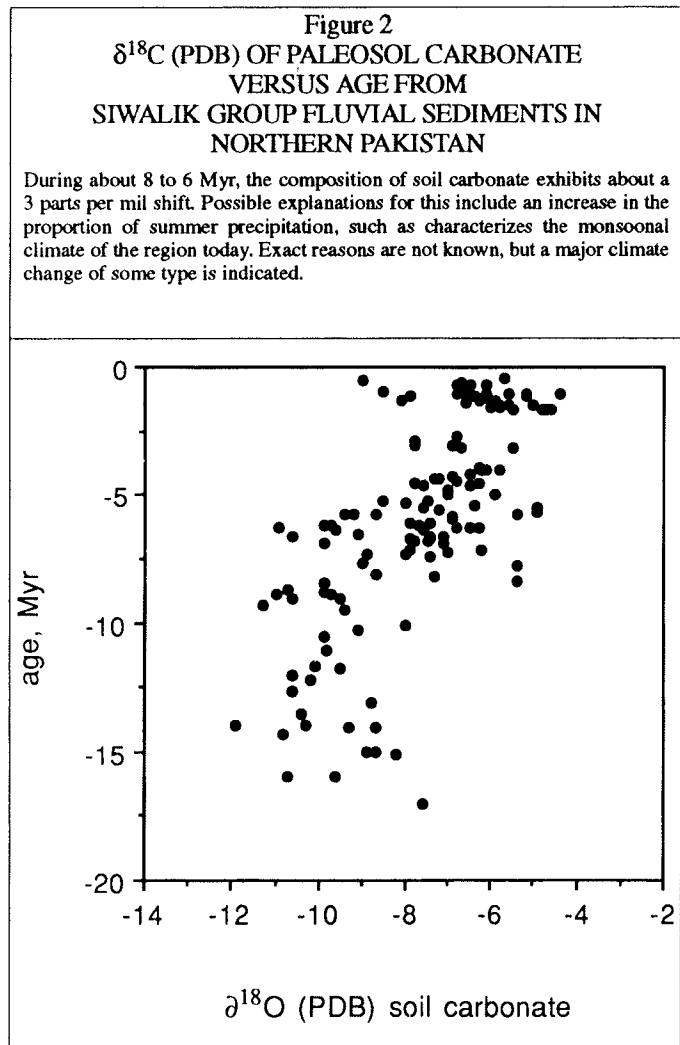
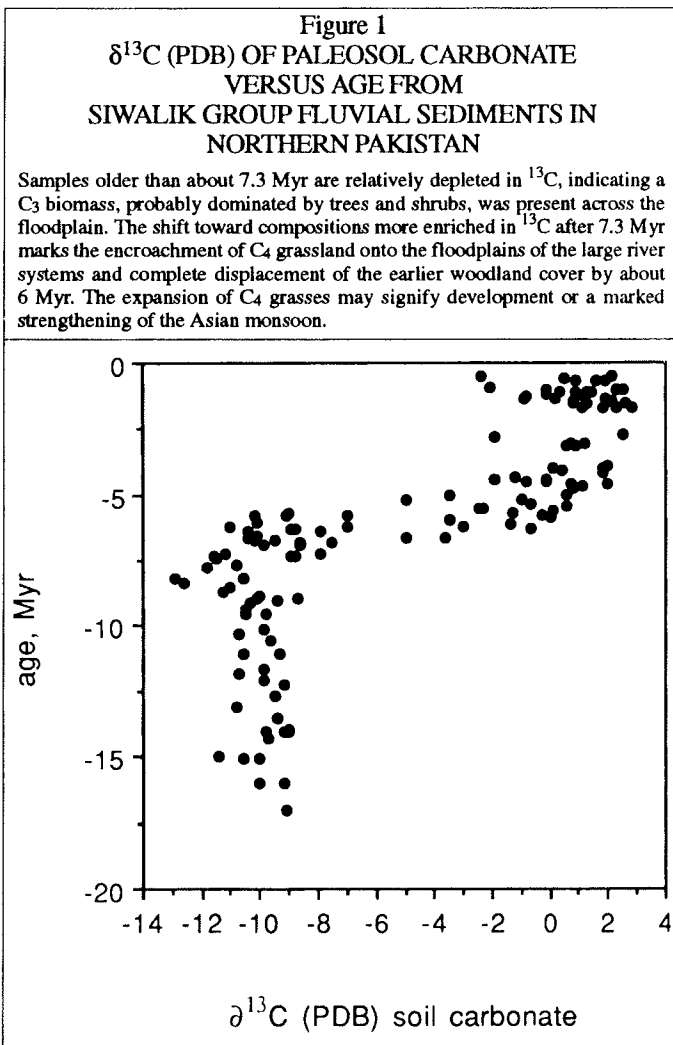
An identical isotopic record occurs in several sections of central and western Nepal, although the age of the biomass shift can only be constrained at this point to between 8 and 6 Myr (Quade Unpub. Data). It is remarkable that the Pakistan and Nepalese records are so similar, since the two areas are 1000 kilometers and 5 degrees of latitude apart.

At the latitude of the Indian subcontinent, C₄ grasses are strongly favored over C₃ grasses because of their superior tolerance for high light intensity and high temperatures. C₃ grasses are known only from high elevations or as a minor component (<10%) in the shaded understory of forests at this latitude. On the other hand, all trees and nearly all shrubs are C₃ plants, irrespective of environmental conditions. Assuming these patterns held for the past, then the nearly pure C₃ biomass indicated by the isotopic composition of soil carbonates and organic matter to be present on floodplains before 7.3 Myr was nearly all trees and shrubs. The C₄ biomass that took over floodplains thereafter was very likely a grassland.

The oxygen isotopic composition of soil carbonate exhibits about a 3 parts per mil shift at about the same time as or just before carbon isotope shift (Figure 2). This can be explained several ways, including:

- Temperature increase,
- Increased proportion of summer rainfall due to higher temperatures,
- Major shift in storm trajectories,
- A broader tropical zone producing a locally steeper gradient in the poleward oxygen isotope depletion of rainwater,
- A combination of the above.

We do not know which alternative, if any, is correct. However, the encroachment of grasses, especially C₄ grasses, after 7.3 Myr suggests climate was increasingly seasonal and a larger proportion of rainfall was falling in summer. Thus, the carbon isotopic evidence suggests the second alternative may have played a role in the oxygen isotope shift.



No matter the exact explanation, a major climate change is indicated, and the carbon isotope evidence would suggest this marks the arrival of a monsoonal climate that favors C₄ grasses over so much of the region today.

Modern Analogs

The carbon isotopic composition and other features of paleosols below the 7- to 8-Myr level all come together in at least one setting on the Indian subcontinent. Soils from those levels usually contain secondary carbonate at 1- to 2-meter depths, arguing against a moist forest setting typified by soils generally leached of carbonate. B horizons are dominated by smectite, although vermiculite, chlorite, and minor kaolinite are also present, all suggesting only moderate leaching conditions. These features — clays indicative of moderate leaching, soil carbonate, and C₃ biomass — come together in soils underlying Sal (*Shorea robusta*) woodland, although soil carbonate is most abundant where parent material is also calcareous, as in western Nepal. Sal woodland is extant in many moderate rainfall areas of India and lowland Nepal. It is most common in broken interfluvial areas — where rainfall is somewhat higher and effects of seasonal fire and flooding, factors that favor grasslands in general, are less pronounced — than in lowland floodplains where C₄ grasses dominate. In areas of Nepal we visited, grasses are rare to absent in the understory of Sal woodland, even in areas that show no evidence of recent grazing.

Chitwan National Park preserves one of the few undisturbed riverine floodplain ecosystems on the Indian subcontinent. C₄ grasses such as *Imperata cylindrica* and *Saccharum mirja* stand more than 2 meters high on the entire floodplain, which is several kilometers wide. Physical appearance of the soils and isotopic composition of the grasses are identical to those of buried paleosols in nearby Plio-Pleistocene paleosols.

Palynological and Faunal Evidence

Palynological evidence from northwest India and Nepal (Mathur 1984) shows that after the late middle Miocene, grass pollen began to become common, mixed with pollen from gymnosperm, tree ferns, herbs, and swamp vegetation. Throughout the Plio-Pleistocene, grass pollen is very common, suggesting grasslands had become a well developed part of the regional ecosystem. The difficulty with pollen studies in the Siwaliks is that much of the pollen has been washed in from higher elevations, and radiometric and paleomagnetic dating have not been done on the sampled sections. Thus, it is not clear exactly when the transition to grassland occurred.

Barry *et al.* (1982 and 1985) have noted several periods of large faunal change in the fossil record over the past 17 Myr. One of these periods begins at 7.5 Myr and coincides with the vegetation transition we have identified using stable isotopes. So distinctive is the change that it is called the “Selenoportax Zone” after the first appearance of a large bovid, *Selenoportax lydekkeri*, which had extremely hypsodont teeth. The nature of the faunal turnover led Barry *et al.* (1985) to believe climate change was involved to some degree. Most interesting is the disappearance between about 8 and 6.5 Myr of animals of apparent forest/woodland affinity, such as four species of tragulids, lorid primates, tree shrews, and *Sivapithecus*, a fossil hominoid allied to the modern tree-dwelling orangutan. Rodents

experienced a major turnover at this time, which Flynn and Jacobs (1982) also related to expansion of grassland in the region.

Tectonic Uplift and Origins of the Asian Monsoon

It has long been known that topography exerts significant control on upper atmosphere flow patterns (Bolin 1950), which, in turn, influence climate at the Earth's surface. The link between the Asian summer monsoon and high topography is well established (Flohn 1950) and has recently been confirmed by global circulation modeling (GCM) (Hahne and Manabe 1975, Kutzbach *et al.* 1989, and Ruddiman and Kutzbach 1989).

Two major processes drive monsoonal circulation (Webster 1987). The specific heat capacity of soil is about half that of water, causing land surface to heat much faster than the ocean. As air is heated at high elevations over the Tibetan Plateau, it rises, causing low pressure to develop. This low pressure draws moisture-laden air off the Indian Ocean, where higher pressure is present due to cooler ocean temperatures. As the moist air masses cross the Indian subcontinent, they rise and cool, and moisture condenses as rain. This condensation leads to release of latent heat, causing additional expansion and rise of air and, thus, intensification of low pressure. Heating at high elevations further steepens the pressure gradient between air masses over the mountains and oceans.

What, then, is the geologic and paleobotanic evidence for uplift of the Himalayas and the Tibetan Plateau, and can this be linked to the onset of the Asian monsoon? The weight of the evidence suggests the Himalayas and the Tibetan Plateau had attained high elevations over large areas by at least the early Pliocene.

The Indian subcontinent probably collided with Asia sometime in the Eocene, when mountain-building presumably began. Molasse deposits in Pakistan derived from the ancestral Hindu Kush date as far back as the late Oligocene. However, fossil evidence indicates there was no significant physical barrier to migration of mammal faunas before the late Miocene or Pliocene (Wang *et al.* 1982, Conroy *et al.* 1982).

Hsu (1978) describes the presence of deciduous Miocene pollen at present-day elevations of 4 to 5 kilometers, where vegetation cover is now scant and aridic. He deduced local uplift rates of as high as 1 km/Myr in the late Cenozoic, with higher rates more recently.

Using pollen and other evidence, Mercier *et al.* (1987) showed that uplift in the Himalayas has increased exponentially in the last 10 Myr, with a minimum of 2 kilometers uplift in that span. Uplift rates inferred from fission-track densities in zircons from the Nanga Parbat area of northern Pakistan (Zeitler 1985) also show a quasi-exponential increase in the last 10 Myr. Some areas are now experiencing about 5 km of uplift per million years. Johnson *et al.* (1982) and Burbank and Johnson (1983) deduced rapid sedimentation and, therefore, high uplift rates since the mid-Miocene in the Himalayan foreland and intermontane basins.

Evidence from the Arabian Sea strongly suggests that while uplift was accelerating in the Himalayas, changes in oceanographic patterns were also taking place. Monsoonally induced upwelling in the Arabian Sea began in the late middle Miocene (Prell *et al.* 1989).

Shraeder (1974) and Burckle (1989) also found this but observed that abundance of diatoms typical of a reversing monsoon markedly increased at 7.3 Myr.

It was suggested that appearance of C₄ grasses in floodplain biomasses beginning about 7.3 Myr signaled the inception or strong intensification of the Asian monsoon. Evidence cited above suggests the event at 7.3 Myr was more likely an intensification and that a weak monsoon was probably in place before that. The evidence also suggests development of a strong monsoon is tied to acceleration of uplift rates beginning sometime in the latter half of the Miocene.

The impact of this uplift on climate may have gone beyond forcing of the Asian monsoon. Raymo *et al.* (1988) found that carbonate sedimentation, calcite compensation depths, and the $\delta^{13}\text{C}$ and ^{87}Sr in biogenic sediments indicate a global increase in river fluxes in the late Miocene. Much of this increase likely came from the Ganges/Brahmaputra system, which contributes a large proportion of total dissolved load to the modern ocean. Increased continental weathering from tectonically active areas like the Himalayas may have caused lowering of atmospheric CO₂. Raymo *et al.* (1988) speculate that this, in turn, may have induced global cooling over the past few million years.

References

- Barry, J.C., N.M. Johnson, S.M. Raza, and L.L. Jacobs. 1985. "Neogene Mammalian Faunal Change in Southern Asia". *Geology* 13:637-640.
- Barry, J.C., E.H. Lindsay, and L.L. Jacobs. 1982. "A Biostratigraphic Zonation of Middle and Upper Siwaliks of the Potwar Plateau of Northern Pakistan". *Palaeogeography Palaeoclimatology Palaeoecology* 37:95-130.
- Bolin, B. 1950. "On the Influence of the Earth's Orography on the General Character of the Westerlies". *Tellus* 2:184-195.
- Burbank, D.W. and G.D. Johnson. 1983. "The Late Cenozoic Chronologic and Stratigraphic Development of the Kashmir Intermontane Basin, Northwestern Himalayas". *Palaeogeography Palaeoclimatology Palaeoecology* 43:205-235.
- Burckle, L.H. 1989. "Distribution of Diatoms in Sediments of the Northern Indian Ocean: Relationship to Physical Oceanography". *Marine Micropaleontology* 15:53-65.
- Cerling, T.E. 1984. "The Stable Isotopic Composition of Modern Soil Carbonate and its Relationship to Climate". *Earth and Planetary Science Letters* 71:229-240.
- Cerling, T.E., J. Quade, Y. Wang, and J.R. Bowman. 1989. "Carbon Isotopes in Soils and Palaeosols as Ecology and Palaeoecology Indicators". *Nature* 341:138-139.
- Conroy, G., R.M. West, and J. Munthe. 1982. "The Siwaliks of Nepal: Recent Contributions to Vertebrate Paleontology and Biostratigraphy". In *Contributions to Himalayan Geology, Vol. 3, Geology of the Western Himalayas*. Ed. V.G. Gupta. New Delhi, India, Hindustan Publishing Corp. pp.52-61.
- Flohn, H. 1950. "Studien zur Allgemeinen der Atmosphere III". *Berliner Deutsches Wetterdienstes* 18:3450.

- Flynn, L.J., and L.L. Jacobs. 1982. "Effects of Changing Environments on Siwalik Rodent Faunas in Northern Pakistan". *Palaeogeography Palaeoclimatology Palaeoecology* 38:129-138.
- Hahne, D.G., and T. Manabe. 1975. "The Role of Mountains in the South Asian Monsoon Circulation". *Journal of Atmospheric Sciences* 32:1515-1541.
- Hsu, J. 1978. "On the Paleontologic Evidence for Continental Drift and Himalayan Uplift". *Paleobotany* 25:131-353.
- Johnson, G.D., M.D. Opdyke, D.W. Johnson, E.H. Lindsey, and R.A.K. Tahirkheli. 1982. "Magnetic Polarity Stratigraphy and Ages of Siwalik Group Rocks of the Potwar Plateau, Pakistan". *Palaeogeography Palaeoclimatology Palaeoecology* 37:1742.
- Kutzbach, J.E., P.J. Guetter, W.F. Ruddiman, and W.L. Prell. 1989. "Sensitivity of Late Cenozoic Uplift in Southern Asia and the American West: Numerical Experiments". *Journal of Geophysical Research* 94:18,393-18,407.
- Mathur, Y.K. 1984. "Cenozoic Palynofossils, Vegetation, Ecology, and Climate of the North and Northwestern Subhimalayan Region, India". In *The Evolution of the East Asian Environment, Vol. 2*. Ed. R.O. Whyte. Centre for Asian Studies, University of Hong Kong. pp. 505-551.
- Mercier, J.L., R. Armijo, P. Tapponnier, E. Carey-Gailhardis, and H.T. Lin. 1987. "Change from Late Tertiary Compression to Quaternary Extension in Southern Tibet During the India-Asia Collision". *Tectonics* 6:275-304.
- Prell, W. L., *et al.* 1989. *Initial Reports, Ocean Drilling Program, Leg 117*. Washington D.C., U.S. Government Printing Office.
- Quade, J., T.E. Cerling, and J.R. Bowman. 1990. "Development of the Asian Monsoon as Revealed by Marked Ecological Shift During the Latest Miocene in Northern Pakistan". *Nature* 342:163-166.
- _____. 1989. "Systematic Variations in the Carbon and Oxygen Isotopic Composition of Pedogenic Carbonate along Elevation Transects in the Southern Great Basin, United States". *Geological Society of America Bulletin* 101:464-475.
- Raymo, M.E., W.F. Ruddiman, P.N. Froelich. 1988. "The Influence of Late Cenozoic Mountain Building on Oceanic Geochemical Cycles". *Geology* 16:649-653.
- Ruddiman, W.F., and J.E. Kutzbach. 1989. "Forcing of Late Cenozoic Northern Hemisphere Climate by Plateau Uplift in Southern Asia and the American West". *Journal of Geophysical Research* 94:18,409-18,427.
- Shraeder, H.J. 1974. "Cenozoic Marine Planktonic Diatom Stratigraphy of the Tropical Indian Ocean". In *Initial Reports of the Deep Sea Drilling Project*. Ed. R.L. Fisher *et al.* U.S. Government Printing Office, Washington DC. 24:887-968.
- Wang, C.Y., Y.L. Shi, and W.H. Zhou. 1982. "Dynamic Uplift of the Himalayas". *Nature* 289:553-556.
- Webster, P.J. 1987. "The Elementary Monsoon". In *Monsoons*. Ed. J.S. Fein and P.L. Stephens. John Wiley and Sons, New York. p.332.
- Zeitler, P.K. 1985. "Cooling History of the NW Himalayas, Pakistan". *Tectonics* 4:127-151.

